# Ninth International Conference on Permafrost

Ninth International Conference on Permafrost
University of Alaska Fairbanks
June 29–July 3, 2008

# Ninth International Conference on Permafrost

# Extended Abstracts

**Edited by Douglas L. Kane and Kenneth M. Hinkel**

**Institute of Northern Engineering**
**University of Alaska Fairbanks**
**2008**

Ninth International Conference on Permafrost
Extended Abstracts
Edited by Douglas L. Kane and Kenneth M. Hinkel



Printed in the United States of America

Cover Photo: Low-Centered Polygons, North Slope, Alaska


Production Editors: Thomas Alton and Fran Pedersen

# Contents

# Preface

One of the looming challenges in organizing an international conference on permafrost is determining the timetable. What should be the deadline for abstract and paper submittals? Early in the process we agreed that we wanted the proceedings published before the conference, and this challenge has become more taxing as the size of the conference has increased. We made a concerted effort to compress the timetable so that papers published in the proceedings were to be submitted only eight and one-half months before the conference. Still, there are those who want to report on their latest research at the permafrost conference. In the recent past, the International Permafrost Association (IPA) introduced the concept of extended abstracts (two pages in this case) that were published in a separate document. The idea was that the collection would represent the latest in permafrost research. It is clear that some researchers, finding the English language challenging, opted instead to submit the shorter extended abstract in lieu of the six-page manuscript. We have one hundred eighty-four extended abstracts that will be presented at the Ninth International Conference on Permafrost; this can be compared with the three hundred fifty-eight papers published in the proceedings. As in the past, the extended abstracts were not reviewed, and except for some minor changes (formatting, deletion of an abstract in the extended abstract, etc.), they are published as they were submitted. As with the proceedings and abstract volumes, we appreciate all the assistance we received from Thomas Alton and Fran Pedersen in producing this volume. We hope that you find these extended abstracts and accompanying poster presentations informative.

— Douglas L. Kane and Kenneth M. Hinkel

# NICOP Sponsors

**Universities**
University of Alaska International Polar Year (Gold plus)
University of Alaska President's Fund (Gold)
Alaska University Transportation Center (Gold)
University of Alaska Fairbanks Institute of Northern Engineering (Silver)
University of Alaska Fairbanks International Arctic Research Center (Silver)
University of Alaska Fairbanks Experimental Program to Stimulate Competitive Research (EPSCoR) (Bronze)
University of Alaska Young Researchers' Network/UA IPY Outreach (Contributor plus)
University of Colorado-National Snow and Ice Data Center (Contributor)

**Government Agencies**
Alaska Division of Geological and Geophysical Surveys, Fairbanks (Gold)
U.S. National Science Foundation (Silver)
U.S. Geological Survey (Silver)
U.S. Army Cold Regions Research and Engineering Laboratory (Bronze)
U.S. Department of Energy (Bronze)
U.S. Arctic Research Commission (Brass)
U.S. Bureau of Land Management (Brass)
Denali Commission (Brass)
North Slope Science Initiative (Brass)
U.S. Minerals Management Service (Contributor plus)
Norwegian Thermal State of Permafrost IPY Project (Sustaining)

**Corporate and Non-Governmental Organizations**
Arctic Foundations, Inc., Anchorage (Gold)
Alyeska Pipeline Company, Anchorage (Silver)
International Permafrost Association (Bronze plus)
Arctic Slope Regional Corp. (Bronze plus)
BP Foundation (Bronze)
Geo-Watersheds Scientific, Fairbanks (Bronze)
Duane Miller & Associates, Anchorage (Bronze)
CH2MHILL Energy & Power, Anchorage (Brass)
ConocoPhillips Alaska (Brass)
EBA Engineering Consultants Ltd., Canada (Brass)
Golder Associates, Anchorage (Brass)
Michael Baker Jr, Inc., Anchorage (Brass)
Shannon & Wilson, Inc. Seattle (Brass)
PND Engineers, Inc, Anchorage (Contributor plus)
RA Kreig & Associates, Anchorage (Contributor plus)
BeadedStream, LLC, Anchorage (Contributor)
DOWL LLC, Anchorage (Contributor)
Kinross Fort Knox Gold Mine (Contributor)
Hawk Consultants, LLC, Anchorage (Contributor)
Houston Advanced Research Center (HARC) (Contributor)
Fairbanks Gold Mining, Inc., Fairbanks (Contributor)
Northern Engineering & Scientific, Anchorage (Contributor)
Northern Geotechnical Engineering, Inc., Anchorage (Contributor)
R&M Consultants, Inc., Anchorage (Contributor)
Tryck Nyman Hayes, Inc., Anchorage (Contributor)
Resource Data, Inc., Anchorage (Sustaining)
URS Corporation, Anchorage (Sustaining)
Usibelli Foundation (Sustaining)
Harley H. Hightower, FAIA, Anchorage (Sustaining)

**ICOP Donor Circle (Contributor)**
Jerry and Celia Brown
Edwin Clarke
Hugh M. French
Don W. Hayley
C.W. "Bill" Lovell
J. Ross Mackay (Honorary Member)
Michael C. Metz
Frederick E. Nelson
Jim and Florence Rooney
Ronald S. Sletten
Sarah M. Springman
Rupert "Bucky" Tart
Ted B. Trueblood
H. Jesse Walker
John Zarling

**Individuals**
Joe Malen

**In-Kind Sponsors**
Elsevier
Rite in the Rain
Fairbanks Convention and Visitors Bureau
American Water Resources Association
UAF Toolik Lake Field Research Station
Pogo Mine
U.S. Army CRREL
U.S. Geological Survey
Permafrost Young Researchers Network
Mountain Studies Institute
University of Cincinnati
University of Colorado at Boulder
Kinross Fort Knox Gold Mine
Institute of Arctic and Alpine Research
BP Exploration (Alaska), Inc.
University of Alaska Fairbanks
ABR, Inc.
U.S. National Park Service
Geo-Watersheds Scientific

UAF International Arctic Research Center
UAF Institute of Northern Engineering
University of Alaska IPY Office
Alaska Division of Geological & Geophysical Surveys
Barrow Arctic Science Consortium
Conoco Phillips Alaska

# Deep Permafrost Studies at the Lupin Mine: Hydrogeological and Geochemical Information for Nuclear Waste Disposal

Lasse Ahonen
*Geological Survey of Finland*
Timo Ruskeeniemi
*Geological Survey of Finland*
Randy Stotler
*University of Waterloo, Canada*
Shaun Frape
*University of Waterloo, Canada*
Kimmo Lehto
*Posiva Oy, Finland*
Ignasi Puigdomenech
*SKB (Swedish Nuclear Fuel and Waste Management Co), Sweden*
Monique Hobbs
*Nuclear Waste Management Organization, Canada*
Paul Degnan
*Nirex, UK (present position CSIRO Exploration & Mining, Australia)*

## Introduction

The deep geological disposal of high-level and long-lived nuclear waste requires a comprehensive understanding of the possible impacts of long-term future climate change on a repository environment and the surrounding rock mass. Despite the general scientific consensus that global warming is underway due to anthropogenic greenhouse gas emissions, future glaciation scenarios have to be taken into account and included in the long-term safety analyses of disposal systems, especially in Fennoscandian countries, Britain, and Canada.

The Lupin gold mine, situated in the territory of Nunavut, Canada, is located in a subarctic tundra environment, where continuous permafrost reaches depths of 400–600 m. The bedrock of the Lupin area consists of Archean metasedimentary crystalline rocks, which are considered to be good analogues for host rocks at potential repository sites in the Fennoscandian Shield. Consequently, several nuclear waste management organizations, together with the Geological Survey of Finland and the University of Waterloo, started a joint venture to study the hydrogeological and hydrogeochemical conditions below and within the permafrost at the Lupin mine (Ruskeeniemi et al. 2003).

Several important uncertainties relating to the potential effects of permafrost on the safety of nuclear waste disposal were identified as follows:

- *Depth range* and rate of formation of permafrost in crystalline rock and the controlling factors.
- *Hydrogeological conditions* in frozen rock, the importance of taliks as possible flow paths and the freezing of water in major fracture zones.
- *Hydrogeochemical effects* of permafrost, formation of saline segregations (cryopegs) in and/or below the frozen rock mass.
- *Methane hydrates, the* abundance and formation of methane in crystalline rock and the nature of any accumulations below the permafrost.

## Research Activities

The research project at the Lupin mine was conducted in three phases. During the first phase, background data on geology and hydrology were compiled, potential fracture zones were identified by a seismic refraction study, and underground waters were sampled (Ruskeeniemi et al. 2002). Phase II activities included an electromagnetic survey (SAMPO), drilling of two research boreholes from inside the mine upwards through the bottom of the permafrost, water and gas sampling, crush and leach studies of the rock material, and freezing experiments of water samples (Ruskeeniemi et al. 2004, Frape et al. 2004).

Phase III (Stotler et al. 2008) focused on the collection of representative data concerning the chemistry and isotopic composition of waters and dissolved components from packed-off boreholes, the long-term monitoring of hydraulic heads in the boreholes, mineralogical studies of fractured rock, and a ground penetrating radar survey.

## Hydrogeological Conditions

In the mine, the bedrock below the permafrost down to about 900 m appeared distinctly dry, as observed along the ramp roadway. Mine statistics indicate pumping rates of about 6 $m^3/h$ (in 2003), of which a major proportion was identified to be fresh water supplied for various purposes in the mining process. Most of the water-producing boreholes situated at the level 1130 m were plugged. At higher levels the seepage of groundwater through frozen bedrock does not appear to take place at all. Measured effective porosities of

the Lupin rocks were less than 0.5%, which indicates that only major fracture systems are likely to serve as significant hydraulic conductors.

Lupin mine is situated near the large freshwater Lake Contwoyto, which—based on its size and elongated form—could potentially maintain a water-conducting talik beneath the surface. A ground penetrating radar study confirmed that there is only a narrow band of frozen ground along the shore of the lake.

Boreholes, most of them situated in the exploration drift at the 1130 m level were packered off with mechanical packers and equipped with valves for water and gas sampling and pressure gauges for monitoring of hydraulic heads. Hydraulic heads were monitored in 9 boreholes for 2 to 3 years, and the highest hydraulic head values measured in 2 of the boreholes correspond to the expected pressures arising from a hydrostatic column of water with its top at the base of the permafrost. Thus, there does not seem to be a clear hydraulic connection between the boreholes and the nearby lake through any non-frozen fracture zone. Lack of uniform hydraulic conductivity of the deep bedrock was also demonstrated by the large differences in hydraulic heads (up to 160 $m_{H2O}$) between monitored boreholes. On the other hand, traces of tritium in the deep saline waters indicate that a small portion of recent surficial water may be recharging to depth.

Drilling through the base of the permafrost indicated that the bedrock was not water-saturated, but a dry zone exists below the permafrost. A cone of depression generated by the mine drainage, together with the very limited recharge of surficial water, is the most likely explanation. However, it is also possible that given the limited potential for recharge, the piezometric surface below the permafrost may fall regionally over the very long time periods involved.

## Hydrogeochemical Conditions and Gases

*Permafrost* waters sampled along the ramp down to the base of permafrost were typically very saline (TDS up to about 40 g/L). Geochemical and isotope studies indicate the contribution of drilling brine used for drilling in cold conditions, but the introduced salt has mixed with a natural salt source and subsequently been altered by the freezing process. Permafrost waters contained a high concentration of sulfate, which could not originate either from the salt used in drilling or from surficial fresh water, but rather indicates oxidation of the sulfide ore body.

The possible formation of saline water by segregation at the *base of the permafrost* was studied by drilling two boreholes at 570 m depth. With time, groundwater contamination by drilling water (labeled with a tracer) and other mine-induced contamination (e.g., nitrate) fade out, and representative water samples seeping from the bedrock were obtained in the upwards-directed borehole. The salinity of the basal permafrost water (TDS 3–5 g/L) was observed to be lower than in waters within the frozen bedrock. No distinct basal cryopeg was observed below the permafrost. Based on molar ratios and isotopic compositions, it is evident that the groundwater at the base of the permafrost is similar to deeper sub-permafrost waters, but more dilute.

Deep *sub-permafrost waters* sampled in one borehole at a depth of 890 m, and in several boreholes of the exploration drift at 1130 m were typically saline (TDS up to about 40 g/L). Interestingly, the salinity of the waters varied not only between different boreholes, but also in the same borehole at different times. Hydraulic connections between fractures are evidently very limited, and the water composition varies between different fracture systems.

Waters contain dissolved gases, mainly methane, in abundance (up to about 0.5L gas/L of water). Isotope compositions of methane samples plot within a relatively narrow range: $\delta D$ = -330 – -350‰, $\delta C$-13 = -45 – -50‰. Isotope geochemical interpretation of the data suggests a thermogenic origin for the methane, but the contribution of bacterial methyl type fermentation cannot be ruled out. A carbon-14 model age of dissolved bicarbonate in deep sub-permafrost water was interpreted to be about 25 ky, while C-14 in methane was below the detection limit. Continuous monitoring of redox potential in a flow-through cell over several days indicated Eh-values around zero and dissolved oxygen concentrations were below detection limit (0.1 mg/L) in all measurements.

## References

Frape, S.K., Stotler, R.L., Ruskeeniemi, T., Ahonen, L., Paananen, M. & Hobbs, M.Y. 2004. *Hydrogeo-Chemistry of Groundwaters at and Below the Base of the Permafrost at Lupin: Report of Phase II*. Ontario Power Generation. Report 06819-REP-01300-10047-R00. Toronto: Ontario Power Generation. 74 pp.

Ruskeeniemi, T., Paananen, M., Ahonen, L., Kaija, J., Kuivamäki, A., Frape, S., Morén, L. & Degnan, P. 2002. Permafrost at Lupin: Report of phase I. *Geological Survey of Finland* Report YST-112.

Ruskeeniemi, T., Ahonen, L., Paananen, M., Blomqvist, R., Degnan, P., Frape, S. K., Jensen, M., Lehto, K., Wikström, L., Morén, L., Puigdomenech, I. & Snellman, M. 2003. Groundwater under deep permafrost conditions. In: *8th International Conference on Permafrost, Zurich, Switzerland, July 20–25, 2003*. Extended abstracts reporting current reserch and new information. Zurich: University of Zurich, 141-142.

Ruskeeniemi, T., Ahonen, L., Paananen, M., Frape, S., Stotler, R., Hobbs, M., Kaija, J., Degnan, P., Blomqvist, R., Jensen, M., Lehto, K., Morén, L., Puigdomenech, I. & Snellman, M. 2004. Permafrost at Lupin: Report of phase II. *Geological Survey of Finland, Report* YST-119.

Stotler, R.L., Frape, S.K., Ruskeeniemi, T., Ahonen, L., Paananen, M., Hobbs, M.Y. & Zhang, M. 2008. *Hydrogeochemistry of Groundwaters at and Below the Base of the Permafrost at Lupin: Report of Phase III*. Ontario Power Generation Report (in print).

# Effect of Fire on Pond Dynamics in Regions of Discontinuous Permafrost: A State of Change Following the Fires of 2004 and 2005?

Garrett Altmann
*School of Natural Resources and Agricultural Sciences, University of Alaska Fairbanks*
Dave Verbyla
*School of Natural Resources and Agricultural Sciences, University of Alaska Fairbanks*
Kenji Yoshikawa
*Water and Environmental Research Center, Institute of Northern Engineering, University of Alaska Fairbanks*
John Fox
*School of Natural Resources and Agricultural Sciences, University of Alaska Fairbanks*

## Introduction

Climate change at high latitudes affects both the disturbance and hydrologic regimes of boreal forests. Throughout Interior Alaska, wildfire is the dominant disturbance regime regulating boreal forests associated with discontinuous permafrost. In recent years, fire activity has signaled a potential shift in this disturbance regime, as significant increases in total burned area and burn severity have occurred. The effects of a potential regime shift may have profound impacts on the permafrost and hydrologic features associated with it.

Previous studies have examined the effects of fire on permafrost and have attributed a deepening of the active layer, as well as increased soil moisture resulting from the removal of insulating vegetation during fire (Yoshikawa et al. 2002, Liljedahl et al. 2007, Burn 1998). Ishikawa et al. (2008) has further implicated fire severity as a significant source of variability among these effects. To examine the relationship between fire, burn severity, and pond dynamics, this study uses remote sensing and GIS to compare ponds affected by fire, to ponds not affected by fire.

## Data and Methods

We use remote sensing and geographic information systems (GIS) to examine the effect of fire on pond sizes throughout four Interior Alaska basins: Tanana Valley, Yukon Flats, Innoko Flats, and Minchumina Basin (Fig. 1). Using Landsat TM/ETM+ imagery and historic fire parameters attained from the Alaska Fire Service, a multi-temporal analysis from 1980 to present is used to observe surface area changes in ponds following fires. To observe pond dynamics in fire-affected areas, historic burn parameters are overlaid on pre-fire and post-fire georeferenced Landsat scenes. All GIS layers are analyzed using the Alaska Alber's Equal Area projection to provide accurate representations of surface area. Pond dynamics within burn areas are then compared to ponds outside burn parameters. Ponds displaying variability are tagged and compared at varying time periods. To evaluate the influence of fire severity, we examine thermal IR (band 6) data within the burn area from imagery attained one year post-burn. As a test of our methodology, a pilot study was applied to the Yukon Flats portion of our study area. Despite the inability to assess pond depth from a remote sensing perspective, we feel confident our methodology will allow us to observe pond dynamics in relation to fire in the remaining study areas.

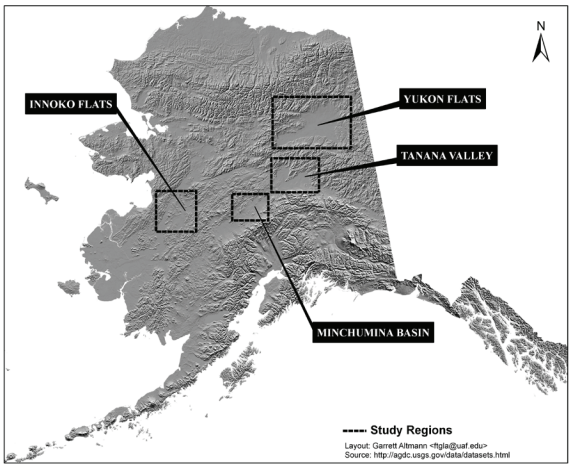


Figure 1. Study area locations.

## Results

Initial results reveal a static state of pond sizes following fires prior to 2004. During the larger, more severe fires occurring in 2004 and 2005, ponds located in burn areas show greater variability in surface area than ponds located outside the burn area. Increased shrinkage was observed within burn areas during the years immediately following the fire. Short-term observations (1–3 years) in burn areas prior to 2004 do not reveal this effect. Periods 5–15 years following a fire show little/no variability in surface area, and fluctuations tend to be dominated by the regional water table. Long-term (15–25 years) reveal similar trends to those experienced during short-term observations associated with high fire severity.

## Discussion

In our initial hypothesis, we expected pond sizes within burn parameters to increase as a result of the removal of a transpiring vegetation layer. Contrary to this hypothesis, we observe a decrease in surface area of ponds in areas

of high burn severity. This is attributed to either the loss and/or depletion of the insolating vegetation that provided protection from incoming solar radiation and prevented evaporation, or to an increase in the active layer thickness which results in more lateral and vertical drainage, and/or thermokarsting. The period 5–15 years following a fire showing little variability in surface area are likely attributed to seasonal refreezing of the active layer. Refreezing of the active layer prevents drainage and talik expansion, thus stabilizing ponds and minimizing changes attributed to fire disturbance. The mechanisms responsible for shrinking during long-term (15–25 years) periods is attributed to a more developed deciduous vegetation community with higher evapotranspiration (ET) flux and reduced levels of moisture availability.

Results from our pilot study in the Yukon Flats reveal evidence that our methodology is capable of attaining desired observations. Even though parameters such as lake depth and permafrost abundance are not quantifiable using this method, we are confident that examining our other study regions will allow us to anticipate changes as a result of fire. Further analysis will include remaining study areas, and results will be presented during the NICOP.

## Acknowledgments

This project was funded through support from the Bonanza Creek LTER (Long-Term Ecological Research) program (funded jointly by NSF grant DEB-0423442 and USDA Forest Service, Pacific Northwest Research Station grant PNW01-JV11261952-231). The authors would like to thank the U.S. Fish & Wildlife service for their assistance in the acquisition of Landsat scenes, as well as the BLM and Alaska Fire Service for providing readily accessible fire history data.

## References

Burn, C.R. 1998. The response (1958–1997) of permafrost and near-surface ground temperatures to forest fire, Takhini River Valley, southern Yukon Territory. *Canadian Journal of Earth Sciences* 35(2): 184-189.

Ishikawa, M. 2008. Heat and water processes of burned and unburned active layer. Presented at the *IARC-JAXA Collaborative Research Plan,* University of Alaska Fairbanks, 28 February 2008.

Liljedahl, A., Hinzman, L., Busey, R. & Yoshikawa, K. 2007. Physical short-term changes after a tussock tundra fire, Seward Peninsula, Alaska. *Journal of Geophysical Research* 112*:* F02S07.

Riordan, B., Verbyla, D. & McGuire, A.D. 2006. Shrinking ponds in subarctic Alaska based on 1950–2002 remotely sensed images. *Journal of Geophysical Research* 111: G04002.

Yoshikawa, K., Bolton W.R., Romanovsky V.E., Fukuda, M. & Hinzman, L.D. 2002. Impacts of wildfire on the permafrost in the boreal forests of Interior Alaska. *Journal of Geophysical Research* 107: 8148.

# Cryological Status of Russian Soils: Cartographic Assessment

T.V. Ananko, D.E. Konyushkov, E.M. Naumov
*V.V. Dokuchaev Soil Science Institute, Russian Academy of Agricultural Sciences, Moscow, Russia*

Soil maps contain valuable information on the cryological conditions encoded in the names of soils and in knowledge of soil morphogenetic properties. In the new Russian soil classification system (Shishov et al. 2004), the presence and character of permafrost are not taken into account (except for an order of the cryoturbated nongley soils, *Cryozems*). A separate classification of soil cryological regimes is suggested (Sokolov et al. 2006). The following criteria are taken into account.

(I) The presence/absence of permafrost and seasonal freeze-thaw processes: (1) *seasonally thawing soils* (the depth of winter freezing exceeds the depth of summer thawing, the freezing layer merges with the permafrost table), (2) *seasonally freezing soils* (permafrost is absent or is below the depth of winter freezing), and (3) *nonfreezing soils* (cryogenic processes are absent).

(II) Duration of the thawed (group 1)/frozen (group 2) state of soils in the root zone (months): *long-term* (> 5), *medium-term* (3–5), *short-term* (1–3), and *very short-term* (< 1). The stability of soil freezing-thawing patterns in interannual cycles (stable, unstable, episodic) is considered as an additional criterion.

(III) The ice content in the transient layer of permafrost (group 1) or in the seasonally frozen soil layer (group 2): *ice-rich* (ice schlieren > 2 mm, the ice volume exceeds soil porosity in the thawed state); *medium-ice* (fine ice segregations, ice volume is approximately equal to soil porosity); *low-ice* (separate ice crystals; ice volume is less than soil porosity); and *dry frost* (no visible ice crystals; soil moisture after thawing is about maximum hygroscopy). For group 2, the ice content in the frozen state can be judged from the soil morphology and from the soil water content before freezing.

(IV) Depth of permafrost table (active layer thickness, seasonal thawing depth, cm) (group 1)/depth of seasonal freezing (group 2): *superficial* (< 25), *shallow* (25–50), *medium* (50–100), *medium deep* (100–150), *deep* (150–250), and *extremely deep* (> 250). The criterion of stability of the thawing/freezing depth may also be introduced (see II).

(V) The dynamics of phase transitions of soil water (freezing-thawing): *Arctic type* (in summer), *Boreal type* (in spring-early summer and in the late summer-fall), and *Subboreal type* (in winter). Additionally, the frequency of phase transitions in the root zone is to be taken into account.

A schematic pedocryological map of the FSU developed by us on a scale of 1:35 M (Fig. 1) contains information on the depth of soil seasonal thawing/freezing, mean annual temperature at the depth of zero seasonal temperature fluctuations, soil temperature characteristics at the depth of 20 cm, duration of the frozen state of soils, merging of permafrost table with the layer of seasonal freezing, the one-sided (from the top) or two-sided (from the top and from the bottom) character of soil freezing, etc. It is considered a part of the integral system of soil maps for the FSU (Ananko et al. 1998) developed for the cartographic assessment of the proper pedogenic, lithogenic, and regime (water and temperature) soil characteristics. The initial soil information was obtained from the *Soil Map of the Russian Federation* (1:2.5 M; 1988) and from the *State Soil Map* (1:1 M). In the presented variant, soil polygons are renamed according to the WRB system (2006) with due account for the earlier elaborated correlation tables (Goryachkin et al. 2002). Estimates of soil cryological characteristics are based on the *Geocryology of the USSR* (1988–1989), the monographs by Dimo (1972) and Romanovskii (1993), and numerous regional works. A fragment of the database to the map is shown in the table below; soil cryological characteristics for the polygons along meridian 120°E are included in it. The estimates are given for predominant soils. The real spatial and temporal variability of the cryological parameters within the polygons is much greater.

Information about cryogenic soil processes (cracking, ice-wedging, heaving, cryoturbation, dehydration, ice segregation, migration of solutes to freezing fronts, etc.) is included in a separate database. Their character and intensity depend on many factors—soil texture, water content, and freezing intensity being the most important.

Mean annual data reflected on the map were obtained from 1950–1980. Since the 1990s, a tendency for some warming of the climate (due to extremely warm winters or extremely warm summers) has been registered in many regions. Climate change results in a certain alteration of the soil cryological conditions (though its range is much less than the range of changes induced by anthropogenic impacts on soils and vegetation). Seasonally freezing soils beyond the permafrost zone become nonfreezing soils, and this phenomenon can be traced not only in the southern parts of European Russia but also in its northern regions (Mazhitova 2008).

In sharply continental regions with a shallow ice-rich and low-temperature permafrost, the buffer role of the latter in regulation of the soil temperature increases. At the same time, the upper layers of permafrost, being involved in seasonal freeze-thaw cycles, are subjected to degradation, which in enhanced by the development of thermokarst and thermal erosion in the case of ice-rich permafrost. A negative feedback in this system may occur due to the more active development of moss layers on the surface of waterlogged soils and a gradual increase in insulation properties of the moss and peat in the summer. In the areas of discontinuous permafrost, soils with a deep active layer merging with the permafrost table may lose their contact with permafrost. In general, the cryological response of soils to climate changes is as diverse and complicated as the diversity of different combinations of cryological parameters in the soil profiles.

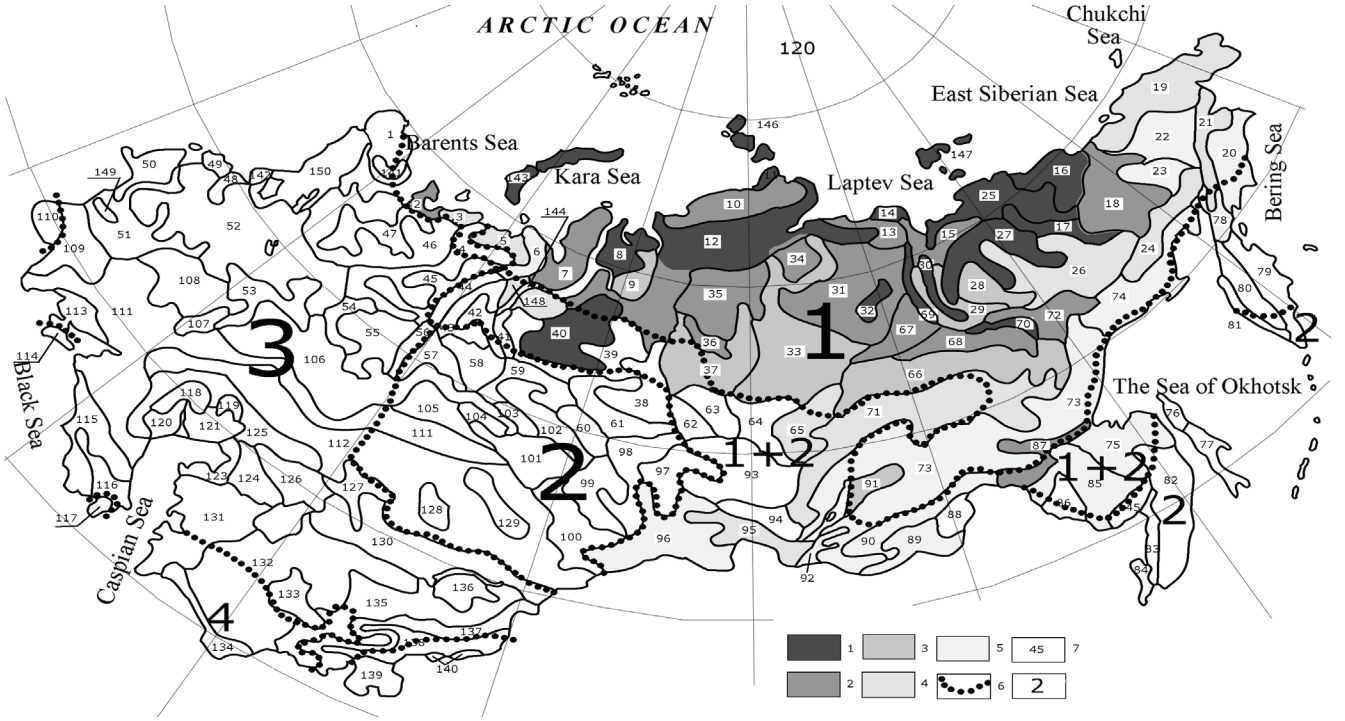


Figure 1. Cryological status of Russian soils. Thawing depths for permafrost-affected soils, cm: (1) < 50, (2) 50–100, (3) 100–150, (4) 150–200, (5) > 200; (6) boundaries of the zones of (**1**) seasonally thawing, (**1 + 2)** seasonally thawing and seasonally freezing, (**3)** seasonally freezing, and (**4**) nonfreezing soils; (7) soil polygon no. in the database; (8) pedocryological zones.

Note: Soil names are given according to the WRB (2006) codes. Soil texture (for predominant soil): S, sand; LS, loamy sand; L, loam; CL, clay loam; LC, loamy clay; Gr, gravelly; St, stony (bouldery). *Soil water content at the moment of freezing in the upper/lower parts of the profile: CR, capillary rupture; FC, field capacity; TC, total capacity; WP, wilting point. **FR, freezing regime: slow (↓) or fast (⇓) freezing from the top and slow (↕) or fast (⇕) freezing both from the top and from the bottom.

Table 1. Cryological parameters of soils along transect 120°E.

| Poly-gon | Dominant soils (WRB) | Texture | Temp. at the depth of $T_{ampl}$ = 0, °C | Annual $T_{ampl}$, °C | Water status* | FR** | Thawing depth, m | Freezing depth, m | Frozen state, months |
|---|---|---|---|---|---|---|---|---|---|
| 13 | CRoa,tu; CR | LS(Gr, St) | <-10 | 13-24 | FC/TC | ⇕↓ | 0.5-1.0 | — | 9-11 |
| 12 | CRgl,tu; CRtu; | L | -5 to -10 | 11-21 | FC/TC | ⇕ | <0.5(1.0) | — | 9-11 |
| 31 | CRoa,tu; | CL | -5 to -10/ -1 to-3 | 13-21 | FC-TC | ↓↕ | 0.5-1.0 | — | 9-11 |
| 32 | HI; GLhi | Peat | -5 to -10 | 13-17 | TC | ↓↕ | <0.5 | — | 9-11 |
| 67 | CRca; CMca,ge | CL | -1 to -3 | >24 | FC-CR/TC | ⇕ | 0.5-1.0 | — | 9-11 |
| 68 | CMlv,ge; CMca,ge | CL | -1 to -3 | >24 | FC-CR/FC | ⇕⇓ | 0.5-1.0 | — | 9-11 |
| 66 | CMeu,ge; CMdy,ge | CL, SL | -2 to -5 | 21->24 | CR-FC/FC | ⇕ | 1.0-2.0 | — | 9-11 |
| 71 | CMca; LPrz | CL,SL(Gr) | +2 to -2 | 13-24 | FC/FC | ⇓ | 1.5-2.5 | 1.5-2.5 | 7-9 |
| 73 | PZet; ARab; CRet,sd | LS(Gr, St) | -1 to -3 | 11-21 | FC/<FC | ↓↕ | 2.5-3.5 | 2.5-3.5 | 7-9 |
| 90 | CMdy | LS (Gr, St) | +2 to -2 | 21-24 | <FC/<FC | ⇓ | — | > 3.0 | 4-7 |
| 88 | PZha; PZet | LS (Gr, St) | +2 to -2 | 21-24 | <FC/<FC | ↓ | — | > 3.0 | >8 |
| 89 | PHha; CH; PHab; KS | CL, LS | +2 to -2 | 17-24 | FC-CR/FC | ↓ | — | > 3.0 | 5-8 |

## References


Ananko, T.E. et al. 1998. A system of soil maps: experience in application of a polycomponent basic soil classification for mapping purposes. *Eurasian Soil Sci.* 31(5): 561-573.

Dimo, V.N. 1972. *The Heat Regime of Soils in the USSR*. Moscow: Kolos, 360 pp. (in Russian).

Goryachkin, S. et. al. 2002. Northern circumpolar soil database and derived soil maps in different classification systems. *17 World Congress of Soil Science. 14–21 August 2002,* Bangkok, Thailand. Transactions. CD-ROM, Vol. II., p. 838-1-9.

Mazhitova, G.G. 2008. Soil temperature regimes in the discontinuous permafrost zone in the East European Russian Arctic. *Eurasian Soil Sci.* 41(1): 48-62.

Romanovskii, N.N. 1993. *Basics of Cryogenesis in the Lithosphere.* Moscow: Mosk. Gos. Univ., 334 pp. (in Russian).

Shishov, L.L. et al. 2004. *Classification and Diagnostic System of Russian Soils*. Smolensk: Oikumena, Russia, 342 pp. (in Russian).

Sokolov, I.A. et al. 2006. Soil cryogenesis. In: *Soil-Forming Processes,* Moscow: Dokuchaev Soil Sci. Inst., 144-166 (in Russian).

# Acoustical Surveys of Methane Plumes Using the Quantitative Echo Sounder in the Japan Sea

Chiharu Aoyama
*Japan's Independent Institute Co., Ltd., Japan*
Ryo Matsumoto
*University of Tokyo, Japan*
Mineo Hiromatsu
*Chiba University, Japan*
Glen Snyder
*Rice University, USA*

## Introduction

Now methane hydrate is spotlighted as a next-generation energy resource to replace oil and natural gas. It is estimated that the methane hydrate deposits around Japan, a nation otherwise poor in energy resources, would be enough to last over 100 years, based on present levels of natural gas consumption (Matsumoto 1997, Sato 2001).

Many echo sounders have been effectively used for fisheries and surveys (McLennan & Simmons 1992). Echo sounders are classified into three types: depth measurement, including the detection of the sediments under sea floor; fisheries echo sounders; and quantitative echo sounders (Urick 1967). Figure 1 shows an echogram of a depth sounder. The horizontal line on the center part of this figure shows a sea floor. This echogram looks like no acoustic data under the water. On the other hand, Figure 2 shows an echogram of a fisheries echo sounder. This "candle-flame" phenomenon is likely due to density differences originated either by gas bubbles, abrupt water temperature anomalies, or the nucleation of gas hydrate crystals in the water column. Accordingly, we used a quantitative echo sounder on acoustical surveys of methane hydrate.

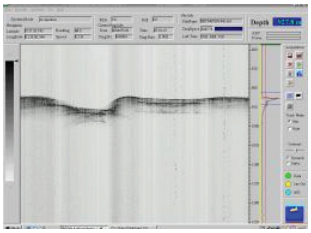

Figure 1. An echogram of a display of a depth sounder. It showed only a sea floor line.

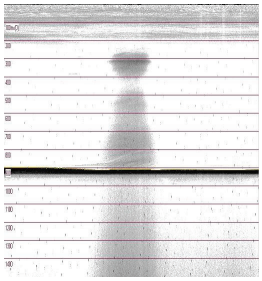

Figure 2. An echogram of a display of a fish echo sounder. It showed a sea floor line and a water column.

*Echo sounder's principle*

Acoustical observations were made using the quantitative echo sounder. The basic components of its hardware function are to transmit sound, receive, filter and amplify, record, and analyze the echoes. Fisheries hydro-acoustics uses sonar to detect fish.

## Experimental Method

Figure 3 shows a schematic diagram of the quantitative echo sounder. As the sound pulse travels through water, it encounters objects that are of different density than the surrounding medium, such as fish that reflect sound back toward the sound source (Jitsuyoshi et al. 1990, Aoyama & Hamada 1997).

To change the ejection amount of methane hydrate bubbles, at the methane hydrate seep point, bubbles were captured with the funnel, whose volume is about 2000 ml (Aoyama et al. 2007), and the MT bottom sampler (inner diameter, 110 mm; length, 285 mm), fixed at the two manipulators of the vehicle that is called Hyper Dolphin (Fig. 3). With bubbles in the funnel and the MT bottom sampler, Hyper Dolphin was moved to 750 m depth underneath *Natsushima*, and then the funnel was turned upside down to release the methane hydrate bubbles from it. The MT bottom sampler was turned upside down to release the methane hydrate bubbles (second ejection). The upwelling of methane hydrate bubbles were observed with the quantitative echo sounder (transducer frequency, 38 kHz) to obtain acoustic data.

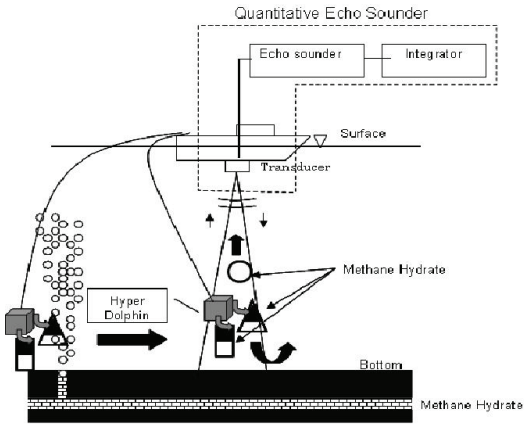


Figure 3. Schematic diagram of the method of the calibration.

Next, to change the depth for bubble release, bubbles were captured with the MT bottom sampler at the methane hydrate bubbles seep point, and Hyper Dolphin was moved to 400 m depth underneath *Natsushima*; then the methane hydrate bubbles were released. The upwelling of methane hydrate bubbles were observed with the quantitative echo sounder (transducer frequency, 38 kHz and 120 kHz) to obtain acoustic data.

## Results

Figure 4 shows the echogram of the calibration experiment. The vertical axis represents depth. The grid lines were added at 250 m intervals. The seabed is at 930 m depth. The horizontal axis represents time; the right region shows the later state. The grid lines were added at 4-min intervals. The trapezoidal line that is in the center-left region of the figure represents the cruise line of Hyper Dolphin. It is obvious that Hyper Dolphin moved again from 750 m depth to 930 m depth. The two diagonal bands in the center region of the figure represent the reflection from released methane hydrates. These two "bands" are parallel, and so it can be understood that the bubbles ascend on the straight toward the ship at constant speed, without depending on the amount of methane hydrates. The left one shows the image of the reflection from the methane hydrates released from the funnel (whose volume is about 1000 ml). The right region shows the reflection from the methane hydrates ejected from the MT bottom sampler (whose volume is about 500 ml). This indicates that as the bubbles ascend, they diffuse while weakening its reflection.

With this, it is possible to study the previously obtained acoustic data of the methane hydrate plume in the past three years, and grasp the approximate state of the real methane hydrate plume.

In addition, the data is obtained with two kinds of transducers of 38 kHz and 120 kHz, concurrently, and then frequency characteristics are calculated.

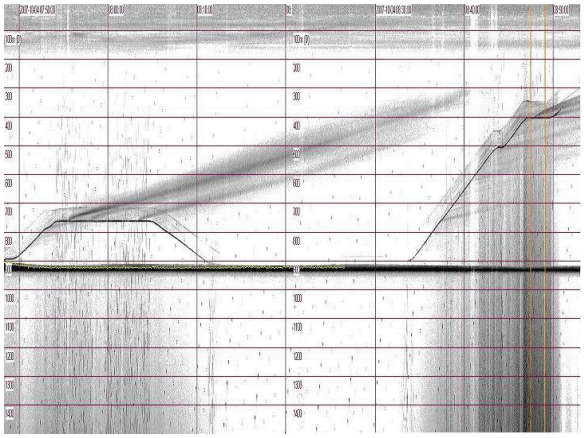

Figure 4. An echogram of the quantitative echo sounder

## Acknowledgments

We would like to thank the many crew members of *Umitaka-maru* and *Natsushima* for their help with the surveys.

## References

Aoyama, C. & Hamada, E. 1999. *Cruise Report of Tokyo Univ. of Fisheries*, May.

Aoyama, C., Matsumoto, R. Okuda, Y. et al. 2004. Acoustical surveys of methane plumes using the quantitative echo sounder in the eastern margin of the Sea of Japan. *2004 Fall Meeting, American Geophysical Union, San Francisco, California.*

Aoyama, C., Matsumoto, R. et al. 2007. Acoustical surveys using a multi narrow beam sonar and a quantitative echo sounder in gas hydrate area off Joetsu, Japan Sea. *Shinkai Symposium, May 2007*.

Jitsuyoshi, J. et al. 1990. *Acoustical Technical Handbook.* Tokyo: Japan Industry News, 18-19.

Matsumoto, R. 1997. Perspective of methane hydrate science. *Japan Energy Soc.* 76(5): 354-361.

McLennan, D.N. & Simmonds, E.J. 1992. *Fisheries Acoustics*. London: Chapman & Hall.

Sato, M. 2001. Distribution, amount of methane and resources of natural gas hydrates in the world and around Japan. *Aquabiology* 23(5): 460-464.

Urick, R.J. 1967. *Principles of Underwater Sound*. McGraw-Hill, 7-8.

# Permafrost Delineation Near Fairbanks, Alaska, Using Geophysical Techniques

Beth N. Astley, Allan J. Delaney
*Cold Regions Research and Engineering Laboratory, Fairbanks Alaska*

## Introduction

Surface geophysical methods can be used to accurately and rapidly map permafrost extent over limited areas and to measure changes in permafrost extent and thickness through time. We investigated discontinuous permafrost sites near Fairbanks, Alaska, using electrical resistivity tomography (ERT), ground-penetrating radar (GPR), and electromagnetic induction (EMI). Discontinuous permafrost in this region is present to depths as great as 60 m, and the active layer ranges from <1 to 3 m.

Between 2004 and 2007, three sites containing discontinuous permafrost were investigated: Fort Wainwright at the base of Birch Hill, Eielson Air Force Base near Mullins Pit, and the CRREL Permafrost Research Site at Farmers Loop Road (Fig. 1). The objectives were to determine permafrost extent and to test the ERT technique compared to more traditional techniques including GPR, EMI (using an EM-31), soil probe, and borehole data.

All three study locations contain relatively flat topography. The Birch Hill and Eielson sites are located on alluvial outwash sands and gravels that contain abandoned river channels. The Farmers Loop Research Site contains approximately 20 m of loess overlying gravels (Linell 1973a). Bedrock at all of these sites is below the depth of investigation. All three sites contain a combination of undisturbed areas and cleared areas.

## Methods

Electrical resistivity has been used to define alpine permafrost (Hauck et al. 2003, Hauck & Kneisel 2006), and northern latitude permafrost (Osterkamp et al. 1980, Gilmore et al. 1995, Fortier et al. 1993). At temperatures less than 0°C, resistivity increases exponentially as ground temperature decreases, making it possible to interpret frozen boundaries. Generally, apparent resistivity values above 2000 Ω-m are considered permafrost in alluvial gravels in this region (Astley & Snyder 2005); however permafrost near 0°C in low-moisture silt can have significantly lower values, and apparent resistivity of clean, frozen alluvial gravels has been measured as high as 18,000 Ω-m.

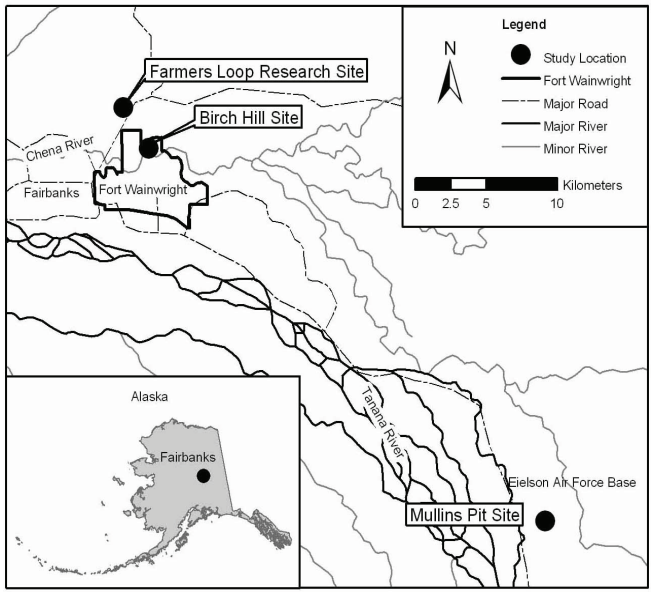


Figure 1. Study site locations near Fairbanks, Alaska.

ERT data were collected with an AGI Supersting R8/IP multi-channel switch resistivity meter and passive cables using Wenner and Dipole-Dipole arrays. Resistivity data were processed using Res2dinv (by Geomoto), a 2-dimensional resistivity inversion program. The inversion process uses forward modeling to produce a best-fit model to the apparent resistivity data (Loke & Barker 1996).

GPR has previously been used to characterize permafrost (Arcone et al. 1998, Lawson et al. 1998, Hinkel et al. 2001). GPR data were collected using GSSI 100- and 400-MHz antennas at the Mullins Pit Site and 50-MHz antennas at the Birch Hill Site. GPR was not attempted at the Farmers Loop Site due to expected signal attenuation in the thick silt there.

EMI methods have been used to map near-surface (<6m) permafrost for decades (Hoekstra & McNeill 1973, Arcone et al. 1979). The advantage to the EM-31 is a relatively fast survey speed compared to other methods. EM-31 data were only collected at the Birch Hill site.

## Results

*Birch Hill, Fort Wainwright*

At the Birch Hill site, a disturbed area appears thawed to depths of 4–19 m. Adjacent, undisturbed areas contain permafrost within 1 m of the surface greater than 30 m thick according to ERT models. We compared the ERT models to EM-31 results and found high correlation for near-surface (<1.5 m) frozen ground. GPR (50-MHz) detected the top of permafrost consistently, but bottom of permafrost was only detected in a few profile segments at depths of 15 to 20 m.

*Mullins Pit, Eielson Air Force Base*

At the Mullins Pit site, we combined ERT with GPR and frost probing. The 400-MHz GPR detected the active layer depth and thaw zones and the 100-MHz detected thaw zones and the bottom of permafrost. A power line clearing that bisects the study area was found to be significantly thawed, with sporadic permafrost based on the ERT and GPR results.

Table 1. Depth to top and bottom of permafrost at three study locations near Fairbanks, Alaska based on ERT, GPR, EMI, soil probing, and borehole data.

| Site | Top (m) | Bottom (m) |
|---|---|---|
| Birch Hill | | |
| Undisturbed | <1 | 17– >30 |
| Cleared | 4–9 | 20–28 or NE |
| Mullins Pit | | |
| Undisturbed | <1 | 18–22 |
| Cleared | 5–10 or NE | 10–17 or NE |
| Farmers Loop Sections | | |
| A. Undisturbed | <1 | |
| B. Trees removed | <1–7 | |
| C. Cleared | 10 | |

NE = not encountered

*Farmers Loop research site*

ERT data were collected from two research plots that were created in 1946 by the U.S. Army Corps of Engineers to study the effects of vegetation cover and climate variability on permafrost (Linell 1973b). Section C (cleared plot) appeared thawed to 10 m, while Section B (trees were removed but not the moss layer) had varying depths of 1 to 7 m to permafrost (Table 1). The top of permafrost was detected within Section A (undisturbed) by probing.

## Conclusion

Permafrost has thawed to depths as great as 9 m or more at Birch Hill, 10 m or more at Mullins Pit, and 10 m at the Farmers Loops site, where land was cleared and graded over 50 years ago and has remained clear of trees since that time.

The ERT technique was the most accurate compared to boreholes in areas where the permafrost boundaries were continuous and horizontal. Areas with sporadic permafrost containing thin (<1 m thick) frozen layers were not always apparent in the ERT model results. The dipole-dipole inversions were the most accurate for detecting shallow permafrost, while the Wenner inversions were most useful for deep permafrost. GPR interpretations of the top of permafrost matched the ERT data to within 0.5 m; however, the interpretations of the bottom of permafrost depth varied between the two methods. ERT data correlated with EMI data for detecting permafrost within 1 m of the surface. Soil probing and EMI are efficient methods for determining the presence of shallow permafrost (<1 m), while ERT and GPR are more useful for detecting deeper permafrost boundaries. For permafrost delineation, the capabilities and limitations of each geophysical technique should be considered in order to select the best methods for a particular location.

## References


Arcone, S.A., Delaney, A.J. & Sellmann, P.V. 1979. Effects of seasonal changes in ground ice on electromagnetic surveys of permafrost. *CRREL Report* 79-23.

Arcone, S.A., Lawson, D.E., Delaney, A.J., Strasser, J.C. & Strasser, J.D. 1998. Ground-penetrating radar reflection profiling of groundwater and bedrock in an area of discontinuous permafrost. *Geophysics* 63(5): 1573-1584.

Astley, B.N. & Snyder, C. 2005. Operable Unit 3 permafrost resistivity investigation, Fort Wainwright, Alaska, *CRREL Letter Report* 05-10.

Gilmore, T.J. & Clayton, E.A. 1995. Mapping the top of the permafrost using surface direct current resistivity survey. *Environmental Geology* 30(1/2): 29-33.

Fortier, R., Allard, M. & Seguin, M.K. 1994. Effect of physical properties of frozen ground on electrical resistivity logging. *Cold Regions Science and Technology* 22: 361-384.

Hauck, C., Mühll, D.V. & Maurer, H. 2003. Using DC resistivity tomography to detect and characterize mountain permafrost. *Geophysical Prospecting* 51(4): 273-284.

Hauck, C. & Kneisel, C. 2006. Application of capacitively-coupled and DC electrical resistivity imaging for mountain permafrost studies. *Permafrost and Periglacial Processes* 17: 169-177.

Hinkel, K.M., Doolittle, J.A., Bockheim, J.G., Nelson, F.E., Paetzoid, R., Kimble, J.M. & Travis, R. 2001. Detection of subsurface permafrost features with ground-penetrating radar, Barrow, Alaska. *Permafrost and Periglacial Processes* 12(2): 179-190.

Hoekstra, P. & McNeill, J.D. 1973. Electomagnetic probing of permafrost. *Proceedings of the Second International Conference on Permafrost, Yakutsk, USSR, 1973*: 517-526.

Lawson, D.E., Arcone, S.A, Delaney, A.J., Strasser, J.D., Strasser, J.C., Williams, C.R & Hall, T.J. 1998. Geological and geophysical investigations of the hydrogeology of Fort Wainwright, Alaska. Part II: North-central cantonment. *CRREL Report* 98-6.

Linell, K.A. 1973a. Risk of uncontrolled flow from wells through permafrost. *Permafrost: North American Contributions Second International Conference, Yakutsk, USSR, July 1973*. National Academy of Sciences, 462-468.

Linell, K.A. 1973b. Long-term effects of vegetative cover on permafrost stability in an area of discontinuous permafrost. *Permafrost: North American Contributions Second International Conference, Yakutsk, USSR, July 1973*. National Academy of Sciences, 688-693.

Loke, M.H. & Barker, R.D. 1996. Rapid least-squares inversion of apparent resistivity pseudosections by a quasi-Newton method. *Geophysical Prospecting* 44(1): 131-152.

Osterkamp, T.E., Jurick, R.W., Gislason, G.A., & Akasofu, S.I. 1980. Electrical resistivity measurements in permafrost terrain at the Engineer Creek road cut, Fairbanks, Alaska. *Cold Regions Science and Technology* 3: 277-286.

# Preparatory Work for a Permanent Geoelectrical Measurement Station for Permafrost Monitoring at the Hoher Sonnblick, Austria

Michael Avian
*Institute of Remote Sensing and Photogrammetry, Graz University of Technology, Austria*
Andreas Kellerer-Pirklbauer
*Institute of Geography and Regional Science, University of Graz, Austria*
Alexander Römer
*Department of Geophysics, Geological Survey of Austria*
Robert Supper
*Department of Geophysics, Geological Survey of Austria*

## Introduction

The thermal and distributional state of permafrost in alpine environments is widely discussed in recent times due to hazardous geomorphic events threatening infrastructure, tourism, or residents. Subterrain processes in environments influenced by permafrost degradation might cause severe problems to alpine infrastructure (e.g., alpine huts, cable-cars). However, such processes are not fully understood so far.

The meteorological observatory at the top of the Hoher Sonnblick (3106 m a.s.l., 47°03′N, 12°57′E, Fig.1) has faced problems of permafrost degradation since the 1990s, leading to intense protection activities during the last years. This observatory has been operating continuously since 1886, presenting one of the longest records of meteorological data in the entire alpine arc. Data from this observatory indicate a rise of the mean annual air temperature (MAAT) by 1.6°C since 1886 (Auer et al. 2002), which is substantially above the global average of 0.74°C (IPCC 2007). The summit area of Hoher Sonnblick is stage of several investigations that focus on the relationship between recent climate change and alterations of a mountain permafrost body in a mountain top detritus environment. One of the most important projects investigates the thermal state of the uppermost 20 m of the summit area monitored at three boreholes—each equipped with 25 temperature sensors—aligned along a south-facing slope (Fig. 2). These three boreholes are the first permafrost boreholes installed within Austria and will therefore deliver important temperature data relevant for the mountain permafrost distribution of the Eastern Alps. However, no temperature data are published so far (Staudinger & Schöner 2008, pers. com.).

In order to get more information about the spatial distribution and temporal changes of the subsurface temperature conditions within shorter periods at Hoher Sonnblick, the installation of a permanent geoelectrical measurement profile is currently carried out. Logistical and technical information regarding the relevant preparatory work is presented here.

## Methods

Geoelectrical investigations of areas underlain by permafrost have been carried out at numerous study areas in the Alps (e.g., Hauck et al. 2003, Kneisel 2004). Hilbich et al. (2008) report from repeated electrical resistivity tomography (ERT) measurements coupled with borehole temperature data at Schilthorn (Switzerland), thereby focusing on active layer dynamics. The application of ERT allows the determination of specific electrical resistivity within the subsurface structure. This parameter is mainly dependent on porosity, water saturation, conductivity of pore fluid and clay content. Minor influence is given by particle shape and pore geometry.

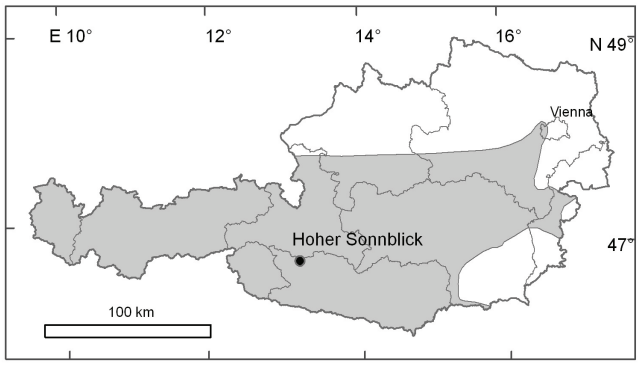


Figure 1. Location of the study area Hoher Sonnblick within Austria, as well as the Austrian part of the European Alps (grey).

Two measurements have been carried out manually so far (August 2006 and March 2007) but are planned to be remote controlled in the next project stage. So this test stage verifies the capability of the GEOMON4D for remote-controlled measurements of geoelectric pseudo-sections. Several requirements have to be considered: high-resolution measurements, possibility of snapshots of the underground, high reliability, and quick availability of data.

## Preparatory Work and Outlook

The first ERT measurements, consisting of 16 electrodes at a spacing of 1 m, were carried out in August 2006 with a Sting RI (AGI) multi-electrode and the GEOMON4D system for comparison. Within the second campaign in March 2007, a permanent profile with 41 electrodes at 0.5 m spacing and 20 m length was installed near the profile of the first campaign. Three thousand measurements were carried out, each sampled for 1000 times. Furthermore, a lightning

protection system was developed in winter 2007/08 to consider the special location on this mountain top.

The ERT profiles were measured with different electrode configurations (Wenner/Schlumberger, Gradient). The results of the inversion for both periods are shown in Figure 3.

Figure 3 indicates an increase of electrical resistivity during winter time. In the measurements of March 2007, high electrical resistivities—representing bedrock or frozen ground—occur in shallow depths in comparison to the measurements of August 2006 (from 1.5–2 m). The overlying structure is characterized by a heterogeneous distribution of resistivity anomalies, ranging from a few hundred up to some thousands of Ohmm. This is addressed as the fragmented/broken rock with some silt fillings, and represents the active layer in such permafrost regions. Therefore, a change of the permafrost table can be interpreted of 1.5 m in 2006 and 0.5 m in 2007 (Fig. 3).

The accomplished test measurements for the installation of a permanent ERT station at the top of Hoher Sonnblick show that observed changes in resistivity allow a monitoring of seasonal changes of the thaw and freeze processes in the active layer. This should lead—in combination with other monitoring techniques—to a better understanding of the processes in the mountaintop detritus of Hoher Sonnblick. After field tests, the permafrost monitoring system will be installed at Hoher Sonnblick in May 2008. The system should then operate completely automatically and can be remote controlled from the Geological Survey of Austria in Vienna.

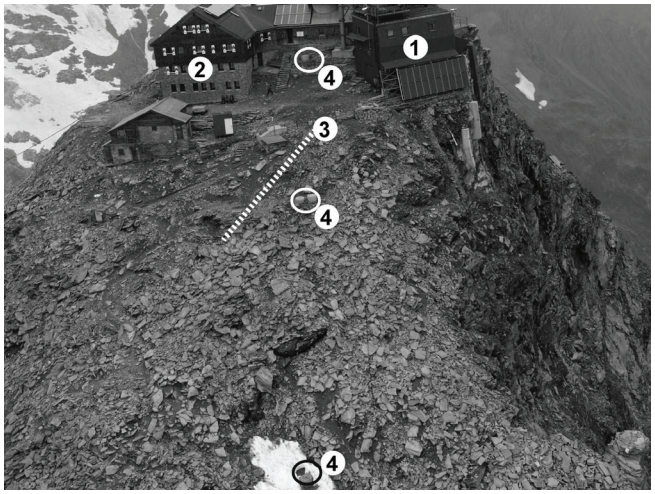


Figure 2. Location of the meteorological observatory (1), alpine hut (2), geoelectric profile (3), and the three boreholes (4). View towards the north. (Photograph kindly provided by M. Staudinger.)

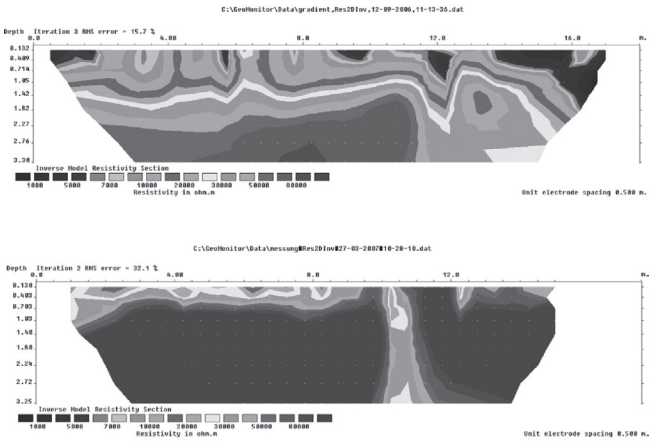


Figure 3. Electrical resistivity tomography (ERT) results from August 2006 and March 2007.

## Acknowledgments

These activities were carried out mainly within the framework of the project ALPCHANGE (www.alpchange.at) funded by the Austrian Science Fund (FWF) through project no. FWF P18304-N10.

## References

Auer, I., Böhm, R., Leymüller, M. & Schöner, W. 2002. Das Klima des Sonnblicks – Klimaatlas and Klimageographie der GAW-Station Sonnblick einschließlich der umgebenden Gebirgsregion. Österreichische Beiträge zur Meteorologie und Geophysik 28: 305 pp.

Hauck, C., Von der Mühll, D. & Maurer, H. 2003. Using DC resistivity tomography to detect and characterize mountain permafrost. *Geophys. Prospect.* 51: 273-284, doi:10.1046/j.1365-2478.2003.00375.x.

Hilbich, C., Hauck, C., Hoelzle, M., Scherler, L., Schudel, L., Völksch, I., Von der, Mühll, D. & Mäusbacher, R. 2008. Monitoring mountain permafrost evolution using electrical resistivity tomography: A 7-year study of seasonal, annual, and long-term variations at Schilthorn, Swiss Alps. *J. Geophys. Res.* 113: F01S90, doi:10.1029/2007JF000799.

IPCC. 2007. *Climate Change 2007: The Physical Science Basis*. Contribution of Working Group I to the Fourth Assessment Report of the Intergovernmental Panel on Climate Change, S. Solomon, D. Qin, M. Manning, Z. Chen, M. Marquis, K.B. Averyt, M. Tignor & H.L. Miller (eds.). Cambridge, U.K. & New York, NY, USA: Cambridge University Press.

# A Provisional Soil Map of the Transantarctic Mountains, Antarctica

Megan R. Balks
*Earth and Ocean Sciences, University of Waikato, Private Bag 3105, Hamilton, New Zealand*
Malcolm McLeod
*Landcare Research, Private Bag 3172, Hamilton, New Zealand*
James G. Bockheim
*Department of Soil Sciences, University of Wisconsin, 1525 Observatory Drive, Madison, WI 53706-1299, USA*

## Introduction

A provisional soil map has been prepared for the Transantarctic Mountain region of Antarctica in three wall-size (A0) sheets, each at a scale of 1:1,000,000. The maps contribute to the ANTPAS (Antarctic Permafrost and Soils) effort to develop a soil map of the Antarctic continent and pdf files of the maps will be made available on the ANTPAS website http://erth.waikato.ac.nz/antpas/.

The Transantarctic Mountains extend 3500 km across the Antarctic continent from 69°S in northern Victoria Land to 87°S in the upper Scott Glacier region. The Transantarctic Mountain region has an ice-free area of 21,000 km$^2$, which constitutes 42% of the total ice-free area (49,500 km$^2$) of Antarctica. The climate ranges from ultraxerous, with temperatures rarely exceeding 0°C, on the inland margins of the Transantarctic Mountains, to subxerous, with temperatures greater than 0°C for several weeks in summer and liquid water present for short periods, on coastal margins (Campbell & Claridge 1987). Soil parent materials are predominantly glacial tills with mixed lithologies, mainly dominated by sandstones, granites, and dolerites. Altitude ranges from sea level to peaks of over 2500 m with many steep valley sides. Topography has a strong influence on local microclimates. Soil surfaces range from Holocene to Pliocene in age. Over much of the area the influence of organisms on soil development is limited to microbial life. In warmer, moister, coastal sites small areas with extensive moss coverage occur and penguins have an impact on soil development, providing guano-rich soils, in small areas of nesting colonies.

While the general pattern and properties of Antarctic soils are well known (e.g., Tedrow & Ugolini 1966, Campbell & Claridge 1987, Bockheim 2002), little attention was paid to mapping the spatial distribution of Antarctic soils until recently, when soil maps of the Wright Valley (McLeod et al. 2008, this proceedings), the McMurdo Dry Valleys (Bockheim & Mcleod 2008), and the Seabee Hook (Hofstee et al. 2006) have been published. This paper is a "partner" to Bockheim et al. (2008, this proceedings), which describes permafrost maps of the Transantarctic Mountains.

## Methods

The soil maps have been compiled from existing data, including published data and data archived by the National Snow & Ice Data Center (http://nsidc.org/cgi-bin/get_metadata.Pl?id-ggd221) and New Zealand Landcare Research (http://www.landcareresearch.co.nz). Scanned and geo-rectified 1:250,000 topographic maps prepared by the U.S. Geological Survey (http://usarc.usgs.gov) were joined in ArcGIS 9.2 and used as a base map. Aerial photograph and topographic map interpretation were used to extrapolate to areas where field data are limited. Because some parts of the region are more readily accessible, with more data available than others, a "confidence" rating was applied to each map unit as described in McLeod et al. (2007). Recent fieldwork was undertaken by the authors in the Darwin Glacier, Wright Valley, and Cape Hallet areas to add to existing data and corroborate our data, topographic map, and photo, interpretations.

Table 1 Provisional physiographic legend.*

| |
|---|
| **Soils of the subxerous coastal regions** |
| *Formed on patterned ground* |
| Typic Haploturbels + Typic Haplorthels |
| *Formed on ice-core drift* |
| Glacic Haploturbels + Glacic Haplorthels |
| *Formed within penguin colonies* |
| Ornithic Haplorthels |
| *Formed on nunataks or rock outcrops* |
| Lithic Haploturbels + Lithic Haplorthels |
| *Formed in areas with patterned ground and rock outcrops* |
| Lithic Haploturbels + Orthic Haploturbels + Lithic Haplorthels + Typic Haplorthels |
| **Soils of the xerous and ultraxerous inland areas** |
| *Formed in areas with dry permafrost to > 70 cm depth and no patterned ground* |
| Typic Anhyorthels |
| *Formed on patterned ground with dry-permafrost to > 70 cm depth* |
| Typic Anhyorthels + Typic Anhyturbels |
| *Formed on patterned ground with ice-cement or seasonally moist soil at < 70 cm depth* |
| Typic Haploturbels + Typic Haplorthels |
| *Formed on patterned ground with ice-cement or seasonally moist soil at < 70 cm depth and rock outcrops* |
| Typic Haploturbels + Typic Haplorthels + Lithic Haploturbels + Lithic Haplorthels |
| *Formed on ice cored drift with dry-permafrost to > 70 cm depth* |
| Glacic Anhyturbels + Glacic Anhyorthels |
| *Formed on nunataks or rock outcrops including areas with dry permafrost to >70 cm depth* |
| Lithic Anhyorthels + Typic Anhyorthels |

* + denotes a soil association.

## Soil Map Units

*Soil classification*

The soils were mapped to the Subgroup level following USDA Soil Taxonomy (Soil Survey Staff 2006). All of the soils key out within the Gelisol Soil Order. Typic Haplorthels, Typic Haploturbels, and Typic Anhyorthels predominate with Lithic, Salic, and Ornithic subgroups also recognised. The Ornithic subgroup has been included to informally distinguish guano-rich soils in penguin colonies.

*Soil associations*

At the small scale of this map, it is impossible to show all the detail of the soil landscape pattern. Where the pattern is predictable from interpretation of the surface topography, soil associations are mapped. The most common soil association occurs where there is patterned ground with Typic Haplorthels in the centre of the polygons and Typic Haploturbels in the strongly cryoturbated polygon margins. In areas where nunataks or rock outcrops occur, a soil association between Lithic and Typic Subgroups is recognised.

*Map legend*

The provisional physiographic legend (Table 1) provides a guide to the soils in relation to their landscape position.

Within the ultraxerous climate region of the dry valleys, seasonally moist soils (Haploturbels and Haplorthels) occur on lake margins and adjacent to ephemeral streams fed from glacial meltwaters. While calcic, salic, nitric, petrosalic, and petronitric soil Subgroups are described in the region they are not recognised on the small scale of these maps.

## Concluding Statement

The maps presented here are an overview of the soils in the Transantarctic Mountains, and are intended to complement similar maps to be prepared by other ANTPAS workers to contribute to a soil map of the Antarctic continent. Work remains to develop a more detailed understanding of the diversity and distribution of Antarctic soils at larger scales (1:50,000 or larger). With over 30,000 tourists predicted to visit Antarctica in the 2008–2009 summer (*www.iaato.org*), one immediate application for a more detailed soil mapping effort is for identification and interpretation of the vulnerability of Antarctic soils to the effects of human activities. Detailed soil maps will also provide a benchmark against which effects of global change can be measured in the future.

## Acknowledgments

The Landcare Research database contains the pioneering Antarctic soil work of Iain Campbell and Graeme Claridge. Thanks to Antarctica New Zealand for Logistic support.

## References

Bockheim, J.G. 2002. Landform and soil development in the McMurdo Dry Valleys: A regional synthesis. *Arctic, Antarctic and Alpine Research* 34: 308-317.

Bockheim, J.G. & McLeod, M. 2008. Soil distribution in the McMurdo Dry Valleys, Antarctica. *Geoderma* 144: 43-49.

Bockheim, J.G., McLeod, M. & Balks M.R. 2008. A provisional permafrost map of the Transantarctic Mountains. *Proceeding of the Ninth International Conference on Permafrost, Fairbanks, Alaska, 29 June–3 July 2008*.

Campbell, I.B. & Claridge, G.G. C. 1987. *Antarctica, Soils, Weathering Processes and Environment. Developments in Soil Science 16.* Amsterdam: Elsevier, 368 pp.

Hofstee, E.H., Balks, M.R., Petchey, F. & Campbell, D.I. 2006. Soils of Seabee Hook, Cape Hallett, Antarctica. *Antarctic Science* 18: 473-486.

McLeod, M., Bockheim, J.G. & Balks, M.R. 2007. A fifth-order reconnaissance map of ice-free ares of the Transantarctic Mountains, Antarctica. *Proceedings of the 10th symposium on Antarctic Earth Sciences. U.S. Geological Survey and the National Academies; USGS F-2007-1047,* Extended Abstract 116.

McLeod, M., Bockheim, J.G. & Balks, M.R. 2008. Soil map of the Wright Valley, Antarctica. *Proceedings of the Ninth International Conference on Permafrost. Fairbanks, Alaska, 29 June–3 July 2008.*

Soil Survey Staff. 2006. *Keys to Soil Taxonomy*, 10th ed. U.S. Department of Agriculture, Natural Resources Conservation Service, 332 pp.

Tedrow, J.C.F. & Ugolini, F.C. 1966. Antarctic soils. In: J.F.C. Tedrow (ed.), *Antarctic Soils and Soil Forming Processes.* Antarctic Research Series. American Geophysical Union, Washington, DC, 8: 161-177.

# Martian Permafrost Depths from Orbital Neutron and Temperature Measurements

Joshua L. Bandfield
*Department of Earth and Space Sciences, University of Washington, Seattle*
William C. Feldman
*Planetary Science Institute, Tucson, Arizona*

## Introduction

The high abundance of hydrogen detected by the Mars Odyssey Neutron Spectrometer (MONS) and High Energy Neutron Detector measurements (e.g., Feldman et al. 2007, Mitrofanov et al. 2004) are consistent with a high concentration of water ice in the shallow subsurface on Mars. Martian high latitudes also have thermal properties consistent with an extensive high thermal inertia layer within a few centimeters of the surface. These results are in agreement with models of theoretical water-ice stability (e.g., Leighton & Murray 1966).

The purpose of this abstract is to show global and local thermally-derived permafrost depths and compare these results with neutron-derived water ice depths. We use the term "permafrost" to describe a buried high inertia surface detected using temperature measurements and "water ice" to describe the high latitude hydrogen concentrations detected using neutron measurements. Both models assume a relatively simple two-layered geometry of relatively dry soil cover on top of a semi-infinite water-rich layer that is assumed constant throughout the measurement field of view. More complicated systems are likely to be common on Mars, but the datasets do not have the leverage to converge on unique solutions with complex geometries.

## Methods and Data

This study utilizes the surface kinetic temperature derived from the Mars Global Surveyor Thermal Emission Spectrometer (TES) and Mars Odyssey Thermal Emission Imaging System (THEMIS). TES data were averaged in bins of 2° latitude, 4° longitude and 4.5° $L_s$ (1/80 year) to construct seasonal surface temperature profiles. THEMIS 100 m/pixel temperature images were acquired over a surface at two seasons to estimate the seasonal cooling rate. We use a thermal model (developed and provided by H.H. Kieffer) to predict surface temperatures. This model allows for customization of a wide variety of parameters such as changes in subsurface thermophysical properties and atmospheric aerosol properties.

The TES- and THEMIS-derived surface temperatures are fit using a non-linear least squares fitting routine. All modeling parameters were fixed except surface cover thermal inertia and depth of the permafrost layer. The seasons used for fitting were restricted to summer and early fall seasons. The model permafrost layer has fixed thermophysical properties, but was allowed to vary from 1.15 to 20.3 diurnal skin depths. As a result, the model and fitting routine is sensitive to permafrost at 0.3–6 and 12–220 cm depths for dusty and rocky surface covers, respectively. Water ice and solid rock have similar thermal inertias (primarily because of offsetting heat capacity and density values), and it is not possible to determine the concentration of water in the permafrost layer from the temperature data. Methods and uncertainties are discussed in detail in Bandfield & Feldman (in press).

The thermal and epithermal neutron currents derived from MONS are translated into the water equivalent hydrogen (WEH) abundance of a semi-infinite buried layer of soil. The top layer has the same composition as that of the bottom layer, but restricted to a WEH abundance of 1 wt. % (e.g., Feldman et al. 2007). The burial depth of the bottom layer is also determined from this model.

## Results and Discussion

A qualitative comparison of Neutron Spectrometer hydrogen and TES permafrost depths displays remarkable agreement, considering the fundamental difference in the measurements (Fig. 1). In the Northern Hemisphere, water ice and permafrost depths are greater within lower latitude, higher surface cover thermal inertia, and low albedo regions. This shows that the water ice depth is generally following its predicted stability, as all three of these properties generally increase the depth of water ice stability. At higher latitudes, all surfaces are characterized by shallow water ice/permafrost depths.

In the Southern Hemisphere, water ice/permafrost depths are shallow at latitudes poleward of ~65°S. A relatively steep increase in depths appears between 60–65°S that, as in the North, coincides with an increase in surface cover thermal inertia and a decrease in latitude and albedo. This is relatively constant with longitude except between ~50–140°E, near the southern rim of Hellas Basin. In these regions, the surface cover thermal inertia remains low and the albedo is relatively high, which allows for water ice to remain stable at relatively shallow depths at lower latitudes.

Despite the similar spatial patterns present in the neutron- and temperature-derived water ice depths, temperature-derived depths are greater than neutron-derived depths at depths greater than ~10 cm. Part of this discrepancy may be explained by differences in the depths of sensitivity of the two techniques. There may also be a physical explanation as well. At greater burial depths, the neutron measurements may be more sensitive to layered hydrated minerals closer to the surface than more deeply buried deeper water ice. An additional explanation for the discrepancy may lie in the simplistic assumptions of a two-layered dry regolith/icy permafrost model. The general agreement of the neutron- and temperature-derived water ice depths adds robustness to the accuracy of both datasets and techniques. However, disagreements between the two sets of results may also lend

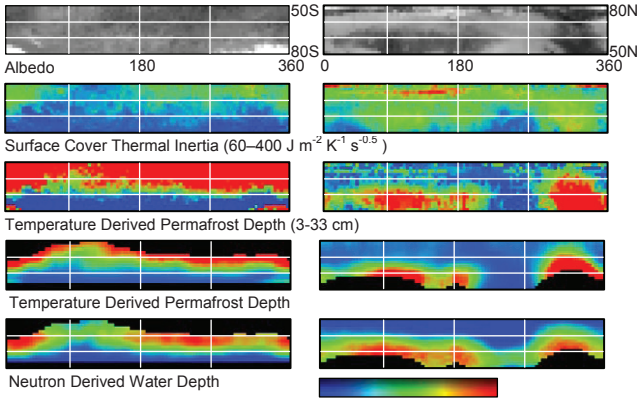


Figure 1. Albedo, surface cover thermal inertia, and permafrost/water depth maps. The temperature-derived depth map is shown twice: at full resolution (third from top) and spatially filtered and masked (fourth from top) to match the coverage and resolution of the neutron-derived water depth maps. The maps cover all longitudes and 50–80 N/S latitude.

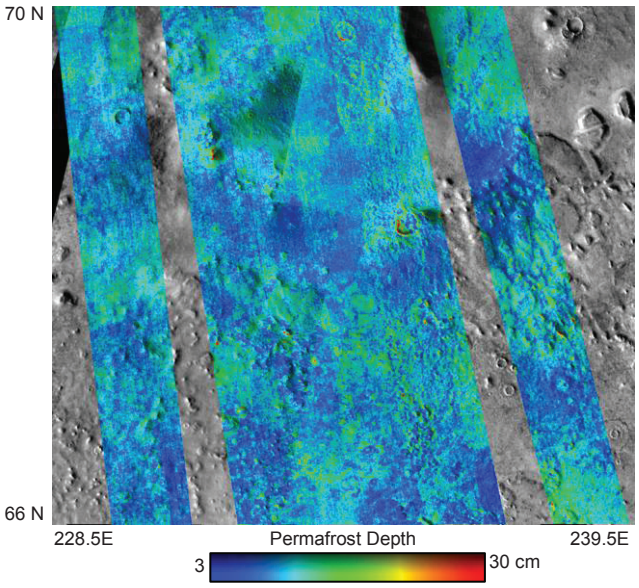


Figure 2. The permafrost depths derived from THEMIS seasonal temperature data are in reasonable agreement with the TES data from the same region. The area shown here includes the primary landing site for the Phoenix spacecraft. The region shown is approximately 250 km across.

insight into their inherent flaws as well as provide clues about the nature of the subsurface structure.

Although a general pattern of increased permafrost depth with decreasing latitude is present globally, the surface cover thermal inertia is also highly correlated with permafrost depth (Fig. 1). A surface with high thermal inertia conducts more energy into the subsurface and to a greater depth than a low thermal inertia surface cover. An exception to this correlation appears between 70–80°N and is concentrated near regions of permanent water ice exposures detached from the main polar cap from ~90–270°E. The most likely explanation for these high surface cover thermal inertia values is that the permafrost is shallow enough to influence the derived surface cover thermal inertia. These exposures are probably extensions of the exposed ice deposits covered by a lag of residual dust.

It is clear that there are regional variations in permafrost depth at the scale of the TES and Neutron Spectrometer measurements. Local slopes, surface cover thermal inertia, and albedo can all have significant effects on the depth of the permafrost. Permafrost depths have been shown to have this variability at the sub-km scale (Bandfield 2007). Figure 2 displays permafrost depths determined from THEMIS seasonal temperature data over the region of the 2007 Mars Scout Phoenix spacecraft landing site. The average permafrost depth retrieved from the TES data for the region is 4.5 cm. The THEMIS data has slightly higher values of 6.2 cm. This comparison shows that the low resolution measurements retain an overall accuracy, but are not able to resolve a large amount of detailed variability that is clearly present. Spatial variability in water ice/permafrost depths is present at all scales and the THEMIS data provide an important bridge between the tens to hundreds of km scales of the TES and Neutron Spectrometer measurements and the <1 m scales to be accessed by the Phoenix Lander.

## Summary

It is possible, and indeed likely, that the current distribution of water ice is attributable to both recession of residual surface ice deposits as well as emplacement via vapor diffusion (Schorghofer 2007). Temperature and neutron measurements show water ice distributions largely consistent with the present stability limits. The subsurface distribution of the water ice may be more complicated than an icy/not-icy model that the simple nature of the datasets restrict us to, however. Climate cycles can be variable in both magnitude and duration, and these variations may leave their imprint on the subsurface water distributions.

## Acknowledgments

We would like to thank Hugh Kieffer for providing guidance and use of the thermal model used in this work.

## References

Bandfield, J.L. 2007. High-resolution subsurface water-ice distributions on Mars. *Nature* 447: 64-67.

Bandfield, J.L. & Feldman, W.C. 2008. Martian high latitude permafrost depth and surface cover thermal inertia distributions. *J. Geophys. Res.* (in press).

Feldman, W.C. et al. 2007. Vertical distribution of hydrogen at high northern latitudes on Mars: The Mars Odyssey Neutron Spectrometer. *Geophys. Res. Lett.* 34: 5201-5204.

Leighton, R.R. & Murray, B.C. 1966. Behavior of carbon dioxide and other volatiles on Mars. *Science* 153: 136-144.

Mitrofanov, I.G. et al. 2004. Soil water content on Mars as estimated from neutron measurements by the HEND instrument onboard the 2001 Mars Odyssey spacecraft. *Solar Sys. Res.* 38: 253-257.

Schorghofer, N. 2007. Dynamics of ice ages on Mars, *Nature* 449: 192-195.

# Time Series Analyses of Active Microwave Satellite Data for Monitoring of Hydrology at High Latitudes

Annett Bartsch
*Institute of Photogrammetry and Remote Sensing, Vienna University of Technology, Austria*

## Introduction

Microwaves can penetrate cloud cover and are independent from daylight conditions. Active systems onboard satellites provide coarse (scatterometer) to medium resolution data (ScanSAR and SAR). An increase of spatial resolution always goes along with reduced revisit intervals. In general, satellites with microwave sensors are polar-orbiting platforms. This means that data coverage increases at higher latitudes due to overlapping footprints and swaths, respectively. Scatterometer can provide here several measurements per day, and medium resolution ScanSAR, up to daily acquisitions.

The backscatter intensity depends on the used wavelength, polarization, incidence angle, and surface conditions (Henderson & Lewis 1998). The latter include dielectric properties and surface structure. Even surfaces such as lakes produce low backscatter compared to forests, where multiple scattering causes higher signal returns. Microwaves have a high application potential in hydrology, since dielectric properties are related to water content. Time series can be used to monitor soil moisture, snowmelt, and inundation. This extended abstract gives an overview of some available datasets and application examples in permafrost areas. Additional information can be found on http://www.ipf.tuwien.ac.at/radar/.

## Near-Surface Soil Moisture

The ERS1 and ERS2 C-band scatterometer have been proven useful for derivation of relative soil moisture (Wagner et al. 1999, Wagner et al. 2007). Such data are available globally with 50km resolution since 1992. The long dataset allows the determination of deviations and thus anomalies. Continuation is ensured due to the launch of Metop in October 2006. The new ASCAT instrument on Metop provides even shorter revisit intervals and increased spatial resolution (25 km; Bartalis et al. 2007).

The near-surface soil moisture can be determined by time series analysis (Wagner et al. 2003). A dry and wet reference is identified for each grid point and each single measurement scaled between these limits. This results in a relative measure of near-surface soil moisture. By application of a simple infiltration model, profile soil moisture is derived (Wagner et al. 1999). The latter is referred to as Soil Water Index (SWI) and is available globally as 25 km grid cells in 10-day intervals (Wagner et al. 2007). The observed near-surface soil moisture variations are related to river discharge (Scipal et al. 2005). Although snowmelt is more important for the magnitude of discharge in high latitudes, a close relationship to soil moisture can be observed during the summer (Bartsch et al. 2007b).

The European satellite ENVISAT has a C-band SAR instrument onboard. This Advanced SAR (ASAR) provides higher resolution data (image mode) as well as medium resolution ScanSAR (Wide Swath and Global Mode). The latter has a wider swath (405 km) than high-resolution modes, which allows coverage of larger regions and provides shorter revisit intervals (with varying incidence angles). Therefore, a similar time series analysis, as developed for scatterometer data, can be applied to ScanSAR data for extraction of near-surface relative soil moisture. This has successfully been carried out for Southern Africa (Bartsch et al. 2007c) and Oklahoma (Pathe et al. 2007). It could be transferred to high latitudes where ENVISAT ASAR Gobal Mode (1km) data provide up to daily measurements (Bartsch et al. in press a). Such medium resolution ScanSAR data can also be used to derive spatial scaling properties, which allow an interpretation of coarse-resolution soil moisture from scatterometer (25 km) at local scale (1 km) (Wagner et al. 2008). Other new microwave sensors, such as the ALOS PALSAR (L-band, 12.5 m in fine beam mode), provide increased spatial and nevertheless low temporal resolution, but have potential for soil moisture retrieval (Bartsch et al. 2007d).

## Snowmelt

C-Band (~5.6 cm) as well as $K_u$-band (~2.1 cm) radars are suitable for snowmelt detection. Changes in the snowpack, however, have a stronger impact on backscatter at shorter wavelengths. The SeaWinds Quikscat is a $K_u$-band scatterometer, which provides measurements with 25 km resolution since 1999. Re-gridded datasets are available with up to 5 km resolution (Long & Hicks 2005). The first entire snowmelt period on the Northern Hemisphere is covered in 2000. Large changes in backscatter between morning and evening acquisitions are characteristic for the snowmelt period, when freezing takes place overnight and thawing of the surface during the day. A change from volume to surface scattering occurs in case of melting. This may cause changes up to 6 dB (Kimball et al. 2004). When significant changes due to freeze/thaw cycling cease, closed snow cover also disappears (Bartsch et al. 2007a). For the identification of melt days over permanently snow- or ice-covered ground, only evening measurements are considered (Ashcraft & Long 2006). Diurnal differences (Bartsch et al. 2007a) on the other hand are calculated for the delimitation of the final spring snowmelt period. The exact day of year of beginning and end of freeze/thaw cycling can be clearly determined with consideration of long-term noise. Such an approach allows not only the monitoring of disappearance of snow. Areas which undergo thaw at a certain day can be identified

as well. The QuikScat-derived thaw patterns relate to spring river discharge in high latitudes (Bartsch et al. 2007b).

## Lakes and Wetlands

Due to the backscatter properties of open water (even surface), lakes can be easily identified with active microwave data. Although wind may increase the surface roughness, lakes can be identified based on time series (Bartsch et al. 2007e, Bartsch et al. in press b). Due to the wider swath and thus increased spatial and temporal coverage of ScanSARs, large regions can be processed. For example, ENVISAT ASAR Wide Swath data with 150 m resolution provide considerably more detailed information in tundra regions than land cover products from MODIS (500 m; Bartsch et al. in press b). The spatial distribution of lakes larger than 2 ha can be used for the determination of tundra wetland extent and also estimation of methane emissions.

Peatlands are characterized by high soil moisture conditions. They can be identified due to the sensitivity of microwaves to moisture/dielectric properties (Bartsch et al. 2007e). ENVISAT ASAR Wide Swath (150 m) as well as Global Mode (1km) time series are suitable for mapping of large regions such as the West Siberian Lowlands (Bartsch et al. in press b).

## Acknowledgments

The author is the recipient of a Hertha Firnberg research fellowship (Austrian Science Fund, T322-N10).

## References

Ashcraft, I.S. & Long, D.G. 2006. Comparison of methods for melt detection over Greenland using active and passive microwave measurements. *International Journal of Remote Sensing* 27: 2469-2488.

Bartalis, Z., Wagner, W., Naeimi, V., Hasenauer, S., Scipal, K., Bonekamp, H., Figa, J. & Anderson, C. 2007. Initial soil moisture retrievals from the METOP-A Advanced Scatterometer (ASCAT). *Geophysical Research Letters* 34: L20401

Bartsch, A., Kidd, R.A., Wagner, W. & Bartalis, Z. 2007a. Temporal and spatial variability of the beginning and end of daily spring freeze/thaw cycles derived from scatterometer data. *Remote Sensing of Environment* 106: 360-374.

Bartsch, A., Wagner, W., Rupp, K. & Kidd, R.A. 2007b. Application of C and Ku-band scatterometer data for catchment hydrology in northern latitudes. In: *Proceedings of the 2007 IEEE International Geoscience and Remote Sensing Symposium, Barcelona, Spain 23–27 July 2007*: 3702-3705.

Bartsch, A., Pathe, C., Sabel, D., Wagner, W. & Doubkova, M. 2007c. Soil Moisture Time Series from Active Radar in Support of Runoff Monitoring on Local, Catchment and Regional Scale. *Proceedings of the Second ESA Space for Hydrology Workshop, Geneva, 12-14 November 2007*.

Bartsch, A., Pathe, C., Sabel, D. & Wagner, W. 2007d. Relative soil moisture from C- and L-band SAR time series. *Proceedings of the First Joint PI Symposium of ALOS Data Nodes, Kyoto, 19–23 November 2007*.

Bartsch, A., Kidd, R., Pathe, C., Wagner, W. & Scipal, K. 2007e. Satellite radar imagery for monitoring inland wetlands in boreal and sub-arctic environments. *Journal of Aquatic Conservation: Marine and Freshwater Ecosystems* 17: 305-317.

Bartsch, A., Wagner, W., Pathe, C., Scipal, K., Sabel, D. & Wolski, P. in press (a). Global monitoring of wetlands: The value of ENVISAT ASAR global mode. *Journal of Environmental Management*.

Bartsch, A., Pathe, C., Wagner, W. & Scipal, K. in press (b). Detection of permanent open water surfaces in central Siberia with ENVISAT ASAR wide swath data with special emphasis on the estimation of methane fluxes from tundra wetlands. *Hydrology Research*.

Kimball, J.S., McDonald, K.C., Frolking, S.E. & Running, S.W. 2004. Radar remote sensing of the spring thaw transition across a boreal landscape. *Remote Sensing of Environment* 89: 163-175.

Henderson, F.M. & Lewis, A.J. 1998. *Principles & Applications of Imaging Radar: Manual of Remote Sensing vol. II*. New York: John Wiley & Sons.

Long, D. & Hicks, B. 2005. *Standard BYU QuikSCAT/ SeaWinds Land/Ice Image Products*. Report Provo, Utah: Brigham Young University.

Pathe, C., Wagner, W., Sabel, D., Bartsch, A., Naemi, V., Doubkova, M. & Basara, J. 2007. Soil moisture information from multi-temporal ENVISAT ASAR ScanSAR data over Oklahoma, USA. *Proceedings of BioGeoSAR 2007, Bari.*

Scipal, K., Scheffler, C. & Wagner, W. 2005. Soil moisture-runoff relation at the catchment scale as observed with coarse resolution microwave remote sensing. *Hydrology and Earth System Sciences* 9: 173–183.

Wagner, W., Lemoine, G. & Rott, H. 1999. A method for estimating soil moisture from ERS scatterometer and soil data. *Remote Sensing of Env.* 70: 191–207.

Wagner, W., Scipal, K., Pathe, C., Gerten, D., Lucht, W. & Rudolf, B. 2003. Evaluation of the agreement between the first global remotely sensed soil moisture data with model and precipitation data. *Journal of Geophysical Research D: Atmospheres* 108 (19): ACL 9(1)-9(15).

Wagner, W., Naeimi, V., Scipal, K., de Jeu, R. & Martìnez-Fernàndez, J. 2007. Soil moisture from operational meteorological satellites. *Hydrology Journal* 15: 121-131.

Wagner, W., Pathe, C., Doubkova, M., Sabel, D., Bartsch, A., Hasenauer, S., Blöschl, G., Scipal, K., Martínez-Fernández, J. & Löw A. 2008. Temporal stability of soil moisture and radar backscatter observed by the Advanced Synthetic Aperture Radar (ASAR). *Sensors* 8: 1174-1197.

# Impact of Permafrost Degradation on Carbon and Nitrogen Stocks Related to Pedogenesis and Ecosystem Functioning

Frank Baumann
*Institute of Geography, University of Tuebingen, Tuebingen, Germany*
Jin-Sheng He
*Department of Ecology, College of Environmental Sciences, Peking University, Beijing, China*
Peter Kühn
*Institute of Geography, University of Tuebingen, Tuebingen, Germany*
Thomas Scholten
*Institute of Geography, University of Tuebingen, Tuebingen, Germany*

## Introduction

The Qinghai-Xizang (Tibetan) Plateau is a key area concerning the environmental evolution of the earth at regional as well as global scales and proves to be particularly sensitive to anthropogenic global change, especially in areas affected by permafrost. It is the youngest, largest, and highest plateau in the world, comprising an area of more than 2.4 million km² with an average altitude exceeding 4000 m a.s.l. and containing the largest high-altitude and low-latitude permafrost area on Earth with 54.3% of its total surface affected by permafrost (Cheng 2005). These areas are characterized by strong diurnal patterns, high radiation on the surface, as well as a distinct geothermal gradient (Wang & French 1994) that mainly control the permafrost distribution and, thus, soil temperature and soil moisture conditions. Further, the proposed decay of Tibetan permafrost will have a strong impact on soil hydrology. Global environmental change, largely caused by human activities, affects climate as well as soils, and consequently reassigns their role in ecosystem functioning (Vitoussek et al. 1997). The major parameters in this context are the organic carbon ($C_{org}$) stock of soils and the decomposition of organic matter, whereas the Qinghai-Xizang (Tibetan) Plateau stores the highest amount of $C_{org}$ and total nitrogen ($N_t$) in Chinese soils (Wang & Zhou 1999). Therefore, periglacial environments of Central China play a major role in the global C and N cycles, especially due to the pronounced sensitivity of this region to climate changes.

During two expeditions in 2006 and 2007, in total 60 sites were investigated on the central-eastern Tibetan Plateau along a 1500 km long northeast–southwest transect. The research focused exclusively on alpine steppe and meadow grassland vegetation. Sites containing continuous or discontinuous permafrost as well as areas without or heavily degraded permafrost were studied for comparison of soil dynamics under changing environmental settings. The main objective was to figure out how carbon and nitrogen contents of the investigated soils on the Tibetan Plateau respond to other pedological parameters, such as texture, acidity and carbonate content, since the sites along the transect show a distinct variety of climate conditions, relief locations and geology. Another major goal was to assess impact of global change on permafrost and its implication concerning the carbon and nitrogen cycles related to the above-mentioned feedback paths. Permafrost, pedogenesis, and ecosystem functioning are, therefore, closely linked. Study of their detangled feedback processes and mechanisms allows a better understanding of the role of geological and anthropogenic factors controlling the development and the functioning of Tibetan Plateau ecosystems.

## Methods

At each site a soil profile pit was established reaching the parent material of soil formation or permafrost, respectively. The detailed field investigations included soil profile description according to FAO (2006) and WRB IUSS Working Group (2007). Soil moisture was determined in the field by TDR-probes connected with a moisture meter type HH2 (Delta-T Devices Ltd, UK). Aboveground and belowground biomass as well as soil respiration and temperature were investigated. Moreover, on-site 1 M KCl extractions for the determination of mineralized N ($N_{min}$) were carried out.

The laboratory analysis included a combined sieving and pipette grain-size analysis. Electrical conductivity (EC) and acidity (pH) were determined potentiometrically. $CaCO_3$ was tested volumetrically with HCl treatment. $N_t$ and $C_{org}$ were measured by heat combustion (CNS-elemental analyzer VARIO EL III, Elementar, Germany). The KCl extractions were analyzed photometrically for $N_{min}$ (Continuous Flow Analyzer SAN Plus, Skalar, Netherlands). Water content was determined gravimetrically.

Climate data for each site was calculated by Kriging out of a 50-year time series of 680 climatic stations in China (1951–2000) (He et al. 2006). The whole dataset was investigated by descriptive statistics, one-way ANOVA, as well as correlation and regression analysis (SPSS for Windows, R) for the relationships of variables.

## Results and Discussion

Highest C and N contents occur in permafrost and groundwater-influenced soils. The lower amount in soils not influenced by permafrost can be explained by shorter duration of pedogenesis and different temperature-moisture regimes. Pedogenesis is described here by acidity, carbonates, grain size distribution, and other soil parameters. Particularly at sites with initial soil formation, frequently influenced by

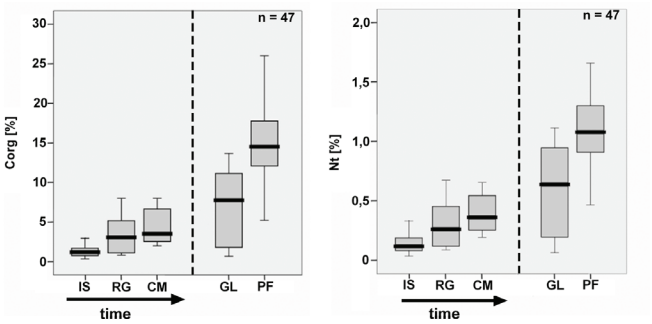


Figure 1. $C_{org}$ and $N_t$ stocks related to the stage of pedogenesis: IS = initially formed soils; RG = Regosols; CM = Cambisols; GL = groundwater influenced; PF = permafrost influenced.

aeolian sedimentation, extremely low contents of C and N combined with a high spatial variability were observed. These layers are composed of sandy and coarse-silty proximal generated material, mostly linked to direct (e.g., overgrazing, construction) and indirect (climate change) human impact. Therefore, the stage of soil development is an important co-variable in explaining the nutrient fluxes in grassland ecosystems on the Tibetan Plateau (Fig. 1). Highly fluctuating C and N contents of topsoils are evident on small spatial scales, mainly controlled by relief position and, in particular, by permafrost distribution in discontinuous permafrost areas. Semi-natural systems like alpine grasslands are generally limited in available plant nutrients. Thus, the productivity of alpine grassland ecosystems is determined by the available nitrogen pool, the amount of nitrogen input, as well as by nitrogen fixation, modified by water availability to plants over the year. Consequently, the degradation processes have severe impact on nutrient supply of plant species and accordingly alter biodiversity patterns.

Botanical and ecological studies on the Qinghai-Xizang (Tibetan) Plateau lead to the assumption that temperature changes alter biodiversity and biomass production in grassland ecosystems and are the main driving parameter for C and N turnover (e.g., He et al. 2006). Moreover, recent research has shown that changes in temperature and moisture conditions will also have serious impact on nitrogen and carbon cycling of soils (e.g., Shaver et al. 2006). Due to the high number of samples and the large-scale transect concept, sophisticated statistical analysis showing significant relationships between pedological parameters as well as carbon and nitrogen contents could be conducted. The results indicate that, in high altitude grassland ecosystems, soil moisture conditions can be determined as the main influencing parameter of C and N stocks, which are in turn closely linked to temperature. Furthermore, similar results are evident for annual precipitation, whereas no significant correlations were found concerning the mean annual temperature or soil temperature (Table 1). Comparable relationships can be shown for the soil respiration measurements. These linkages are in close connection to feedback mechanisms with temperature, which is predominantly affected by permafrost, aeolian sedimentation, and the stage of soil development. Permafrost and aeolian sedimentation are again a function of relief

Table 1. Correlations: C/N stock and selected control parameters.

| | MAT (°C) | MAP (mm/a) | Soil Moisture (%) | Sand (%) |
|---|---|---|---|---|
| $N_t$ (%) | n.s. | 0.54 (**) | 0.57 (**) | -0.38 (**) |
| $C_{org}$ (%) | n s. | 0.53 (**) | 0.55 (**) | -0.37 (**) |
| $NO_3^-$ (mg/l) | 0.28 (**) | n.s. | n.s. | n.s. |
| $NH_4^+$ (mg/l) | n.s. | 0.30 (**) | 0.30 (**) | n.s. |

(**) correlation is significant (0.01 two-sided).
(*) correlation is significant (0.05 two-sided).
(n.s.) correlation is not significant.

position, parent material, and seasonal climatic fluctuations, with an overall impact of climatically and human-induced degradation processes.

An evident trend of climate parameters in the above-mentioned direction to warmer conditions was observed during the past decades on the Qinghai-Tibetan Plateau (Yang et al. 2004), obviously leading to permafrost degradation (Cheng 2005). A relatively quick turnover rate of organic matter is expected for the turf-like upper layers in only some tens of years (Hirota et al. 2006). This process will be amplified if warming is accompanied by drier conditions.

## References

Cheng, G. 2005. Permafrost Studies in the Qinghai-Tibet Plateau for Road Construction. *Journal of Cold Regions Engineering* 19(1): 19-29.

He, J.-S., Wang, Z., Wang, X., Schmid, B., Zuo, W., Zhou, M., Zheng, C., Wang, M. & Fang, J. 2006. A test of generality of leaf trait relationships on the Tibetan Plateau. *New Phytologist* 170: 835-848.

Hirota, M., Tang, Y., Hu, Q., Hirata, S., Kato, T., Mo, W., Cao, G. & Mariko, S. 2006. Carbon Dioxide Dynamics and Controls in a Deep-water Wetland on the Qinghai-Tibetan Plateau. *Ecosystems* 9: 673-688.

Shaver, G.R., Giblin, A.E., Nadelhoffer, K.J., Thieler, K.K., Downs, M.R., Laundre, J.A. & Rastetter, E.B. 2006. Carbon turnover in Alaskan tundra soils: effects of organic matter quality, temperature, moisture and fertilizer. *Journal of Ecology* 94: 740-753.

Vitousek, P.M., Mooney, H.A., Lubchenco, J. & Melillo, J.M. 1997. Human domination of earth's ecosystems. *Science* 277: 494-499.

Wang, B. & French, H.M. 1994. Climate Controls and High-Altitude Permafrost, Qinghai-Xizang (Tibet) Plateau, China. *Permafrost and Periglacial Processes* 5: 87-100.

Wang, S. & Zhou, C. 1999. Estimating soil carbon reservoir of terrestrial ecosystem in China. *Geogr. Res.* 18: 349-356.

Yang, M., Wang, S., Yao, T., Gou, X., Lu, A. & Guo, X. 2004. Desertification and its relationship with permafrost degradation in Qinghai-Xizang (Tibet) plateau. *Cold Regions Science and Technology* 39: 47-53.

# DC Resistivity Soundings Across a Pebbly Rock Glacier, Kapp Linné, Svalbard

Ivar Berthling
*Norwegian University of Science and Technology, Trondheim, Norway*
Håvard Juliussen
*UNIS – The University Centre in Svalbard, Longyearbyen, Norway*

## Introduction

Recently, Ikeda and Matsuoka (2006) have drawn attention towards what they call "pebbly" rock glaciers that differ from "bouldery" rock glaciers both with respect to lithological content, mean size of clasts, and rock glacier dimensions. The present paper reports on pebbly rock glaciers close to Isfjord Radio on Kapp Linné, Svalbard, and their internal structure based on a detailed DC resistivity profiling campaign. A working hypothesis is proposed for their development.

## Setting

Kapp Linné is located on the northern part of the coast of Nordenskiølds land, western Svalbard (Fig. 1). The pebbly rock glaciers have developed along Griegaksla at the transition between talus slopes and the strandflat area, a topographical position similar to that of the rock glaciers on Prins Karls Forland (Berthling et al. 1998, 2007) and rock glaciers further south on the coast of Nordenskiølds land (Kääb et al 2002, Farbrot et al. 2005).

The western flank of Griegaksla is composed of phyllitic bedrock that weathers to matrix-supported highly frost-susceptible debris. The lower part of the mountain wall is covered by talus deposits that in some cases have developed into small rock glaciers.

## Fieldwork and Methods

The DC resistivity measurements where carried out in July 2007 on the largest of these rock glaciers (Fig. 1), as part of the IPY project "Permafrost Observatory Project: A Contribution to the Thermal State of Permafrost in Norway and Svalbard (TSP Norway)." The investigated rock glacier is from 50 to 100 m long and has a frontal slope with a height of about 30 m.

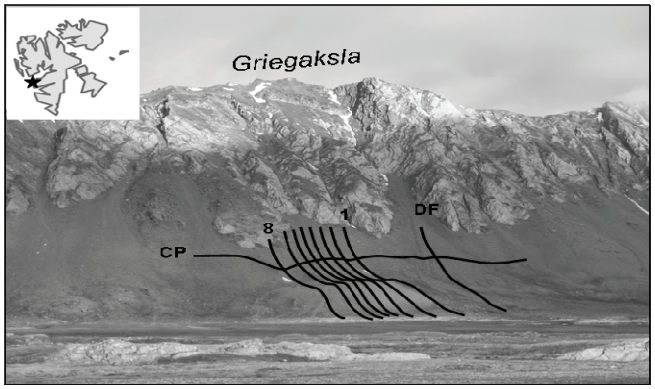


Figure 1. The study site at Griegaksla, Kapp Linné (arrow on Svalbard map). 1–8 are the resistivity lines along the talus slope–rock glacier system. CP is the cross profile and DF is a resistivity profile along a talus slope with debris-flow tracks.

We used ABEM equipment, with an along-slope electrode spacing of 10 m. Spacing between resistivity lines were 10 m (profiles 1–7) and 20 m (profile 7–8). We also collected a resistivity profile along a neighboring talus slope and a profile across the talus (Fig. 1). The topography of all profiles was established using differential GPS.

## Results

The resistivities are highest in the talus cone, while on the rock glacier itself, resistivity decreases (Fig. 2). On the northern part of the rock glacier (profile 7–8), higher resistivity reaches further down into the rock glaciers. The northern part of the rock glacier is longer, lacks an inner depression, and does not display a very sharp transition between rock glacier surface and front. Resistivities in talus areas outside of the rock glacier system are lower, but comparable to that of the rock glacier itself.

## Discussion and Conclusions

The results obtained underline the importance of processes operating in talus slopes for the development of rock glaciers. The environmental conditions along Griegaksla are fairly similar, and it is a question why rock glaciers have only developed along parts of the more or less continuous talus sheet found here. However, it seems to be a pattern that these rock glaciers are developed beneath areas where the talus slope is shorter than elsewhere. One possible explanation is that a larger and more active talus slope, including snow avalanche and debris flow processes, will tend to erode the upper part of the talus cone and transport debris to its lower part. This will set up a tendency for melting at the bottom of the active layer, inhibiting accumulations of segregation ice beneath the active layer, while at the same time lowering shear stresses within the talus cone. On a less active talus, especially one composed of frost-susceptible debris, the potential for water migration into the permafrost, segregation ice development, and aggradation of permafrost will be higher.

## Acknowledgments

The "Permafrost Observatory Project: A Contribution to the Thermal State of Permafrost in Norway and Svalbard (TSP Norway)" is led by Hanne H. Christiansen, UNIS, who was in charge of the field campaign at Kapp Linné. Andreas Kääb, University of Oslo, calculated the DGPS data. The assistance provided in the field by Jaran Wasrud is greatly appreciated.

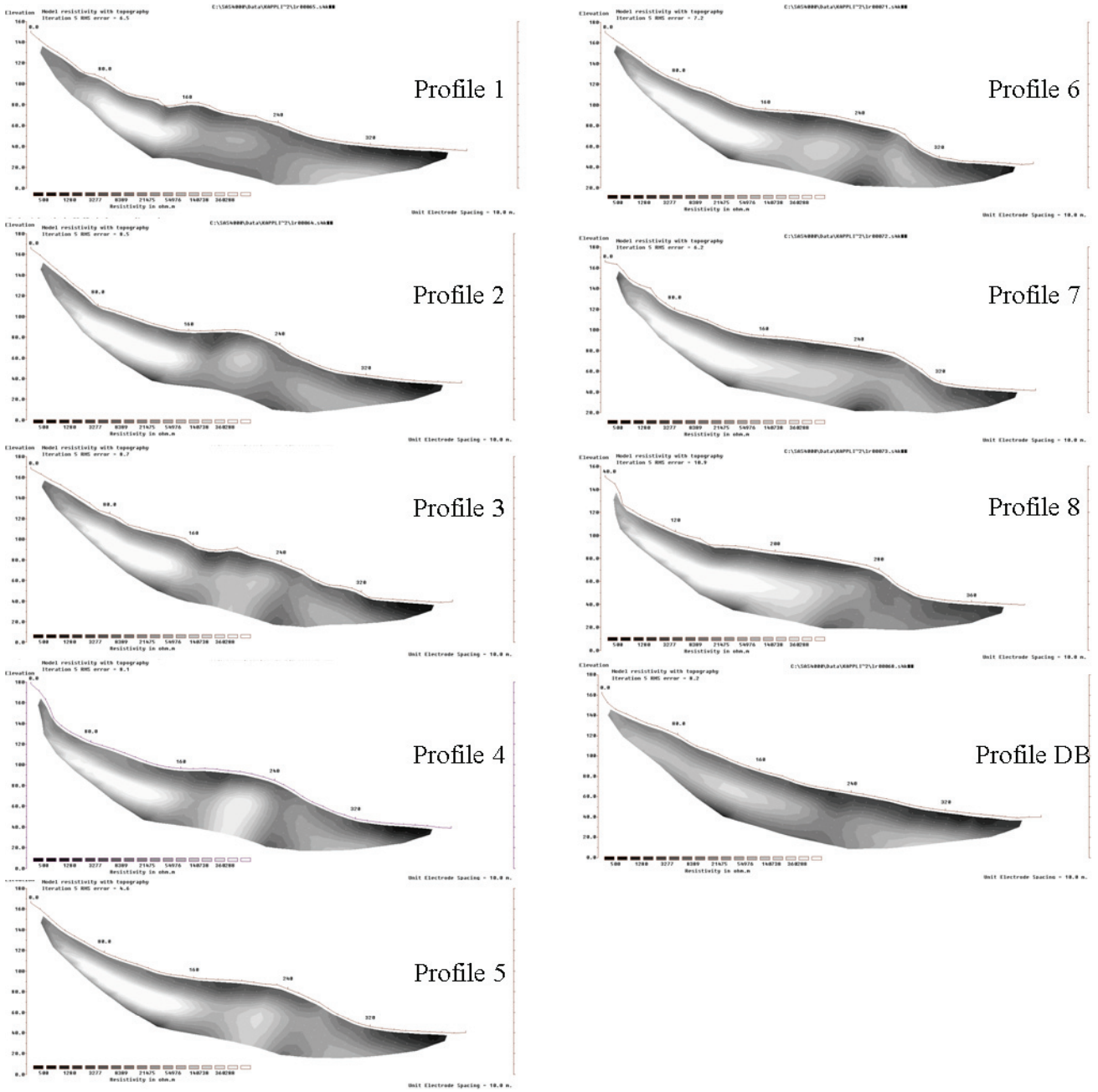


Figure 2. Results from the resistivity profiling. Light tones indicate high resistivities (around 400 KΩm). For position of profiles, see Figure 1. The cross profile is not shown.

## References

Berthling, I., Etzelmuller, B., Eiken, T. & Sollid, J.L. 1998. Rock glaciers on Prins Karls Forland, Svalbard. I: Internal structure, flow velocity and morphology. *Permafrost and Periglacial Processes* 9: 135-145.

Berthling, I., & Etzelmuller, B. 2007. Holocene rockwall retreat and the estimation of rock glacier age, Prins Karls Forland, Svalbard. *Geogafiska Annaler* 89A: 83-93.

Kääb, A., Isaksen, K., Eiken, T. & Farbrot, H. 2002. Geometry and dynamics of two lobe-shaped rock glaciers in the permafrost of Svalbard. *Norsk Geografisk Tidsskrift – Norwegian Journal of Geography* 56: 152-160.

Farbrot, H., Isaksen, K., Eiken, T., Kääb, A. & Sollid, J.L. 2005. Composition and internal structures of a rock glacier on the strandflat of western Spitsbergen, Svalbard. *Norsk Geografisk Tidsskrift - Norwegian Journal of Geography* 59: 139-148.

Ikeda, A. & Matsuoka, N. 2006. Pebbly versus bouldery rock glaciers: morphology, structure and processes. *Geomorphology* 73: 279-296.

# Modeling Thermal and Moisture Regimes of Permafrost with New Deep Soil Configuration in CLASS

Jean-Philippe Blanchette, Laxmi Sushama, René Laprise
*Centre pour l'étude et la simulation à l'échelle régionale, Université du Québec à Montréal, Montréal, Canada*
*Canadian Regional Climate Modelling and Diagnostics Network, Montréal, Canada*
*Consortium Ouranos on Regional Climate and Adaptation to Climate Changes, Montréal Canada*

## Introduction

Most of the climate models, including Regional Climate Models (RCMs), employ land-surface schemes that vary in depth between 3 and 10 m; for example, the current version of the Canadian Regional Climate Model (CRCM) has a physically-based land surface scheme, CLASS (Canadian Land Surface Scheme; Verseghy et al. 1991, Verseghy 1993), which is 4.1 m deep, with three soil layers that are 0.1, 0.25, and 3.75 m thick, respectively. As shown by many recent studies (Smerdon & Stieglitz 2006, Alexeev et al. 2007, Nicolsky et al. 2007, Stevens et al. 2007), such shallow-soil models, though coupled, cannot simulate active-layer and near-surface permafrost realistically. To simulate realistic soil thermal and moisture regimes in the CRCM, it is intended to use the latest version (v. 3.3) of CLASS, which is particularly suitable for permafrost studies due to its more flexible layering scheme and bottom boundary conditions. Sensitivity of the soil thermal and moisture regimes to the soil model depth/configuration is assessed using offline simulations with this latest version of CLASS, which is presented in this paper.

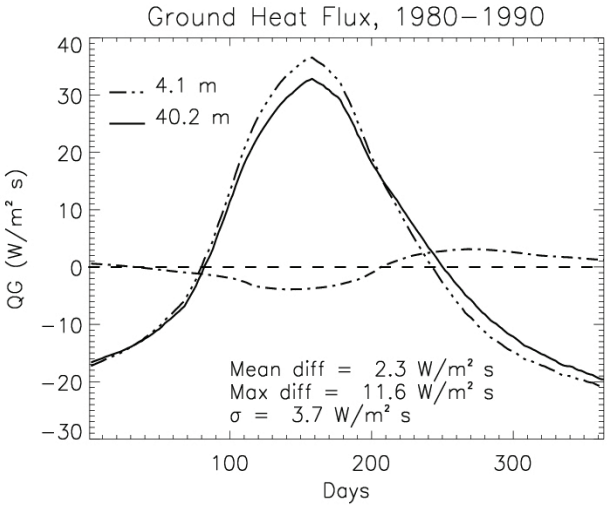


Figure 1. Average ground heat flux for the 1980–1990 period, for 6 (dash-multidotted line) and 10-layer (solid line) configurations, and their differences (dash-dotted line). The annual maximum difference, the annual mean difference, and the standard deviation are also indicated in the Figures.

## Experiments and Model Configuration

The offline simulations were performed with CLASS for a location in northern Québec with continuous permafrost, for the 1961–1999 period. The input variables (downward visible and infrared radiation, precipitation, atmospheric pressure, surface air temperature, specific humidity, and wind) required to drive the soil model were specified using the European Re-analysis datasets (ERA-40, Uppala et al. 2005). The soil properties were specified using the land surface datasets developed by Wilson and Henderson-Sellers (1985), according to which the bedrock is at 0.1 m below surface for the chosen location. Three experiments were performed, with the lower boundary at 4.1, 40.2, and 133.7 m below surface, respectively. The layer thickness varies exponentially from top to bottom (0.10, 0.17, 0.31, 0.57, 1.04, and 1.91 m for the first six layers and so on), and accordingly the number of layers for the three cases is 6, 10, and 12, respectively. The initial profile is determined by iteratively running the soil model from chosen conditions using 1961 data, until equilibrium is reached.

## Results

Preliminary results confirm that adding deeper layers to CLASS, and in doing so, lowering the bottom boundary with zero soil heat conduction flux, changes the thermal regime, as shown in Figures 1, 2, and 3, comparing the six and ten-layer configuration. The thermal inertia brought by new deeper

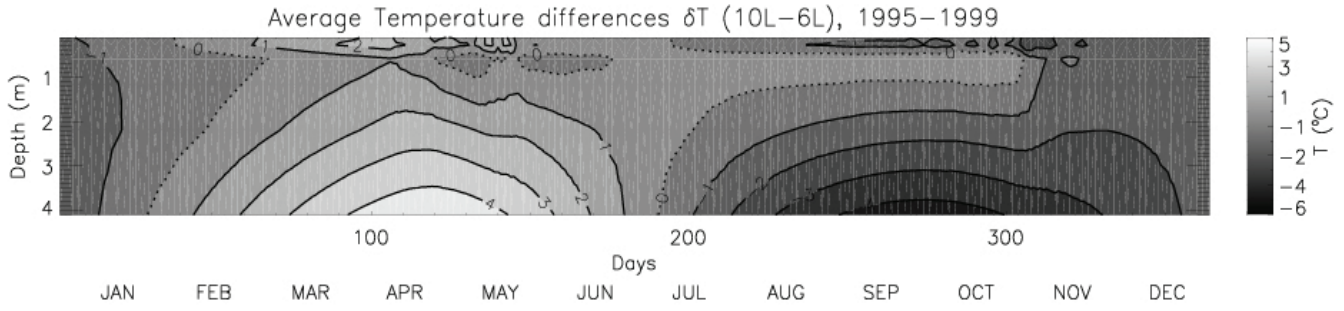


Figure 2. Average temperature differences between the 10- and 6-layer configuration for the 1995–1999 period.

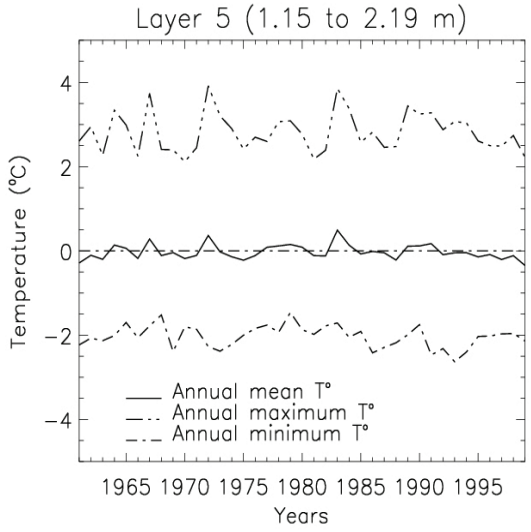


Figure 3. Evolution of the differences in the annual minimum (upper dash-multidotted line), average annual (solid line), and annual maximum (bottom dash-dotted line) temperatures of layer 5, for the period 1961–1999, between the 6- and 10-layer configuration. The annual minimum (maximum) temperature is warmer (colder) in the deeper version compared to the shallow one. The mean annual temperature of both models, however, is very similar.

layers modifies the heat fluxes and, thus, the heat storage of the soil. With deeper soil, the top 4 m soil temperature is colder in summer and fall, and warmer during winter and spring. Figure 2 suggests differences of 5°C at 4 m during March to May. The influence of these changes on the surface fluxes and on other fields (albedo, latent heat flux, runoff, etc., not shown here) need to be further explored. However, it appears that the impact is significant during the snowmelt period or during the beginning of the snow accumulation. For example, the snow cover accumulation starts earlier in the deeper model, because of the colder soil temperature present in early fall, which is reflected by higher accumulation in the 10-layer model. However, the higher soil temperature in spring for the 10-layer model compared to the 6-layer one causes early snowmelt. This is also reflected in the liquid and solid water content of the first layer. The ratio of solid to liquid soil water content is higher at the beginning of the freezing period for the 10-layer configuration, and inversely, the ratio is lower at the beginning of the snowmelt.

Further tests need to be conducted with deeper bedrock, organic matter, etc., which will be followed by coupled simulations to understand the importance of the deeper soil on surface fluxes.

## Acknowledgments

Jean-Philippe Blanchette is supported by the Réal-Décoste/ Ouranos Scholarships, the Canada Graduate Scholarship (CGS M) from NSERC, and by the partial GEC3 Graduate Student Stipend.

## References

Alexeev, V.A., Nicolsky, D.J., Romanovsky, V.E. & Lawrence, D.M. 2007. An evaluation of deep soil configurations in the CLM3 for improved representation of permafrost. *Geophys. Res. Lett*. (34): L09502.

Nicolsky, D.J., Romanovsky, V.E., Alexeev, V.A. & Lawrence, D.M. 2007. Improved modeling of permafrost dynamics in a GCM land-surface scheme. *Geophysical Research Letter* (34): L08501.

Stevens, M.B., Smerdon, J.E., Gonzalez-Rouco, J.F. & Stieglitz, M. 2007. Effects of bottom boundary placement on subsurface heat storage: Implications for climate model simulations. *Geophys. Res. Lett*. (34): L02702.

Uppala, S.M. et al. 2005. The ERA-40 re-analysis. *Q.J.R.Meteorol. Soc* (131): 2961-3012.

Verseghy, D.L. 1991. CLASS – A Canadian land surface scheme for GCMs, I. Soil model and coupled runs. *International Journal of Climatology* (11): 111-133.

Verseghy, D.L., McFarlane, N.A. & Lazare, M. 1993. CLASS – A Canadian land surface scheme for GCMs, II. Vegetation model and coupled runs. *International Journal of Climatology* (13): 347-370.

Wilson, M.F. & Henderson-Sellers, A. 1985. A global archive of land cover and soil data for use in general circulation climate models. *Journal of Climatology* (5): 119-143.

# A Provisional Permafrost Map of the Transantarctic Mountains

J.G. Bockheim
*Department of Soil Science, University of Wisconsin, 1525 Observatory Drive, Madison, WI 53706-1299, USA*
M. McLeod
*Landcare Research, Private Bag 3127, Hamilton, New Zealand*
M.R. Balks
*Department of Earth and Ocean Sciences, University of Waikato, Private Bag 3105, Hamilton, New Zealand*

## Introduction

The Transantarctic Mountains (TAM) extend 3,500 km across the Antarctic continent from 69°S in northern Victoria Land to 87°30′S in the upper Scott Glacier region. The TAM form a natural barrier between ice in East and West Antarctica and record the history of Cenozoic glaciations of Antarctica (Lyons & Elliot 2006). The TAM have an ice-free area of 20,910 km$^2$, which constitutes 42% of the total ice-free area (49,500 km$^2$) of Antarctica.

Bockheim (1995) prepared the first permafrost map of Antarctica. He showed that permafrost was limited to ice-free areas and that all of East Antarctica and most of West Antarctica contain continuous permafrost. More recently, Bockheim and others (2007) prepared a provisional permafrost map of the McMurdo Dry Valleys portion of the TAM (6,700 km$^2$), reporting that buried ice, ice-cemented permafrost, and dry-frozen permafrost comprised 2, 55, and 43% of the area, respectively. A task force under the auspices of the IPA and Scientific Committee on Antarctic Research (SCAR), identified as the Antarctic Permafrost and Soils (ANTPAS) Group (http://erth.waikato.ac.nz/antpas/), is preparing a series of permafrost and ground-ice maps of Antarctica. The text that will accompany these maps is included in this volume (Bockheim et al. 2008). The poster accompanying the present abstract displays permafrost distribution in the TAM on three maps at scales of 1:1 million.

## Methods

To prepare a permafrost map of the TAM, we used 62 scanned and geo-rectified 1:250K topographic maps prepared by the US Geological Survey (http://usarc.usgs.gov/drg_dload.shtml). We joined these seamless maps in ArcGIS 9.2 and used the composite map as a base map. To display the entire TAM, we divided the mountains into three regions: northern Victoria Land (69°30′–75°S), central Victoria Land (75–80°30′S), and southern Victoria Land (80°30′–86°30′S). Each map could be displayed as a standard A0 wall size (841 x 1188 mm) at a scale of 1:1 million.

Expert permafrost scientists working in Antarctica prepared a legend that includes the following map units: (i) buried or ground ice within the upper 100 cm, (ii) ice-cemented permafrost with a surface within 70 cm, (iii) ice-cemented permafrost with a surface below 70 cm (excluding dry-frozen permafrost), and (iv) dry-frozen permafrost with an ice-cemented surface below 70 cm. To determine the distribution of these permafrost forms throughout the TAM, we used published data and data archived by the National Snow & Ice Data Center (http://nsidc.org/cgi-bin/get_metadata.Pl?id-ggd221) and New Zealand Landcare Research (http://www.landcareresearch.co.nz). In northern Victoria Land, we used data from Denton and others (1986) and Guglielmin and French (2004). In central Victoria Land, we used data collected by Bockheim and others (1989, 2007). For southern Victoria Land, data were used from Claridge and Campbell (1968) and Bockheim and others (1990). For unmapped areas we extrapolated the database using the following criteria: ice-cored drift was identified from a stippled pattern on topographic maps; ice-cemented permafrost was identified from patterned ground on remotely sensed images and proximity to streams, lakes, and ponds; and dry-frozen permafrost comprised the remaining areas, particularly in interior mountains and broad central valleys.

Polygons were drawn on the base maps, numbered, and identified in the accompanying attribute table by permafrost form. The maps were prepared using an agreed upon colour scheme for continuous permafrost that included: dark brown = buried or ground ice; dark green = ice-cemented permafrost <70 cm; dark purple = ice-cemented permafrost >70 cm (excluding dry-frozen permafrost); dark red = dry-frozen permafrost with an ice-cemented surface below 70 cm. The areal distribution of permafrost by form was determined using a GIS.

## Results

Buried ice comprised 12% of the total permafrost in the TAM and was most abundant in northern Victoria Land. Ice-cemented permafrost, with the surface at <70 cm, comprised 44% of the area and was most abundant in the McMurdo Dry Valleys. Few sites (2%) had the surface of ice-cemented permafrost deeper than 70 cm. These sites were primarily in coastal areas of central Victoria Land. Dry-frozen permafrost occurred in the upper 70 cm in 44% of the TAM. Dry-frozen permafrost is particularly abundant in the Beardmore Glacier region.

## Discussion

The distinction between soils with ice-cemented permafrost <70 cm and dry-frozen permafrost with an ice-cemented surface below 70 cm is based on both direct observation during field work and insights gained during fieldwork. Where there are large areas with no observations we have

used a distance from coast rule to determine the nature of the permafrost, reasoning that soils closer to the coast are likely to have greater moisture recharge and thus ice-cemented permafrost at <70 cm. However, our field observations suggest that ice-cemented permafrost at <70 cm can occur at other locations where soil moisture is being recharged. Examples of recharge areas include land where snow has accumulated in discrete patches in predominantly snow-free regions or land below snow or ice patches which melt producing downslope subsurface flow. Unfortunately, such areas as these are not readily identifiable on the 1:250,000 scale topographic maps. Inland nunataks have generally been allocated dry permafrost form using the a priori reason that they predominantly have very shallow soils over rock or are comprised of rock only.

Because of the large area and relatively sparse density of observations in many locations, the permafrost map is a dynamic document with further contributions welcome following individuals review or field observation in the future.

## Acknowledgments

This work was largely unfunded and conducted by the authors on their own time. One author (MM) received a capability development travel grant from Landcare Research to initiate the work. Anne Sutherland and Craig Briggs are thanked for tireless GIS assistance. We gratefully acknowledge the support of ANTPAS personnel.

## References

Bockheim, J.G. 1995. Permafrost distribution in the Southern Circumpolar Region and its relation to the environment: a review and recommendations for further research. *Permafrost and Periglacial Processes* 6: 27-45.

Bockheim, J.G., Wilson, S.C., Denton, G.H., Andersen, B.G. & Stuiver, M. 1989. Late Quaternary ice-surface fluctuations of Hatherton Glacier, Transantarctic Mountains. *Quaternary Research* 31: 229-254.

Bockheim, J.G., Wilson, S.C., & Leide, J.E. 1990. Soil development in the Beardmore Glacier region, Antarctica. *Soil Science* 149: 144-157.

Bockheim, J.G., Campbell, I.B. & McLeod, M. 2007. Permafrost distribution and active layer depths in the McMurdo Dry Valleys, Antarctica. *Permafrost and Periglacial Processes* 18: 217-227.

Bockheim, J.G. & McLeod, M. 2007. Soil distribution in the McMurdo Dry Valleys, Antarctica. *Geoderma*, doi: 10:10.16/j.geoderma.2007.10.015.

Bockheim, J.G., Campbell, I.B., Guglielmin, M. & López-Martínez, J. 2008. Distribution of types of permafrost and buried ice in ice-free areas of Antarctica.

Claridge, G.G.C. & Campbell, I.B. 1968. Soils of the Shackleton Glacier region, Queen Maud Range, Antarctica. *New Zealand Journal of Science* 11: 171-218.

Denton, G.H., Bockheim, J.G., Wilson, S.C. & Schlűchter, C. 1986. Late Cenozoic history of Rennick Glacier and Talos Dome, northern Victoria Land, Antarctica. In: E. Stump (ed.), *Geological Investigations of Northern Victoria Land*. American Geophysical Union, Antarctic Research Series 46: 339-375.

Guglielmin, M. & French, H.M. 2004. Ground ice in the Northern Foothills, northern Victoria Land, Antarctica. *Annals of Glaciology* 39: 495-500.

Lyons, W.B. & Elliot, D.H. 2006. Transantarctic Mountains Transition Zone Project. *Proceedings of a Workshop on Multi-disciplinary Research in the Central and Southern Transantarctic Mountains.* http://www-bpre.mps.ohio-state.edu/workshops/tam_2006.php.

# Alpine Permafrost Distribution at Massif Scale: Assessment of Mean Surface Temperatures During Winter Equilibrium Period Thanks to Topoclimatic and Geomorphological Data (Combeynot Massif, French Alps)

Xavier Bodin
*University Paris Diderot-Paris 7/Institute of Alpine Geography, Joseph Fourier University, Grenoble, France*
Philippe Schoeneich
*Institute of Alpine Geography, Joseph Fourier University, Grenoble, France*
Monique Fort
*UMR 8586 PRODIG, University Paris Diderot-Paris 7*

## Introduction

Statistical modeling using BTS (Bottom Temperature of the Snow cover; Haeberli 1985) have been attempted by authors (e.g., Hoelzle 1992, Gruber & Hoelzle 2001, Lewkovicz & Ednie 2004) to model mountain permafrost distribution. Field validations generally show good agreement with rock glaciers, which are the most common geomorphological evidences of the permafrost. The main limit of this approach is the necessity of well-distributed BTS data over the studied area.

In the Combeynot massif (Hautes Alpes, France – around 45.0°N, 6.4°E), numerous rock glaciers may be observed on various topoclimatic contexts, whereas BTS datasets are available on some limited areas (Bodin 2007). In order to get a spatialized overview of the surface temperature, and hence of the permafrost presence, a linear relationship between the main topoclimatic parameters (air temperature and solar radiation) and the WEqT is proposed.

## A Spatial Model of the WEqT

*Starting hypothesis*

In order to quantify respective influences of the main parameters, the following hypotheses are made:

- The WEqT is equal to the mean annual air temperature (MAAT), to which is added, or subtracted, the influences of the solar radiation and the debris cover.
- The thermal influence of the solar radiation (α), positive, is linearly related to the potential solar incoming radiation (PSIR) during summer (June–July–August) and proportional to the PSIR/PSIRmax ratio.
- The thermal influence of the openwork debris mantles (β) is negative and, on yearly average, homogeneous independently of other factors.
- For similar topoclimatic conditions, WEqT is equal from one place to the other.

*Parameterization of the linear model*

Within the linear model of WEqT, the α and β parameters were parameterized by minimizing the sum of residuals in two steps:

1. First, for rock glaciers with topoclimatic conditions close to those of the root of the Laurichard rock glacier, where BTS in 2004 shows a mean WEqT of -3.44°C. Due to very low PSIR, α was minimal, and the adjustment led to β = -3.9°C.

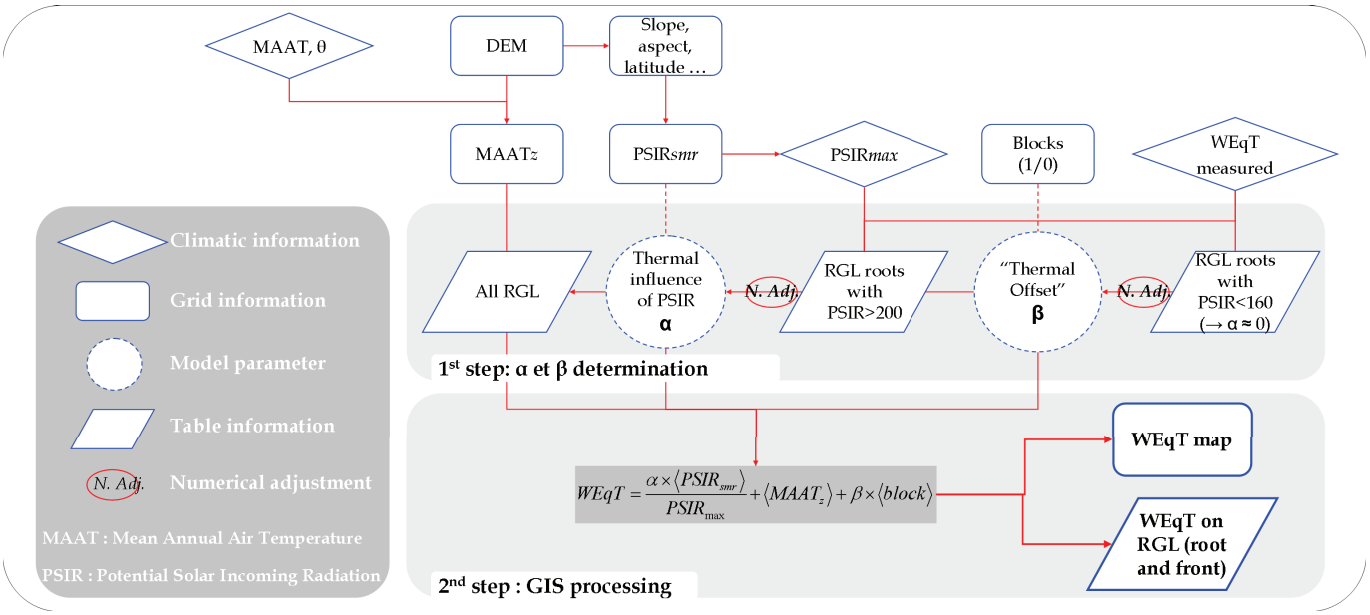


Figure 1. Processing steps (1 = calibration of α and β by numerical adjustment; 2 = GIS processing) to model WeqT.

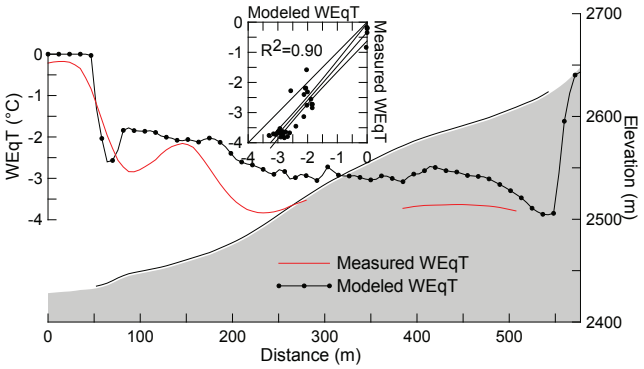


Figure 2. Comparison between modeled WEqT and measured BTS on the Laurichard rock glacier (Combeynot Massif, Hautes Alpes, France).

2. Second, for locations with high PSIR and using the previously defined β, the BTS values of the Pradieu Valley give α = 2.9°C.

The flow chart of the model describes the different datasets used and the main steps of the process (Fig. 1).

## Results at Different Spatial Scales

*The Laurichard rock glacier case*

A first validation of the model is given by comparing the extrapolated WEqT to the measured BTS on the whole surface of the Laurichard rock glacier.

The model correctly reproduces the measured BTS on the rock glacier (Fig. 2), and suggests that the general trend of the WEqT is, at this scale, visibly driven by the solar radiation received during summer.

*The WEqT on the rock glaciers of the Combeynot Massif*

The mean modeled WEqT at the rooting zone of the rock glaciers of the Combeynot massif amounts to -3.4°C, whereas it reaches -2.9°C at the front of the landforms. Some fronts, nevertheless, are located on warmer conditions, mainly when glacier is or has been, historically, present on the rooting area.

## Conclusion

A statistical model of the WEqT has been presented in which the influences of solar radiation and coarse debris presence have been adjusted thanks to BTS measurements. Though local processes (e.g., permafrost creeping) or influences of other parameters (e.g., snow) are not taken into account, the validation of the model on the Laurichard rock glacier encourages the use of this kind of topoclimatic approach for permafrost study at massif scale.

## Acknowledgments

This work was funded by the French Ministry of Education and Research. S. Gruber (Univ. of Zürich) is greatly acknowledged for running the TEBAL model to get the PSIR map of the Combeynot massif, as well as for his advice concerning the presented model.

## References

Bodin, X. 2007. *Géodynamique du pergélisol de montagne : fonctionnement, distribution spatiale et évolution récente. L'exemple du massif du Combeynot (Hautes Alpes)*. PhD, University of Paris-Diderot Paris 7, 274 pp.

Gruber, S. & Hoelzle, M. 2001. Statistical modeling of mountain permafrost distribution: local calibration and incorporation of remotely sensed data. *Permafrost and Periglacial Processes* 12(1): 69-77.

Haeberli, W. 1973. Die Basis-Temperature der winterlichen Schneedecke als möglicher Indikator für die Verbreitung von Permafrost in den Alpen. *Zeitschrift für Gletscherkunde und Glazialgeologie* 9: 221-227.

Hoelzle, M. 1992. Permafrost occurrence from BTS measurements and climatic parameters in the Eastern Swiss Alps. *Permafrost and Periglacial Processes* 3: 143-147.

Lewkovicz, A.G. & Ednie, M. 2004. Probability mapping of mountain permafrost using the BTS method, Wolf Creek, Yukon Territory, Canada. *Permafrost and Periglacial Processes* 15: 67-80.

# Cryogenic Formations of the Caucasus and the Significance of Their Impact on the Natural Phenomena of the Region

Igor V. Bondyrev
*Vakhushti Bagrationi Institute of Geography, Ministry of Education and Sciences of Georgia, Tbilisi*

Cryogenic or periglacial phenomena are widespread within the high mountain Caucasian region. The modern area of spreading cryogenic processes on the south slope of the Central Caucasus (Georgia) forms 3300 km$^2$ and within the Republic of North Osetia-Alanya, 5400 km$^2$, but in Kabardino-Balkaria, 4600 km$^2$ (1, 2). These processes are widely spread as well on the territory of the Pontides Mountains and the Iranian upland, covering 14,200 km$^2$. The set of factors defining the genesis and morphology of the forms of periglacial relief changes depending on the height of the area. Three hypsometric levels are singled out:

1. The upper belt occupies the whole area of the nival zone and is limited from underneath by snow line lying at the height of 3000–3200 m a.s.l. Frost weathering and gravitational talus processes, which play the leading role in formation of present-day relief forms, take place here.

2. The middle belt is situated below snow line and practically coincides with the alpine and sub-alpine landscape zones (1750–2300 m). Here prevail slope (solifluction, rock-streams, stone and snow avalanches, talus trains, mud flows, etc.) and plane (polygonal-structural groundboulder pavement, thufurs).

3. Relict cryogenic formations (fluvioglacial deposits, cryoturbation, etc.) are spread in the lower belt down to 1400–1600 m a.s.l.

The given formations are characterized by the following regularities of their spatial distribution:

1. Formations related to rocky ground occupy the belt of tops, ridges of watersheds, and steep slopes of high mountains.

2. Formations related to rudaceous ground and pebbles are mainly placed on gentle slopes and at the foot of mountain ridges and massifs within 2700–1900 m a.s.l.

3. Formations related to fine detrital and rock debris are well observed on the high mountain plateaus in the zone of Neocene-quaternary volcanism.

4. Formations related to loamy and turf/soddy surfaces cover quite a large area, mostly alpine and sub-alpine meadows and alluvial soils of high mountain zones (see the scheme of classification of periglacial formations of the Caucasus).

Widespread morainic mantles and sheets and gravitational talus processes define the existence of numerous "fossil" glaciers (dead ice), on their part testifying to the regression of the glaciation process. The value of seasonal freezing of ground soil is an important feature for determining main relief-forming processes in high mountains. Information on these parameters helps with decisions about engineering-geological, building, agro-biological, and other problems. We offered theoretical determination for the values of seasonal freezing depth for different points in periglacial areas in Georgia, having minimum information on those areas. For this purpose, the formula of Budnikov was used with some amendments of ours on the high-mountainous relief character, the height of snow cover, and influence of wind (2, 3, 6, 8). Comparison of meteorological yearbook records of the Hydrometeorological Institute of Georgia with ours on the depth of seasonal freezing showed little discrepancy (not more than 3–6 cm). The gained records are well founded only for subhorizontal surfaces deprived of mantle and vegetative cover, with similar mechanical composition and equal humidity value. Calculations were carried out per formula:

$$h_{np} = 5k\left[\sqrt{Tn - \frac{50\ell\left(n_1 + L\right)}{t\sqrt{H \cdot V}}}\right] \qquad (1)$$

Table 1. Experimental evaluation of the rate of frosty weathering of mountain rocks (5).

| Number of version | Mean amplitude of temperature fluctuation during the experiment | Area of frozen surface (sm$^2$) | Initial weight of sample (r) | Weight of frozen sample | Number of "freezing-thawing" cycle | Weight of disintegrated particles | Velocity of disintegration of frozen surface a day/gr/m$^2$.a day/ | Velocity of disintegration/ mm/year/ |
|---|---|---|---|---|---|---|---|---|
| 1 – over-moistured | 28.2°C | 22.56 | 31.70 | 31.74 | 80 | 0.73 | 4.0514 | 0.288 |
| 2 – dry | | 31.34 | 41.10 | 41.47 | 80 | 0.07 | 0.2819 | 0.040 |
| 3 – over-moistured | | 34.23 | 41.94 | 42.03 | 70 | 0.53 | 2.2079 | 0.672 |
| 4 – dry | | 37.84 | 25.19 | 25.45 | 70 | 0.10 | 0.3790 | 0.047 |

where $\sqrt{Tn}$ = Budnikov formula, $k$ = lithological coefficient, provisionally equal to unity, $T$ = mean air temperature during winter, $t$ = mean ground surface temperature during winter, $n$ = longness of the period with temperature below zero, $n_1$ = the same with temperature above zero during winter, $H$ = area altitude above sea level, $V$ = winter wind mean velocity (m/sec), $L$ = thickness of snow cover /average for winter (3).

Therefore, we have conducted a number of experiments studying the rate of frosty weathering in different types of rock. With this purpose different types of rock were taken. Core sample No. 1 was taken from the well on Tbilisi site and represents carbonate fine-grained rock of Eocene age (marl), taken at a 2574–2580 m depth. The other sample was a monolith of andezite-dacitic lava (SiO2-50%) from the top of Emlikli massif (2750–2800 m a.s.l., Southern Georgia).

The conditions similar to those of high mountain natural conditions were specially created. Experiments went on for 31 days.

About 315 regimes of "freezing-thawing" changed one after another. As a result, it became possible to find the decisions of such issues as estimation of the rate of disintegration of mountain rocks under frosty weathering. Data are given in Table 1, estimating the rate of frosty weathering of separate units depending on the lithology of mountain rocks and extent of their moistening.

## References

Bondyrev, I.V. & Maisuredze, G.M. 1978. Some particularities of dynamics, morphogenesis and spatial distribution of frozen ground in the Caucasus. In: *Cryogenic Phenomena in High Mountains*. Novosibirsk: Nauka, 43-59

Bondyrev, I.V. 1987. Main problems of study and development of high mountain regions in Georgia, Tbilisi: GruzNIINTI, 72 pp.

Bondyrev, I.V., Tatashidze, Z.K., Singh, V.P., Tsereteli E.D. & Yilmaz, A. 2004. Impediments to the sustainable development of the Caucasus-Pontdes region: New global development. *Journal of International & Comparative Social Welfare* Twentieth Anniversary Special 20(1): 33-48

Bondyrev, I.V., Tatashidze, Z.K. & Tsereteli, E.D. 2004. Actual ecological situations in the territory of mountain regions and biodiversity problems (the case of Georgia). *NATO ARW Seminar: Environmental Security and Sustainable Land Use of Mountain and Steppe Territories of Mongolia and Altay, Barnaul, Russia, October 25–27, 2004*: 89-98.

# Modeling Potential Climatic Change Impacts on Mountain Permafrost Distribution, Wolf Creek, Yukon, Canada

Philip P. Bonnaventure, Antoni G. Lewkowicz
*Department of Geography, University of Ottawa, Ottawa, Canada*

## Introduction

Differences in air temperature, precipitation, and vegetation cover that develop across hundreds of kilometres in lowland areas can be generated by a few hundred metres of elevation change in mountainous regions. Consequently, a mountain basin located in the discontinuous permafrost zone may span the entire range of permafrost conditions, from isolated patches at low elevations on north-facing slopes to continuous permafrost on summits (Lewkowicz & Ednie 2004). It is reasonable to infer that within such a basin there will be terrain present at temperatures close to 0°C that can be affected by changes in climate. If unfrozen, this terrain may become permafrost during sustained climate cooling, or if permafrost, it may thaw during sustained warming or long-term increases in snow depths. Consequently, mountain basins with permafrost may be particularly sensitive to climate change. However, the complexity of permafrost distribution within them means that there have been relatively few attempts to model climate change impacts (e.g., Janke 2005). Our goal here is to present a method that can be used to explore the potential effects of past and future climate change on mountain basins with permafrost.

## Study Area

Wolf Creek Basin (60°30′N, 135°10′W) is a mountainous watershed of approximately 190 km$^2$, with elevations ranging from 700–2080 m a.s.l. and located 20–30 km south of Whitehorse in the Yukon Territory. The climate is continental with dry, cold conditions (Wahl et al. 1987), and the basin falls within the zone of sporadic, discontinuous permafrost zone according to the Permafrost Map of Canada (Heginbottom et al. 1995). Basin vegetation comprises boreal forest, with sub-alpine forest, a shrub zone, and an alpine tundra zone at progressively higher elevations. Under current conditions, permafrost probability models in Wolf Creek indicate that 38 to 43% of the area is underlain by permafrost (Lewkowicz & Ednie 2004, Lewkowicz & Bonnaventure 2008).

## Methodology

BTS measurements were collected in Wolf Creek during the winters of 2001 and 2002 (Lewkowicz & Ednie 2004). The spatial field of BTS was modeled in a GIS using elevation and Potential Incoming Solar Radiation (PISR) as independent variables. Logistic regression was used to relate the modeled BTS temperatures to the presence or absence of permafrost at numerous sites within the basin in late-summer. The end result of this procedure is a map of permafrost probability at a grid cell resolution of 30 x 30 m.

The effects on permafrost distribution of climate cooling or warming scenarios can be simulated by respectively increasing or decreasing the values of the elevation throughout the study area (Janke 2005). This alters the modeled BTS field which in turn affects the predicted permafrost probabilities. We used a standard environmental lapse rate of 6.5°C/1000 m to calculate the necessary change of elevations, a value which is less than the BTS lapse rate (8.2°C/1000 m) (Lewkowicz & Bonnaventure 2008). Temperature changes of -2 to +5°C were used in order to examine how permafrost distributions might have appeared under equilibrium conditions similar to those of the Little Ice Age, when temperatures in the basin were lower (e.g., Farnell et al. 2004), and for future changes through to the most aggressive temperature warming scenarios proposed by the Intergovernmental Panel on Climate Change (IPCC 2007). As in previous work, we assume that permafrost probability can be equated over many grid cells to permafrost extent.

## Results and Discussion

It should be emphasized that model predictions are for equilibrium states; the model does not account for lag times associated with permafrost formation and degradation. Given these lag effects, the model outputs are best thought of as referring to the upper few metres of permafrost only.

Under cooler-than-present conditions, permafrost area within the basin expands, doubling to about 75% for a temperature reduction of 2°C. The form of the change is approximately linear within this range (Fig. 1). Spatially, permafrost zones become more extensive at intermediate elevations and the boundary between continuous and extensive discontinuous permafrost (90% probability) descends from about 1600 m to 1250 m, while that between extensive and sporadic permafrost (50% probability) changes from 1400 to 1100 m.

Under warming conditions, such as those expected under IPCC projections, permafrost extent is substantially reduced in a nonlinear fashion. An increase of only 1°C halves the permafrost extent in the basin, and a further 1°C change reduces it to less than 10% of the basin area (Fig. 1). Boundaries of permafrost zones within the basin move upwards so that a 1°C change causes the continuous permafrost boundary to rise to 1700 m. At an increase of 2°C, permafrost is present only on high elevation mountain tops and upper elevation north-facing slopes. A 4°C increase reduces permafrost extent to less than 1% of the basin area, and probabilities exceed 10% only on the highest mountain peaks above 1850 m.

The changing slope of the line in Figure 1 relates to the hypsometry of the basin (Fig. 2). The elevation zones with the most area occur from 1200–1500 m a.s.l., and these have intermediate permafrost probabilities under the current climate. Cooling enhances permafrost probability in these extensive zones, and permafrost also moves downwards into lower terrain. Even a warming of 1°C reduces probability substantially in these extensive areas. For large increases in temperature, permafrost is confined to the highest peaks which occupy only a small part of the basin, so there is little further loss as warming continues.

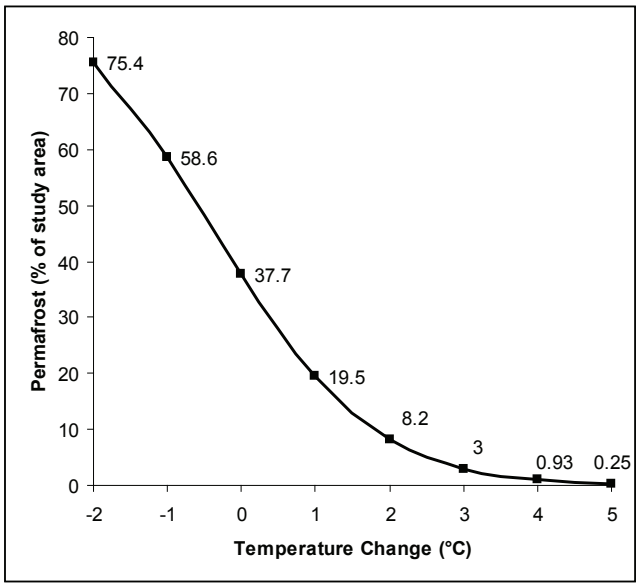


Figure 1. Predicted percent of Wolf Creek basin underlain by permafrost for climate change scenarios of -2 to +5°C.

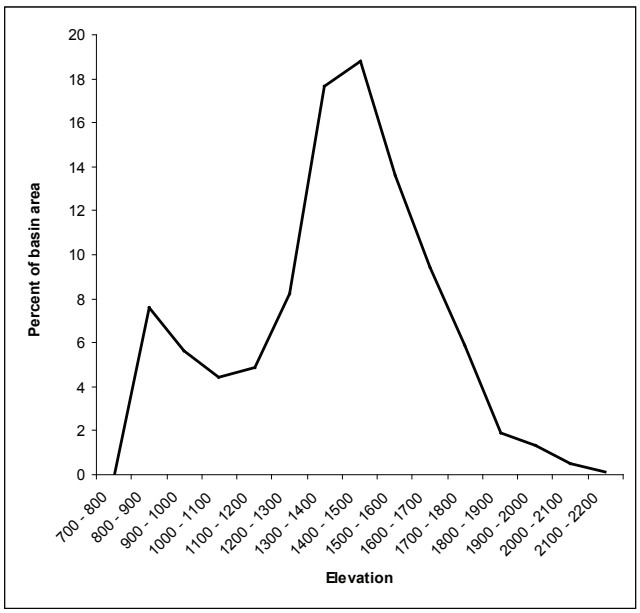


Figure 2. Hypsometric curves illustrating the percent area of Wolf Creek basin in each elevation band.

## Conclusions

This simple equilibrium modeling indicates that substantial change in permafrost extent has probably occurred in Wolf Creek since the Little Ice Age, and loss of permafrost can be expected as the climate warms. Mountain permafrost is highly sensitive to climatic change as ground thermal conditions vary spatially, and thus there is always permafrost on the point of thaw (warming scenarios) or nonpermafrost areas ready to become perennially frozen (cooling scenarios). Although not shown here, the modeling produces a spatial field of permafrost probabilities that may be useful for purposes such as distributed hydrological modeling or hazard mapping.

## Acknowledgments

Funding was provided by NSERC, the Canadian Foundation for Climate and Atmospheric Sciences, the Yukon Geological Survey, the Geological Survey of Canada and the University of Ottawa.

## References

Bonnaventure, P.P. & Lewkowicz, A.G. Mountain permafrost probability mapping using the BTS method in two climatically dissimilar locations, northwest Canada. *Canadian Journal of Earth Sciences* (in press).

Farnell, R., Hare, P.G., Blake, E., Bowyer, V., Schweger, C., Greer, S. & Gotthardt, R. 2004. Multidisciplinary investigations of alpine snow patches in southwest Yukon. *Arctic* 57: 247-259.

Heginbottom, J.R., Dubreuil, M.A. & Harker, P.T. 1995. Canada Permafrost. (1:7,500,000 scale). In: *The National Atlas of Canada*, 5th ed., sheet MCR 4177. Ottawa: National Resources Canada.

Janke, J.R. 2005. Modeling past and future alpine permafrost distribution in the Colorado Front Range. *Earth Surface Processes and Landforms* 30: 1495-1508.

IPCC. 2007. http://www.ipcc.ch/ipccreports/assessments-reports.htm.

Lewkowicz, A.G. & Bonnaventure, P.P. 2008. Interchangeability of mountain permafrost probability models, Northwestern Canada. *Permafrost and Periglacial Processes* 19 (in press).

Lewkowicz, A.G. & Ednie, M. 2004. Probability mapping of mountain permafrost using the BTS method, Wolf Creek, Yukon Territory, Canada. *Permafrost and Periglacial Processes* 15: 67-80.

Wahl, H.E., Fraser, D.B., Harvey, R.C. & Maxwell, J.B. 1987. *Climate of Yukon.* Canadian Government Publishing Centre.

# A Hypothesis: A Condition of Growth of Thick Ice Wedges

Anatoli Brouchkov
*Tyumen State Oil and Gas University*

So-called Ice Complex or "edoma" in Siberia, which represents extremely ice-rich and perennially-frozen sediments with thick polygonal ice wedges, is formed in territories acting as terrestrial accumulation basins during the Pleistocene. It sometimes consists of more than 90% ice by volume. Simplifying, a decrease of temperature causes soil to shrink and cracks to form; then water seeps into the cracks in spring. It freezes and expands when it is chilled by permafrost. This cycle continues to enlarge the wedges year by year until the soil above the wedges is pushed up and finally almost disappears around. However, details of the mechanism of thermal contraction cracking and ice wedge formation still remain unclear (French 1996). Ice is known to be able to flow under loads, and it probably could be easier for ice to be pressed up than for soil. Why do we observe the result of soil pushing up only, not ice, and what is the mechanical condition of the process?

Water freezing and expanding when it is chilled by permafrost can be expressed by the Clapeyron equation. Stresses can be estimated approximately as 13.4 MPa per a decrease in negative temperature by 1°C. In the case of mechanical equilibrium, if horizontal stresses $\sigma_z$ are equal in soil and ice, the heaving strain of about 9% of volume of freezing water $\varepsilon_f$ is connected to mechanical compression of frozen soil ($d\sigma_z * l_{fr}/E_{fr}$) and ice ($d\sigma_z * l_{ice}/E_{ice}$), being of $l_{fr}$ and $l_{ice}$ in size and having the strain modulus $E_{fr}$ and $E_{ice}$, respectively:

$$d\sigma_z = \frac{d\varepsilon_f}{\frac{l_{fr}}{E_{fr}} + \frac{l_{ice}}{E_{ice}}} \quad (1)$$

If, for example, $\varepsilon_f$ is 0.0045 m as a result of freezing of 0.05 m of water, $l_{fr}$ = 5 m and $l_{ice}$ = 0.5 m, and the long-temp compression modulus $E_{fr}$ = 20 MPa and $E_{ice}$ = 50 MPa, then stress $\sigma_z$ = 0.017 MPa. In many cases, the value of $\varepsilon_f$ is even less then 0.05 m; for example 0.001–0.003 m only in Barrow (Black 1951), and 0.002–0.01 m in Kolyma plain (Berman 1965). Due to higher modulus values, compression of soil reaches 4.33 and ice 0.17 mm consequently. The size of the deformed soil area varies, for example, near Fairbanks in the range of 0.3–3 m (Pewe 1962). The lateral strains depending on Poisson's ratio will be less than compression, but probably they will be more for soil than for ice. Stresses are small and perhaps unable to make considerable structural changes of soil mass. Repeating a thousand times, it results in ice wedge thickness of about 4 m. This is generally in agreement with the point that soil is pushed up during ice wedge formation. However, it was found that soil layers at a certain distance from the ice wedge are almost not affected (Popov 1965).

An area of high density of deformed soil should be created on contact with an ice wedge to give space to ice, and that area should be gradually increased in size in accordance with an increase of wedge thickness. One reason for the deformed area to remain small is the stress distribution in soil mass. The stresses are basically not equal and become smaller with distance from an ice wedge. Using $q$/unit length on the surface of a semi infinite soil mass, or if the excess stress is according to the Boussinesq equation (Ahlvin & Smoots 1988), the stress can be found approximately:

$$\Delta\sigma_z \sim \frac{\sigma_z}{z^n} I \quad (2)$$

where $n$ changes from about 1 to 2, $I$ = influence factor for the load, and $z$ = distance from the ice wedge. Formula (1) should be adjusted then according (2). If horizontal stress $\sigma_z$ = 0.017 MPa near an ice wedge, it is about $\sigma_z$ = 0.004 MPa only on distance of 2 m. Thus, stresses might be too small to cause deformations far from the ice wedge, but they are big enough to move soil particles and pore ice near the ice wedge. Another reason for the deformed area to be small is perhaps because of gradual movement of attached ice soil towards the surface together with ice caused by pressure and buoyancy.

Signs of diapirism and soil circulation are widespread in periglacial areas (Hallet & Waddington 1991). Buoyancy can be an effective driving force in the case of ice wedges due to different densities of frozen soil (1.5–1.7 and more cm$^3$/g) and ice (0.9–1 cm$^3$/g). If the size of polygons are more than or equal to the height of an ice wedge $h$, and the viscosity of ice $\eta_i$ is much less than the viscosity of the surrounding soil $\eta_s$, the rate of vertical movement of an ice wedge wall $\upsilon$ will be (Artyushkov 1969):

$$\upsilon \sim \frac{\Delta\rho g h^2}{\eta_s} \quad (3)$$

where $\Delta\rho$ = difference of densities of soil and ice; $g$ = gravity acceleration, 9.81 m/sec; $\eta_s$ = viscosity of surrounding soil, Pa*s. However, the assumption that the viscosity of ice is less than the viscosity of the surrounding soil is far from being acceptable: relationship is opposite. The ice viscosity can be assumed as $10^{12}$–$10^{13}$ Pa*s, and frozen soil viscosity as $10^{10}$–$10^{11}$ Pa*s. The buoyancy of an ice wedge and its vertical movement $z$ can still be found from the similar Navier-Stoks equation:

$$z \sim vt \sim \frac{\Delta\rho g l^2}{18\eta_s} t \quad (4)$$

where $t$ = time; $l$ = width of ice wedge. If the width of the ice wedge $l$ = 1 m, and time $t$ is 1000 years, then resurfacing of ice can reach about 1.5 m. That value of vertical movement may change the shape of ice wedges drastically, especially in saline or high-temperature permafrost. Vertical orientation of

rod-shaped air bubbles (Kurdyakov 1965), "echelon breaks" (Pewe 1962), and the foliated structure of ice can serve as indirect evidence of it. Sometimes soil layers near an ice wedge look like they are "drawing in ice" (Pewe 1962). Flexures of soil layers near ice wedges are mostly directed up (Popov 1965) probably because of vertical ice flow. Unusual deformations of soil layers under an ice wedge, described by Kostyaev (1965) in the Yana River terrace, can also be a result of buoyancy. Ice wedges flowing upward 1–3 m, like diapers, were described by Black (1983).

Therefore, the thick ice wedges can be formed easier in conditions of low values of the soil creep threshold $\sigma_0$ and their higher deformability; it is a condition of their growth by the cracking-fullfiling-freezing mechanism. Stresses induced by freezing are small and perhaps unable to make considerable structural changes of soil mass. However, creep threshold $\sigma_0$ values of frozen saline soil are low, and that gives a vital reason for wide distribution of thick ice wedges in regions of saline permafrost. Ice is able to flow at any stress, and should be flowing up during ice wedge formation. A number of features appears to be created during the evolution of ice wedge shape due to the flow; among them irregular shapes of underground ice are common. Buoyancy can be another effective driving force in the case of ice wedges due to the difference of densities of frozen soil and ice. An estimation shows the buoyancy of ice can reach substantial values.

## References


Ahlvin, R.G. & Smoots, A.V. 1988. Construction *Guide for Soils and Foundation*. New York: John Wiley & Sons.

Artyushkov, E.V. 1969. About pressing of ice-wedges by surrounded deposits. In: *Problems of Cryolithology*, Issue 1. Moscow University Press, 34-37 (in Russian).

Berman, L.L. 1965. Underground ice in northern part of Kolyma plain. In: *Underground Ice,* Issue 1. For the 7th International Congress on Quarternary (INQUA), USA. Moscow University Press, 112-119 (in Russian).

Black, R.F. 1951. Structure in ice wedges of Northern Alaska. *Geol. Soc. Am. Bull*. 62, Pt. 2.

Black, R.F. 1983. Three superposed systems of ice wedges at McLeod Point, northern Alaska, may span most of the Wisconsian stage and Holocene. *Proceedings of the Fourth International Conference on Permafrost, July 17–22, 1983.* Washington, DC: National Academy Press, 68-73.

French, H.M. 1996. *The Periglacial Environment,* 2nd ed. Longman, Harlow, 1-341.

Hallet, B. & Waddington, E.D. 1991. Buoyancy forces induced by freeze-thaw in the active layer: Implications for diapirism and soil circulation. In: J.C. Dixon & A.D. Abrahams (eds.), *Periglacial Geomorphology*. John Wiley and Sons Ltd., 251-279.

Kostyaev, A.G. 1965. Ice wedges and convective instability of soils. In: *Underground Ice*, Issue 1. For the 7th International Congress on Quarternary (INQUA), USA. Moscow University Press, 133-140 (in Russian).

Kurdyakov, V.S. 1965. Polygonal ice-wedges in Amguema river basin. In: *Underground Ice,* Issue 1. For the 7th International Congress on Quarternary (INQUA), USA. Moscow University Press, 87-103 (in Russian).

Pewe, T.L. 1962. Ice wedges in permafrost, Lower Yukon river near Galena Alaska. *Biuletyn Peryglacjalny* 11. Lodz.

Pewe, T.L. 1966. Ice wedges in Alaska: Classification, distribution and climatic significance. *Proceedings of the First International Conference on Permafrost.* National Academy of Science: National Research Council of Canada, Publication 1287, 76-81.

Popov, A.I. 1965. Underground ice. In: *Underground Ice*, Issue 1. For the 7th International Congress on Quarternary (INQUA), USA. Moscow University Press, 7-39 (in Russian).

# Modeled Continual Surface Water Storage Change of the Yukon River Basin

Rena Bryan
Larry D. Hinzman
Robert C. Busey
*International Arctic Research Center, University of Alaska Fairbanks, Fairbanks, Alaska, USA*

## Introduction

Climate change in high latitudes, occurring at an observable pace, provides a window into changes the rest of the earth may experience over a longer time scale (Shaver et al. 1992). Large-scale datasets of surface water, groundwater, and permafrost dynamics serve as prerequisites in a variety of other analyses and applications (Lehner et al. 2008). This study models continual surface water storage change in the Yukon River Basin. The project is the underpinning for carbon dioxide and methane flux; taiga-tundra shift; regional surface energy balance; regional weather pattern; migratory waterfowl habitat availability; and infrastructure, building, and community stability studies.

The purpose of this study is to determine how the future surface water storage of the Yukon Basin will compare to present. The project considers the changes to surface water storage as affected by warming climate, permafrost degradation, and the vertical flux of water, but ignores changes induced by altered evapotranspiration or lateral flow. Transition from birch forests to fens and bogs has been documented over the last twenty years in the Tanana Flats (Jorgenson et. al. 2001). Also in the last twenty years, thermokarst lakes developed and initiated large taliks that completely penetrated the permafrost near Council, Alaska. As a result, drier environments than before exist near Council (Yoshikawa & Hinzman 2003). In areas of discontinuous permafrost, where projected permafrost will be warm enough to degrade, (1) if the local hydraulic gradient is upwards, the surface will be inundated with water and (2) if the hydraulic gradient is downwards, existing surface water will drain. In areas of continuous permafrost, where projected permafrost will be warm enough to degrade, the surface will subside and surface ponds may increase. To investigate this hypothesis, we utilize synoptic meteorology, permafrost thermal composition, and potentiometric surface algorithms.

*Background*

According to the International Permafrost Association *Circum-Arctic Map of Permafrost and Ground-Ice Conditions* (Brown et al. 1998), discontinuous permafrost dominates the interior of the basin. Continuous permafrost is second most prominent and present in the northern rim of the basin and at Yukon-Kuskokwim Delta. Sporadic permafrost exists in southern Yukon Territory. Isolated permafrost can be found sparsely in the glaciated region at the river's source. Closer examination of local variation in vegetation, soil moisture and thermal properties, and snow cover produces finer resolution permafrost thermal composition (Smith & Riseborogh 1996). Continuous permafrost, frozen ground (0°C and below) in spatial continuity, provides an impervious barrier to groundwater movement. Because of overall permafrost stability, much of the Arctic is spotted by ponds perched above the permafrost. Most groundwater-surface water interactions occur in areas of discontinuous permafrost. In areas where the hydraulic gradient is downwards, as the confining layer of permafrost degrades and an open talik forms, surface water formerly underlain by permafrost can drain into the subpermafrost groundwater. In contrast, where the local hydraulic gradient is upwards, subpermafrost groundwater may discharge at the surface.

*Methods*

Referencing topographic features, the weather forecast model, National Weather Service Global Forecast System, is synoptically represented and accounts for topographically driven processes. TopoClimate is developed at the International Arctic Research Center, University of Alaska Fairbanks by Atkinson and Gourand. Driven by high-resolution surface air temperatures available from TopoClimate, the TTOP model is a numerical model using surface n-factors, bulk thermal conductivities, and freezing and thawing indices. TTOP was originally developed by Smith & Riseborough (1996) (Busey et al. 2008). The model is applied to estimating the permafrost thermal composition in the Yukon Basin. Extracting steepness and relative elevations from the digital elevation model, modeled potentiometric surfaces generate a hydraulic gradient map. (1) The surface air temperature, (2) permafrost thermal composition, and (3) hydraulic gradient maps in concert assess surface water storage change. This study reviews existing observations of spring, aufeis, and lake size and distribution change locations in order to calibrate the model. Remote sensed imagery analysis has defined some areas of lake change. Thermal conductivity, thermokarst, and $\delta\ ^{18}O$ field observations validate the model. Thermal conductivity measurements and thermokarst documentation validate permafrost thermal composition modeled by TTOP and permafrost destabilization. The $\delta\ ^{18}O$ values from lakes with a deep groundwater component are distinct from those lacking connection to the groundwater. Lakes possessing a deep groundwater component as revealed by isotope analysis validate the hydraulic gradient model. Model validation data will be collected in Innoko National Wildlife Refuge, Yukon Flats National Wildlife Refuge, and locations throughout the road system of Alaska and the Yukon Territory.

*Implications to surface water storage change*

Projecting ecosystem dynamics will moderate concerns and help us plan for a warming Arctic and its effects on

the rest of the globe. Drying of soils allows increased $O_2$ levels to penetrate the soil deeper and may therefore increase the release of $CO_2$ to the atmosphere (Oechel et al. 2000). Expansion of thaw lakes due to thawing of permafrost, increasing the expanse of waterlogged soils, may increase the release of $CH_4$ into the atmosphere (Walter et al. 2006). Closer examination of the taiga-tundra ecotone reveals a more complex situation than the simple northward migration of trees in response to warming (Skre et al. 2002). Permafrost thawing, surface water drainage, and drying of soils in areas of low precipitation are likely to lead to a shift to grassy tundra vegetation (Callaghan et al. 2004). Wet systems of relatively continental climates, for example wet sedge tundra, experience high evapotranspiration, cool surface, and, therefore, a high latent heat flux. Dry systems, for example dry heath, have a warm surface and experience high sensible heat flux (McFadden 1998). The regional surface energy balance forces regional weather patterns. Global climate change is made up of long-lasting regional weather changes. Habitat for migratory waterfowl, affected by the availability of surface water, is an issue of concern to wildlife managers. This is also a region where societal impacts are acute. Town and village infrastructure will likely experience a variety of changes due to permafrost and surface water changes. Changes in permafrost cause the pavement to heave and slump on Farmers Loop Road in Fairbanks, and uncontrolled flow from wells damaged houses in the same area. This area of upwelling holds potential danger. Traditional travel routes, berry picking, and hunting places are likely to be affected.

## Acknowledgments

Support for this research is provided by the U.S. National Science Foundation (Grant No. 0327664).

## References

Brown, J., Ferrians Jr., O.J., Heginbottom, J.A. & Melnikov, E.S. 1998. Revised February 2001. *Circum-Arctic map of permafrost and ground-ice conditions.* Boulder, CO: National Snow and Ice Data Center/World Data Center for Glaciology. Digital Media.

Busey R.C., Hinzman, L.D., Cassano, J.J. & Cassano, E. 2008. Permafrost distributions on the Seward Peninsula: Past, present, and future. *Proceedings of the Ninth International Conference on Permafrost, Fairbanks, Alaska, June 29–July 3, 2008.*

Callaghan, T.V., Björn, L.O., Chernov, Y., Chapin, T., Christensen, T.R., Huntley, B., Ims, R.A., Johansson, M., Jolly, D., Jonasson, S., Matveyeva, N., Panikov, N., Oechel, W., Shaver, G., Schaphoff, S. & Sitch, S. 2004. Effects of changes in climate on landscape and regional processes, and feedbacks to the climate system. *Royal Swedish Academy of Sciences Ambio* 33(7): 459-468.

Jorgenson, M.T., Racine, C.H., Walters, J.C. & Osterkamp, T.E. 2001. Permafrost degradation and ecological changes associated with a warming climate in central Alaska. *Climatic Change* 48: 551-579.

Lehner, B., Verdin, K. & Jarvis, A. 2008. New Global Hydrography Derived from Spaceborne Elevation Data. *EOS* 89(10): 93-94.

McFadden, J.P., Chapin III, F.S. & Hollinger, D.Y. 1998. Subgrid-scale variability in the surface energy balance of arctic tundra. *Journal of Geophysical Research* 103: 28,947-28,961.

Oechel, W.C., Vourlitis, G.L., Hastings S.J., Zulueta R.C., Hinzman, L.D. & Kane, D.L. 2000. Acclimation of ecosystem $CO_2$ exchange in the Alaskan Arctic in response to decadal climate warming. *Nature* 406: 978-981.

Shaver, G.R., Billings, W.D., Chapin III, F.S, Giblin, A.E., Nadelhoffer, K.J., Oechel, W.C. & Rastetter E.B. 1992. Global Change and the Carbon Balance of Arctic Ecosystems. *BioScience* 42(6): 433-441.

Skre, O., Baxter, R., Crawford, R.M.M., Callaghan, T.V. & Fedorkov, A. 2002. How will the tundra-taiga interface respond to climate change? *Swedish Royal Academy of Sciences, Ambio Special Report* 12: 37-46.

Smith, M.W. & Riseborough, D.W. 1996. Permafrost monitoring and detection of climate change. *Permafrost and Periglacial Processes* 7: 301-310.

Walter, K.M., Zimov, S.A., Chanton, J.P., Verbyla, D. & Chapin III, F.S. 2006. Methane bubbling from Siberian thaw lakes as a positive feedback to climate warming. *Nature* 443(7107): 71-75.

Yoshikawa, K. & Hinzman, L.D. 2003. Shrinking thermokarst ponds and groundwater dynamics in discontinuous permafrost near Council, Alaska. *Permafrost and Periglacial Processes* 14: 151-160.

# Freeze/Thaw Properties of Tundra Soils, with Applications to Trafficability on the North Slope, Alaska

Christina F. Bryant
*Geo-Watersheds Scientific, College Station, USA*
Ron F. Paetzold
*Geo-Watersheds Scientific, College Station, USA*
Michael R. Lilly
*Geo-Watersheds Scientific, Fairbanks, USA*

## Introduction

This abstract focuses on the application of soil temperature profile data and its relationship to tundra-travel management on the North Slope of Alaska, with particular attention to winter travel. Current standards regulate tundra-travel on the North Slope of Alaska to conditions at or below -5°C at a depth of 30 cm in the soil profile (Bader 2005). These regulations are meant to ensure adequate soil strength for such activities. Additionally, six inches of snow cover is needed in the Coastal Plain region for tundra-travel to be open.

Frozen water affects tundra soils through added strength from the addition of solids (ice) in soil pore spaces, which decreases slipping between soil particles. Soil cohesive properties are also augmented by frozen water, which "cements" soil particles to one another (Lilly et al. 2008). Thus, in areas where soil water content is high, soil strength increases during winter freezes, and conversely decreases in conjunction with summer thaws.

Little or no data are available to assess travel limitations resulting from seasonal freeze/thaw cycles of tundra soils on the North Slope, especially in areas of interest to those involved in the oil and gas exploration and field operations.

Although this abstract makes no suggestions pertaining to revisions or alterations to current management standards, the knowledge gained in respect to freeze/thaw time constraints and conditions on tundra-travel will aid others when making such decisions. Data analysis is specifically useful when assessing seasonal time limits on ice-road construction and use as a basis of frozen soil freeze/thaw properties.

## Methods

A system of twelve weather stations was set up in northern Alaska in fall of 2006 and has since been collecting soil moisture data by TDR, and soil temperature data from Thermisters each hour at 0, 5, 10, 15, 20, 40, 60, 80, 100, 120, 135, and 150 cm depths (Fig. 1). These depths may vary for some sites due to local soil conditions and the depth of the active layer during sensor installations. Relative humidity, dew point, wind speed and direction, wind chill, snow depth, solar radiation, net radiation, and snow and rain precipitation data are also available from the data network. Station dataloggers are connected to radios, allowing for near real-time measurement, which is specifically applicable when analyzing current conditions for tundra-travel.

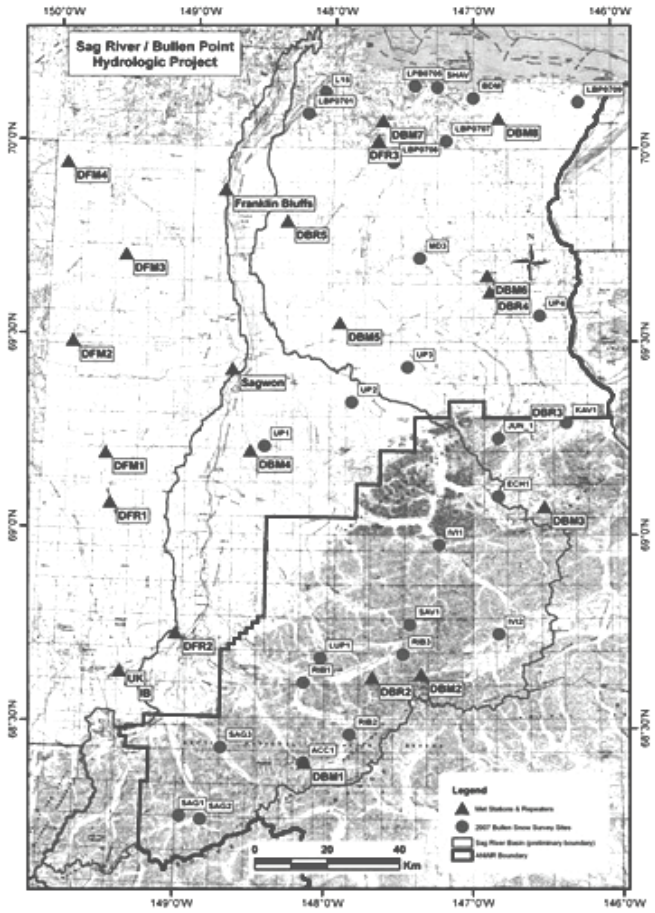


Figure 1. Map of meteorological station locations along the North Slope, Alaska.

Soil temperature data were analyzed to show temporal variation in one-degree incremental temperature conditions in the freezing soils. Analyzing the differences in dates that soils reach these one-degree temperatures helps illustrate the potential differences in timing of tundra-travel openings when using different soil temperatures**.** Soil temperature data were also spatially examined to display the effects of relative location on timing of one-degree changes during the annual freeze/thaw cycle in the active layer.

## Results and Discussion

Current data analyses include plotted freeze/thaw cycles from winter 2006 to summer 2007 for stations DMB2,

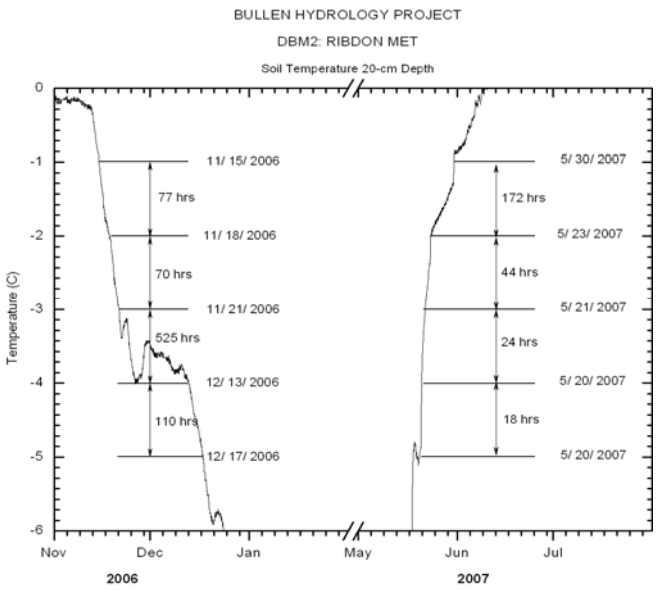


Figure 2. Soil temperature and water content for the 20 cm depth at DBM2 Ribdon met.

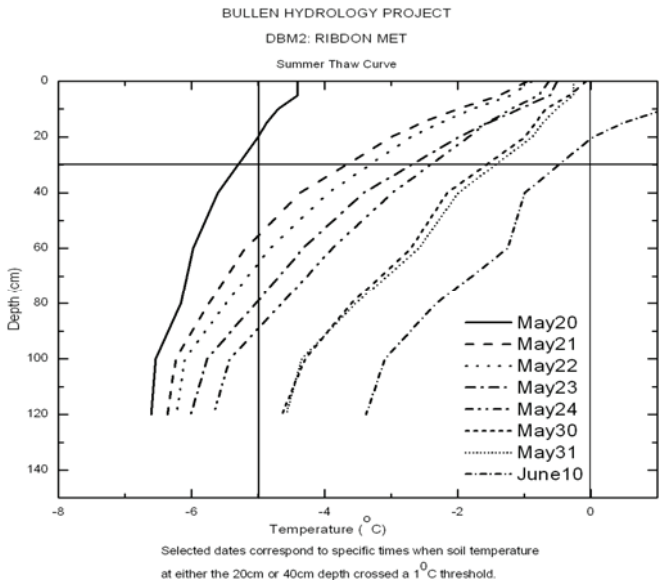


Figure 3. Soil temperature profile for the 2007 summer at DBM2 Ribdon met.

DMB4, DMB5, and DMB6, respectively. Note that data are not available at the regulated 30 cm depth, and so must be interpolated by averaging data from the 20 and 40 cm depths. (See Figure 2 for an example of the 2006/2007 freeze/thaw curve at the 20 cm depth for DBM2 Ribdon met.) Relaxing tundra-travel regulations from -5°C to -2°C would add approximately 34 days of travel time at station DBM2, approximately 28 days of travel time at station DBM4, approximately 30 days of travel time at station DBM5, and approximately 29 days of travel time at station DBM6. In all four cases, the majority of additional travel time would occur during the winter freeze, as tundra soils freeze slower than they thaw. At each of the aforementioned sites, the ratio of additional winter travel time to additional summer travel time was at least 1:1.4, with the mean ratio being 1:2.8, and the maximum ratio being 1:4.9.

Profile curves showing temperature changes based on soil depth were also created for stations DBM2, DBM4, and DBM6. The dates selected on these plots correspond to specific times when soil temperature at either the 20 or 40 cm depth crossed a 1°C incremental threshold. (See Figure 3 for an example of a temperature profile curve for DBM2 Ribdon met for the 2007 summer period.) Of the analyzed stations, DBM2 had both the earliest freeze and earliest thaw dates. In respect to DBM4 and DBM6, DBM2 is the furthest station from the coastline. Soils at DBM4, the westernmost station analyzed, began both the freeze cycle and thaw cycle on the latest dates.

## Summary

Soil temperature data were collected and analyzed from a system of 12 weather stations. This data can be used to help evaluate tundra-travel management policy along the North Slope of Alaska. Variation in incremental one-degree conditions in the freezing soils was used to illustrate the potential differences in timing of tundra-travel openings. Relaxing tundra-travel regulations from -5°C to -2°C would add an average of 30 days of travel time throughout the analyzed stations, with the majority of additional time occurring during winter freeze-up. Freeze/thaw curves had the earlier start times at the inland locations, as compared to those locations closer to the coastline.

To better assess freeze/thaw tundra soil conditions, a larger quantity of data must be analyzed. Other station locations as well as current winter freeze data should be plotted to broaden the depth of analyzed trends. Spatial analyses of data will also be performed. Soil parameters associated with freeze/thaw cycles will be compared between coastal and foothill sites, as well as resulting variations from east/west locations. Current data for the 2007/2008 freeze curve will also be compared to data from the previous winter. Soil-strength measurements on a variety of soils as a function of temperature and water content are also needed to better relate travel conditions to soil parameters.

## References

Bader, H.R. 2005. *Tundra Travel Research Project: Validation Study and Management Recommendations*. Alaska Department of Natural Resources, 20 pp. http://www.dnr.state.ak.us/mlw/tundra/validation2005final_with_figures.pdf.

Lilly, M.R., Paetzold, R.F. & Kane, D.L. 2008. Tundra soil-water content and temperature data in support of winter tundra travel. *Proceedings of the Ninth International Conference on Permafrost, Fairbanks, Alaska, June 29–July 3, 2008.*

# Discontinuous Permafrost Distribution and Groundwater Flow at a Contaminated Site in Fairbanks, Alaska

Andrea E. Carlson
*Shannon & Wilson, Inc., Fairbanks, Alaska, USA*
David L. Barnes
*Civil & Environmental Engineering, Water and Environmental Research Center, University of Alaska Fairbanks (UAF), Fairbanks, Alaska, USA*

## Introduction

Permafrost distribution substantially influences groundwater hydrology. Permafrost can affect hydrologic processes of water distribution, movement, and storage capacity, controlling zones of recharge and groundwater flow pathways (Anderson 1970, Prowse & Ommanney, 1990, Hinzman et al. 2005). These effects are noticeable in discontinuous permafrost regions because of lateral and vertical variability in frozen and unfrozen soil distribution.

Borehole and monitoring well installations revealed the variable nature and distribution of discontinuous permafrost during a site investigation to characterize and delineate the extent of groundwater contamination at a site in Fairbanks, Alaska.

We compiled borelogs and field observations and used ArcGIS to create thematic maps of groundwater elevations and the top of the permafrost surface below the ground. The groundwater elevation maps were overlain on the permafrost distribution map to investigate if changes in groundwater flow direction and gradient could be correlated to or were associated with areas of frozen soil. We measured water levels in nested wells to determine if vertical gradients due to frozen soils were affecting the groundwater flow regime.

## Site Environment

The site is in the Alaskan subarctic, located in the zone of discontinuous permafrost. Environmental consulting reports (Shannon & Wilson 2002–2007) documented that several contaminants, including trichloroethylene and benzene, are present in the area's soil and groundwater. In an effort to characterize and delineate site contamination, monitoring wells and soil borings were installed and sampled over the past 16 years.

Soils at the site consist of 2 feet to 20 feet of surficial silt and organics underlain by sand and gravel deposits. Swale and slough channels cut through the area and are filled with finer grained silt and sand. Soil borings encountered seasonal frost to a thickness of 20 feet, and discontinuous permafrost was encountered from the surface to greater than 65 feet at some locations. The majority of frozen soils were bonded with no excess visible ice.

## Methods

We compiled consultant reports (Shannon & Wilson 2002–2007), field data, borelogs, and analytical geochemical data for geostatistical analysis. Northing and easting data are in Alaska State Plane North America Datum 1983, Zone 3 (NAD '83); elevation data are in National Geodetic Vertical Datum of 1929 (NGVD '29). Using Environmental Systems Research Institute (ESRI), ArcGIS Desktop software, version 9.2 released in 2006, we created interpolated surfaces and contour maps of the top of the permafrost below ground surface and groundwater elevations. ArcGIS Desktop Extension, including Spatial Analyst and 3-D Analyst, were the primary geostatistical analysis tools.

To determine if vertical gradients could be affecting groundwater movement, groundwater elevation data was collected once a week over a two-month period in three sets of nested wells where permafrost was not encountered during well installation. The depth to groundwater below the top of the well casing was measured using a handheld water level indicator, and the elevation was calculated based on the top of casing elevation.

## Results

The permafrost distribution map (Fig. 1) shows the elevation of the top of the permafrost relative to NGVD '29; the approximate ground surface elevation at the site is 435 feet above mean sea level. The permafrost map was created using data from 54 locations, including 38 monitoring well borings, 13 well point installations, and 3 geotechnical-investigation borings in the vicinity. The depth to permafrost varies across the site, from the ground surface to greater than 60 feet; the elevation of the top of permafrost ranges from less than 370 feet to the ground surface (435 feet). Groundwater elevation maps were created for two 24-hour periods for each data collection event (six total maps). The groundwater elevations ranged from 421.59 feet to 423.52 feet during October 2004; from 419.87 feet to 422.08 feet in April 2006; and from 421.38 feet to 424.94 feet in October 2007. The mapped configurations of the elevations illustrate localized variations in groundwater flow direction and velocity.

Groundwater elevations, recorded for two sets of the nested wells, did not show significant differences in elevations between the deep (50 feet) and shallow (20 feet) wells. However, measurements taken at one location did have significant differences in head between the deep and shallow wells, ranging from 0.07 feet to 0.19 feet, with an average difference of 0.10 feet during the period of measurement.

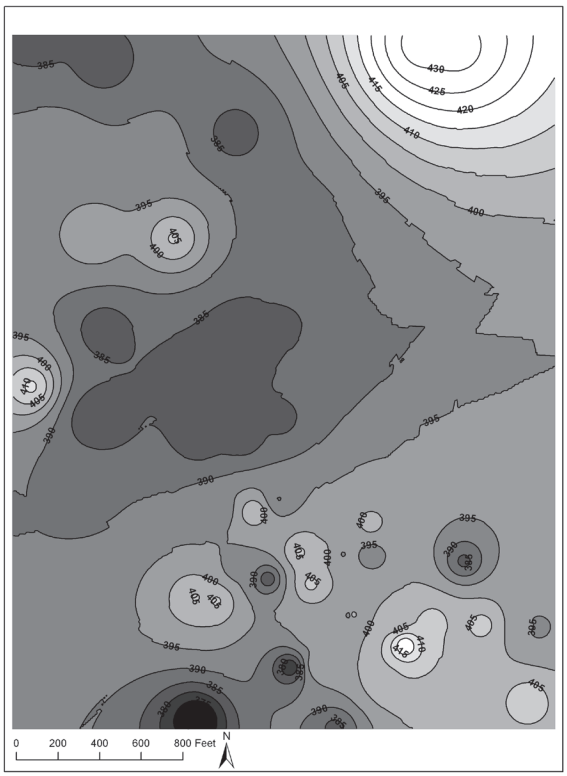


Figure 1. Permafrost distribution map showing contours of the elevation of the top of permafrost below the ground surface; the permafrost contour interval is 5 feet. The dark areas represent areas where the top of permafrost is at a greater depth below the ground surface; light areas represent where the top of permafrost is closer to the ground surface.

## Discussion

*Permafrost distribution*

The permafrost distribution map illustrates that the top of the permafrost is highly variable within short horizontal distances across the study site. The southeastern portion of the map has a larger number of sample points, and discontinuities are better represented. The central area of the site shows an area where permafrost was not encountered during the well installations. The wells were installed to 50 feet in this location, which represents a "hole" in the permafrost. In the northwestern area of the site, shallow permafrost was encountered at 20 feet to 25 feet below the ground surface. The thickness of the permafrost masses is unknown; and none of the wells in the area extend through permafrost. There are very few sample points in the northeast section of the map, as this area is outside the delineated contaminant plume boundary; it is likely discontinuities exist on the same scale as in the other portions of the site.

*Groundwater elevations*

A general groundwater trend towards the northwest is evident in the groundwater elevation maps (not shown). In addition to the regional trends, each of the groundwater elevation configurations exhibit patterns with varying gradients that show changing groundwater directions and velocities. Several regions of the project site have similar groundwater contours during each sampling event. By comparing the permafrost distribution with the converging and diverging groundwater flow-paths, the variances in groundwater flow can be attributed to areas of discontinuous permafrost.

Vertical gradient measurements in the nested wells also indicate that masses of discontinuous permafrost likely affect the hydraulic gradient in those areas.

## Conclusions

The permafrost distribution map shows a high degree of lateral and vertical variability between frozen and unfrozen soils at the site. The groundwater elevation maps demonstrate that the heterogeneity of subsurface hydraulic conductivities, attributable to areas of discontinuous permafrost, affect lateral and vertical groundwater flow. Vertical gradients were measured in the aquifer and are likely a result of the distribution of frozen soils.

## Further Work

The permafrost distribution and groundwater elevation maps served as a starting point for further research to investigate the relationship between contaminant movement and areas of discontinuous permafrost. Thematic maps of contaminant concentrations were also created and overlain on the permafrost distribution and groundwater gradient maps to assess spatial and temporal trends in the concentration data that may be correlated to areas of discontinuous permafrost.

## Acknowledgments

The authors would like to acknowledge input and support provided by project managers at Shannon & Wilson Inc, and the Alaska Department of Environmental Conservation.

## References

Anderson, G.S. 1970. Hydrological Reconnaissance of the Tanana Basin, Central Alaska: *U.S. Geological Survey Hydrologic Investigations Atlas* HA-319.

Hinzman, L.D., Kane, D.L. & Woo, M.K. 2005. Permafrost hydrology. In: M.G. Anderson (ed.), *Encyclopedia of Hydrological Sciences*. John Wiley & Sons, Ltd., 2679-2693.

Prowse, T.D. & Ommanney, C.S.L. 1990. *Northern Hydrology: Canadian Perspectives. National Hydrology Research Institute*. Science Report No. 1, 308 pp.

Shannon & Wilson, Inc. 2002–2007. *Groundwater Quality Assessments ADOT & PF Peger Road Operations and Maintenance Facility, Fairbanks, Alaska*.

# Thermal Regime Within an Arctic Waste Rock Pile: Observations and Implications

Jim W. Cassie
*BGC AVOT Ingenieria Ltda., Santiago, Chile*
Lukas U. Arenson
*BGC Engineering Inc., Vancouver, BC, Canada*

## Introduction

As part of the advanced exploration for diamond mining projects in Canada's north, a small waste rock pile of run of mine materials was constructed at the Snap Lake Diamond Project to investigate its long-term thermal behavior. The site is located approximately 220 km northeast of Yellowknife (Fig. 1), and it is in continuous permafrost with a mean annual air temperature (MAAT) of -8.3°C (Fig. 2). The maximum active layer thicknesses at the location of TH 12 (Fig. 3) varied between 5.93 m (9/29/2001) and 5.21 m (9/28/2004).

*Test cell configuration and materials*

The 8 m high "test cell" (Fig. 4) was instrumented with two horizontal thermistor cables at the base of the rock pile: one cable from west to east (TH 9) and one from south to north (TH 10). The cables were installed to confirm the expected subzero nature of the rock pile, along with measurements of active layer depths within the rockfill material. The test cell consists of clean to sandy gravel. Temperature measures from the base of the rock pile are available for a period of five years. Unfortunately, the rockfill material from the test cell was later excavated to make room for the full-scale mine.

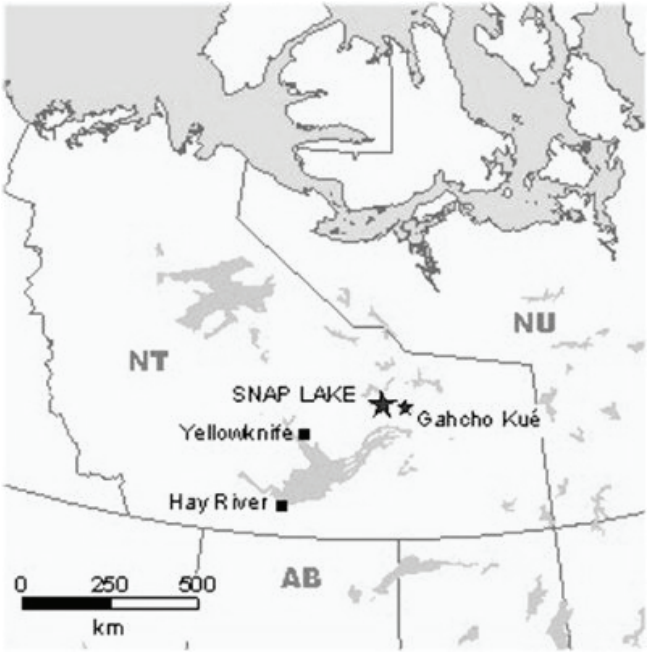


Figure 1. Location of Snap Lake (De Beers Canada).

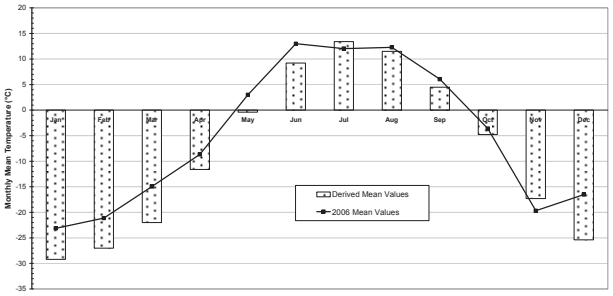


Figure 2. Mean monthly air temperatures for Snap Lake (1998–2006).

## Thermal Monitoring

Temperature trends from the south-to-north thermistor are presented in Figure 6 as one-year moving averages. There is a clear cooling trend for all locations as well as a dampening of the seasonal variations close to the boundaries of the test cell. The cooling rates change with distance from the edge and are highest (~0.7–0.8°C/year) at the edge and the centre of the pile and lowest (~0.3°C/year) half way into the

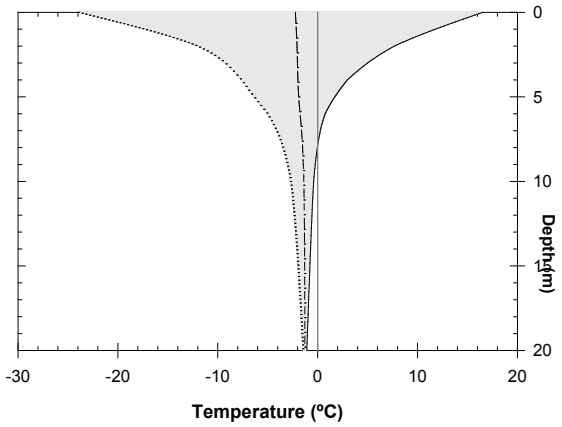


Figure 3. Temperature trumpet (2000–2005). The borehole (TH 12) is located approximately 100 m from the shoreline of Snap Lake.

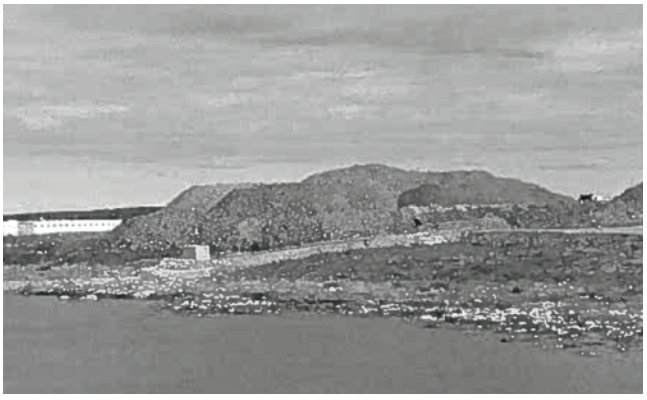

Figure 4. View of the test cell form the southeast (Photo: J.W. Cassie, 2003).

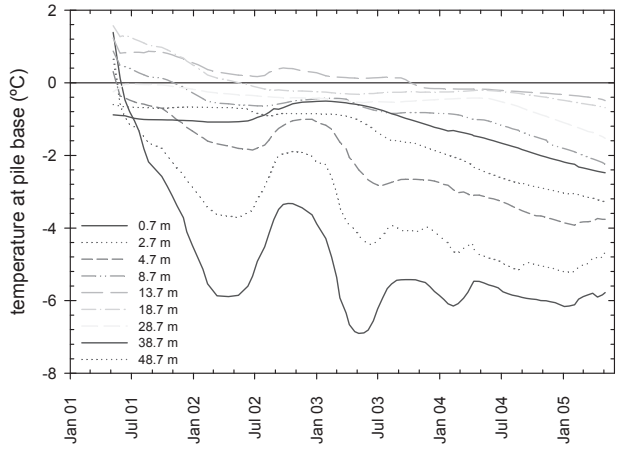


Figure 5. One-year moving average temperature trends for TH 10.

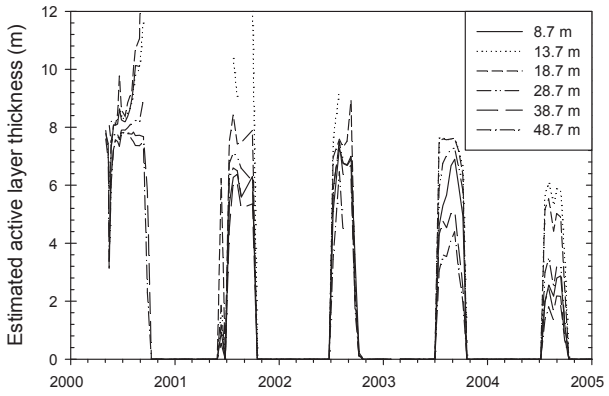


Figure 6. Estimated active layer thickness at different distances from the edge in the waste rock test cell calculated from the temperatures at the base.

pile. This difference can be explained by the formation of convective cells within the pile that force cold air to funnel down the centre of the pile, therefore, generating increased cooling.

## Active Layer Depths/Permafrost Aggradation

Changes in the active layer depth underneath the test cell had to be estimated from the horizontal temperature readings at the base of the waste rock. At a distance of 2.7 m from the edge, the temperatures stayed below 0° during the whole summer after construction. TH 9 showed subzero temperatures even at a distance of only 0.7 m from the edge, whereas TH 10 seemed to stay at a zero curtain. No positive ground temperatures, however, were recorded on this side. These readings show that, at the edge of the waste rock pile, the active layer thickness is in the order of 2 m, assuming a slope angle of 37°, which is the angle of repose for the rockfill material.

In order to estimate the active layer of the waste rock test cell, temperatures at the edge and the base were compared. It was assumed that the ground surface temperature at the top of an 8 m pile is similar to the temperatures measured at the edge of the test cell. By linearly comparing this temperature with the temperature at the base, an active layer thickness can be calculated. The cooling, hence permafrost aggradation in the waste pile, can be followed by the thinning active layer thickness (Fig. 6). It can be noted that the active layer thickness also decreases with distance from the edge. In the centre of the test cell (i.e., 28.7–48.7 m), the active layer thickness is reduced from 8 m to 2–3 m during this 5-year period. A thicker active layer was noted closer to the edge. However, the active layer thickness was still reduced by 2 m.

*Test cell excavation observations*

In summer 2005, the test cell had to be excavated. Observations made during this excavation confirmed the temperature readings, in that the core of the test cell was frozen in only 5 years.

## Conclusions

The thermal regime within coarse-grained mine waste rock piles is of particular importance when designing short- and long-term mine facilities in cold regions. To investigate the temperatures at the base of a gravelly rock pile, thermistors were placed at the base of a test cell at Snap Lake, and temperatures were recorded between 2000 and 2005 before the pile had to be excavated to make room for the full-scale mine. The pile temperatures cooled rapidly, and permafrost under the pile was reestablished within 5 years of operation. The active layer completely remained within the pile. The cooling rates differ spatially within the pile confirming the development of convective circles during winter. Cold surface air penetrates down the center of the waste rock pile. The pile excavation further confirmed that ice built; that is, permafrost aggradation occurred at the location of the test cell.

These measurements confirm predictions from various numerical simulations recently published that suggest accelerated cooling within coarse-grained waste rock piles in the Arctic.

The composition and internal thermal behavior has to be considered in the design of waste rock piles, in particular for permafrost aggradation/degradation under warming climate conditions. These results provide further evidence as to the water balance of waste rock piles in cold regions.

## Acknowledgments

The authors would like to thank De Beers Canada for their support and for allowing the publication of these results.

# Seasonal and Interannual Variability of Active Layer Development in Permafrost Wetland Systems

C.M. Chiu
*Department of Agronomy, Purdue University, West Lafayette, IN, USA*
L.C. Bowling
*Department of Agronomy, Purdue University, West Lafayette, IN, USA*

## Introduction

Over the last decades, the arctic region has been warming at an accelerated rate with sometimes puzzling effects on lakes and wetlands. Wetlands are common landscape characteristics in the northern high latitudes. Permafrost and seasonal frost can be a powerful factor affecting wetland hydrology. The interaction of soil thermal and moisture regimes controls the structure of the seasonally thawed active layer and hydrological response in permafrost regions. Soil thermal and moisture properties regulate the transfer of heat though the active layer, thus affecting the annual thaw and frost depth. The maximum active layer thickness can vary substantially with annual soil temperature change, given similar moisture conditions (Brown & Hinkel 2000). Spatially, the active layer thickness can vary over short lateral distances due to differences in heat transfer under different soil moisture conditions subject to freezing and thawing (Outcalt et al. 1990). For example, Woo and Xia (1996) found that a wetland site had shallower maximum thaw depth than a drier site due to the buffering effect of the large ice content. The spatial variation may also reflect the interaction of a large number of highly localized factors, including vegetation type, snow cover, organic layer thickness, soil thermal properties, microtopography, and the operation of nonconductive heat transfer processes (Outcalt et al. 1990). This study will examine the spatial and temporal variation of soil temperature and soil moisture content in a continuous permafrost environment and how they relate to the duration and thickness of seasonal active layer in upland and wetland systems. In particular, the ability of the Variable Infiltration Capacity (VIC) land surface model to reproduce the observed relationship between moisture condition and maximum annual thaw depth will be evaluated

## Study Area

The study area is the 471 km$^2$ Putuligayuk River watershed located on the coastal plain south of Prudhoe Bay on the Alaskan North Slope. Observations of soil temperatures and weather are taken from the Betty Pingo weather station (70°16′46.3″N, 148°53′44.5″W) operated by the University of Alaska Fairbanks. The watershed is dominated by drained lakes and numerous permafrost features such as high- and low-centered polygons, pingos, hummocky terrain, frost boils, and strangemoor ridges (Kane et al. 2000). The poor drainage results in extensive wetlands, ponds, and lakes. The maximum thickness of the permafrost along the arctic coast is about 600 m, whereas the maximum depth of thaw of the active layer was about 53 cm between 1993 to 2002 (Brown & Hinkel 2000). The vegetation in this area is dominated by sedge tundra, with shrubs in wetter areas and tussock tundra in higher and drier areas. Observed meteorological and soil temperature data for the period 1994–2004 was obtained through the National Snow and Ice Data Center (Kane & Hinzman 1997).

## Model Description

The Variable Infiltration Capacity (VIC) model is a macroscale hydrologic model which has been applied to many environmental studies associated with global climate and land use change prediction (Liang et al., 1994). VIC model features relevant to this application include (1) a finite difference soil thermal solution (Cherkauer & Lettenmaier 1999, Cherkauer & Lettenmaier 2003) and (2) representation of the surface storage and energy dynamic of sub-grid lakes and wetlands (Bowling 2003, Cherkauer & Lettenmaier 2003). In this study, we will examine the ability of the VIC model to simulate upland and wetland soil temperature, soil moisture, and active layer depth. The VIC model is run as a single point centered on the two sites. A constant temperature bottom boundary condition is used with a fixed temperature of -10°C at 4 m damping depth. Two scenarios are run with contrasting initial moisture conditions, bulk density and base flow parameters to simulate the contrasting moisture conditions of the site.

## Preliminary Result

Adjacent upland and wetland sites were instrumented by UAF beginning in 1994. The upland site was instrumented with 12 temperature probes vertically arranged at depths of 0, 1, 2, 3, 4, 5, 6, 7, 8, 15, 35, and 60 cm. The adjacent wetland site was also instrumented with 12 temperature probes vertically arranged at depths of 0, 0.5, 1, 2, 3, 4, 5, 6, 15, 30, 50, and 75 cm. Mean annual soil temperatures for the upland and wetland sites derived from hourly observations between 1996–2001 are shown in Figure 1. The patterns at both sites are very similar, although observed annual average temperatures are 0.27 to 0.74°C warmer for the wetter soils. The simulated temperatures are 0.35 to 0.6°C warmer for the wetter soil. In the wetter soil, water or ice displaces air in soil pores, increasing the bulk conductivity as well as the soil heat capacity. Thus, more energy may be required to change the temperature within the same depth resulting in a shallower active layer depth and shorter thawed period in the wetter soil (Figs. 2, 3).

As shown in Figure 2, simulated annual average active layer depth is slightly underestimated for the wetland site (58.78 cm). Since the 60 cm temperature sensor at the upland site exceeds 0°C in most years, the annual active layer depth is unknown, but still deeper than wetland. Figure 3 illustrates that both the observed and simulated frost-free period is longer in the upland than in the wetland site.

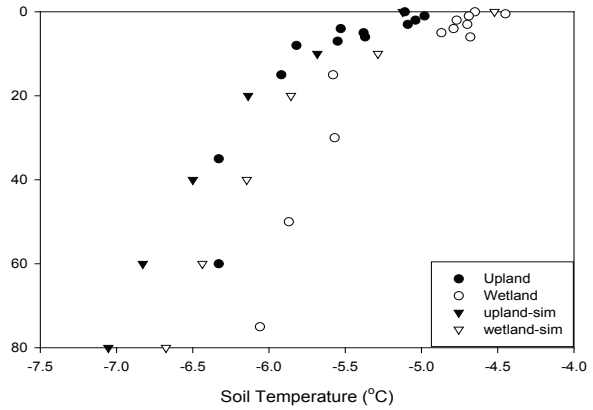


Figure 1. Mean annual soil temperature at 12 probe levels from 1996 to 2001 at upland and wetland site at Betty Pingo, Alaska.

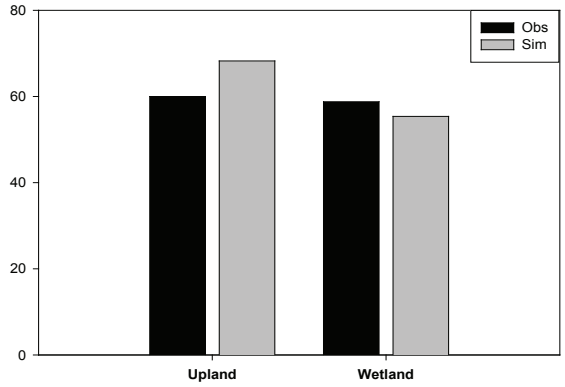


Figure 2. Observed and simulated maximum active layer depths (depth to the 0° isotherm) from 1996 to 2001 at upland and wetland site at Betty Pingo, Alaska. (The maximum temperature sensor in upland site is located at 60 cm.)

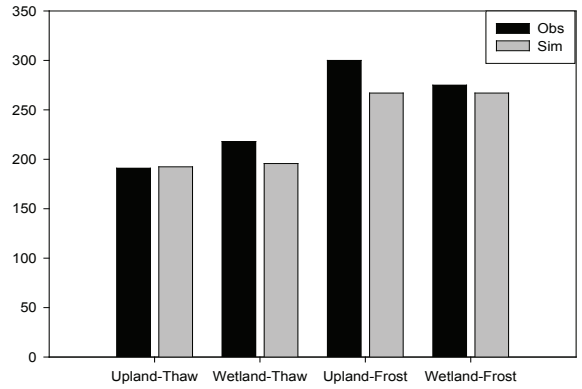


Figure 3. Observed and simulated mean Julian day that soil thaw reaches 50 cm (Thaw) and Julian day that soil freezes to within 1 cm (Frost) from 1996 to 2001 at upland and wetland site at Betty Pingo, Alaska.

## Summary

The wetter wetland site is observed to have higher average soil temperature than the dryer upland site. The higher water or ice content in the soil retards the development of the active layer and results in a shallower active layer and shorter thawed period than the upland site. The VIC soil temperature predictions appear to be less sensitive to the soil moisture differences due to heat capacity and bulk conductivity, although the actual difference in moisture content between the sites is unknown. Future work will focus on the active layer seasonal dynamic and hydrology response above continuous permafrost at the watershed scale.

## Acknowledgments

This research has been supported and funded by NASA through the Northern Eurasia Earth Science Partnership Initiative (NEESPI). The observed data was collected by Water and Environmental Research Center, University of Alaska Fairbanks.

## Reference

Brown, J. & Hinkel, K. 2000. Circumpolar Active Layer Monitoring (CALM) Network. Available online: http://www.geography.uc.edu/~kenhinke/CALM/sites.html.

Bowling, L.C. 2002. *Estimating the freshwater budget of high-latitude land areas.* Ph.D. dissertation. Univ. of Washington, Seattle.

Cherkauer, K.A. & Lettenmaier, D.P. 1999. Hydrological effects of frozen soils in the upper Mississippi River basin. *J. of Geophysical Research* 104: 19559-19610.

Cherkauer, K.A., Bowling, L.C. & Lettenmaier, D.P. 2003. Variable infiltration capacity cold land process model updates. *Global and Planetary Changes* 38: 151-159.

Kane, D.L. & Hinzman, L.D. 1997. updated 2003. *Meteorological and hydrographic data, Kuparuk River Watershed*. Boulder, CO: National Snow and Ice Data Center, World Data Center for Glaciology. Digital media.

Kane, D.L., Hinzman, L.D., McNamara, J.P., Zhang, Z. & Benson, C.S. 2000. An overview of a nested watershed study in Arctic Alaska. *Nordic Hydrology* 31(4/5): 245-266.

Liang, X., Lettenmaier, D.P., Wood, E.F. & Burges, S.J. 1994. A simple hydrogically based model of land surface water and energy fluxes for GSMs. *J. Geophys. Res.* 99(D7): 14415-14428.

Nixon, J.F. 1975. The role of convective heat transport in the thawing of frozen soil. *Canadian Geotechnic Journal*. 12: 425-429.

Outcalt, S.I., Nelson, F.E. & Hinkel, K.M. 1990. The zero curtain effect: heat and mass transfer across and isothermal region in freezing soil. *Water Resour. Res.* 26: 1509-1516.

Woo, M.K. & Xia, Z.J. 1996. Effects of hydrology on the thermal conditions of the active layer. *Nordic Hydrology*. 27: 129-142.

# Twelve-Year Thaw Progression Data from Zackenberg, Northeast Greenland

Hanne H. Christiansen
*The University Centre in Svalbard, UNIS*
Charlotte Sigsgård
*Institute of Geography and Geology, University of Copenhagen*

## Introduction

In Greenland, it is only in the northeast part, at 74°30′N in Zackenberg, that a continuous CALM data series exists since 1996 (Christiansen et al., in press). Circumpolar Active Layer Monitoring (CALM) data are collected as part of the Zackenberg Ecological Research Operations (ZERO) monitoring programme GeoBasis, which is maintained by the National Environmental Research Institute and the University of Copenhagen. As this programme has been manned during entire summer seasons since 1996, progressive summer thaw data have been collected to allow full season annual thaw progression data collection.

The CALM monitoring at Zackenberg was designed to investigate, at site scales, the effects of interannual temporal and spatial changes in snow cover, as determined by air temperature, wind speed, dominant wind direction and snow precipitation on thaw progression and active layer thickness. This is done by operating two different so-called ZEROCALM sites. The ZEROCALM-1 (ZC1) site consists of 121 grid points, covering a 100 m x 100 m area, with 10 m grid size. It is located on a flat marine abraded ground moraine (Christiansen 2004). The ZEROCALM-2 (ZC2) site has 208 grid points, covering 120 m x 150 m and also has a 10 m grid size. ZC2 is located in and around a natural snowdrift site (Christiansen 2004). The two sites are located 750 m apart in the Zackenberg lowlands, and are located between 20 and 37 m a.s.l. They are numbered G1 and G2, respectively, in the CALM database (Brown et al. 2000).

## Thaw Progression

Probing of ZC1 and ZC2 from early June to the end of August for the last 12 years, including from 6 to 11 sets of measurements in ZC1 and from 6 to 13 sets in ZC2, has enabled continuous summer thaw progression curves (Fig. 1). In the ZC1 grid, thawing was quick down to around 50 cm, and below was significantly slower. In the end of the summer, the curves show very little to no increase in thaw thickness, which is when the active layer was established, typically in mid to late August. Some refreezing was registered when measurements were done in September.

In the ZC2 site, the thaw rate was relatively homogeneous for most of the summer, with average rates below ZC1. In the end of summer, only little or no additional thawing happened, like in ZC1, when the active layer was reached. Also in the ZC2 site, some refreezing was registered in years when measurement proceeded into early September.

The difference in thaw progression between the ZC1 and ZC2 sites is mainly controlled by the different rate of annual

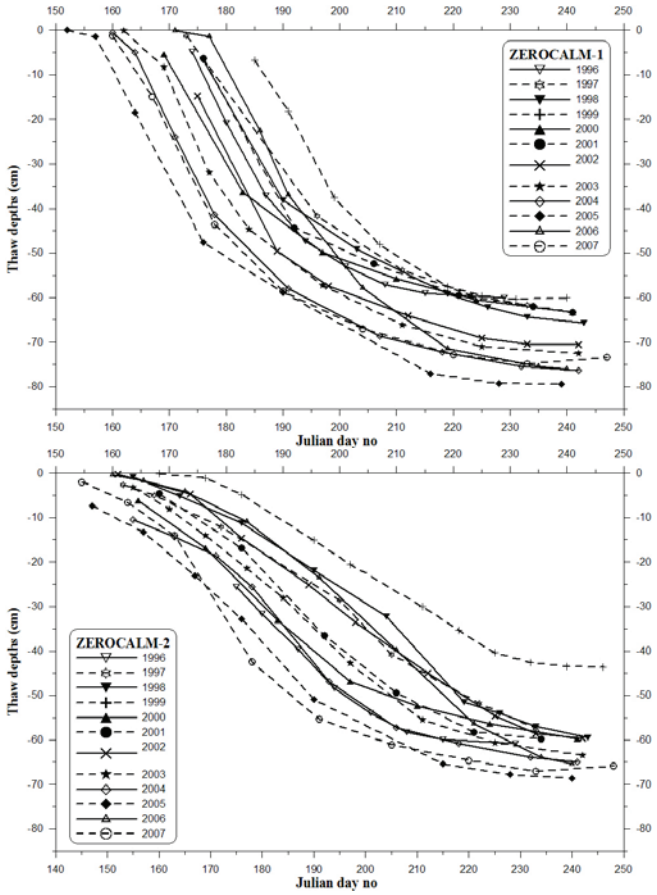


Figure 1. Thaw progression calculated as the mean of 121 points in ZEROCALM-1 site and as the mean of 208 points in the ZEROCALM-2 site.

snow depletion in the two sites (Christiansen 2004, Fig. 4). Ground thawing only starts when the snow has melted. As the ZC2 site is completely containing the snowpatch, its gradual backmelting during summer allows still more grid points to start thawing, and, therefore, a less steep thawing curve is established for the entire grid. The year 1999 was special in that the snowpatch stayed through the summer, which caused a much-reduced active layer of only 44 cm in ZC2, as several grid points did not melt at all.

## Active Layer Thickness

The active layer thickness (ALT) in the ZC1 and ZC2 sites varied, respectively, 20 cm and 26 cm in the 12-year period, with the deepest thaw in 2005 (ZC1 80 cm, ZC2 70 cm) and the thinnest in 1999 (ZC1 60 cm, ZC2 44 cm) for both sites (Fig. 1). Generally, the interannual ALT

variation was 20 cm in ZC1, but only 10 cm in ZC2, when excluding the 1999 snowdrift-affected year. This shows that the influence of the snowdrift seems to be larger than any other meteorological factor in this type of landscape setting, where the combination of topography and meteorology lead to snowpatch accumulation. The snowdrift size is controlled by the amount of winter snow, but mainly by the late winter wind activity causing snowdrifting (Christiansen 2004).

Comparing the ZEROCALM sites with the UNISCALM site in Svalbard, the nearest CALM site on the opposite site of the Greenland Sea is interesting. There is no simple correlation of ALT between the two CALM sites. The deepest thaw in Svalbard occurred in 2007 (Christiansen & Humlum 2008), while this was in 2005 for both sites in northeast Greenland (Fig. 1). In 2005, Svalbard actually experienced the shallowest active layer since measurements started in 2000.

## Air Temperature Control on Active Layer Thicknesses

Traditionally, the relationship between ALT and TDD of the thaw period is established using the Stefan solution to investigate the influence of air temperature forcing or other factors on ground thawing (Hinkel & Nelson 2003). Just 10 m south of the ZC1 site, the ZEROCALM official meteorological station is located. Air temperature is a standard parameter measured at this station, enabling calculations of thawing degree-days (TDD) of the thaw period.

The correlations between ALT and the square root of the TDD are shown for the entire 12-year period for both ZC1 and ZC2 in Figure 2. Clearly, ZC1 has a relatively high correlation to positive air temperatures in the thawing season, but also ZC2 has some correlation. Interestingly, both sites have a significantly better correlation than what has been found for a flat site in neighboring Svalbard based on 8 years of data ($r^2 = 0.004$) (Christiansen & Humlum 2008). Previously, based on the 7 first years of observations in the ZC1 and ZC2 sites, reduced correlations (ZC1: $r^2 = 0.53$ and ZC2: $r^2 = 0.00$) were also found for these sites (Christiansen 2004). This indicates that longer data series, such as the 12-year record from Zackenberg, must be collected to analyze with confidence the air temperature influence on ground thawing.

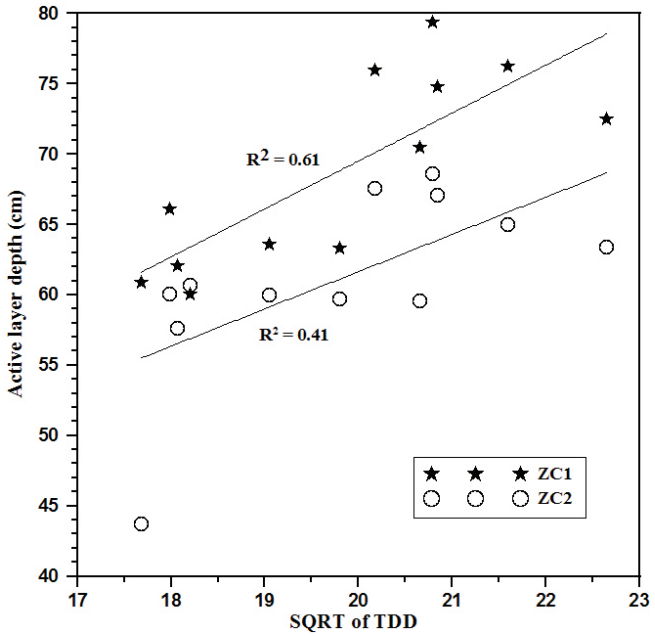


Figure 2. ZEROCALM-1 and ZEROCALM-2 active layer thickness correlated to the square root of the thawing degree-days until the time of the active layer measurement in the 1996–2007 period.

## Acknowledgments

The data collection of thaw depths is the responsibility of the Zackenberg Ecological Research Operations monitoring programme GeoBasis, to which we extend our sincere thanks for keeping this basic monitoring running and thus providing a rather unique CALM data series from Greenland.

## References

Brown, J., Hinkel, K.M. & Nelson, F.E. 2000. The Circumpolar Active Layer Monitoring (CALM) Program: Research designs and initial results. *Polar Geography* 24: 165-258.

Christiansen, H.H. 2004. Meteorological control on interannual spatial and temporal variations in snow cover and ground thawing in two northeast Greenlandic Circumpolar-Active-Layer-Monitoring (CALM) sites. *Permafrost and Periglacial Processes* 15: 155-169.

Christiansen, H.H., Sigsgaard, C., Humlum, O., Rasch, M. & Hansen, B.U. In press. Permafrost and periglacial geomorphology at Zackenberg. *Advances in Ecological Research* 40.

Christiansen, H.H. & Humlum, O. 2008. Interannual variations in active layer thickness in Svalbard. *Proceedings of the Ninth International Conference on Permafrost, Fairbanks, Alaska, June29–July 3, 2008*.

Hinkel, K.M. & Nelson, F.E. 2003. Spatial and temporal patterns of active layer thickness at Circumpolar Active Layer Monitoring (CALM) sites in northern Alaska, 1995–2000. *Journal of Geophysical Research* 108: D2: ALT 9, 1-13.

# Continued Permafrost Warming in Northwest Alaska as Detected by the DOI/ GTN-P Borehole Array

Gary D. Clow
*U.S. Geological Survey, Lakewood CO 80225, USA*

The U.S. Department of the Interior contributes to the Global Terrestrial Network for Permafrost (GTN-P) with a 21-element deep borehole array located in northwest Alaska. The majority of the holes are located on the Arctic Coastal Plain (ACP) with the remainder being in the northern foothills of the Brooks Range (Fig. 1). All but two of the boreholes penetrate the base of permafrost which is situated between 210 and 410 m in this region.

The U.S. Geological Survey began monitoring temperatures in the DOI/GTN-P boreholes in the late 1970s, soon after the holes were drilled. This was done by periodically relogging the wells with a portable temperature logging system (PTLS) developed especially for this purpose at USGS. While the original PTLS was limited to an incremental or "stop-and-go" logging mode, improvements allowed the PTLS to acquire "continuous" temperature logs by the mid-1980s. Further refinements have reduced the standard uncertainty of the ITS-90 temperature measurements obtained with this system to less than 3.3 milliKelvin. Early results which focused on interpretation of the curvature of the borehole temperature profiles for past climatic changes were reported by Lachenbruch and Marshall (1986) and Lachenbruch et al. (1988).

Monitoring the thermal response of permafrost to contemporary climate change has been the primary research focus of the DOI/GTN-P monitoring network for the last decade. Due to logistical constraints, our current protocol is to relog the entire borehole array every five years with a few key wells being relogged annually. Measurements in the wells show that near-surface temperature fluctuations in NW Alaska were generally small during the late 1970s and most of the 1980s, except for a short cold period during 1983–84. Permafrost temperatures began warming dramatically in 1989. By 2002–03, near-surface permafrost temperatures had warmed 3 K on average across the array relative to 1989. The coastal plain portion of the borehole array was relogged again during 2007 in support of the international Thermal State of Permafrost (IPY/TSP) project. These new measurements show that shallow permafrost temperatures have continued to warm on the ACP since 2002–03; the magnitude of the warming since 2002–03 ranges 0.0 to 1.0 K (mean = 0.4 K), depending on local site conditions. The total average (shallow) permafrost warming in this region since 1989 is now ~ 3.5 K (Fig. 1).

Data from the co-located DOI/GTN-P active layer/ meteorological network show that the 2002–03 borehole measurements coincided with a peak in mean annual air temperatures in NW Alaska. Mean annual air temperatures cooled substantially during 2004, but have been rising since and are now warmer than those experienced during 2002–03. Permafrost temperatures have not tracked the post-2004 air temperature warming due to the effects of changing snow cover.

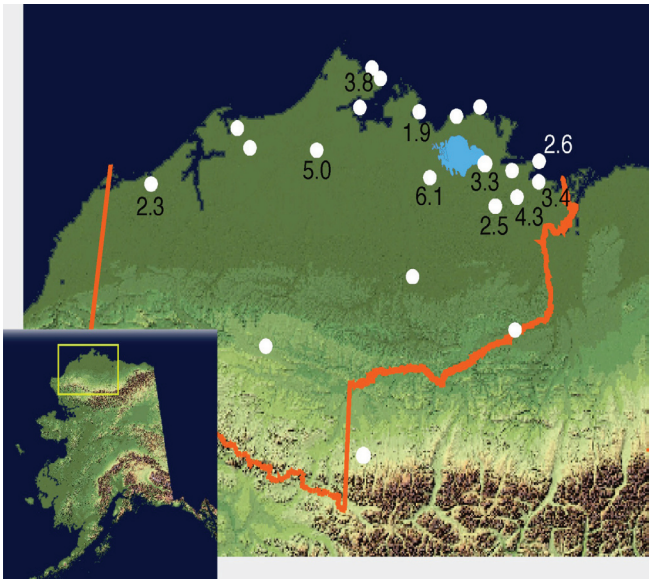


Figure 1. Location of the DOI/GTN-P boreholes in northwest Alaska. Also shown is the magnitude (degrees Kelvin) of shallow permafrost warming at various well sites on the coastal plain between 1989 and 2007.

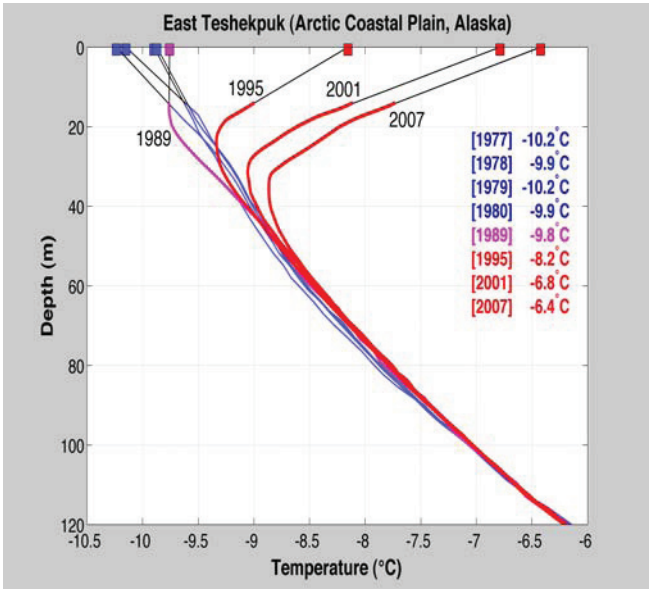


Figure 2. Sample permafrost temperatures measured in one of the coastal plain DOI/GTN-P boreholes (East Teshekpuk) since 1977. Extrapolated mean annual surface temperatures have increased about 3.6 K at this site since the late 1970s, close to the average for the entire array.

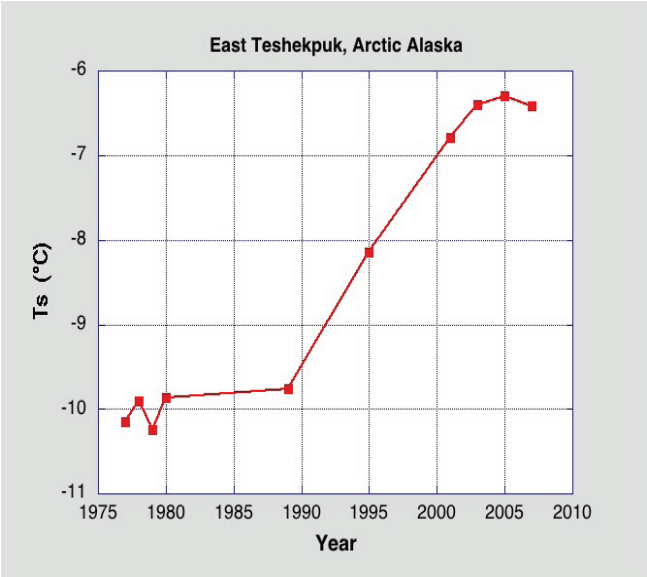


Figure 3. Time series of extrapolated mean annual surface temperatures derived from the borehole temperature measurements at the East Teshekpuk well site.

## References

Lachenbruch, A.H. & Marshall, B.V. 1986. Changing climate: geothermal evidence from permafrost in Alaska. *Science* 234: 689-696.

Lachenbruch, A.H., Cladouhos, T.T. & Saltus, R.W. 1988. Permafrost temperature and the changing climate. *Proceedings of the Fifth International Conference on Permafrost, 1988*: 9-17.

# Landsliding Following Forest Fire on Permafrost Slopes, Klondike Area, Yukon, Canada

Jim Coates, Antoni G. Lewkowicz
*Department of Geography, University of Ottawa, Ottawa, Ontario*

## Introduction

In the boreal forest, fire is often followed by widespread active layer detachment sliding (McRoberts & Morgenstern 1974a, 1974b, Lewkowicz & Harris 2005a, 2005b). Forest fire, with a recurrence interval of 25–300 years, kills adult trees, destroys much of the insulating mossy organic layer, and blackens the ground surface (Dyrness et al. 1986).

Seasonal thaw depths (active layer thickness) generally increase in the years following forest fire (Yoshikawa et al. 2003), although this can vary according to the slope aspect and state of vegetation (Swanson 1996, Lewkowicz & Harris 2005b). When the heat reaches the permafrost, it may thaw the ice-rich transient layer, which lies just below the average maximum depth of thaw (Shur et al. 2005). Water released by this process may raise soil porewater pressures sufficiently to destabilize slopes and cause active layer detachment sliding (McRoberts & Morgenstern 1974a).

Active layer detachment failures occur when all or a portion of the active layer separates from the permafrost beneath and moves as a semi-competent, unsaturated mass downhill over the lubricated slip surface of the thaw plane. Failures occur within the active layer or the transient layer and are triggered by high porewater pressures over frozen ground (Lewkowicz & Harris 2005b). The depth of the initial failure plane is limited by the position of the permafrost table (Harris & Lewkowicz 2000).

## Klondike Detachment Failures

Numerous forest fires occurred during the summer of 2004 in the Klondike Goldfields region of the Yukon Territory, an area of extensive discontinuous permafrost. Significant detachment failure landslide activity developed in subsequent weeks in Steele Creek, a small drainage basin located about 60 km south of Dawson City at approximately 63°35′N and 138°59′W.

Preliminary observations of the failures and near-surface thermal regime were made through freeze-up of 2004 and continued in the summers of 2005 and 2006. Detachment failures were mapped, and individual sites were surveyed. Two-dimensional DC resistivity transects were used to examine subsurface conditions in the area.

Thirty-five detachment failures occurred in 2004 along a 3.7 km section of the main Steele Creek Valley and on slopes within its tributaries. Five new failures developed by mid-August 2005, and several failures from 2004 reactivated. No more failures developed in the summer of 2006.

Table 1. Failure characteristics ($n$ = 37).

| | Mean | Max | Min |
|---|---|---|---|
| Failure Angle | 23 | 32.0 | 12.0 |
| Length (m) | 32 | 105.5 | 5.0 |
| Width (m) | 7 | 23.0 | 1.6 |
| Depth (cm) | 48 | 160.0 | 17.0 |
| Scar (m) | 23 | 88.5 | 2.0 |
| Length/Width ratio | 4 | 10.6 | 1.2 |

## Form

The failures in the Steele Creek Valley varied in length from 5–105 m, in width from 7–23 m, and in depth from 17–160 cm (Table 1). Only elongate detachment failures were observed (length-to-width ratio >1; e.g., Lewkowicz & Harris 2005a). The majority of these took place in coarse-grained soils with high pore-water pressures at the time of failure. Headscarps were coincident or proximal to convex breaks-of-slope. At the headscarps of nearly all the failures, tension cracks were observed with roots stretched across them. These tension cracks were more common on convex breaks-of-slope which are concentrations of stress. Near many of the failures, the organic mat was thinner near the headscarp but thicker downslope as a result of burning or pre-fire vegetation conditions.

Failure surfaces were generally higher than the inferred frost plane and dipped towards the centre of the failure scar. Displaced soil and organic material in most debris piles was highly disturbed. Trees were left standing in debris piles, indicating that the organic layer moved without overturning until it lost momentum or reached material that would not detach. It then piled up with liquefied mineral soil sandwiched between folded layers of the original surface organics. At some of the larger failures, the moving mass acquired sufficient weight and momentum to scour down to the permafrost table. Failure angles were all moderate (Fig. 1), with none below 10°.

## Mechanism

Forest fire contributed to detachment failure activity on permafrost slopes by destroying the surface organic mat, causing burned surface temperatures to rise, thawing active layers by up to 20 cm (+30%) deeper than adjacent unburned slopes and weakening the surface root structures. Deeper thaw melted transient layer ground ice, raising soil pore-water pressures.

These landslides appeared to have behaved as flows within unfrozen soils. The permafrost affected the failures by providing an aquiclude, which raised pore-water pressures, and by supplying water released from the transient layer due to thermal disequilibrium caused by the forest fire.

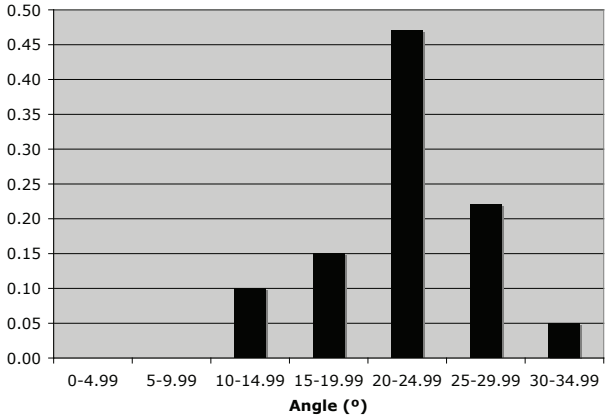


Figure 1. Histogram of landslide failure angles ($n$ = 37).

Failures in Steele Creek occurred where the subsurface mineral soil consisted of completely saturated coarse-grained material with low cohesion, the organic mat was weak on the break of slope but strong below, and there was significant downslope stress. The saturated soil mass liquefied and began to flow below the organic mat, which was elevated above, and detached from, the mineral soil. Tree roots that were still anchored in the mineral soil supported the suspended organic mat.

## Significance

The failures are similar in planar dimensions to those described previously in other permafrost regions (e.g., Lewkowicz & Harris 2005a, 2005b, McRoberts & Morgenstern 1974b). However, they are towards the upper end of the range of slope angles observed, and no low-angled forms were present. Moreover, in contrast to most other shallow failures over permafrost, the frost table did not act as a failure plane, and soil materials were cohesionless and coarse-grained. The critical role of permafrost in Steele Creek was to release water from upslope as the transient layer thawed, and by acting as an aquiclude, to generate high pore-water pressures near the base of the slope.

Fossil failures in the Steele Creek Valley and other Yukon locations (e.g., Lipovsky et al. 2006) indicate that detachment failure is an episodic process controlled by fire. In unglaciated areas such as Steele Creek, given a fire recurrence interval in the order of 100 years, this process has likely occurred thousands of times during the Pleistocene and may be responsible for elements of the form of the region's slopes. These include permafrost slopes having a generally gentler gradient and more defined mid-slope break of slope than nonpermafrost slopes.

The potential for climate change-induced thaw of permafrost as well as larger and hotter forest fires raise the possibility of greater active layer detachment failure activity in the future (McCoy & Burn 2005, Lipovsky et al. 2006).

## Acknowledgments

Financial Support came from NSERC through its Northern Internship Program and Discovery Grant (to A. Lewkowicz), the Yukon Geological Survey, Northern Scientific Training Program (Indian and Northern Affairs Canada), University of Ottawa (to A. Lewkowicz). We are also grateful for support from Klondike Star, Indian River Farm, EBA Engineering Consultants Ltd., Cam Arkinstal, Yukon Client Services and Inspections, Gimlex Mining, Mike Schultz, Geoff Hodgeson, Martina Knopp, Yukon Geological Survey, Dr Bernd Etzelmüller, Phil Bonaventure, and Emily Schultz.

## References

Dyrness, C.T., Viereck, L.A. & Van Cleve, K. 1986. Fire in taiga communities of interior Alaska. In: K. Van Cleve, F.S. Chapin III, P.W. Flanagan, L.A. Viereck & C.T. Dyrness (eds.), *Ecological Series* 57: *Forest Ecosystems in the Alaskan Taiga.* New York: Springer-Verlag, 74-86.

Harris, C. & Lewkowicz, A.G. 2000. An analysis of the stability of thawing slopes, Ellesmere Island, Nunavut, Canada. *Canadian Geotechnical Journal.* 37: 449-462.

Lewkowicz, A.G. 1988. Slope processes. In: M.J. Clarck (ed.), *Advances in Periglacial Geomorphology.* Chichester: Wiley, 325-368.

Lewkowicz, A.G. & Harris, C. 2005a. Morphology and geotechnique of active-layer detachment failures in discontinuous and continuous permafrost, northern Canada. *Geomorphology* 69: 275-297.

Lewkowicz, A.G. & Harris C. 2005b. Frequency and magnitude of active-layer detachment failures in discontinuous and continuous permafrost, northern Canada. *Permafrost and Periglacial Processes* 16: 115-130.

Lipovsky, P.S., Coates J, Lewkowicz, A.G. & Trochim, E. 2006. Active layer detachments following the summer 2004 forest fires near Dawson City, Yukon. In: D.S. Edmond, G.D. Bradshaw, L.L. Lewis & L.H. Weston (eds.), *Yukon Exploration and Geology 2005*. Yukon Geological Survey, 175-194.

McCoy, V.M. & Burn, C.R. 2005. Potential alteration by climate change of the forest-fire regime in the boreal forest of central Yukon Territory. *Arctic* 58: 276-285.

McRoberts, E.C. & Morgenstern, N.R. 1974a. The stability of thawing slopes. *Canadian Geotechnical Journal* 11: 447-469.

McRoberts, E.C. & Morgenstern, N.R. 1974b. Stability of slopes in frozen soil, Mackenzie Valley, N.W.T. *Canadian Geotechnical Journal* 11: 554-573.

Shur, Y., Hinkel, K. & Nelson, F. 2005. The Transient Layer: Implications for Geocryology and Climate-Change Science. *Permafrost and Periglacial Processes* 16: 5-17.

Swanson, D.K. 1996. Susceptibility of permafrost soils to deep thaw after forest fires in interior Alaska, USA, and some ecologic implications. *Arctic and Alpine Research* 28: 217-227.

Yoshikawa, K., Bolton, W.R., Romanovsky, V.E., Fukuda, M. & Hinzman, L.D. 2003. Impacts of wildfire on the permafrost in the boreal forests of Interior Alaska. *Journal of Geophysical Research* 107: 8148.

# A Permafrost Model Incorporating Dynamic Variable Soil Depth and Properties

Richard Coppell
*School of Geography, University of Leeds, Leeds, UK*
*Met Office – Hadley Centre for Climate Prediction and Research, Exeter, UK*
Sergey Venevsky
*School of Geography, University of Leeds, Leeds, UK*
*Met Office – Hadley Centre for Climate Prediction and Research, Exeter, UK*

## Introduction

Recent dynamic global vegetation models, for example, LPG, SEVER (Sitch et al. 2003, Venevsky & Maksyutov 2007), and land surface schemes, for example, IMOGEN, MOSES (Cox et al. 1999), have deficiencies in their representations of thermal and hydrological dynamics in the permafrost zone. These deficiencies are related to the following:

(a) Inadequate representation of thaw/freeze processes (absence of frozen soil water fraction). This relates to differing thermal conduction regimes between frozen (high conduction) and unfrozen (lower conduction) surface layers that experience thawing and freezing, particularly seasonally (see French 2007).

(b) Absence of the upper soil organic layer (moss/lichen). Distinctions may be made between thermal and hydrological properties of moss-dominated and lichen-dominated soils (Beringer et al. 2001), also modified by the influence of sedges (Usowicza et al. 2006).

(c) Inadequate parameterisation of soil properties. The number of types of soils represented within models may be expanded to test if this is also a sensitive parameter.

## Methods

Permafrost data (Brown 1998, International Permafrost Association Standing Committee on Data Information and Communication [comp.] 1998, 2003) is being compared with representations in SEVER, considering active layer depth, seasonal variation, time precision, temperature profile, soil moisture profile, and physical and biological soil constituents.

Peatland soil profiles and vegetation cover develop over periods of thousands of years, and a MATLAB model reproducing this based on Frolking et al. (2001) is also being assessed.

This will provide the opportunity to create a dynamic soil and vegetation representation within SEVER in place of more static representations of peatland and soil types.

## Acknowledgments

Richard Coppell is in receipt of UK NERC scholarship NE/F008341/1 with CASE funding from the Hadley Centre.

## References

Beringer, J., Lynch, A.H., Chapin, F.S., Mack, M. & Bonan, G.B. 2001. The representation of Arctic soils in the land surface model: The importance of mosses. *J. Climate* 14(15): 3324-3335.

Brown, J. 1998. Circumpolar Active-Layer Monitoring (CALM) Program: Description and data. In: M. Parsons & T. Zhang (eds.), *Circumpolar Active-Layer Permafrost System, version 2.0.* International Permafrost Association Standing Committee on Data Information and Communication. Boulder, CO: National Snow and Ice Data Center/World Data Center for Glaciology.

Cox, P.M., Betts, R.A., Bunton, C.B., Essery, R.L.H., Rowntree, P.R. & Smith, J. 1999. The impact of new land surface physics on the GCM simulation of climate and climate sensitivity. *Climate Dynamics* 15(3): 183-203.

French, H.M. 2007. *The Periglacial Environment*. Chichester, UK: Wiley, 478 pp.

Frolking, S., Roulet, N.T., Moore, T.R., Richard, P.J.H., Lavoie, M. & Muller, S.D. 2001. Modeling northern peatland decomposition and peat accumulation. *Ecosystems* 4(5): 479-498.

International Permafrost Association Standing Committee on Data Information and Communication (comp.). 1998. *Circumpolar Active-Layer Permafrost System, Version 1.0*. Edited by J. Branson, J. Brown & M.O. Leibman. Boulder, CO: National Snow and Ice Data Center/World Data Center for Glaciology. CD-ROM.

International Permafrost Association Standing Committee on Data Information and Communication (comp.). 2003. *Circumpolar Active-Layer Permafrost System, Version 2.0*. Edited by M. Parsons & T. Zhang. Boulder, CO: National Snow and Ice Data Center/World Data Center for Glaciology. CD-ROM.

MacDonald, G.M., Beilman, D.W., Kremenetski, K.V., Sheng, Y., Smith, L.C. & Velichko, A.A. 2006. Rapid early development of circumarctic peatlands and atmospheric $CH_4$ and $CO_2$ Variations. *Science* 314(5797): 285-288.

Sitch, S., Smith, B., Prentice, I.C., Arneth, A., Bondeau, A., Cramer, W., Kaplan, J.O., Levis, S., Lucht, W., Sykes, M.T., Thonicke, K. & Venevsky, S. 2003. Evaluation of ecosystem dynamics, plant geography and terrestrial carbon cycling in the LPJ dynamic global vegetation mode. *Global Change Biology* 9: 161-185.

Usowicza, B., Lipieca, J., Marczewskib, W. & Ferreroc, A. 2006. Thermal conductivity modelling of terrestrial soil media: A comparative study. *Planetary and Space Science* 54: 1086-1095.

Venevsky, S. & Maksyutov, S. 2007. SEVER: A modification of the LPJ global dynamic vegetation model for daily time step and parallel computation. *Environmental Modelling and Software* 22: 104-109.

# Seasonal Sources of Soil Respiration from High Arctic Landscapes Dominated by Polar Stripes

Claudia I. Czimczik
*Department of Earth System Science, University of California, Irvine, CA 92614, USA*
Susan E. Trumbore
*Department of Earth System Science, University of California, Irvine, CA 92614, USA*
Jeffrey Welker
*Environment and Natural Resources Institute and Biology Department, University of Alaska Anchorage*

## Introduction

Carbon (C) cycling studies in the Arctic have largely focused on Low Arctic wet sedge and tussock tundra ecosystems, with studies in the High Arctic only recently contributing to our understanding of the complete Pan Arctic C biogeochemistry. It is becoming increasingly clear that High Arctic soils contain significant amounts of soil C that previously have been underestimated by up to an order of magnitude (Horwath 2007). In addition, we now recognize that soil C pools in portions of the High Arctic landscape may be spatially heterogeneous (horizontally and vertically), especially in areas where pattern ground is extensive such as landscapes, where polar strips result in vegetated troughs and barren ridges. In addition, because this region is warming at some of the highest rates across the entire biome, increasing levels of microbial decomposition and soil respiration may provide an important positive feedback to global warming that warrants quantification.

We studied the seasonal pattern of $CO_2$ evolved from the soil surface (soil respiration) and its production within the mineral soil to 60 cm depth from a High Arctic prostrate dwarf shrub tundra (polar semi-desert) ecosystem in northwest Greenland as part of a NSF Biocomplexity project on C cycling in cold, dry ecosystems. We used radiocarbon to (1) partition the net flux of soil respiration into plant-derived C sources (C cycling on a time scale of days to a few years) and microbial-derived sources (slower cycling C) and (2) to investigate whether microorganisms are currently accessing very old C pools that used to be unavailable under previous climatic conditions.

## Material and Methods

*Study site*

Samples were taken at two locations near Thule Air Base, northwest Greenland (76°32′N, 68°50′W) throughout the growing season from June to August 2007. The landscapes were dominated by classic polar stripes formed from frost cracking, aeolian in-filling, colonization by higher plants, and freeze thaw dynamics resulting in troughs dominated by *Dryas integrifolia* and *Salix arctica* and ridges that were non-vegetated. This landscape type represents about one-third of the entire High Arctic terrestrial land cover.

*Sampling*

Soil respiration rates were measured with paired, dynamic chambers ($n$ = 3) in troughs and ridges, together with measurements of air and soil temperature. In addition, we monitored the concentration and isotopic signature ($\delta^{13}C$, $\Delta^{14}C$) of $CO_2$ within the soil profile to 60 cm depth as well as the isotopic signature of $CO_2$ in ambient air. Gas fluxes and concentrations were monitored approximately weekly. The isotopic signature of $CO_2$ was measured monthly. $CO_2$ was sampled with evacuated canisters.

At UC Irvine, $CO_2$ was cryogenically purified, reduced to graphite, and analyzed for its stable isotope signature (IRMS) and radiocarbon content (AMS) (Xu et al. 2007). The isotopic signature of the main soil respiration sources (roots and microorganisms) were investigated using laboratory incubations or freshly-cut roots and intact soil cores. In addition, we measured the content and isotopic composition of C and nitrogen in each core.

## Results and Discussion

In vegetated troughs, soil respiration rates peaked in the summer, when temperatures were highest (Fig. 1). $CO_2$ concentrations in the soil pore space reached a plateau in the summer. Respiration rates from ridges were low throughout

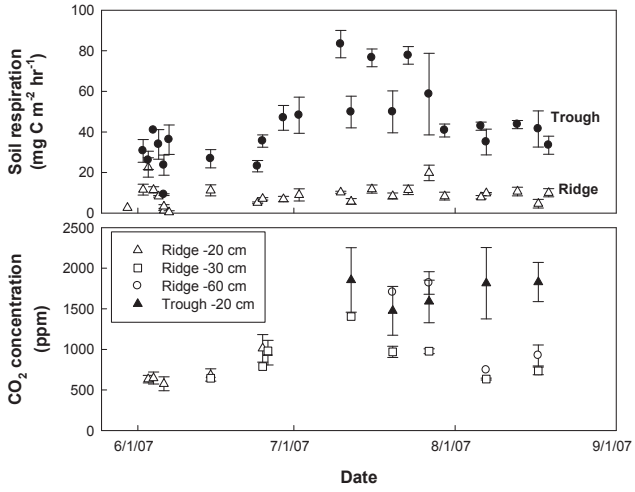


Figure 1. Flux of $CO_2$ from the soil surface (top panel) and concentration of $CO_2$ in the soil pore space (bottom panel) throughout the growing season.

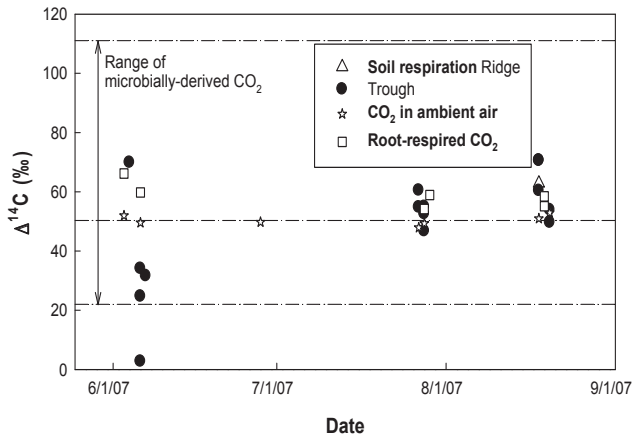


Figure 2. Radiocarbon signature of soil respiration, root- and microbially-respired $CO_2$ (from incubations), and of $CO_2$ in ambient air throughout the growing season.

the growing season. Pore space $CO_2$ concentrations were also lower, and peaked during the summer.

Although soil C pools had mean ages of up to 5000 years, the $^{14}C$ signature of all $CO_2$ respired from the soil surface, roots, and soil cores, as well as the $CO_2$ in the soil pore space, was modern (fixed by photosynthesis post-1950) (Fig. 2). Throughout the growing season, soil respiration had $^{14}C$ signatures higher than the current atmospheric $CO_2$, indicating that the source is C cycling on decadal time scales. At the end of winter, the source of soil respiration was a mixture of older and modern C, indicated by modern signature lower than that of current atmospheric $CO_2$. A clear source portioning into plant- and microbial-derived sources was complicated by a very high spatial variability of the $^{14}C$ signature of microbial-derived $CO_2$.

High Arctic soils contain considerable amounts of old C currently protected from microbial decomposition by cold temperatures. The mobilization of these pools could act as a positive feedback to global climate change. However, during the growing season, $CO_2$ fluxes from High Arctic soils were dominated by modern (post-1950) C. Erosion of older C sources was observed at the end of winter when plants were largely dormant, but measurements were complicated by low flux rates and very high 3D-spatial variability of potential C sources.

## Acknowledgments

We thank M. Rogers, H. Kristenson, and K. Nagel for their assistance in the field, and Thule Air Base for logistical support. This work was funded by the U.S. NSF Biocomplexity Program.

## References

Horwath, J.L. 2007. *Quantification and Spatial Assessment of High Arctic Soil Organic Carbon Storage in Northwest Greenland*. PhD Thesis. Seattle, WA, USA: Department of Earth and Space Sciences, University of Washington.

Xiaomei, X. Trumbore, S.E., Zheng, S., Southon, J.R., McDuffee, K.E., Luttgen, M. & Liu, J.C. 2007. Modifying a sealed tube zinc reduction method for preparation of AMS graphite targets: Reducing background and attaining high precision. *Nuclear Instruments and Methods in Physics Research* B 259: 320–329, doi:10.1016/j.nimb.2007.01.175.

# Greenland Permafrost Temperature Simulations

R.P. Daanen
*Geophysical Institute, University of Alaska Fairbanks, Fairbanks, Alaska*
V.E. Romanovsky
*Geophysical Institute, University of Alaska Fairbanks, Fairbanks, Alaska*
S.S. Marchenko
*Geophysical Institute, University of Alaska Fairbanks, Fairbanks, Alaska*
J.H. Christensen
*Danish Meteorological Institute, Copenhagen, Denmark*
M. Stendel
*Danish Meteorological Institute, Copenhagen, Denmark*
T. Ingeman-Nielsen
*Technical University of Denmark, Copenhagen, Denmark*

## Introduction

Tourism in Greenland has increased in recent years and has put more stress on infrastructure. Expansion of airstrips and roads to accommodate increased travel in conjunction with climate warming (IPCC 2001, ACIA 2004) requires an assessment of permafrost in the area. Complex topography and coastal configurations are key characteristics of the Alaskan and Greenland regions on which this study will focus. This requires high-resolution simulation of climate as well as permafrost distribution. We used a numerical simulation model called GIPL 2.1 (Tipenko & Romanovsky 2001, Sergeev et al. 2003) for simulating spatially distributed ground temperatures over Greenland.

## Results

The permafrost in this country is dominated by areas of frozen bedrock with pockets of sediments and organic matter. For this study, we split the simulation in two categories: bedrock simulations and sediment simulations. Snow is treated the same for sediment areas and bedrock areas, and taken from HIRHAM snow water equivalent predictions. It was corrected for a constant density (0.15 gr/cm$^3$) and shows a fairly close fit for some of the observed years in the dataset from Illulisat (Fig. 1).

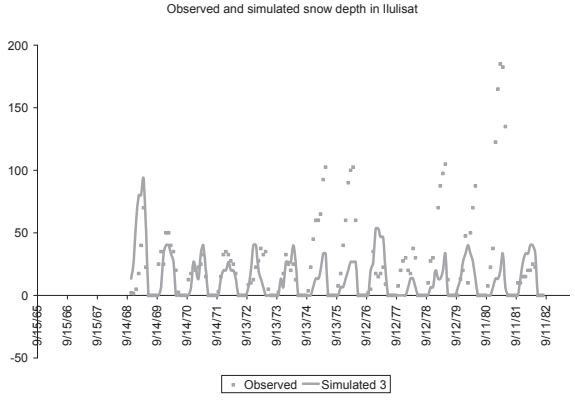


Figure 1. Observed and simulated snow depth for the Illulisat region.

Figure 2 shows the temperature distribution in bedrock material over entire Greenland at a 25 km resolution. The first image is the result of a ten-year-average ground temperature from 1955 till 1965 for a depth of 2 m; the second image is for the same depth at the end of the simulation period from 2065 till 2075.

The simulation data does not show a large difference over the simulation period. In bedrock, the temperature fluctuation between summer and winter are larger then in the sediment, due to a lack of ice or liquid water that buffers the temperature fluctuation. Figure 3 shows the active layer depth for the beginning of the simulation period and the end of the simulation period.

For sediment we find cooler average temperatures due to the thermal offset in the organic materials in the upper soil layers. In addition, there is a larger quantity of liquid water present and a larger amount of ice in the winter. The results for the sediment simulations are given in Figure 4 for the 2 m temperature and in Figure 5 for the active layer depth.

## Discussion

The data provided in this abstract are average data over ten years and show little change over the simulation period from 1950 till 2075. Even the higher spatial resolution simulated in this study is relatively coarse when comparing it with the heterogeneity of the landscape.

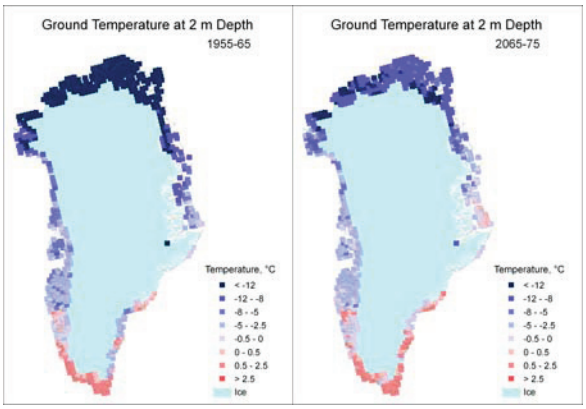


Figure 2. Bedrock temperature distribution at 2 m depth.

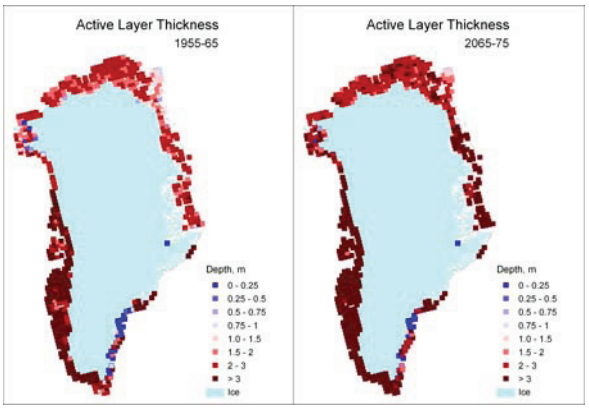


Figure 3. Active layer depth distribution in bedrock.

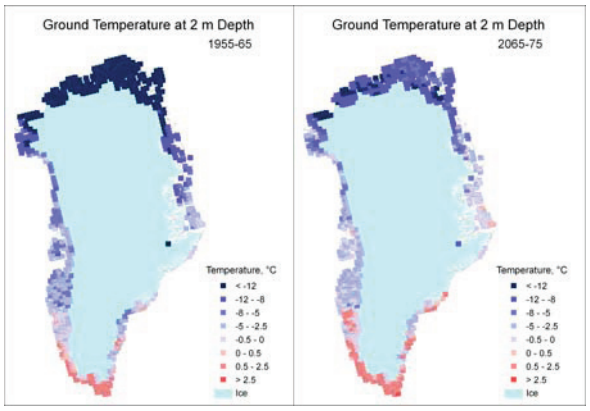


Figure 4. Annual average ground temperature distribution at 2 m depth in sediment with organic layer.

Temperatures in the northern part of Greenland seem to be most affected by the warming climate for bedrock and for the sediment simulation.

The active layer seems to be sensitive to the warming trend over the simulation period. Active layer depth increases at some locations in bedrock from 2 to 3 m. The eastern portion of Greenland shows soil warming, but the southwestern portion shows active layer depths in bedrock greater then 3 m as well. For sediment areas, which are important for infrastructure, the active layer deepens in the western portion of the country.

## Conclusion

Permafrost temperatures are simulated for Greenland, and it was found that most areas are warming as the climate warms over the period from 1950 till 2075.

Permafrost temperatures in the northern portion of the country are strongly affected by warming winter temperatures, whereas the temperatures in the south are buffered by disappearing ground ice.

The active layer depths are increasing with time for bedrock and sedimentary substrates. Increases of the active layer with 1 m are commonly seen in the southern portion of the country.

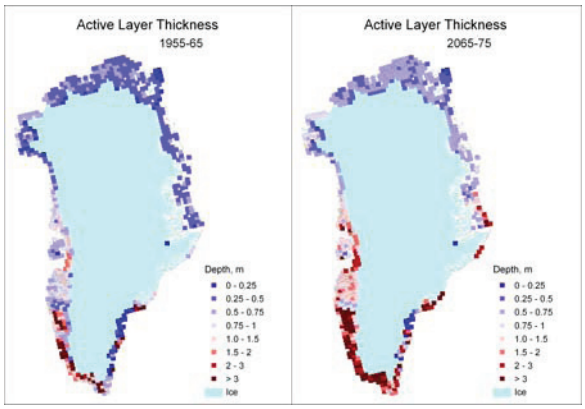


Figure 5. Active layer depth distributions for areas with sediments and organic matter.

## Acknowledgments

Funding for this project was provided by the National Science Foundation under grant no. ARC-0612533.

We would also like to thank our collaborators from ASIAQ, the DMI, DTU, and ARSC.

## References

ACIA. 2004: *Impacts of a Warming Arctic*. *Arctic Climate Impact Assessment (Highlights)*. Cambridge, UK: Cambridge University Press, 110 pp.

IPCC. 2001: *Summary for Policy Makers: Climate Change 2001: The Scientific Basis*. Contribution of Working Group I to the Third Assessment Report of the Intergovernment Pannel on Climate Change. J.T. Houghton, Y. Ding, D.J. Griggs, M. Noguer, P.J. van de Linden, X. Dai, K. Mashell, & C.A. Johnson (eds.). Cambridge, UK & New York, NY, USA: Cambridge University Press, 1-20.

Sergeev, D.O., Tipenko, G.S. & Romanovsky, V.E. 2003. Mountain permafrost evolution under long term climate fluctuations (results of numerical simulation). *Proceedings of the Eighth International Conference on Permafrost, Balkema, Zurich*: 1017-1021.

Tipenko, G.S. & Romanovsky, V.E. 2001. Simulation of soil freezing and thawing: Direct and inverse problems. *EOS*, *Trans. AGU* 82(47), Fall Meet. Suppl., Abstract, F551.

# The Importance of Snow Cover Evolution in Rock Glacier Temperature Modeling

Matteo DallAmico
*Department of Civil and Environmental Engineering, University of Trento, Italy*
Stefano Endrizzi
*Department of Civil and Environmental Engineering, University of Trento, Italy*
Riccardo Rigon
*Department of Civil and Environmental Engineering, University of Trento, Italy*
Stephan Gruber
*Department of Physical Geography, University of Zurich, Switzerland*

## Introduction

The snow cover evolution is one of the crucial factors affecting the thermal and hydraulic regime of rock glaciers (Mittaz et al. 2000), as snow strongly controls soil energy balance through its high albedo and insulating properties. Therefore, accurate modeling of the snowpack is absolutely necessary to reliably describe soil temperatures. The importance of accurate snow modeling entails the use of sophisticated models based on the solution of the snow energy balance and, consequently, on a good parameterization of radiation and turbulent fluxes (e.g., Jordan 1991). An advance or delay in estimating the time of snow disappearance would cause a strong error in the calculation of the energy balance at the soil surface, altering the ground heating or freezing and, therefore, affecting the soil temperature profile for the whole summer.

The goal of this work is to simulate and discuss the rock glacier snow evolution in order to analyze the influence of the snow cover and accumulation/melting time on the temperature regime of the active layer of a rock glacier.

## Modeling Features and Case Study

The model used in the simulation is GEOtop (Rigon et al. 2006), a distributed physically-based model which jointly solves the energy and water balance of soil (Bertoldi et al. 2006) and snow (Zanotti et al. 2004), and accounts for the geotechnical parameters of unsaturated soils affecting slope stability (Simoni et al. 2007). The model has been improved recently to include a correct treatment of frozen soil (Endrizzi et al. 2008) and to model snow with a multilayer scheme capable of describing snow metamorphism and water circulation and refreezing in the snowpack (Endrizzi 2007).

Commonly, in alpine climates the soil exchanges heat directly with the atmosphere only in a short time window, roughly spanning from June to October, whereas during winter and early spring, heat transfer between soil and atmosphere is mediated by the snowpack. Consequently, the heat flux reaching the soil surface is strongly reduced due to high snow albedo, which reduces net energy input, and to snow insulating properties, which cause heat conduction to be very small below the upper snow layers. In fact, the snow energy balance equation can be written as follows (Oke 1990):

$$\Delta Q_S + \Delta Q_M = R_n + P - H - L - G \qquad [\mathrm{W/m^2}] \qquad (1)$$

where the terms in the left-hand side (LHS) represent the heat storage rate in the snowpack due to sensible heat ($\Delta SQ_S$) and to latent heat ($\Delta Q_M$, melting/refreezing and rain on snow). In the right-hand side (RHS), $R_n$ is the net all-wave radiation, $P$ is the sensible heat flux supplied by precipitation, $H$ and $L$ are, respectively, the sensible and latent heat fluxes exchanged between the surface (be it snow or soil) and the atmosphere, and $G$ is the heat flux reaching the soil surface acting as soil energy input. When the ground is snow-free, the LHS in equation (1) is null, and $G$ is equal to the net energy flux exchanged with the atmosphere. On the other hand, for snow covered ground, $G$ is proportional to the temperature gradient at the snow-soil interface, namely:

$$G_{sn} = -K \frac{T_{sn} - T_S}{\frac{1}{2}(D_{sn} + D_S)} \qquad [\mathrm{W/m^2}] \qquad (2)$$

where $K$ is the snow-soil averaged thermal conductivity calculated as a harmonic mean, $T_{sn}$ is snow temperature in the layer close to the soil surface, $T_S$ is the soil surface temperature, and $D_{sn}$ and $D_S$ are the depths of the snow and surface layer, respectively.

*Investigated site*

Simulations have been carried out on the active rock glacier Murtèl (Upper Engadin, Swiss Alps: 46°26′N, 9°49.5′E, 2670 m a.s.l., 15° slope with NW aspect) in which the oldest temperature time series of Alpine Permafrost has been measured (Vonder Mühll & Haeberli 1990, Hoelzle et al. 1999). Input data include incoming shortwave radiation (both direct and diffuse), incoming longwave radiation, air temperature, wind speed and direction, air pressure, and precipitation.

## Simulations and Results

The simulation spans a period of two hydrological years beginning from October 1997. As the first snowfall normally occurs in November, this choice allows the avoidance of the problem of determining the initial condition of snow on the surface. Most of the parameters used by the snow model of GEOtop were simply taken from literature, for example, snow reflectance and snow thermal and hydraulic properties. As only total precipitation was available, the calibration was reduced to the definition of the threshold air temperatures above (below), where precipitation is considered to occur as rain (snow).

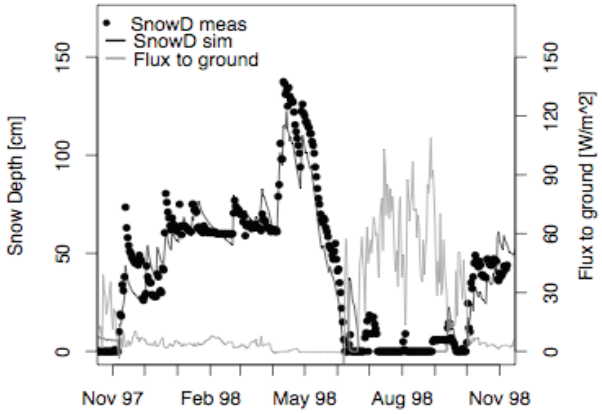


Figure 1. Simulated vs. measured snow depth and energy flux input to the ground in the Murtèl rock glacier.

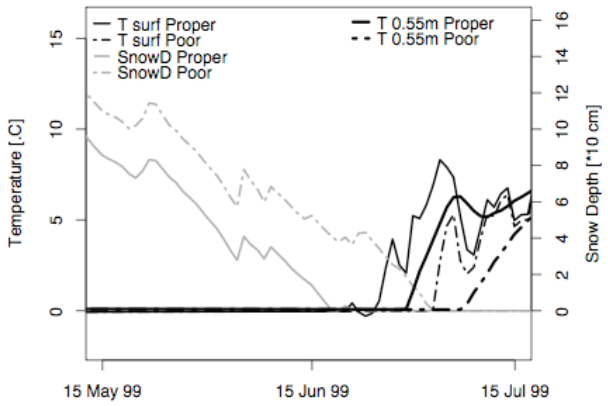


Figure 2. The error in temperature profile depends on snow modeling and becomes bigger the deeper in the ground. "Proper" and "Poor" refer to real measures and delayed modeling, respectively

As can be seen in Figure 1, the model proves to simulate well both the snow depth and the time when snow is completely ablated. The heat flux reaching the soil surface clearly depends on snow presence. When soil is snow free, the flux is of the order of 50 W/m$^2$, but it can drop by an order of magnitude or more when snow is present.

A delay (anticipation) in the estimation of the snow cover complete ablation date may lead to an underestimation (overestimation) of the ground surface temperature and of the temperature profile of the layers below. For example, in Figure 2 the temperature behavior at the soil surface and at 55 cm depth during the snow melting period is reported, considering a "proper" snow simulation (full grey line) and a "poor" delayed snow simulation (dotted grey line). The surface temperature increases as the snow is melted, and the delay between the two scenarios is disappear after few days. At 55 cm depth, instead, the delay in the temperature evolution is still visible after one month, indicating that the error in snow model will propagate and increase as we go deeper in the soil.

## Conclusions

The work shows that the model is capable of reproducing the evolution of the snow cover and the temperatures in the active layer of the rock glacier. Snow evolution, together with the thermal and hydraulic parameters (DallAmico et al. submitted), is a crucial process to take into consideration when the thermal regime of an active layer is to be modeled. A proper representation of the snow evolution can provide the right time window of direct soil exposure to solar radiation and, in turn, a reliable quantification of the soil energy fluxes. Conversely, a poor representation may lead to significant errors that propagate and increase the deeper we go in the ground.

## References

Bertoldi, G., Rigon, R. & Over, T.M. 2006. Impact of watershed geomorphic characteristics on the energy and water budgets. *J. Hydrometeorology* 7: 389-403.

DallAmico, M., Endrizzi, S., Rigon, R. & Gruber, S. Submitted. Modelling the thermal regime of a rock glacier active layer using GEOtop. *Proceedings of the Ninth International Conference on Permafrost, Fairbanks, Alaska, June 29–July 3, 2008.*

Endrizzi, S. 2007. *Snow cover modeling at local and distributed scale over complex terrain.* Ph.D. dissertation. Dept. of Civil and Environmental Engineering, University of Trento, Italy.

Endrizzi, S., Rigon, R. & DallAmico, M. 2008. A soil freeze/thaw model through the soil water characteristic curve. *Extended Abstracts, Ninth International Conference on Permafrost, Fairbanks, Alaska, June 29–July 3, 2008.*

Hoelzle, M., Wegman, M. & Krummenacher, B. 1999. Miniature temperature dataloggers for mapping and monitoring of permafrost in high mountain areas: first experience from the Swiss Alps. *Permafrost and Periglacial Processes* 10: 113-124

Jordan R. 1991 A one-dimensional temperature model for a snow cover. *Technical documentation for SNTHERM 89*. CRREL, Hanover, NH, USA.

Mittaz, C., Hoelzle, M. & Haeberli, W. 2000. First results and interpretation of energy-flux measurements of Alpine permafrost. *Annals of Glaciology* 31: 275-280.

Oke, T.R. 1990. *Boundary Layer Climates*. Routledge.

Rigon, R., Bertoldi, G. & Over, T.M. 2006. GEOtop: A distributed hydrological model with coupled water and energy budgets. *J. of Hydromet.* 7: 371-388.

Simoni, S., Zanotti, F., Bertoldi, G. & Rigon, R. 2007. Modelling the probability of occurrence of shallow landslides and channelized debris flows using GEOtop-FS. *Hydrological. Processes.*

Vonder Mühll, D. & Haeberli, W. 1990. Thermal characteristics of the permafrost within an active rock glacier (Murtèl/Corvatsch, Grisons, Swiss Alps). *Journal of Glaciology* 36(123): 151-158.

Zanotti F., Endrizzi, S., Bertoldi, G. & Rigon, R. 2004. The GEOTOP snow module. *Hydrological. Processes* 18: 3667-3679. doi:10.1002/hyp.5794.

# The Account of Long-Term Air Temperature Changes for Building Design in Permafrost

I.V. Davidova
*The Moscow State University, The Faculty of Geology, 119992, GSP-2, Moscow, Lenin Mountains, Russia*
L.N. Khroustalev
*The Moscow State University, The Faculty of Geology, 119992, GSP-2, Moscow, Lenin Mountains, Russia*

## Introduction

One of the main parameters defining permafrost-bearing capacity as a base of buildings is their temperature depending on air temperature. According to meteorological supervision, it is established that air temperature increase became practically appreciable since 1970, and it is expected that, to the middle of the 21st century, increase of mean annual air temperature will reach from 1.5 to 7.0°C.

A rise in soil and air temperature leads to an increase of rated building base temperature, which defines rated resistance of frozen ground. Knowing rated resistance decrease during the time, it is possible to plan engineering actions which will provide necessary bearing capacity of the building under condition of climate warming. On a design stage the main action is the increase of supporting structure of foundation, that is, increase of reliability factor. Thus the problem is divided into three interconnected problems: the forecast of mean annual air temperature, the forecast of ground temperature, and the definition of reliability factor.

## The Forecast of Mean Annual Air and Permafrost Temperature

Laws of long-term changes of mean annual air temperature were established by the method of autoretrospective analysis of meteorological supervision series. The method is based on harmonious decomposition of time series and considers cyclic, trend, and casual changes in meteorological series. In detail the method is described in the work of Khroustalev et al. (2000).

Received forecast air temperatures were used for modeling of temperature ground conditions. For the forecast of permafrost temperature, a numerical method—the final difference method—was used. The mathematical model of permafrost evolution was the Stefan problem. Calculations were carried out in the program "Warm," developed on the Geocryological Faculty of the Geological Department of the Moscow State University (Khruostalev et al. 1994). The mathematical model has been realized by us for 10 settlements located in Sakha-Yakutia Republic (6 items) and in Western Siberia (4 items).

Obtained data have been estimated by us from a position of the reliability theory.

## Reliability Estimation of the Building Foundations in Permafrost

At first we defined a cost optimum reliability of the bases without taking into account climatic changes, taking as the base data from the boundary year (standard reliability).

The analytical calculation method for optimum reliability of the building foundations when construction is built with principle I (we consider only this case in the report) has been developed by Pustovoit (Khrustalev & Pustovoit 1988). Its basis is minimization of the total expenses consisting of the building initial cost ($C_0$) and expenses connected with possible damage before the termination of the operation life ($C_R$).

Except for optimum reliability, another important parameter is the optimum factor of reliability ($K_{H,0}$), which corresponds to optimum reliability.

The factor of reliability allows the connection of two determined approaches which are put in a basis of normative documents and developed by us as probability-statistical. This factor depends on many parameters: climatic, geological, constructive, and economic. Therefore, it cannot be appointed directly, but should be calculated separately for each area.

The calculated result of optimum reliability and reliability factors for the residential building bases in 10 areas allow the following conclusions to be drawn:

Optimum reliability increases, and optimum reliability factor decreases when air temperature decreases and foundation depth increases. These changes occur in interval $P(te) = 0.747 - 0.998$ and $K_{H,0} = 1.1 - 2.5$.

Casual fluctuations of mean annual air temperature influence the optimum reliability and optimum reliability factor. When air temperature fluctuation increases, the optimum reliability decreases and the optimum reliability factor increases. For example, at practically identical air temperature in areas of Chekurdah ($\sigma = 1.3$) and Tiksi ($\sigma = 1.86$), in the first case optimum reliability is above, and optimum reliability factor is below, than in the second.

Greater building cost (smaller value of economic factor) should correspond to greater base reliability and greater optimum reliability factor. Unfortunately, this trivial conclusion does not find reflection in operating normative documents.

After definition of optimum values of reliability and reliability factor, the forecast of the base reliability for a residential building on the pile foundation for the nearest 50 years has been executed, considering variability of air and ground temperatures and depth of seasonal thawing during the time.

For Nadym city, the optimum value of reliability factor is 1.697, if long-term changes of air temperature do not occur (a modeling problem), function of reliability changes a little,

Table 1. Recommended values of reliability and reliability factor for residential buildings during the period 2000–2050.

| Area | $T_{air}$, °C | $g$, °C/year | $l$=6m | | $l$=8m | | $l$=12m | |
|---|---|---|---|---|---|---|---|---|
| | | | $P(t_e)$ | $K_H$ | $P(t_e)$ | $K_H$ | $P(t_e)$ | $K_H$ |
| | | | | | Yakutia | | | |
| Chekurdah | -11.1 | 0.01 | 0.992 | 1.214 | 0.996 | 1.16 | 0.998 | 1.104 |
| Tiksi | -10.7 | 0.02 | 0.984 | 1.411 | 0.990 | 1.301 | 0.995 | 1.190 |
| Verhoyansk | -7.3 | 0.033 | 0.986 | 1.263 | 0.991 | 1.198 | 0.996 | 1.129 |
| Ust-Maya | -4.0 | 0.042 | 0.913 | 1.403 | 0.923 | 1.316 | 0.943 | 1.214 |
| Mirniy | -3.4 | 0.031 | 0.746 | 1.183 | 0.773 | 1.646 | 0.804 | 1.436 |
| Tuoy-Haya | -2.8 | 0.032 | 0.949 | 1.549 | 0.958 | 1.451 | 0.966 | 1.319 |
| | | | | | Western Siberia | | | |
| Beliy island | -8.6 | 0.006 | 0.983 | 1.344 | 0.989 | 1.255 | 0.995 | 1.165 |
| Salehard | -2.02 | 0.02 | 0.727 | 2.222 | 0.777 | 1.892 | 0.824 | 1.581 |
| Nadim | -1.64 | 0.017 | 0.73 | 2.62 | 0.79 | 2.21 | 0.849 | 1.823 |
| Poluy | -0.56 | 0.013 | 0.63 | 3.96 | 0.767 | 2.99 | 0.878 | 2.21 |

and reliability remains high enough. In a real case, reliability intensively tends to zero, reaching value 0.08 at the end of operation. This means that the building will be destroyed before the termination of operation period with probability of 92%. At reliability factor $K_H = 2.62$, the reliability at the initial stage surpasses reliability of the modeling problem, and then decreases to 0.73. Thus the material damage caused by reliability decrease remains the same as in case of the modeling problem.

Values of reliability $P(t_e)$ and the factor of reliability $K_H$ for all 10 considered areas have similarly been calculated (Table 1).

## References


Khroustalev, L.N., Emeljanov, N.V., Pustovojt, G.P. & Jakovlev, S.V. 1994. *The Calculation Program of Thermal Interaction of Engineering Constructions with Permafrost*. The Certificate 940281. RosAPO.

Khroustalev, L.N. & Pustovoit, G.P. 1988. Calculations of the building bases in permafrost. *Novosibirsk: the Science*. 253 pp.

Khroustalev, L.N., Medvedev, A.V. & Pustovoit, G.P. 2000. Long-term change of air temperature and construction stability projected in permafrost area. *Cryosphere of the Earth* IV(3): 35-41.

Pavlov, A.V., Ananev, G.V & Drozdov, D.S. 2002. Monitoring of seasonal thawing layer and temperature of frozen ground in the north of Russia. *Cryosphere of the Earth* VI(4): 30-39.

Pavlov, A.V. 2003. Permafrost and climatic change in the north of Russia: supervision, forecast. *Proceedings of the Russian Academy of Sciences* 6: 39-50.

Pustovoit, G.P. 1997. The account of climate variability at maintenance of construction base reliability in permafrost area. *Cryosphere of the Earth* I(4) :50-53.

SNiP 2.02.04-88. 1990 *The Bases and the Foundations in Permafrost*. Moscow: Stroyizdat, 53 pp.

# The Combined Isotopic Analysis of Late Quaternary Ice Wedges and Texture Ice at the Lena-Anabar Lowland, Northern Siberia

Alexander Dereviagin
*Moscow State University, Faculty of Geology, Vorobievy Gory, 119899, Moscow, Russia*
Hanno Meyer
*Alfred Wegener Institute for Polar and Marine Research, Research Unit Potsdam, Telegrafenberg A43, 14473 Potsdam, Germany*
Alexander Chizhov
*Moscow State University, Faculty of Geology, Vorobievy Gory, 119899, Moscow, Russia*
Diana Magens
*Alfred Wegener Institute for Polar and Marine Research, Am Alten Hafen 26, 27568 Bremerhaven, Germany*

## Introduction

Different types of ground ice are fed by meteoric water sources and are considered to be a unique archive of paleoenvironmental and paleoclimatic information (Mackay 1983, Meyer et al. 2002). The isotopic signal of an ice wedge is indicative for winter temperatures. Texture ice (both segregated and pore ice) may be assumed as a mixture of summer and winter precipitation. Isotope variations within sediment columns are difficult to interpret in paleotemperature terms, because of various processes involved such as seasonality of precipitation, amount of rain and snow feeding the active layer, fractionation during evaporation, melting and freezing may influence its isotopic composition. This study focuses on the combined isotopic analysis of Late Quaternary ice wedges and texture ice in an ice-rich sedimentary complex named Ice Complex. The isotopic composition ($\delta^{18}O$, $\delta D$) of ground ice dating to ca. 60 ka was studied in the framework of Russian-German multidisciplinary research expeditions at the Laptev Sea coast.

## Study Sites and Methods

The investigations were carried out at two sites located in the Lena-Anabar lowland at the Laptev Sea coast at Bykovsky Peninsula (eastern part of Lena Delta): at Mamontovy Khayata outcrop, 71°60′N, 129°20′E (site 1) and at Cape Mamontov Klyk, 73°36′N, 117°10′E (site 2).

The region is characterized by a continental Arctic climate. Mean annual air temperatures (MAAT) at site 1 are about -14°C, mean January temperatures ($T_J$) are about -34°C and mean winter temperatures ($T_w$) are about -22°C (data of Tiksi). MAAT at site 2 are about -15°C, $T_J$ are about -33°C, and $T_w$ are about -23°C (data of Cape Terpey-Tumasa). Annual precipitation reaches 300 mm, with a maximum (about 75%) in summer. The region belongs to the zone of continuous permafrost with a thickness of about 300–500 m and mean annual ground temperature around -12°C. The coastal lowland is characterized by widespread Ice Complex remains, composed of ice-rich silty fine-grained sand with peaty paleosol horizons and huge syngenetic polygonal ice wedges (heights of 20–40 m and widths of 2–6 m) and columns of frozen sediments (width of 2–4 m) with belt-like cryostructure.

The formation of Late Pleistocene Ice Complex is usually associated with Karginsky and Sartansky periods of the Russian stratigraphy, which correspond to MIS-3 and MIS-2 of the global classification. According to AMS dates, Ice Complex formation at Bykovsky Peninsula was between 58.4 ka (at sea level) and 12.2 ka BP (Schirrmeister et al. 2002). At Cape Mamontov Klyk, Ice Complex formation took place between 31–28 ka and 10.7 ka BP (Schirrmeister et al. 2008). At both sites, Ice Complex is partly covered by a 2 m thick horizon of peat-rich, silty sediments with Holocene ice wedges. Holocene ground ice was also studied in alases, thermo-erosional and river valleys.

The investigations are based on the combined application of stable isotopes to both ice wedges and texture ice sampled in parallel. Measurements of isotope composition ($\delta^{18}O$, $\delta D$) were carried out at the Alfred Wegener Institute in Potsdam. The stable isotopic composition is given in ‰ vs. V-SMOW standard. The 1σ errors for H and O isotopes are better than 0.8‰ and 0.10‰, respectively.

## Results and Discussion

The available data of isotope analyses are presented in Table 1. Both wedge and texture ice differs considerably in their isotopic composition between Holocene and Pleistocene, with 3–8‰ lower $\delta^{18}O$ in Pleistocene ice following the global warming trend. The isotopic composition of both Late Pleistocene wedge and texture ice is very close at site 1 and site 2. This can be evidence both of the similarity of ice complex formation and climatic conditions in the region.

The mean $\delta^{18}O$ of ice wedges differs by 0.1‰ in Sartansky (MIS-2) time, and by 1.6‰ in Karginsky (MIS-3) time between both sites. For texture ice, the differences are about 0.1‰ in Karginsky time. In Holocene, differences in mean $\delta^{18}O$ reach about 3‰ for ice wedges and 0.7‰ for texture ice between both sites. The observed differences of Holocene ice wedges are likely the result of different ages of the sampled ice wedges at sites 1 and 2. At site 1, many Early Holocene ice wedge samples were taken at the top of the Ice Complex.

The ice wedge isotopic composition is similar in Karginsky and Sartansky with more negative minimum values (of -33.9 to -34.9‰) in Karginsky time. This leads to the assumption

Table 1. Isotopic composition (‰) of ice wedges and texture ice: mean (in bold)/min./max. values). *N* = number of samples.

| Ice wedges | | | | Texture ice | | | |
|---|---|---|---|---|---|---|---|
| N | $\delta^{18}O$ | δD | $d_{ex}$ | N | $\delta^{18}O$ | δD | $d_{ex}$ |
| **Site 1 (Bykovsky Peninsula)** | | | | | | | |
| Holocene (MIS-1) | | | | | | | |
| 184 | **-27.5** | **-203.5** | **13.5** | 14 | **-20.8** | **-155.5** | **11.2** |
| | -30.2 | -224.3 | 8.5 | | -23.3 | -173.1 | 7.0 |
| | -22.5 | -168.5 | 17.8 | | -17.7 | -134.8 | 15.1 |
| Sartansky (MIS-2) | | | | | | | |
| 178 | **-29.7** | **-231.2** | **6.1** | no data | | | |
| | -32.1 | -253.5 | 1.9 | | | | |
| | -23.1 | -174.5 | 13.3 | | | | |
| Karginsky (MIS-3) | | | | | | | |
| 158 | **-30.6** | **-241.3** | **3.7** | 40 | **-23.8** | **-193.1** | **-2.5** |
| | -33.9 | -267.5 | -3.9 | | -29.5 | -231.7 | -11.7 |
| | -25.6 | -208.3 | 7.9 | | -18.9 | -158.5 | 14.0 |
| **Site 2 (Cape Mamontov Klyk)** | | | | | | | |
| Holocene (MIS-1) | | | | | | | |
| 54 | **-24.1** | **-182.9** | **10.0** | 13 | **-20.1** | **-150.8** | **9.7** |
| | -27.3 | -212.6 | 6.1 | | -28.2 | -204.5 | 5.2 |
| | -20.4 | -155.5 | 14.3 | | -17.2 | -130.6 | 21.4 |
| Sartansky (MIS-2) | | | | | | | |
| 120 | **-29.8** | **-234.3** | **4.5** | 51 | **-27.6** | **-210.3** | **10.4** |
| | -31.9 | -253.4 | 0.4 | | -31.6 | -242.1 | -7.3 |
| | -26.1 | -199.6 | 9.4 | | -19.5 | -147.0 | 24.2 |
| Karginsky (MIS-3) | | | | | | | |
| 62 | **-29.0** | **-227.5** | **4.4** | 20 | **-23.7** | **-186.3** | **3.6** |
| | -34.9 | -272.2 | -0.6 | | -27.7 | -215.3 | -16.8 |
| | -24.0 | -180.6 | 14.6 | | -16.7 | -150.4 | 19.2 |

that winter conditions in Sartansky were slightly less severe than in Karginsky time.

The isotopic composition of texture ice is always less negative than the isotopic composition of ice wedges (Table 1), because of the influence of summer precipitation (as well as fractionation effects). Texture ice from Karginsky time is about -23.7‰ for both sites, whereas Holocene texture ice is much heavier ($\delta^{18}O$ around -20‰), again showing the similarity between both sites and the relatively warmer Holocene. In contrast, texture ice from Sartansky time is characterized by very light isotopic composition (-27.6‰) close to that of ice wedges (-29.8‰). This may correspond to extremely cold summer temperatures and/or a relatively smaller amount of summer precipitation taking part in texture ice formation at that time. The late glacial maximum (LGM) apparently is visible only in summer.

The higher differences between isotopic composition of ice wedges and texture ice (as well as the heavier $\delta^{18}O$ of texture ice) in Karginsky time may reflect relatively warm summer conditions. Additionally, the negative $\delta^{18}O$ values of ice wedges point to severe winter conditions at that time.

$\delta^{18}O$ and δD of ice wedges at both sites are aligned parallel to GMWL with slopes close to 8. This indicates that the isotopic composition of initial meteoric water-formed ice wedges was not subject to pronounced fractionation processes. In contrast, isotopic composition of texture ice crosses the GMWL with slopes of 6.8 (site 1) and 7.2 (site 2). This is a result of fractionation processes during evaporation and freezing as well as mixing of both snowmelt and rainwater, also reflected in *d* excess. In general, low *d*-excess values of texture ice point to fractionation during evaporation and reflect the influence of rainwater enriched in heavy isotopes. High *d*-excess values can be considered a result of fractionation during freezing.

## Conclusions

The isotopic records of ground ice correlate well with the global climatic trend, and show progressive warming from MIS-3 to MIS-1. Ice wedge isotopic composition is indicative for $T_w$. $\delta^{18}O$ values of texture ice allow estimating summer climatic conditions (by comparing with ice wedges). The *d* excess, well known as an indicator of precipitation sources, also reflects fractionation processes during ground ice formation.

Negative $\delta^{18}O$ of ice wedges reflect (stable) cold winter conditions during Karginsky (MIS-3) and Sartansky (MIS-2) time with minimum in Karginsky time. Differences of $\delta^{18}O$ values between ice wedges and texture ice point to relatively warmer summers in Karginsky time and colder summer periods in Sartansky time. This let us believe that the LGM in the region is visible only in summer indicators.

The combined isotopic analysis of both ice wedges and texture ice extends considerably the quantitative and qualitative capabilities of paleoenvironmental interpretation.

## References

Mackay, J.R. 1983. Oxygen isotope variations in permafrost, Tuktoyaktuk Peninsula area, Northwest Territories. *Current Research, Part B, Geological. Survey of Canada* Paper 83-1B: 67-74.

Meyer, H., Dereviagin, A., Siegert, C. & Hubberten, H.-W. 2002a. Paleoclimate studies on Bykovsky Peninsula, North Siberia. Hydrogen and oxygen isotopes in ground ice. *Polarforschung* 70: 37-52.

Schirrmeister, L., Grosse, G., Kunitsky, V., Magens, D., Meyer, H., Dereviagin, A., Kuznetsova, T., Andreev, A., Babiy, O., Kienast, F., Grigoriev, M. & Preusser, F. 2008. Periglacial landscape evolution and environmental changes of Arctic lowland areas during the Late Quaternary (Western Laptev Sea coast, Cape Mamontov Klyk). *Polar Research* (accepted).

Schirrmeister, L., Siegert, C., Kuznetsova, T., Kuzmina, S., Andreev, A.A., Kienast, F., Meyer, H. & Bobrov, A.A. 2002. Palaeoenvironmental and palaeoclimatic records from permafrost deposits in the Arctic region of Northern Siberia. *Quaternary International* 89: 97-118.

# Adaptating and Managing Nunavik's Transportation Infrastructure

Guy Doré
*Laval University*
Anick Guimond
*Quebec Ministry of Transportation*
Gilles Grondin
*Quebec Ministry of Transportation*

## Introduction

In Nunavik (Quebec, Canada), an important increase in mean annual temperatures has occurred over the last 15 years. As a result, permafrost is degrading and is threatening the integrity of roads and airfields in 13 Inuit communities. This study was initiated by the Quebec Ministry of Transportation in order to adapt transportation embankments to the new climatic reality. The purpose of this study is to identify the consequence of global warming on the transportation infrastructure, to carry out a performance assessment of the Nunavik runways and access roads since their construction, and to develop a management strategy in order to effectively maintain a safe airport and access road network in Nunavik.

## Problem Statement

Damages observed on Nunavik's airstrips and access roads caused by degrading permafrost have led the Quebec Ministry of Transportation to take action. Research has been undertaken to assess current and foreseeable impacts on northern infrastructures, recommend adaptation strategy and propose a management plan for these transportation infrastructure networks.

## Condition of Nunavik's Airports and Access Roads

The study led to the identification of six unstable runways and two unstable access roads. Depressions along airstrip edges and roadsides and water ponding in drainage ditches are the most frequent problems observed in Nunavik. These problems are mainly caused by snow accumulation on the side-slopes and by climate warming. As a result, the ground temperature under the embankments and more specifically under side-slopes tends to increase, causing permafrost degradation and loss of support if the permafrost is ice-rich.

## Experimentation of Protection Techniques

Three protection techniques that have the potential for large-scale application in Nunavik have been chosen to mitigate permafrost degradation under transportation infrastructures in Nunavik. Air convective embankment, heat drain, and reflective surfaces have been selected for their operational and economical feasibility. The intent is to use these techniques in cases of severe degradation on recently paved access roads and on airstrips. The use of protection technique should extend the service life or reduce the maintenance requirements of Nunavik's transportation infrastructure. The heat drain was developed at Laval University (Beaulac & Doré 2006). This technique allows heat extraction from the embankment during winter through a highly permeable geocomposite placed in the embankment shoulder. The air convection embankment, developed in Alaska (Goering 2003), uses convective flow in large pores of a uniform-size stone material to activate heat loss in embankments during winter. Use of reflective surfaces can reduce the *n*-factor and has proven to be effective in reduction of the depth of thaw penetration in permafrost regions. Reflective surfaces, based on the use of white paint applied on pavement surfaces, have been tested in several experimental projects in Alaska (Reckard 1985).

The solutions based on heat extraction (heat drain and convection embankment) have been tested in a laboratory on small-scale embankments built in a cold room. Laboratory testing has demonstrated the effectiveness of the heat drain and of the air convection embankment. The results showed that it is possible to lower ground temperature significantly during winter when these techniques are used in the embankment. Temperature differences reaching 7°C have been observed between the two protection techniques and the reference embankment. The testing program will continue to support thermal modeling and development of design parameters for these techniques.

The reflective surface has been tested at the Laval University Road Experimental Site (SERUL) and the results of the experiment are discussed in (Stuhr-Jorgensen & Doré 2007). All these techniques are also being tested in the field on the Salluit airport access road and on the embankment of the Tasiujaq airstrip. The objective of the experimental program is to assess the technical, operational, and economical feasibility of these techniques and to identify those having the best potential for large-scale application. The Salluit test site, including six test sections, was constructed in summer 2006 to determine the operational and economical feasibility of the techniques (initial construction cost, maintenance cost, labour and materials cost, heavy equipment location cost, and shipping cost). The three protection techniques described above have been used alone (3 sections) and by combining the reflective surface with both heat extraction techniques (2 sections). An additional section is used as a reference to assess the relative effectiveness of the protection techniques.

The Tasiujaq airstrip project involves the experimentation of the air convection embankment and the heat drain in the shoulder of the embankment. The project also includes a

Figure 1. Installation of the heat drain in the shoulder of the Tasiujaq airstrip embankment.

gentle slope section to measure the benefit of modifying the embankment geometry in order to reduce problems caused by snow accumulation along the embankment. Figure 1 illustrates the installation of the heat drain section besides the air convection section in Tasiujaq, Nunavik. Thermistor strings have been installed in the test sections. Data is recorded by automatic data acquisition systems every four hours for the duration of the project (3 years). Thermal regimes in the test sections will be the basic information used to quantify the performance of each technique used. Despite numerous operational problems, some encouraging data trends were observed during the first months of operation.

It is expected that the use of protection techniques will increase the service life of the Nunavik transportation infrastructure.

## Management Strategy

The last step of the research project was to develop the framework of a management strategy for the transportation infrastructure of Nunavik. The strategy is based on four coordinated groups of activities:

1. Data collection
   a. Identification of thaw sensitive areas along airstrips and access roads
   b. Characterization of thaw sensitive areas including thaw and settlement rates as well as characteristics of soils in the top part of the permafrost
2. Identification of applicable solutions, and assessment of their effectiveness and economical benefit
3. Implementation of the selected solution
4. Long term monitoring of the performance of the selected solution

## Conclusion

The study led to the identification of six unstable runways and two unstable access roads. Three mitigation methods and a management plan are proposed to reduce permafrost degradation at Nunavik transportation infrastructures. The protection techniques include heat drains, air convective embankments, and reflective surfaces. These techniques have been experimented with in controlled conditions in order to assess their relative effectiveness and to determine design parameters in view of their application on road and airfield embankments. They are also being tested in a full-scale test embankment on the Salluit access road and the Tasiujaq airstrip in Nunavik. The management plan involves the identification of thaw-sensitive areas in the Nunavik airport and access roads network. It also involves monitoring the rate of evolution of these problem areas and investigation of permafrost conditions beneath the embankments. Finally, the management plan involves the development of a series of maintenance and construction actions in order to maintain the transportation network in safe and good condition.

## References

Beaulac, I. & Doré, G. 2006. Development of a new heat extraction method to reduce permafrost degradation under highway and airfield embankments, *Compte Rendu de 13th Int. Conf. on Cold Region Engineering Orono, ME, 2006*: CDROM.

Goering, D.J. 2003. Thermal response of air convective embankments to ambient temperature fluctuations. *Proceedings of the Eighth International Conference on Permafrost, Zurich, Switzerland, 20–25 July 2003*: 291-296.

Reckard, M.K. 1985. *White Paint for Highway Thaw Settlement Control*. Fairbanks, Alaska, USA: Alaska Department of Transportation and Public Facilities. Report no. FHWA-AK-RD-85-16: 1-7.

Stuhr-Jorgensen, A. & Doré, G. 2007. *Use of Reflective Surfaces on Roadway Embankment*. Tempere, Finland: ISCORD.

# Human Experience of Cryospheric Change in Nunavut, Canada: Preliminary Findings

Nancy Doubleday
*Carleton University, Ottawa, Canada*
Shawn Donaldson
*Carleton University, Ottawa, Canada*
Tatiana Vlasova
*Russian Academy of Sciences, Moscow, Russia*
Anita Kushwaha
*Carleton University, Ottawa, Canada*
Morgan Ip
*Carleton University, Ottawa, Canada*

There is a significant consensus within both scientific and northern communities: dramatic change is occurring in the Arctic (e.g., ACIA 2005, Hinzman 2005, Duerden 2004) and the transformation of the cryosphere itself provides a critical focal point for research contributing to our understanding of health and well-being. Despite debates about the relative importance of drivers of change (e.g., Zalasiewicz et al. 2008), the occurrence of environmental change, both gradual and rapid, is not at issue (although many elements of landscape processes and impacts still require further study). The necessity of adaptation at all scales of both human organization and landscape dynamics is not in dispute either. However, in moving forward from identification of processes of environmental change to definition of impacts, then to development of strategies for mitigation and adaptation, we enter stormy and contested regions. Why? Because integration of physical and social science perspectives, along with those of actors who engage locally, regionally, nationally, and internationally with realities of a changing cryosphere, is necessary in order to build effective policy and to set priorities for mitigation and for adaptation. In reaching for multiparty consensus on actions, we face limitations of knowledge, of knowledge interoperability, and of decision-making processes; as well as potentially conflicting goals and objectives, priorities, and visions. Lack of agreement and cooperation can affect both capacities for communication and adaptation as well as resources available for mitigation. Standard approaches to decision-making in the south and the north see government agencies consulting with stakeholder representatives, usually at a point after an issue has been defined and after measures available to address it have already been scoped, but before a final decision is taken. This process is also a reflection of past practice with respect to knowledge creation, and assumes that community and other "local" interests are farther removed from expert knowledge. Here, by positioning local or traditional knowledge as complementary source, in conjunction with social and physical sciences in current research, we are building transdisciplinary knowledge (Wilcox 2008) as a starting point for multiparty consensus around environmental change in Nunavut, Canada, and for inclusive strategies for mitigation and adaptation, emphasizing local communities and their concerns.

*Preliminary findings*

Practically, we integrate physical and social science of northern environmental change by situating our research at the nexus of environment, health, and well-being, as framed by northerners themselves, in a series of specific studies constructed to include both research and design elements in methods of enquiry. We report briefly on five related studies currently under investigation: (1) food choice among women and men, and thus impacting health and well-being; (2) local perceptions and understanding of ecological changes linked to a changing cryosphere through investigation of spatial and temporal variation in observations of plants and as interpreted from photographs; (3) design choices in arctic architecture as represented by a healing centre, directly contributing to health and well-being; (4) integration of data from these substudies, and refinement of mixed methods for advancing transdisciplinary work, as steps in the iterative research process; and (5) development of protocols modeled on Canadian standards for ethical and just research involving humans that yield both point-in-time images ("snapshots") of social, environmental, and economic conditions, as well as in-depth profiles at selected sites. The purpose of this research is to understand adaptation, mitigation, and community resilience, in the face of cryospheric environmental change, using mixed methods to achieve social-ecological systems integration.

In Nunavut, Canada, we are documenting food choice among women and men. Previously, Donaldson investigated factors influencing food choice, and Kushwaha documented Inuit traditional knowledge of the effects of environmental change on sea ice and ringed seal. Results here indicated that multiple factors are involved both in food choices and in traveling and hunting decisions. We note that uncertainty plays a larger role: for example, the thickness, extent, and stability of sea ice in the Cape Dorset area have changed in recent years, making it increasingly difficult to travel and hunt; and weather patterns have also changed. While hunters report ringed seals in the surrounding area to be

physically healthy, they have become increasingly difficult to hunt, as the occurrence of sinking seals has become more common. Local residents have been responding and coping to environmental changes primarily by adapting their subsistence hunting practices. These findings are consistent with Reidlinger and Berkes' (2001) earlier work in the Western Arctic, and suggest that adaptation to rapid cryological change is occurring in the Foxe Basin, off Baffin Island, as well.

During preliminary site visits to Sanikiluaq, Rankin Inlet, and Baker Lake in 2007, other community observations and reports of impacts confirmed the regional nature of change. While the form of environmental expression varied (i.e., skinny seals in marine environments and thicker willows inland), the reports all pointed to systemic change.

We find these "social observations" (Vlasova 2006) to be an extremely sensitive detector of environmental change. The challenge is then to communicate these findings so that they can be integrated with studies that model change on global or regional scales. If synergies among multiple factors across scales are in fact the case, as the regional variability of the warming trends suggest, then strategies for adaption and mitigation must be capable of recognizing and addressing local and regional factors implicated in these changes. Additionally, linking the data generated by physical environmental studies with social impacts requires social data. The fine-grained "social observations" approach may contribute most significantly here. We anticipate additional data on this question from the second project "plants and photographs through time," which provides a direct link to daily life, focusing spatial and temporal observations of plants, and using photographs to derive anecdotal information.

In terms of proactive adaptation through design, the third study, investigating appropriate architecture, offers a critical view of past practice and resulting increases in risk associated with cryospheric change. Next steps will address incorporation of community values in design of a healing centre. The fourth project is iterative, and will integrate results from the other studies as they become available. The fifth project to develop protocols for social, environmental, and economic observations is well underway, with a consultation meeting scheduled in April 2008.

These projects are contributions to PPS Arctic, an international study of the impacts of a changing tree line, led by Annika Hofgaard of Norway. We will conduct a second season of fieldwork on all five studies in 2008–09. In the longer term, we plan to continue transdisciplinary work and welcome connections with other researchers who are similarly engaged.

## Acknowledgments

We thank the people of the communities of Nunavut, the Nunavut Research Institute, the International Polar Year Office of the Government of Canada, Carleton University, and the Russian Academy of Science, Institute of Geography. We also thank the organizers of NICOP 2008.

## References

ACIA 2005. *Arctic Climate Impact Assessment*. Cambridge University Press, 1042 pp. Web site: http://www.acia.uaf.edu (accessed 10 March 2007).

Duerden., F. 2004. Translating climate change impacts at the community level. *Arctic* 57(2): 204-212.

Furgal, C. & Seguin, J. 2006. Climate change, health, and vulnerability in Canadian northern aboriginal communities. *Environmental Health Perspectives* 114(12): 1964-1970.

Hinzman, L.D., Bettez., N.D., Bolton, W.R., Chapin, F.S., Dyurgerov, M.B., Fastie, C.L., Griffith, B., Hollister, R.D., Hope, A., Huntington, H.P., Jensen, A.M. Jia, G.J., Jorgenson, T., Kane, D.L., Klein, D.R., Kofinas, G., Lynch, A.H., Lloyd, A.H., Mcguire, A.D., Nelson, F.E., Oechel, W.C., Osterkamp, T.E., Racine, C.H., Romanovsky, V.E., Stone, R.S., Stow, D.A., Sturm, M., Tweedie, C.E. Vourlitis, G.L., Walker, M.D., Walker, D.A., Webber, P.J., Welker, J.M. 2005. Evidence and implications of recent climate change in northern Alaska and other Arctic regions. *Climatic Change* 72: 251-298.

Reidlinger D, & Berkes F. 2001. Responding to climate change in northern communities: Impacts and adaptations. *Arctic* 54(1): 96-98.

Vlasova, T. 2006. Arctic residents' observations and human impact assessments in understanding environmental changes in boreal forests: Russian experience and circumpolar perspectives. *Mitigation and Adaptation Strategies for Global Change* 11: 897-909.

Wilcox, B. & Kueffer, C. 2008. Transdisciplinarity in EcoHealth: Status and future prospects. *EcoHealth* doi:10.1007/s10393-008-0161-5 (accessed 21 March 2008).

Zalasiewicz, J., Williams, M., Smith, A., Barry, T.L., Coe, A.L., Bown, P.R., Brenchley, P., Cantrill, D., Gale, A., Gibbard, P., Gregory, F.J., Hounslow, M.W., Kerr, A.C., Pearson, P., Knox, R., Powell, J., Waters, C., Marshall, J., Oates, M., Rawson, P. & Stone, P. 2008. Are we now living in the Anthropocene? *GSA Today* 18(2): 4-8.

# HiRISE Observations of Fractured Mounds in the Martian Mid-Latitudes

Colin M. Dundas
*The University of Arizona, Department of Planetary Sciences, Tucson, AZ, USA*
Alfred S. McEwen
*The University of Arizona, Department of Planetary Sciences, Tucson, AZ, USA*

## Introduction

The planet Mars has widespread permafrost, much of it ice-rich. Some ground ice features such as thermal contraction cracks have been confidently identified based on orbital imagery (e.g., Mellon 1997). The possibility of other periglacial features has been considered; in particular, a number of authors have suggested various Martian features as pingos (Judson & Rossbacher 1979, Parker et al. 1993, Cabrol et al. 2000, Soare et al. 2005, Burr et al. 2005, Page & Murray 2006). However, low resolution of orbital imagery made it difficult to assess detailed morphologies of such features, and in several cases, later work has indicated different formation mechanisms (Farrand et al. 2005, Martinez-Alonso et al. 2005, Jaeger et al. 2007). This has left the possibility of pingos on Mars an open question. The issue is of particular importance, since pingos would provide information about the state and history of water on Mars, with implications for the origins of other water-related features such as young gullies (Malin et al. 2000).

The High Resolution Imaging Science Experiment (HiRISE) camera on the Mars Reconnaissance Orbiter (MRO) spacecraft has returned several thousand images of the Martian surface with scale as small as 26 cm/pixel. This resolution allows assessment of fine-scale morphologies in much more detail than previously possible. Early images revealed fractured mounds, similar to pingos on Earth in some respects, in both northern and southern mid-latitudes (Dundas et al. 2008). Dundas et al. (2008) also used lower-resolution images to examine the distribution of flat-topped mounds (matching the approximate shape of some of the observed features) and found that in the northern plains region of Utopia Planitia, the mounds occurred in the latitudinal band where gullies are most common. This study uses HiRISE images to examine the planet-wide distribution and range of morphologies in order to better compare these mounds with pingos on Earth.

## HiRISE Observations

*HiRISE survey*

HiRISE images from across Mars were examined in order to assess the distribution of fractured mounds. This is a non-genetic definition that could encompass a range of morphologies and origins, used here in order to ensure a comprehensive survey of possible pingos. We search for features where fracturing occurs only on the mound or is distinctly enhanced there, since much of the Martian surface has fractures of various origins. We specifically exclude outcrops of jointed rock and knobs with superposed polygonal cracks occurring as part of a widespread network (e.g., thermal contraction cracks).

To date, 1350 HiRISE images have been incorporated into this survey. All images obtained through orbit 2150 were used; among images from subsequent orbits, only those from latitudes 20°–60° of each hemisphere were examined.

*Fractured mound morphologies*

A wide range of morphologies fitting the loose definition of fractured mound have been observed. Some are isolated, while others, typically smaller, are clustered. In several instances, roughly radial fracture patterns are observed, but in other cases the fractures are irregular. Mounds are found in pits or small impact craters at several sites, often in association with other fractured features. The breadth of the definition also includes some anomalous forms, such as irregular, few-hundred-meter scale raised plateaus with distinct fracturing.

This breadth prevents any feature from being truly typical, but several broad categories are observed. Fractured mounds in the Southern Hemisphere are generally found on the floors of multi-kilometer diameter impact craters, often with gullied walls. This group includes both isolated mounds (e.g., Fig. 1) and clusters of fractured features. A group of flat-topped mounds in Utopia Planitia displays distinct summit fracturing, often radially oriented, and is often found

Figure 1. Fractured mound in HiRISE image PSP_007522_1480. The mound is approximately 100 m across and lies on the floor of an impact crater with gullied walls. Illumination is from the right and north down in this non-map-projected image.

in conjunction with irregular mounds in small craters. A third major class encompasses those mounds found on lineated valley fill. These are often irregular or degraded and, in some cases, may include remnants of a mantling deposit.

*Fractured mound distribution*

Despite the scope of the definition, the mounds exhibit notable latitudinal control. They are generally found between 30°–45° in each hemisphere. The distribution also exhibits some longitudinal variation; fractured mounds are generally absent from the volcanic provinces of Tharsis and Elysium, although some portion of this variation may be due to biases in HiRISE image coverage, which is concentrated over certain areas.

## Discussion

Fractured mounds are a broad category, which may include features of multiple origins. The apparent latitudinal control suggests that these features have origins related to water or ice activity, particularly since the latitude bands of the mounds are also the locations of other water- or ice-related features (e.g., Milliken et al. 2003).

Several of the fractured mounds appear to be very good morphological analogues for terrestrial pingos, particularly the isolated examples near the base of gullied slopes. Since gullies may indicate shallow groundwater outflow (Mellon & Phillips 2001), these could be similar to hydraulic pingos. In other cases, a pingo-like origin is less likely: at least some of the mounds on lineated valley fill may be degraded impact craters with inverted relief (Mangold 2003) or eroding mantling material. The mounds in Utopia Planitia are morphologically similar to pingos in several ways, including scale and (frequently) distinct radial fractures, but often have distinctly trapezoidal profiles and are found in level terrain rather than in depressions or at the base of slopes.

The possible effects of different Martian conditions on morphology complicate interpretation. Different processes could produce similar resulting landforms, and Mars may have a different range of ground ice processes than Earth. However, the mounds discussed here include the best morphological analogues for pingos yet observed on Mars. Further coverage from HiRISE will clarify the range of morphologies and settings and allow more detailed analysis of formation mechanisms.

## Acknowledgments

We thank the HiRISE science and operations teams for their work in producing outstanding images and the MRO project for support.

## References

Burr, D.M., Soare, R.J., Wan Bun Tseung, J.-M. & Emery, J.P. 2005. Young (late Amazonian), near-surface, ground ice features near the equator, Athabasca Valles, Mars. *Icarus* 178(1): 56-73.

Cabrol, N.A., Grin, E.A. & Pollard, W.H. 2000. Possible frost mounds in an ancient Martian lake bed. *Icarus* 145: 91-107.

Dundas, C.M., Mellon, M.T., McEwen, A.S., Lefort, A., Keszthelyi, L.P. & Thomas, N. 2008. HiRISE Observations of fractured mounds: Possible Martian pingos. *Geophysical Research Letters* 35(4): L04201.

Farrand, W.H., Gaddis, L.R. & Keszthelyi, L. 2005. Pitted cones and domes on Mars: Observations in Acidalia Planitia and Cydonia Mensae using MOC, THEMIS and TES data. *Journal of Geophysical Research (Planets)* 110(E5): E05005.

Jaeger, W.L., Keszthelyi, L.P., McEwen, A.S., Dundas, C.M. & Russell, P.S. 2007. Athabasca Valles, Mars: A lava-draped channel system. *Science* 317(5845): 1709-1711.

Judson, S. & Rossbacher, L. 1979. Geomorphic role of ground ice on Mars. *NASA Technical Memo 80339*: 229-231.

Malin M.C. & Edgett, K.S. 2000. Evidence for recent groundwater seepage and surface runoff on Mars. *Science* 288(5475): 2330-2335.

Mangold, N. 2003. Geomorphic analysis of lobate debris aprons on Mars at Mars Orbiter Camera scale: Evidence for sublimation initiated by fractures. *Journal of Geophysical Research (Planets)* 108(E4): CiteID 8021.

Martinez-Alonso, S., Jakosky, B.M., Mellon, M.T. & Putzig, N.E. 2005. A volcanic interpretation of Gusev Crater surface materials from thermophysical, spectral and morphological evidence. *Journal of Geophysical Research (Planets)* 110(E1): CiteID E01003.

Mellon, M.T. 1997. Small-scale polygonal features on Mars: Seasonal thermal contraction cracks in permafrost. *Journal of Geophysical Research* 102(E11): 25,617-25,628.

Mellon, M.T. & Phillips, R.J. 2001. Recent gullies on Mars and the source of liquid water. *Journal of Geophysical Research* 106(E10): 23,165-23,180.

Milliken, R., Mustard, J.F. & Goldsby, D.L. 2003. Viscous flow features on the surface of Mars: Observations from high-resolution Mars Orbiter Camera (MOC) images. *Journal of Geophysical Research (Planets)* 108(E6): CiteID 5057.

Page, D.P. & Murray, J.B. 2006. Stratigraphical and morphological evidence for pingo genesis in the Cerberus plains. *Icarus* 183(1): 46-54.

Parker, T.J., Gorsline, D.S., Saunders, R.S., Pieri, D.C. & Schneeberger, D.M. 1993. Coastal geomorphology of the Martian northern plains. *Journal of Geophysical Research* 98(E6): 11,061-11,078.

Soare, R.J., Burr, D.M. & Wan Bun Tseung, J.-M. 2005. Possible pingos and a periglacial landscape in northwest Utopia Planitia. *Icarus* 174(2): 373-382.

# A Soil Freeze-Thaw Model Through the Soil Water Characteristic Curve

Stefano Endrizzi
*Department of Civil and Environmental Engineering, University of Trento, Italy*
Riccardo Rigon
*Department of Civil and Environmental Engineering, University of Trento, Italy*
Matteo DallAmico
*Department of Civil and Environmental Engineering, University of Trento, Italy*

## Introduction

The mathematical description of the freeze-thaw behavior of soil mainly depends on its texture. Usually coarse-grained soils follow a moving boundary with phase change, commonly referred to as the *Stefan problem*, whereas fine-grained soils show the existence of a "frozen-fringe" (Fowler & Krantz 1994) of partially frozen soil between frozen and unfrozen regions. Therefore, the possibility of including the freezing characteristic of soil in a model (Hansson et al. 2004) appears promising, as it allows the description of the freezing/thawing cycles of natural soils.

The goal of this work is to propose a freezing soil scheme based on soil freezing characteristic curves and to test it against the analytical solution of the Neumann problem.

## The Freeze-Thaw Model

The freezing soil model can be explained by the following equations:

$$\begin{cases} C_T \dfrac{\partial T}{\partial t} + L_f \dfrac{\partial W}{\partial t} = \dfrac{\partial}{\partial z}\left( \lambda_T \dfrac{\partial T}{\partial z} \right) \\ \rho_w \dfrac{\partial \theta_w}{\partial t} = -\rho_i \dfrac{\partial \theta_i}{\partial t} = \dfrac{\partial W}{\partial t} \end{cases} \tag{1}$$

The first term represents the energy budget equation where $\theta_w$ and $\theta_i$ (-) are the volumetric content of water and ice, respectively; $n$ is the porosity, $\rho_w$ and $\rho_i$ (Kg/m$^3$) are the density of water and ice, respectively; $W$ (Kg/m$^3$) is the quantity of water in the control volume subject to phase change; $L_f$ (J/Kg) is the latent heat of fusion; $T$ (°C) is the temperature; and $z$ (m) is the soil depth coordinate. $C_T=C_s(1-n)+c_w\theta_w\rho_w+c_i\theta_i\rho_i$ (J m$^{-3}$ K$^{-1}$) is the total thermal capacity of the soil, where $C_s$ is the volumetric heat capacity of the soil, and $c_w$ and $c_i$, the mass heat capacity of liquid and ice, respectively. $\lambda_T=K_e(\lambda_s^{(1-n)}\lambda_w^{\theta w}\lambda_i^{\theta i})+(1-K_e)\lambda_{dry}$ (W m$^{-1}$ K$^{-1}$) represents the thermal conductivity of the soil matrix and follows the formulation of Farouki (1981), where $\lambda_s$, $\lambda_w$, and $\lambda_i$ are the thermal conductivities of soil, water, and ice, respectively; $\lambda_{dry}$ is the thermal conductivity of the dry soil (Johansen 1975); and $K_e$ is the Kersten number.

The second equation in (1) is a closure relation and is usually known as the "no flow condition"; that is, the water flux during phase change may be neglected (Fuchs et al. 1978). The left-hand side (LHS) of the second equation represents the freezing/thawing rate and may be described by proper equilibrium and closure relations as follows:

$$\begin{cases} \dfrac{1}{g} \cdot \dfrac{p_w}{\rho_w} = \dfrac{L_f \cdot T}{g \cdot 273.15} = \psi_{eq}(T) \\ \dfrac{\theta_w - \theta_r}{(n - \theta_r)} = \left[ 1 + \left( -\alpha \cdot \psi_{eq} \right)^{\beta} \right]^{\left(1-\frac{1}{\beta}\right)} \end{cases} \tag{2}$$

The first equation represents the thermodynamic equilibrium during phase change, when pressure head $\psi$ (m) and $T$ (°C) satisfy the Clapeyron equation (Christoffersen & Tulazczyk 2003). The second equation represents the unsaturated soil condition by using the soil water characteristic curve (SWCC) according to the Van Genuchten (1980) model, where $\alpha$ (m$^{-1}$) and $\beta$ (-) are Van Genuchten parameters and $\theta_r$ is the residual water content.

Eventually, the allowed unfrozen water content can be plotted against the temperature, and becomes the soil freezing characteristic curve (SFCC) (see Fig. 1). Applying the chain rule to $\partial\theta_w/\partial t=\partial\theta_w/\partial\psi \bullet \partial\psi/\partial T \bullet \partial T/\partial t$ the first equation in (1) may be rewritten as:

$$\left[ C_T + \rho_w C_H \frac{L^2 f}{g \cdot 273.15} \right] \frac{\partial T}{\partial t} = \frac{\partial}{\partial z}\left( \lambda_T \frac{\partial T}{\partial z} \right) \tag{3}$$

where $C_H=\partial\theta_w/\partial\psi$ (m$^{-1}$) is the hydraulic capacity of the soil. The term in squared brackets is often referred to as the *apparent heat capacity* (Williams & Smith 1989) and accounts for both sensible and latent heat capacity of soils.

*The numerical scheme*

The numerical model follows a finite difference discretization with a Crank Nicholson scheme. At the first iteration, the system is solved neglecting phase change in order to calculate the temperature at the time step $k+1$ ($T^{k+1}$): if $T^{k+1}<0$ or $\theta_i>0$, then the freezing soil module is activated. Given the unfrozen water content $\theta_u^{eq}$ at the equilibrium, four alternatives may occur: (a) $T^{k+1}<T^k$ and $\theta_u>\theta_u^{eq}$: cooling soil and excess water content; (b) $T^{k+1}>T^k$ and $\theta_w>\theta_w^{eq}$: warming soil and excess water content; (c) $T^{k+1}<T^k$ and $\theta_u<\theta_u^{eq}$: cooling soil and defect water content; and (d) $T^{k+1}>T^k$ and $\theta_u<\theta_u^{eq}$: heating soil and defect water content. If the current point does not lay on the curve, it has to be moved to equilibrium curve. Under the alternatives (a) and (d) a vertical path at constant temperature is followed, where the unknown in the energy budget equation becomes $W$, that is, the water to be frozen/thawed to reach equilibrium. Under the alternatives (b) and (c), a horizontal path at constant $\theta_u$ is followed, and

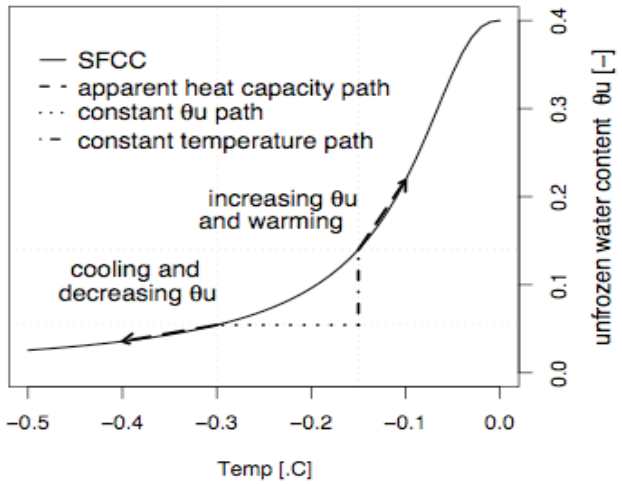


Figure 1. Soil freezing characteristic curve (SFCC) and paths for freezing and thawing calculations.

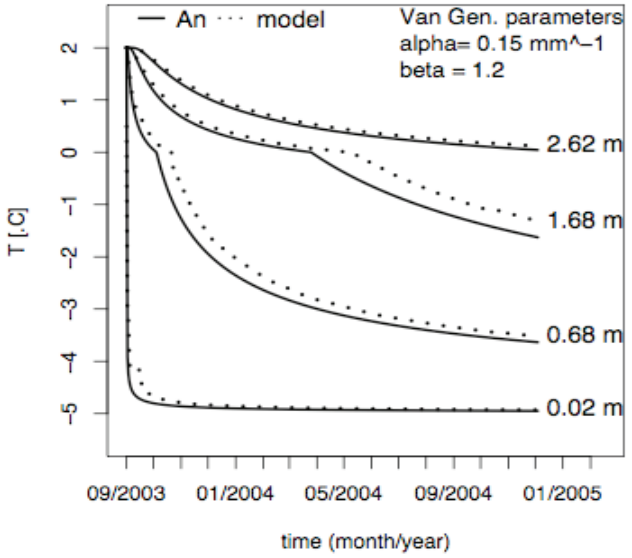


Figure 2. A comparison between the model and the analytical solution at various depths.

the unknown is the temperature $T_{eq}$ at the equilibrium. When the equilibrium curve is reached, the model follows the curve with linearized paths using the apparent heat capacity formulation.

## Application

The model has been tested against the Neumann problem, a simple case of a moving boundary. Nakano and Brown (1971), following the approach described by Carslaw and Jaeger (1959) for a homogeneous substance, give the analytical solution of an initially frozen soil bound to a constant Dirichlet boundary condition at the top. We applied the same formulation to a saturated soil initially thawed at an initial temperature $T_i$=2°C, and later forced to a freezing boundary condition $T_s$=-5°C at the surface.

The results in Figure 2 show that the model follows the analytical solution at the surface, whereas at depths, a little delay is maintained in the frozen part of the curve, progressively increasing with depth. As the same thermal parameters (conductivity and capacity) are given both to the analytical solution and to the model, it seems that the uncertainty relies on the choice of the Van Genuchten parameters, upon which depends the unfrozen water content and the apparent heat capacity. Further investigations are being taken at present to evaluate the influence of these parameters through a sensitivity analysis.

## Conclusions

This work describes a new freezing soil paradigm based on the soil freezing characteristic curves. The model, tested against the analytical solution of the Neumann problem with a moving boundary, seems to be very sensitive to the Van Genucthen parameters and therefore to the shape of the SFCC.

## References

Carslaw, H.S. & Jaeger, J.C. 1959. *Conduction of Heat in Solids*. Oxford: Clarendon Press.

Christoffersen, P. & Tulaczyk, S. 2003. Response of subglacial sediments to basal freeze-on: 1. Theory and comparison to observations from beneath the West Antarctica Ice Sheet. *J. Geophys. Res.* 108: 2222.

Farouki, O.T. 1981. The thermal properties of soils in cold regions. *Cold Regions Sci. and Tech.* 5: 67-75.

Fowler, A.C. & Krantz W.B. 1994. A generalized secondary frost heave model. *SIAM Journal on Applied Mathematics* 54(6): 1650-1675

Fuchs, M., Campbell, G.S. & Papendick, R.I. 1978. An analysis of sensible and latent heat flow in a partially frozen unsaturated soil. *Soil Sci. Soc. Am. J.* 42(3): 379-385.

Hansson, K. et al 2004. Water flow and heat transport in frozen soil: Numerical solution and freeze-thaw applications. *Vadose Zone Journal* 3(2): 693-704.

Johansen, O. 1975. *Thermal Conductivity of Soils.* Ph.D. dissertation. Trondheim: Norwegian Technical Univ.

Nakano, Y. & Brown, J. 1971. Effect of a freezing zone of finite width on the thermal regime of soils. *Water Resources Research* 5: 1226-1233.

Van Genuchten, M.Th. 1980. A closed-form equation for predicting the hydraulic conductivity of unsaturated soils. *Soil Sci. Soc. Am. J.* 44: 892-898.

Williams, P.J. & Smith, M.W. 1989. *The Frozen Earth: Fundamentals of Geocryology*. Cambridge: Cambridge University Press.

# Mapping and Modeling the Distribution of Permafrost in the Nordic Countries

Bernd Etzelmüller, Herman Farbrot, Ole Humlum
*University of Oslo, Norway*
Hanne Christiansen, Håvard Juliussen
*The University Centre in Svalbard, Norway*
Ketil Isaksen
*Norwegian Meteorological Institute, Norway*
Thomas V. Schuler
*Norwegian Water and Energy Directorate and University of Oslo, Norway*
Rune S. Ødegård
*University College of Gjøvik, Norway*
Hanne Ridefelt
*University of Uppsala, Sweden*

## Introduction

In the Nordic countries (Norway including Svalbard, Sweden, Finland, and Iceland) permafrost is widespread and ranges from continuous permafrost in Svalbard, to widespread discontinuous permafrost in high-mountain regions of Iceland and the Scandes, to isolated patches related to palsas, especially in Iceland and northern Scandinavia. Numerous studies exist, especially in Norway and Svalbard, addressing the distribution and thermal regime of permafrost. Here we present the status of permafrost mapping for the Nordic countries, present a map including new borehole information, and draw lines to actual monitoring programmes (TSP NORWAY – Thermal state of permafrost IPY project) and numerical modeling projects (CRYOLINK).

## The Regional Nordic Permafrost Map

As a basis, a simple climate-permafrost relationship has been used to generate a permafrost map of the Nordic countries (Fig. 1). The approach used the relation of gridded mean annual air temperature (1961–90, MAAT) values to permafrost existence, not considering snow conditions and topographic heterogeneity (Etzelmüller et al. 2007). The resulting permafrost distribution was compared with observations in the different regions in Norway, Sweden, and Iceland (e.g., Isaksen et al. 2002, Heggem et al. 2005, Farbrot et al. 2008, Ridefelt et al. in press, Etzelmüller et al. 2007). All validation showed that the general permafrost pattern is well reproduced, indicating a decrease in the lower permafrost limit from west to east in Scandinavia. In Iceland, a southwards increase in altitude of the permafrost limit is due to more maritime and snow-rich conditions in southeastern Iceland.

## Borehole Information – The TSP NORWAY Project

Boreholes for ground thermal monitoring exist especially in Norway and Iceland. The deepest boreholes down to 130 m

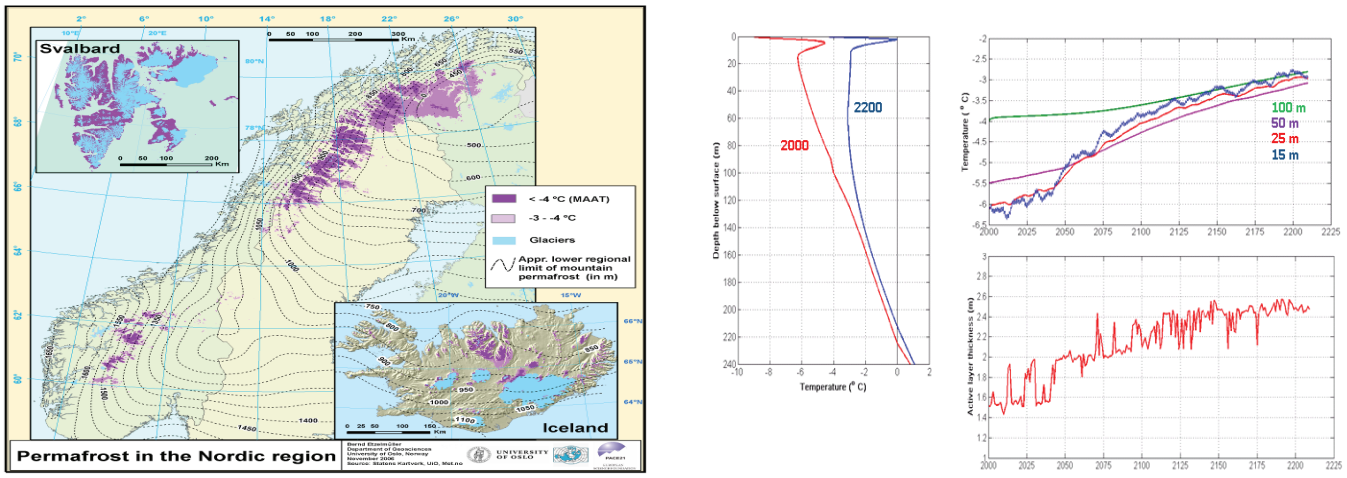


Figure 1. Left: Map of mean annual air temperatures, indicating permafrost distribution in the Nordic countries. This study uses this map as a basis. Information about local permafrost mapping and ground temperature recordings will be added. Right: Projected ground temperatures and active layer depth on Jansonhaugen, Svalbard. A 1D heat-flow model was calibrated based on borehole temperatures, and forced by monthly air temperatures generated from the Hadley Center 1B scenario, down-scaled to Longyearbyen (REGCLIM, e.g., Hanssen-Bauer et al. 2005).The initialization and calibration was based on ground temperature measurements in a borehole (100 m) and extrapolation with depth. Left inlet: Start condition and simulated temperature at end of simulation run. Upper right: Temperature development in various depths. Lower left: Modeled active layer thickness development.

are related to the European PACE project, which commenced in 1997 (Harris et al. 2001). Several shallow boreholes are drilled using nationally funded projects, such as the ongoing IPY project TSP NORWAY (Permafrost Observatory Project: A Contribution to the Thermal State of Permafrost in Norway and Svalbard) (Christiansen et al. NICOP extended abstract), the long-term monitoring programme on Dovrefjell, southern Norway (Sollid et al. 2003), and the currently finished project "Mountain permafrost in Iceland" (Farbrot et al. 2007). All boreholes will be shown on the map, and key parameters will be indicated (average active layer depth, TTOP temperature, ground and surface air temperatures). Furthermore, selected ground temperature profiles will be given as inlets.

## Inlet Maps of Local Permafrost Studies

In addition to the regional map, inlet maps are provided to display permafrost distribution in local settings. These maps comprise the areas of Jotunheimen, Dovrefjell (Isaksen et al. 2001, 2002) and Sølen-Elgå (Heggem et al. 2005) in southern Norway, the Gaissane Mountains in northern Norway (Farbrot et al. 2008), and the Abisko area in Sweden (Ridefelt et al. in press). These larger scaled maps are compiled from multiple logistic regressions of BTS measurements or GIS-based multi-criteria analysis (MCA).

## Future Permafrost Modeling – The CRYOLINK Project

Regional spatial modeling in mountains until now mainly used empirical or statistical modeling approaches (Riseborough et al. 2008). A newly started project funded by the Norwegian Research Council aims to apply existing and develop new numerical modeling tools to address the near-surface heat transfer processes, the spatial distribution of surface and ground temperatures, and the seasonal ground thaw and freeze. As a first step we use a 1D heat flow model on the PACE borehole located at Janssonhaugen, Svalbard (Isaksen et al. 2001) to address thermal responses in the ground to atmospheric forcing. An example is given in Figure 1. Furthermore, the project aims to establish appropriate relations, describing the influence of snow and vegetation (surface offset) and ground type (thermal offset) for the near-surface energy exchange processes as a basis for further spatial modeling of permafrost and seasonal frost. The Norwegian Water and Energy Directorate and the Norwegian Meteorological Institute have developed gridded air temperature and snow data (daily, ground resolution 1 km), enabling the calculation of *N*-factors, GST, TTOP, and permafrost thickness in space. The project's ultimate aim is to develop a spatially distributed model which yields spatial information of ground surface temperatures, ground temperatures, active layer thickness and timing, and seasonal ground freezing depth and duration, as a response to past and future climate changes.

## References


Etzelmüller, B., Farbrot, H., Guðmundsson, Á., Humlum, O., Tveito, O.E. & Björnsson, H. 2007. The regional distribution of mountain permafrost in Iceland, *Permafrost and Periglacial Processes* 18: 185-199.

Farbrot, H., Etzelmüller, B., Gudmundsson, A., Schuler, T.V., Eiken, T., Humlum, O. & Björnsson, H. 2007. Thermal characteristics and impact of climate change on mountain permafrost in Iceland. *Journal of Geophysical Research* 112: F03S90, doi:10.1029/2006JF000541.

Farbrot, H., Etzelmüller, B. & Isaksen, K. 2008. Present and Past Distribution of Mountain Permafrost in Gaissane Mountains, Northern Norway. *Proceedings of the Ninth International Conference on Permafrost, Fairbanks, Alaska, 29 June–3 July 2008.*

Hanssen-Bauer, I., Achberger, C., Benestad, R.E., Chen, D. & Forland, E.J. 2005. Statistical downscaling of climate scenarios over Scandinavia. *Climate Research* 29: 255-268.

Harris, C., Haeberli, W., Vonder Mühll, D. & King, L. 2001. Permfrost monitoring in the high-mountains of Europe: the PACE project in its global context. *Permafrost and Periglacial Processes* 12: 3-12.

Heggem, E.S.F., Juliussen, H. & Etzelmüller, B. 2005. The permafrost distribution in central-eastern Norway. *Norsk Geografisk Tidskrift* 59: 94-108.

Isaksen, K., Hauck, C., Gudevang, E., Ødegård, R.S. & Sollid, J.L. 2002. Mountain permafrost distribution on Dovrefjell and Jotunheimen, southern Norway, based on BTS and DC resistivity tomography data. *Norsk Geografisk Tidsskrift* 56: 122-136.

Isaksen, K., Holmlund, P., Sollid, J.L. & Harris, C. 2001. Three deep alpine permafrost boreholes in Svalbard and Scandinavia. *Permafrost and Periglacial Processes* 12: 13-26.

Ridefelt, H., Etzelmuller, B., Boelhouwers, J. & Jonasson, C. in press. Mountain permafrost distribution in the Abisko region, sub-Arctic northern Sweden. *Arctic. Antarctic and Alpine Research.* Submitted.

Riseborough, D., Etzelmuller, B., Gruber, S., Marchenko, S. & Shiklomanov, N.I. 2008. Space, time, and permafrost: Recent advances in permafrost modeling. *Permafrost and Periglacial Processes.* Submitted.

Sollid, J.L., Isaksen, K., Eiken, T. & Ødegård, R.S. 2003. The transition zone of mountain permafrost on Dovrefjell, southern Norway. *Proceedings of the Eighth International Conference on Permafrost, Zurich, Switzerland*: 1085-1090.

# First Results of Ground Surface Temperature Modeling in Finnmark, Northern Norway

Herman Farbrot
*Department of Geosciences, University of Oslo, Norway and Norwegian Meteorological Institute, Oslo, Norway*
Bernd Etzelmüller
*Department of Geosciences, University of Oslo, Norway*
Ketil Isaksen
*Norwegian Meteorological Institute, Oslo, Norway*
Thomas V. Schuler
*Norwegian Water Resources and Energy Directorate, Oslo, Norway*
Ole Einar Tveito
*Norwegian Meteorological Institute, Oslo, Norway*
Hanne H. Christiansen
*The University Centre in Svalbard, Longyearbyen, Norway*

## Introduction

The main objective of the Norwegian IPY project "Permafrost Observatory Project: A Contribution to the Thermal State of Permafrost in Norway and Svalbard" (TSP NORWAY) (http://www.tspnorway.com) is to measure and model the distribution of permafrost in northern Norway and Svalbard, as well as to assess its thermal state, thickness, and influence on periglacial landscape-forming processes.

The inner part of Finnmark (Fig. 1), the northernmost county of mainland Norway, is a plain, having strong

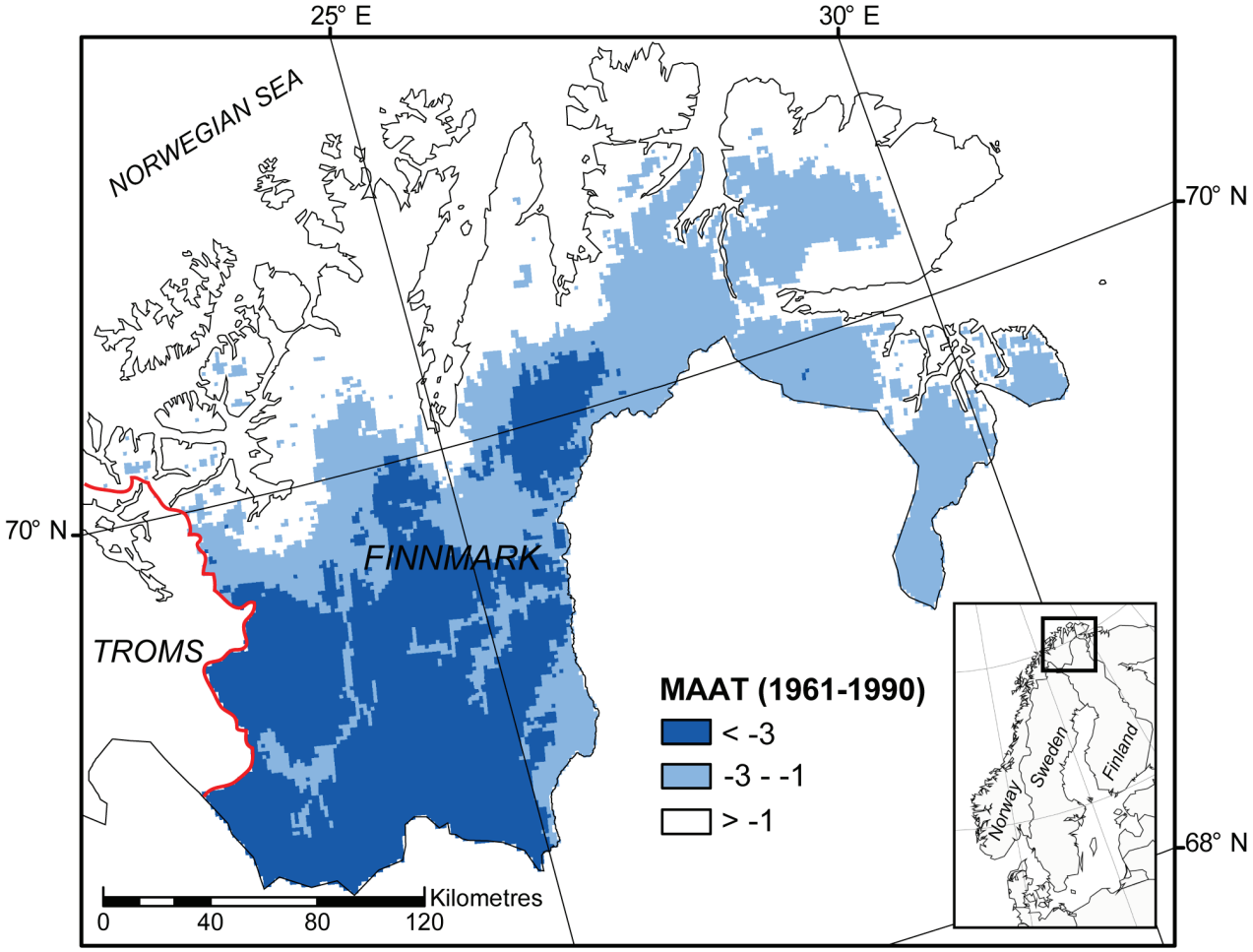


Figure 1. Location map showing three classes of mean annual air temperature (MAAT, 1961–1990) in Finnmark (based on Tveito et al. 2000). The dark grey shows areas where MAAT is lower than -3°C, light grey shows areas where MAAT is between -3°C, and -1°C, and white is MAAT higher than -1°C.

continentality and the lowest MAAT when reduced to sea level in Norway. Typically in this area MAAT is -2.5°C to -4°C, with mean summer temperature of 8°C to 10°C and mean winter temperature -15°C to -20°C. In winter, mean maximum snow depth is 25–75 cm. The current knowledge on the extent and the thermal conditions of permafrost is scarce (Isaksen et al. 2008). Thawing of permafrost in this area may lead to subsidence of the ground surface, having a substantial impact on, for example, the stability of mountain slopes and infrastructure. It is important, therefore, to delineate the distribution of permafrost.

## Modeling the Distribution of Mountain Permafrost

Regional permafrost modeling in southern Norway has so far been based on maps of gridded mean annual air temperature (MAAT), indicating permafrost as probable in non-glaciated mountain areas where MAAT is below -3°C (Etzelmüller et al. 1998, 2003). This crude approach does not take into consideration the effects of the uneven thickness and timing of the winter snow cover as well as the vegetation cover. In Finnmark, permafrost is presumably absent in large forested areas although MAAT < -3°C (Isaksen et al. 2008). The reason is the influence of the forest, where more snow is accumulated than at wind-exposed locations. The low thermal conductivity of snow efficiently insulates the ground surface from the atmosphere at locations having considerable snow cover. Aiming for a better spatial representation of ground temperature and, thus, permafrost conditions in Finnmark, ongoing work elaborates on the connection between MAAT and mean annual ground surface temperature (MAGST) through the Canadian "temperature at the top of permafrost" (TTOP) model. The TTOP model uses seasonal *n*-factors and air temperatures to model MAGST, and a ratio of thawed-to-frozen conductivity of the ground to model the average TTOP (Smith & Riseborough 2002). In a first step, we derive seasonal *n*-factors based on records of air and ground surface temperatures for different land cover and of snow parameters. As input to a regional MAGST model, we use a land-cover map of Finnmark and gridded data of snow thickness and freezing and thawing degree-days sum of air at a resolution of 1 × 1 km. This poster presents first results of this ground surface temperature modeling.

## References

Etzelmüller, B., Berthling, I. & Sollid, J.L. 1998. The distribution of permafrost in Southern Norway; a GIS approach. *Proceedings of the Seventh International Conference on Permafrost, Quebec, PQ, Canada*, Centre d'Etudes Nordiques, Universite Laval, Collection Nordicana 57: 251-257.

Etzelmüller, B., Berthling, I. & Sollid, J.L. 2003. Aspects and concepts on the geomorphological significance of Holocene permafrost in southern Norway. *Geomorphology* 52: 87-104.

Isaksen, K., Farbrot, H., Blikra, L.H. & Sollid, J.L. 2008. Five year ground surface temperature measurements in Finnmark, Northern Norway. *Proceedings of the Ninth International Conference on Permafrost, Fairbanks, Alaska, 29 June–3 July 2008*.

Smith, M.W. & Riseborough, D.W. 2002. Climate and the limits of permafrost: A zonal analysis. *Permafrost and Periglacial Processes* 13: 1-15.

Tveito, O.E., Førland E.J., Heino, R., Hanssen-Bauer, I., Alexandersson, H., Dahlström, B., Drebs, A., Kern-Hansen, C., Jónsson, T., Vaarby-Laursen, E. & Westman, Y. 2000. Nordic Temperature Maps. *DNMI Klima 9/00 KLIMA*, 54 pp.

# Historical Changes in the Seasonally Frozen Ground Regions of the Russian Arctic

Oliver W. Frauenfeld, Tingjun Zhang, Andrew J. Etringer, Roger G. Barry
*CIRES National Snow and Ice Data Center, University of Colorado, Boulder, Colorado, USA*
David Gilichinsky
*Soil Cryology Laboratory, Institute of Physico-Chemical and Biological Problems in Soil Sciences, Russian Academy of Sciences, Pushchino, Moscow Region, Russia*

## Introduction

Seasonal freezing and thawing processes in cold regions play an important role in ecosystem diversity, productivity, and the Arctic hydrological system (Hinzman et al. 1991, Kane et al. 1991, Woo 1992, Osterkamp et al. 2000, Nelson 2003). Long-term changes in seasonal freeze and thaw depths are also useful indicators of climate change (Frauenfeld et al. 2004). However, only sparse historical measurements of seasonal freeze and thaw depths are available for permafrost and seasonally frozen ground regions. In previous work, we applied mean monthly soil temperature data for 1930–1990 at 242 sites located throughout Russia, and employed a simple interpolation scheme to determine the depth of the 0°C isotherm based on soil temperature data measured at 13 depths between 0.2 m and 3.2 m. The relationship between available observed annual maximum freeze and thaw depths and our interpolated values indicates a perfect correlation, and thereby verifies our methodology (Frauenfeld et al. 2004).

In this analysis, we improve on our previous work by employing a greatly expanded station database with soil temperatures for 423 sites with updated observations through the year 2000. These 423 stations are located throughout Russia (Fig. 1) and can be obtained from the Frozen Ground Data Center (http://nsidc.org/fgdc/). The addition of 181 sites throughout the Russian Arctic combined with 10 more years of observations allows for a significantly more comprehensive evaluation. Furthermore, the addition of 1991–2000 allows us to quantify changes in the soil thermal regime during a decade when accelerated climate warming has potentially occurred.

## Data and Methods

Detailed descriptions of soil temperature measurements in the former Soviet Union were provided by Gilichinsky et al. (1998), by Zhang et al. (2001), and in the instruction manuals of the State Committee of the U.S.S.R. for Hydrometeorology and Environmental Control (1985). Observations are available for the 0.2 m, 0.4 m, 0.6 m, 0.8 m, 1.2 m, 1.6 m, 2.0 m, 2.4 m, and 3.2 m depths. We linearly interpolated the depth of the 0ºC isotherm throughout the 0.2 m–3.2 m temperature profile (recognizing that this is not necessarily the same as the "true" freeze/thaw depth). The 423 stations were first classified as either permafrost or seasonally frozen ground, depending on soil temperature at the 3.2 m depth. If, for the entire record, a station's soil temperature at 3.2 m was positive, that station was classified as a seasonally frozen ground station; 387 of the 423 stations qualified. We also employ kriging to improve data quality and in-fill missing observations, and produce nearly continuous station time series for 1930–2000. For the seasonally frozen ground stations, the freeze depth was interpolated between those layers where the temperature switched from negative to positive. The maximum depth of freezing was selected from the months of March, April, and May only. An average time series was generated by averaging all available stations' maximum annual freezing depth departures (with respect to each station's long-term mean) in the seasonally frozen ground region of the Russian Arctic. Linear least-squares regression was then applied to the time series to quantify its long-term changes.

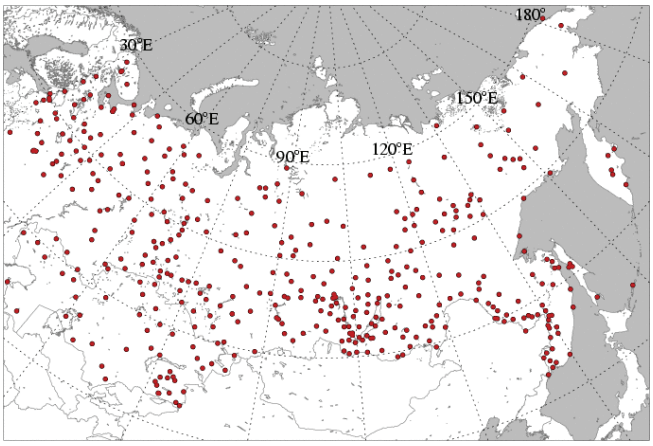

Figure 1. Location of the 428 soil temperature observing sites in Russia.

## Results and Discussion

In our previous work the long-term trend for the 1930–1990 period based on 211 seasonally frozen ground stations indicated a decrease in seasonal freeze depths of approximately 4.4 cm decade$^{-1}$, or 27 cm overall (Fig. 2). This trend is statistically significant (95%-level). However, because prior to the mid-1950s there were too few stations to produce a robust trend (Fig. 2), this 27 cm change had to be interpreted cautiously. Based on the 1956–1990 period, when 100 or more stations contribute to each year's mean value, the overall change is approximately -34 cm (not shown). Note that while a total of 211 stations were available to generate the time series, a maximum of 158 stations contribute at any given year, as most individual station time series are incomplete and have gaps due to missing data.

With the addition of 176 new sites in seasonally frozen ground regions, more data for the original 211 sites, and

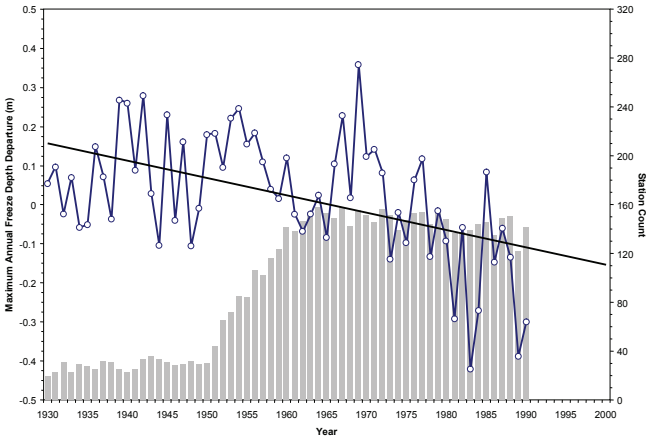


Figure 2. Mean 1930–1990 time series, based on a total of 211 stations, of the maximum annual freeze depth departures. Included also is the linear trend (-4.4 cm decade$^{-1}$). The number of stations contributing to each year's mean value is indicated by the grey bars.

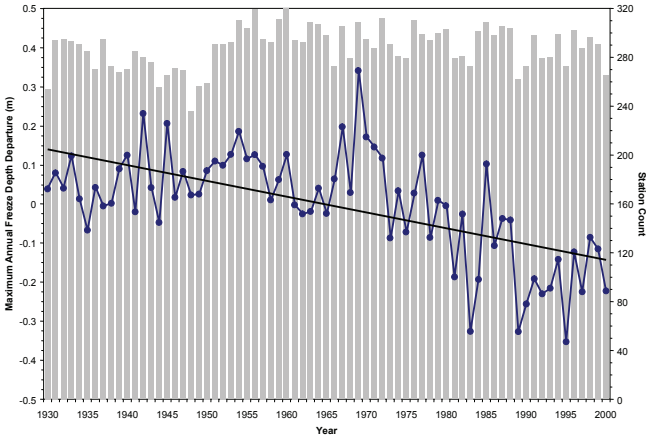


Figure 3. Mean 1930–2000 time series, based on a total of 387 stations, of the maximum annual freeze depth departures. Included also is the linear trend (-4.0 cm decade$^{-1}$). The number of stations contributing to each year's mean value is indicated by the grey bars.

our kriging efforts, we are now able to provide much more robust trend estimates. As shown in Figure 3, up to 320 (of the total 387) stations now contribute to each year's mean freeze depth departure. For the same period as shown in Figure 2, 1930–1990, the trend indicates a decrease of only 17 cm in seasonal freeze depth (not shown). It appears as if the early period prior to 1956 indeed biased our long-term trend estimation in our earlier work. However, the 1956–1990 trend, based on these more complete data, shows an overall decrease of 48 cm. This change is 30% greater than previously reported in Frauenfeld et al. (2004).

The overall change for the 71-year period from 1930–2000 is a statistically significant (95%-level) -4.0 cm decade$^{-1}$, or an overall decrease of 29 cm (Fig. 3). Interestingly, this time series also indicates some patterns of interdecadal variability (and we need to exercise caution, therefore, in applying linear regression). Freeze depths actually increased slightly until ~1970, followed by a sharp decrease until ~1990. From 1990 on, freeze depths may actually be increasing again. In our ongoing efforts, we are trying to establish the degree to which these interdecadal patterns are real or potentially caused by changes in the amount and quality of available data.

## Acknowledgments

This work was funded by the U.S. National Science Foundation under grants ARC-0612431, OPP-0229766, and OPP-0352910, and the International Arctic Research Center, University of Alaska Fairbanks, under the auspices of the NSF cooperative agreement number OPP-0327664.

## References

Frauenfeld O.W., Zhang, T., Barry, R.G. & Gilichinsky. D. 2004. Interdecadal changes in seasonal freeze and thaw depths in Russia. *J. Geophys. Res.* 109: D05101, doi:10.1029/2003JD004245.

Gilichinsky, D.A. et al. 1998. A century of temperature observations of soil climate: Methods of analysis and long-term trends. In: A.G. Lewkowicz & M. Allard (eds.), *Proceedings of the 7th International Conference on Permafrost*, Ste.-Foy, Canada: Centre d'Études Nordiques, Université Laval, 313-317.

Hinzman, L.D., Kane, D.L, Gieck, R.E. & Everett, K.R. 1991. Hydrologic and thermal properties of the active layer in the Alaskan Arctic. *Cold Reg. Sci. Technol.* 19: 95-110.

Kane, D.L., Hinzman, L.D. & Zarling, J.P. 2003. Thermal response of the active layer to climatic warming in a permafrost environment. *Cold Regions Sci. Technol.* 19: 111-122.

Nelson, F.E. 2003. (Un)frozen in time. *Science* 299: 1673-1675.

Osterkamp T.E., Viereck, L., Shur, Y., Jorgenson, M.T. Racine, C., Falcon, L., Doyle, A. & Boone, R.D. 2000. Observations of Thermokarst and its Impact on Boreal Forests in Alaska, U.S.A. *Arct. Antart. Alp. Res.* 32: 303-315.

State Committee of the U.S.S.R. for Hydrometeorology and Environmental Control. 1985. *Instructions for Meteorological Stations and Posts* Vol. 3, Part 1 in Meteorological Observations at Stations, Gidrometeoizdat, Leningrad.

Woo, M.-K. 1992. Impacts of Climatic Variability and Change on Canadian Wetlands. *Can. Water Resour. J.* 17: 63-69.

Zhang, T., Barry, R.G., Gilichinsky, D., Bykhovets, S.S., Sorokovikov, V.A. & Ye. J. 2001. An amplified signal of climatic change in soil temperatures during the last century at Irkutsk, Russia. *Clim. Change* 49: 41-76.

# Rock Glaciers in the Kåfjord Area, Troms, Northern Norway

Regula Frauenfelder
*Department of Geosciences, University of Oslo, Norway,*
*currently at Norwegian Geotechnical Institute, Oslo, Norway*
Jon Tolgensbakk
*Department of Geosciences, University of Oslo, Norway*
Herman Farbrot
*Department of Geosciences, University of Oslo, Norway*
Tom Rune Lauknes
*NORUT AS, Forskningsparken, Tromsø, Norway*

## Introduction

Rock glacier distribution in mainland Norway was inventoried on a macro scale by Sollid & Sørbel (1992). They found that active rock glaciers exist in the high mountain areas of southern and northern Norway, while relict rock glaciers can be found in low-lying areas near the coast of northern Norway and in higher inland areas.

Detailed geomorphological mapping in Troms by Tolgensbakk & Sollid (1988) revealed the existence of more than 100 rock glaciers in the Kåfjord area on the eastern side of Lyngenfjorden. Most of the area lies inside the glacial limit of the Younger Dryas (YD) ice sheet (Andersen et al. 1995), with the youngest YD moraines situated at the valley entrances. Compared to surrounding areas with similar relief and geology, the high frequency of rock glaciers in this region is quite striking. The mapped rock glaciers are mostly of talus-derived origin and are found between the present coastline and the highest mountains in the area (c. 1360 m a.s.l.). Most of the rock glaciers seem to be associated with rockslides caused by neotectonic activity, which was very pronounced in the region during the early Holocene (Tolgensbakk & Kverndal 1995, 1996, Dehls et al. 2000). Due to the general orientation of the main fault (NW–SE trending normal fault, cf. Dehls et al. 2000), the majority of the rock glaciers is concentrated in the sectors SW-W-NW (Fig. 1).

While most of these rock glaciers seem to be relict today, exceptions can be found. Velocity measurements carried out in the early 1990s on one of the rock glaciers showed surface movement in the order of less than 1 cm $a^{-1}$ (Tolgensbakk & Kverndal 1995, 1996). Measurements on this rock glacier, hereafter called Sannjarriep'pi rock glacier, were continued during summer 2006, and the findings are reported in the following.

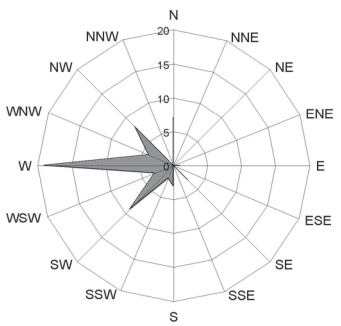


Figure 1. Main aspect of talus-derived rock glaciers in the Kåfjord area ($n$ = 59).

The Sannjarriep'pi rock glacier is situated on the orographic right side of Nordmannvikdalen, a tributary valley to the Lyngenfjord. The rock glacier lies on the western slope of a 1207 m high peak, is approximately 700 m long and 700 m wide, and is situated between 580 and 780 m a.s.l.

## Methods

The deformation of Sannjarriep'pi rock glacier was tracked by two different methods: (a) by polar survey using an electronic theodolite (Wild DI 3000 Distomat), and (b) by space-borne Differential SAR interferometry (DInSAR) using ERS SAR imagery covering the period 1992–1999 (e.g., Bamler & Hartl 1999).

For two-dimensional resistivity tomography (ERT) over one of the lobes of the rock glacier, an ABEM Lund multi-electrode, high-resolution 2D resistivity system was used, applying the Wenner configuration (Reynolds 1997).

Miniature temperature data logger devices have been installed at three locations on the rock glacier in summer 2006. These loggers record the ground surface temperature (GST) at shallow depths in a 2 h interval.

Measurements of Schmidt-hammer rebound values—a proxy for rock hardness, that is, the rock weathering degree—were performed on three different transects perpendicular to the central flow line of the rock glacier. Samples for cosmogenic nuclide exposure dating have been taken on two conspicuous ridges and at the front of the rock glacier (see Fig. 2a for location of measurements).

## Results

The velocity measurements from summer 2006 show that the lower northern lobe of the Sannjarriep'pi rock glacier has been stagnant during the last 17 years (1989–2006), while the upper southern lobe has been steadily moving with c. 1 to 6 mm $a^{-1}$; maximum movement is in the order of 10 cm in 17 years. The DInSAR survey confirms these measurements, with maximum displacement values of -4.9 mm $a^{-1}$ for the southern lobe (Fig. 2b).

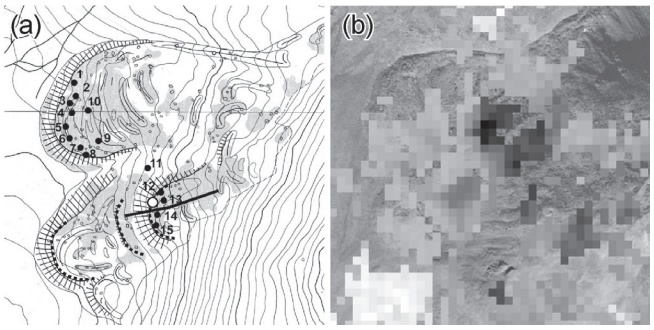


Figure 2. (a) Location of measurements on the Sannjarriep'pi rock glacier: black dots = bolts for terrestrial survey, white dot = location of miniature temperature data loggers, stippled lines = Schmidt-hammer rebound measurement transects, black line = electrical resistivity tomography (ERT) profile. (b) Results of DInSAR measurements: black = -4.9 mm $a^{-1}$, white = stagnant.

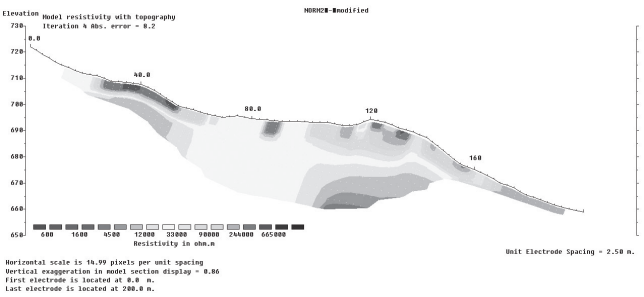


Figure 3. Result of the Electrical resistivity tomography (ERT) measurements. The active layer is highly heterogeneous, characterized by large air voids in the very coarse blocky surface layer. Below the active layer, maximum resistivity values are in the order of 30 to 100 kOhm.m, being indicative for ice.

Mean air temperature at Sørkjosen lufthavn during 2006–2007 was +3.2°C. Applying a lapse rate of -0.005°C/m yields a mean air temperature at the front of the rock glacier (580 m a.s.l.) of c. +0.3°C for the same period. During this period, mean ground surface temperature (GST) on the rock glacier was between +1.0°C (at 10 cm depths, within fine debris) and +1.6°C (below 7 cm thick moss cover on top of large boulder). Mean air temperature measured in an air void of the coarse blocky layer was 1°C (Fig. 4).

The results of the Schmidt-hammer rebound measurements show that the rock glacier is, indeed, a continuous landform with increasing surface age from its source zone (close to the foot of the rock-free face behind it) to its tongue. This result is a prerequisite for the correct interpretation of cosmogenic nuclide exposure dating.

## Acknowledgments

Fieldwork has been financially supported by the Department of Geosciences, University of Oslo and the Swiss Academy of Sciences (Reisestipendien in Botanik, Zoologie und Erdwissenschaften). The ERS-1/2 data set is provided by the European Space Agency (ESA) under the project AOALO.3668. Further thanks go to Christian Hauck for his help with the interpretation of the geophysical results and to Trond Eiken for the post-processing of the distance measurements.

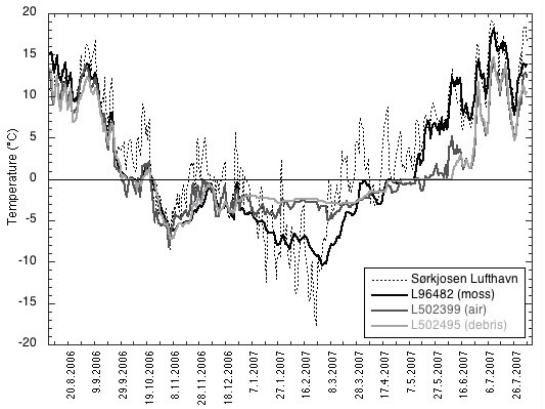


Figure 4. Ground surface temperatures (GST) and air void temperature in the blocky surface layer of the Sannjarriep'pi rock glacier during the period 2006–2007. Air temperature at Sørkjosen Lufthavn, 20 km northeast of Sannjarriep'pi rock glacier is given for comparison.

## References

Andersen, B.G., Mangerud, J., Sørensen, R., Reite, A., Sveian, H., Thoresen, M. & Bergstrøm, B. 1995. Younger Dryas ice-marginal deposits in Norway. *Quaternary International* 28: 147-169

Bamler, R. & Hartl, P. 1998. Synthetic aperture radar interferometry. *Inverse Problems* 14: R1.

Dehls, J., Olesen, O., Olsen, L. & Blikra, L.H. 2000. Neotectonic faulting in northern Norway; the Stuoragurra and Nordmannvikdalen postglacial faults. *Quaternary Science Reviews* 19: 1447-1460

Reynolds, J.M. 1997. *An Introduction to Applied and Environmental Geophysics*. Chichester: John Wiley & Sons, 796 pp.

Sollid, J.L. & Sørbel, L. 1992. Rock glaciers in Svalbard and Norway. *Permafrost and Periglacial Processes* 3: 215–220.

Tolgensbakk, J. & Sollid, J.L. 1988. *Kåfjord, kvartærgeologi og geomorfologi,* 1:50,000, 1634 II. Geographical Institute, University of Oslo (map).

Tolgensbakk. J. & Kverndal A.-I. 1995. Fjellskred og steinbreer I Kåfjordområdet, Troms. *Geonytt* 22: 70.

Tolgensbakk. J. & Kverndal A.-I. 1996. Rock glaciers and Neotectonics in the Kåfjord area, North Norway. *Abstracts of the 28th International Geographical Congress*: 471–472.

# Snowpack Evolution on Permafrost, Non-Permafrost Soils, and Glaciers in the Monte Rosa Massif (Northwest Alps, Italy)

M. Freppaz
*Di.Va.P.R.A. - LNSA, Università di Torino, Grugliasco (TO), Italy*
M. Maggioni
*Di.Va.P.R.A. - LNSA, Università di Torino, Grugliasco (TO), Italy*
S. Gandino
*Comando Truppe Alpine - Servizio Meteomont, Bolzano, Italy*
E. Zanini
*Di.Va.P.R.A. - LNSA, Università di Torino, Grugliasco (TO), Italy*

## Introduction

Snow cover evolution is governed by several variables, such as meteorological factors, local topography, and snow characteristics. Different types of substrata might present different surface temperatures, influencing therefore the temperature gradient within the snowpack and its evolution.

In non-permafrost soils, a thick early winter snow cover maintains soil temperature close to 0°C, independently from air temperature (Edwards et al. 2007). In permafrost soils, beneath at least a 1 m cover of snow, the ground temperature during February and March is below -2 to -3°C (Haeberli 1973, Hoelzle 1992). For glaciers, less literature exists. Kuhn et al. (1998) found an interface temperature between snow and ice of about -5°C.

The aim of this study is to follow the evolution of the snow cover on three different substrata (permafrost, non-permafrost soils, and glacier) in the Monte Rosa Massif on the Italian Northwest Alps.

## Materials and Methods

*Study area*

The three study sites are located in the area of the Monte Rosa Massif in the northwestern Italian Alps. The permafrost site is at an elevation of 2910 m a.s.l. on a northwest-oriented slope of about 10° of inclination; the non-permafrost site is placed at an elevation of 2900 m a.s.l., on horizontal terrain; and the glacier site is located on Indren Glacier at an elevation of 3400 m a.s.l., with a southwest aspect and about 10° of inclination.

*Nivometeorological data*

Snow pits were dug periodically, according to the accessibility of the sites, from December 2006 to July 2007: 9 surveys at the permafrost site, 8 surveys at the non-permafrost site, and 6 surveys at the glacier site. Snow temperature was measured every 10 cm with 10 cm long dial stem thermometers. Snow density measurements were made using a 0.5 L stainless steel core in each layer of the snowpack, where also grain type and dimension were recorded. Continuous measurements of the temperature at the interface between snow and the three different substrata have been made through dataloggers (UTL-1).

Meteorological data in the area, such as wind speed and direction, air temperature, and humidity, were registered by an automatic station of the Italian Army (Comando Truppe Alpine-Servizio Meteomont) located at 2901 m a.s.l. near the three sites.

## Results and Discussion

In the study area, winter 2006–2007 was characterized by a lack of snow cover in the early winter and relatively high air temperature, with a minimum of -17.9°C recorded on January 26. As in Phillips & Schweizer (2006), the characteristics of the snow cover above the three different substrata are summarized in Table 1 and described briefly in the following sections.

*Non-permafrost site*

In the non-permafrost site, the maximum snow depth was recorded on April 4 (180 cm), while until the end of February, the amount of snow was less than 80 cm. Seventy-five percent of the snow profiles were weak-based, with a bottom layer of faceted and depth hoar crystals due to the medium-high temperature gradient recorded mainly in the early winter season. The average snow/soil interface temperature was greater than -1°C.

*Permafrost site*

In the permafrost site, the maximum snow depth was recorded on May 7, greater than in the other two sites. Fifty-six percent of the snow profiles were characterized by faceted and depth hoar crystals, due to the high temperature gradient (recorded especially during March) closely related to the low air temperature, as this site is on a northwest-oriented slope. But 22% of the snow profiles were also characterized by small rounded crystals, typical of an equi-temperature gradient, revealing how the lower ground temperature may induce a lower temperature gradient (Keller & Gubler 1993). The average snow/permafrost interface temperature was -5.1°C, 4.2° colder than the interface temperature between snow and non-permafrost soil.

*Glacier site*

In the glacier site, the maximum snow depth was recorded on May 16. Except for the last snow profile, the snow cover was characterized by a bottom layer of faceted crystals,

Table 1. Snow cover characteristics for the three sites. Except for snow depth and the snow/substratum interface temperature, the other parameters are average values computed on data from manual snow profiles ($N$ = 8 at non-permafrost site, $N$ = 9 at permafrost site, $N$ = 6 at glacier site).

| Parameter | Non-permafrost | Permafrost | Glacier |
|---|---|---|---|
| max snow depth (cm) | 180 | 230 | 125 |
| grain type in bottom layer of snowpack | 5a, 4a | 5a, 4a, 3a | 4c |
| maximum grain size in bottom layer (mm) | 2.4 | 1.8 | 1.7 |
| hand hardness index in bottom layer | 1.8 | 2.2 | 5.0 |
| snow/substratum interface temperature* (°C) | -0.9 | -5.1 | -4.8 |
| temperature gradient within the snowpack (°C/m) | -6.5 | -7.4 | -2.1 |
| density ($Mg/m^3$) | 0.305 | 0.273 | 0.389 |
| Effective heat conductivity (W/mK) | 0.131 | 0.116 | 0.257 |

* average values computed on data recorded by dataloggers (12/29/2006–04/20/2007).

often well bonded together. The snow hardness was very high (level 5), higher than in the other sites. The average snow/glacier interface temperature was -4.8 °C.

The main differences between the three sites can be summarized in the following points:

• A very hard bottom layer was present on the glacier in respect to a snow hardness of 2 for the other two sites; the assumption is that the cold temperature of the glacier surface together with the high density and low gradient might create good conditions for the snow crystals to bond well together.

• The permafrost and glacier sites presented similar interface temperatures, close to -5°C, before reaching isothermal conditions.

• The average temperature gradient at the glacier site was lower than in the other two sites. The possible reason is that the air temperature was higher, as this site is southwest exposed, resulting then in a lower temperature gradient.

In all the sites, the interface temperature remained constant around a certain value (non-permafrost soil -0.9°C, permafrost -5.1°C, glacier -4.8°C) without great oscillations when the snow cover was deep enough to insulate the substrata.

## Conclusions

The main purpose of this work was to analyze the evolution of the snow cover on different substrata to understand if they might generate appreciable differences in the snow cover characteristics.

Our results shows that the main differences in the evolution of the snow cover on permafrost, non-permafrost, and glacier substrata are related to hand hardness in the bottom layer (higher on glacier), snow/substrata interface temperature (higher on non-permafrost soil), and temperature gradient (lower on glacier).

Moreover, an important outcome of this work is that the temperature at the snow/substrata interface remains constant around certain values, without oscillating in relation to air temperature, when enough snow covers the substrata, showing the important insulating effect of the snow.

## Acknowledgments

Fot the technical support we thank MonterosaSki, Roberto Cilenti, Corpo Guide Alpine di Alagna Valsesia, Regione Autonoma Valle d'Aosta-Ufficio Neve e Valanghe, Hervè Jaccond, Emil Squinobal, and Antoine Brulport.

## References

Edwards, A.C., Scalenghe, R. & Freppaz, M. 2007. Changes in the seasonal snow cover of alpine regions and its effect on soil processes: A review. *Quaternary International* 162-163: 172-181.

Haeberli, W. 1973. Die Basis-Temperatur der winterlichen Schneedecke als morfologischer Indikator fuer die Verbreitung von Permafrost in den Alpen. *Zeitschrift fuer Gletscherkunde und Glazialgeologie* 9: 221–227.

Hoelzle, M. 1992. Permafrost occurrence from BTS measurements and climatic parameters in the Eastern Swiss Alps. *Permafrost and Periglacial Processes* 3: 143-147.

Keller, F. & Gubler, H. 1993. Interaction between snow cover and high mountain permafrost; Murtèl/Corvatsch, Swiss Alps. *Proceedings of the Sixth International Conference on Permafrost, Beijing, China, 5-9 July 1993. Proceedings*. Guangzhou, China: South China University of Technology Press, 1: 332-337.

Kuhn, M., Haslhofer, J., Nickus, U. & Schellander, H. 1998. Seasonal development of ion concentration in a high alpine snow pack. *Atmospheric Environment* 32(23): 4041-4051.

Phillips, M. & Schweizer, J. 2007. Effect of mountain permafrost on snowpack stability. *Cold Regions Science and Technology* 47: 43-49.

# Climate Change in Permafrost Regions in North America

Maria K.Gavrilova
*Melnikov Permafrost Institute SB RAS, Yakutsk, Russia*

## Introduction

In North America, permafrost occurs in three-fourths of Alaska, half of Canada, and along the coasts and below ice sheets in Greenland.

## Method

Weather station records have been used to analyze climate variations during the last centuries. The method of 10-year moving averages has been used in the analysis, which excludes casual errors.

## Results and Discussion

For the Barrow station (the northern coast of Alaska*)* which has a relatively long record spanning from the 1910s to 2000s, the change of air temperature in winter was within the limits of similar values of mean annual temperature for January (-25.8°C) from the 1920s to 1970s. Significant cooling occurred in the 1910s (up to-29°C). Then, intensive warming was observed in the 1970s. The winter air temperature lowered nearly to the long-term average in the 1990s and began to increase again in the 2000s.

Summer temperatures changed less, within the limits of ±1–1.5°C. Warming was observed in the 1920s, cooling in the 1950s, and warming in the 1990s. The mean annual temperature which dictates whether the ground is frozen or unfrozen varied within ±1–1.5°C. Significant warming occurred in the 1930s, cooling was observed from the 1940s through the 1970s, and rapid warming has occurred since the 1990s to the end of the century. The latter warming was due to increases in both winter and summer temperatures observed in the last decades.

For Fairbanks (central Alaska), the length of the record is 20 years shorter than at Barrow. Significant cooling of winter temperatures of up to -30° (the long-term average is -23.2°) in the 1960s–1970s and significant warming in the late 1970s–1980s (up to -19°) are evident. In the 1990s and 2000s, temperatures decreased to the long-term average.

Summer temperatures were lower than the average from the 1930s to 1960s, and have been persistently higher than the average since the 1970s. Mean annual temperatures were below the long-term average of -2.9° prior to the mid 1970s (up to -4°C), and have been higher since the mid 1970s (up to -2°).

St. Bethel (southwestern Alaska) shows nearly the same variations as Fairbanks, but only with a smaller range.

Mt. Washington is situated in southern Alaska, and records are available since 1940. A significant increase in winter temperatures was observed from the mid 1940s to mid 1960s, when temperatures reached -12.5°C, while the long-term mean is -15°. Then, cooling occurred in the 1960s–1980s (up to -17°). This cooling was followed by warming from the mid 1980s to mid 2000s. The last warming, however, was less in magnitude than the warming of the 1950s. Then, temperatures began decreasing again.

Summer temperatures are surprisingly stable, varying within the limits of ±0.5°C. The mean annual temperature also varied more or less stable. Slight warming occurred in the mid 1950s, extended cooling from the mid 1950s–1980s and a steady temperature increase in the 1990s. All these variations were within the range of ±0.5°C.

Unfortunately, in northern *Canada,* meteorological observations were begun later, and recent data, probably, are not published.

At the Alert station located on the most northern extremity of the Canadian Archipelago, observations were apparently begun in the 1950s and ended in the 1990s. During this period, there were two peaks in winter temperatures: a smaller one in the 1950s and a larger one in the 1970s (-29° at the mean of -32°). Then temperatures began to decrease.

Summer temperatures were above the long-term average in the 1950s–1960s and have been below the average since the latter half of the 1980s. There has been a slight increasing trend in recent years. The mean annual temperature varied ±0.5°C.

Along the northern coast of the continent (Aklavik station) there were alternating cold and warm winters within the range of typical variation. Unfortunately, only the data prior to the mid 1960s are available for us.

For the Frobisher Bay station (Baffin Island) data are available from the 1940s to 2000s. Winter warming was observed in the 1960s and the 1980s, similar in magnitude (-24°, while the long-term mean is -26.5°). In the mid 1940s, late 1980s and 1990s, winter temperatures lowered to -29°C.

After significant cooling in the mid 1980s and in the 1990s, summer and mean annual temperatures have increased by 1–1.5°C in the early 2000s.

The longest record for the permafrost region at our disposal is from the Churchill station, where observations began in the 1890s. January temperatures increased significantly in the 1940s and, in similar magnitude, in the 1980s and the 1990s. During these warmer periods, temperatures were -25° to -25.5°, while the long-term average is -27.2°C.

Increases in summer temperature were observed in the second half of the 1930s and in the 1990s. The mean annual temperature increased noticeably during the last decades of the 20th century, having reached -5.5° (the long-term normal is -7°C).

Greenland stations, for which records are available, are situated on the western coast. The longest record is from the

station where observations were started in the 1870s. At the Upernavik station (central coast), significant warming began in the 1920s which reached -13° in 1940 (the long-term average is -19°C). This warming apparently is related to the proximity to the warm Gulf Stream, which had the greatest influence on the stations of Western Europe.

Summer temperature variations are within the range of ±1–1.5°C. Mean annual temperatures varied within ±2°C.

Jodhab station records show variations similar to Upernavik, with significant cooling from the 1970s to the early 20th century, and significant warming from the 1920s to the end of the 20th century.

Summer temperatures were highest in the 1930s and in the 1960s (-6° to -5.5°, the long-term average = -8.6°C). Warmer winter and summer temperatures resulted in higher mean annual temperatures. In the 1930s and 1960s, they exceeded the "norm" (-1.4°C) by 1–1.5°C and frequently approached 0°C; that is, unstable permafrost conditions occurred now and then.

## Conclusions

The coldest years in North America during the period of instrumental observations occurred from the late 19th century to the 1910s–1920s. Arctic warming was not reflected in Alaska and Canada records, and some locations experienced cooling. But the stations in Greenland responded well to the Arctic warming. Recent climate warming occurred in Alaska in the 1980s, in Canada in the 1970s and in Greenland in the 1960s. In the end of the 20th century, mean annual temperatures at many stations increased by 1–1.5°C compared to the long-term average (Gavrilova 1998, 2003).

## Acknowledgments

The author thanks her assistant, Tamara Sofroneeva, for helping.

## References

Gavrilova, M.K. 1998, 2003. *Climates of Earth's Cold Regions*. Yakutsk: 2008 pp.

# Maximizing Construction Season in a Subarctic Environment, Fort Wainwright, Alaska

Quentin Gehring
*Shannon & Wilson, Inc.*
Frank J. Wuttig
*Shannon & Wilson, Inc.*

## Introduction

The Denali Village housing project involves the construction of approximately 200 housing units (50 buildings) on a partially-developed site along the banks of the Chena River, encompassing approximately 150 acres on Fort Wainwright near Fairbanks, Alaska. Common construction practice on Fort Wainwright has been to replace frost-susceptible foundation soils with nonfrost-susceptible fills, mitigating the risk of undesirable frost-related movements. However, the design build team proposed founding the housing units on frost-protected shallow foundations to reduce both construction and costs.

Construction of the project provided several design challenges from a frozen-ground standpoint. This presentation describes the design of frost-protected shallow foundations outside standard design criteria, and lists strategies we considered to provide temporary frost protection for overwintered unfinished buildings and building pads. The desired outcome of temporary frost protection was to lengthen the construction season and accelerate the construction schedule.

## Climate

ASCE 32-01 has developed a standard for the design and construction of frost-protected shallow foundations. The standard applies to areas free of permafrost, to areas where the mean annual air temperature is greater than 0°C, and to areas where the design air-freezing index is less than 2,500°C-days.

Interior Alaska, including Fort Wainwright, has a continental climate characterized by large daily and annual temperature ranges. Mean annual temperatures are slightly below freezing. The mean annual air freezing index exceeds 3,000°C-days. The recorded freezing index for Fairbanks is plotted in Figure 1. The 100-year mean return period design freezing index developed by the U.S. National Oceanic and Atmospheric Administration (NOAA) is 3,900°C-days.

The mean daily temperatures typically rise above freezing in mid-April and fall below freezing in mid-October, providing about a six-month construction season. Foundation construction in frost-susceptible soils generally begins after the seasonal frost has thawed, delaying the start of construction until late spring. Seasonal frost depths can extend several meters into the ground in cold, low-snow years. In areas kept clear of insulating snow cover, frost depths can exceed 4 m.

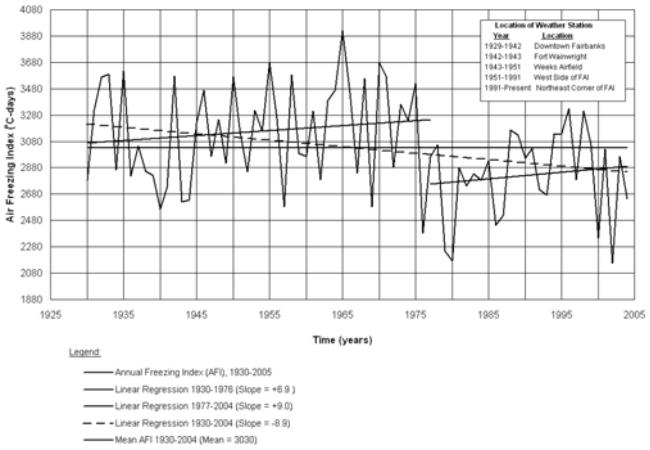


Figure 1. Climate information.

## Site Conditions

The site is on the Chena River floodplain. Prior to construction, the site was primarily wooded with birch and spruce with an under-story of alder and willow. A portion of the site was developed as a campground, including gravel roads, parking areas, and trails.

Exploratory drilling by the U.S. Army Corp of Engineers and follow-up drilling by our firm showed that the site is underlain by a surficial layer of silty frost-susceptible soils overlying generally nonfrost-susceptible (NFS) sands and gravels. Localized areas of both shallow and deep permafrost were encountered across the site, which affected the foundation design. Groundwater levels were 3 m or more below the planned finished floor elevation, but past experience in the area indicates the water table can fluctuate seasonally 1 m to 2 m.

## Foundation Design

The housing units are being founded on shallow, thickened-slab foundations with in-slab radiant floor heat bearing on controlled nonfrost-susceptible fills. A typical section of a frost-protected shallow foundation is shown in Figure 2. Frost protection is provided with either perimeter insulation designed to keep the soils below the foundations in a permanently thawed state, or by excavating and replacing frost-susceptible soils beneath the foundation system with a NFS fill. For this project, given the variation in subsurface conditions, four distinct foundation design solutions were proposed to address permafrost and frost-susceptibility issues.

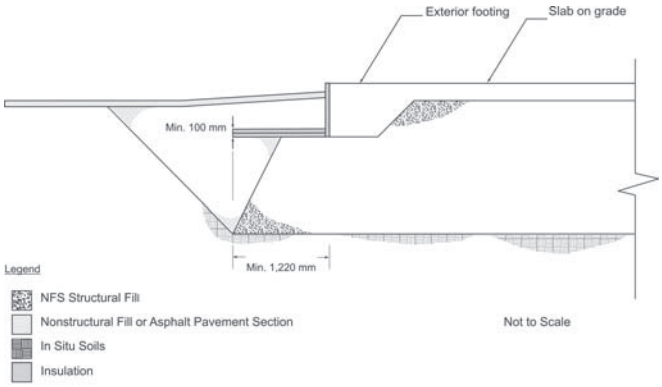


Figure 2. Typical frost-protected shallow foundation section.

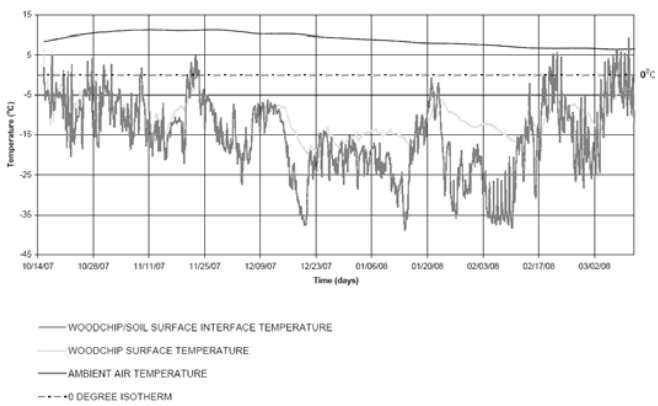


Figure 3. Foundation monitoring temperature data.

The climate parameters for Fort Wainwright are outside the ASCE design standard for the design and construction of frost-protected shallow foundations. In addition, discontinuous permafrost underlies portions of the site. To determine the insulation requirements for a frost-protected foundation design in areas without permafrost, thermal analyses were conducted using Temp/W, a finite element simulation package developed by Geoslope International, Inc., in Calgary, Alberta. Based on the results of the analyses, we recommended a 100-mm-thick wing of insulation, 1.22 m wide, extending out horizontally from the base of the foundation around the entire perimeter of the frost-protected slab foundations.

Complete excavation of frost-susceptible soils was recommended in permafrost areas.

## Temporary Frost Protection Strategies

The short construction season placed limitations on the schedule for such a large construction project. Foundations that had been started had to be heated by the end of the construction season to prevent frost-susceptible foundation soils from freezing. Furthermore, deep seasonal frost would delay foundation construction in the spring. The following strategies were considered to reduce the affects of seasonal frost on the construction schedule:

1. Complete removal of frost-susceptible soils below planned foundations.
2. Use of board insulation, laid horizontally across pads and recycled the following spring for use as slab and foundation insulation.
3. Use of on-site soils or chipped organics as insulation over building pads designed for frost-protected foundations.
4. Continuous heating of pads and foundations throughout winter with glycol heating loops.

Using a combination of these strategies, the majority of the foundations were prepared in the first construction season. The following spring, construction began without the need to wait until the seasonal frost had thawed, effectively and efficiently achieving the desired outcome for temporary frost protection.

## Foundation Monitoring

Little data is available on the use of on-site organics to provide temporary frost protection for a construction project; therefore, two prepared foundation pads were instrumented with thermistor strings and monitored for temperatures over the winter, in addition to monitoring air temperatures.

Woody plants, including small trees up to 0.3 m in diameter, were chipped/shredded during the 2007 construction season. Selected pads were covered with roughly 1 m of this material which was then covered with plastic sheeting to reduce the potential for natural convection. Thermal simulations were conducted to assist the contractor in determining the thickness of recycled on-site organics necessary for temporary frost protection.

Temperatures were monitored throughout the 2007/2008 winter. The temperatures plotted in Figure 3 show that the chips were effective at preventing building pads from freezing. Figure 3 also suggests some possible heat generation due to organic decomposition.

## References

American Society of Civil Engineers (ASCE). 2001. *Design and Construction of Frost-Protected Shallow Foundations.* ASCE 32-01.

# Pleistocene Sand-Wedge, Composite-Wedge, and Complex-Wedge Growth in Flanders, Belgium

G. Ghysels
*Department of Geography, Ghent University, Krijgslaan 281-S8, Ghent, Belgium*
I. Heyse
*Department of Geography, Ghent University, Krijgslaan 281-S8, Ghent, Belgium*
J.-P. Buylaert
*Nordic Laboratory for Luminescence Dating, Department of Earth Sciences, University of Aarhus, Risø National Laboratory, DK-4000, Roskilde, Denmark*
A.S. Murray
*Nordic Laboratory for Luminescence Dating, Department of Earth Sciences, University of Aarhus, Risø National Laboratory, DK-4000, Roskilde, Denmark*
D. Vandenberghe
*Department of Geology and Soil Science, Ghent University, Krijgslaan 281-S8, Ghent, Belgium*
F. De Corte
*Laboratory of Analytical Chemistry, Institute for Nuclear Sciences, Ghent University, B-9000 Ghent, Belgium*
P. Van den haute
*Department of Geology and Soil Science, Ghent University, Krijgslaan 281-S8, Ghent, Belgium*

## Introduction

Reconstruction of former periglacial environments in Europe heavily relies on the identification of relicts and pseudomorphs of thermal-contraction-cracking wedges in soils (Vandenberghe & Pissart 1993). During the past seven years, a large number of these wedge-shaped sedimentary structures have been identified in lowland Belgium (Ghysels & Heyse 2006, Ghysels 2008). Wedge forming processes have been carefully reconstructed, providing new information on Pleistocene palaeoenvironmental and palaeoclimatic conditions of the Flemish sandy lowlands. Investigation methods included field observations, sedimentological analysis, and optically stimulated luminescence (OSL) dating.

## Results

A key observation includes the identification of composite-wedge pseudomorphs, relict sand wedges, and complex wedges. Their appearance was variable. Some structures showed a typical wedge shape (Fig. 1), while others appeared as irregular features with branching sand veins and bundles (Figs. 1, 2). The majority of the wedges comprised a laminated infill, although some showed a massive infill. Besides mature wedge forms, elementary sand-filled veins and groups of sand-filled veins similar to Murton's (1996) sand veins in Canadian sand sheets were also identified. The veins and wedges penetrated Weichselian aeolian and fluvio-aeolian sand sheets (Fig. 3), but sometimes extended into underlying Tertiary sands and clays (Figs. 2, 3).

All these structures suggest thermal-contraction-cracking of frozen soils in a former cold periglacial environment. Their windblown infill points to sand transport on a sparsely vegetated ground surface with a limited snow cover during wedge growth (Murton et al. 2000).

## Discussion

The results point to a greater complexity of wedge-forming processes and palaeoenvironments compared to those of previous studies. The latter stressed the dominance of ice-wedge pseudomorphs (e.g., De Moor et al. 1978, Heyse 1983, 2000, Vandenberghe & Pissart 1993, Huijzer & Vandenberghe 1998). Therefore, former reconstructions may have been biased towards conditions suitable for ice-wedge growth. Sparse vegetation and snow covers during wedge growth may also have favored efficient cooling

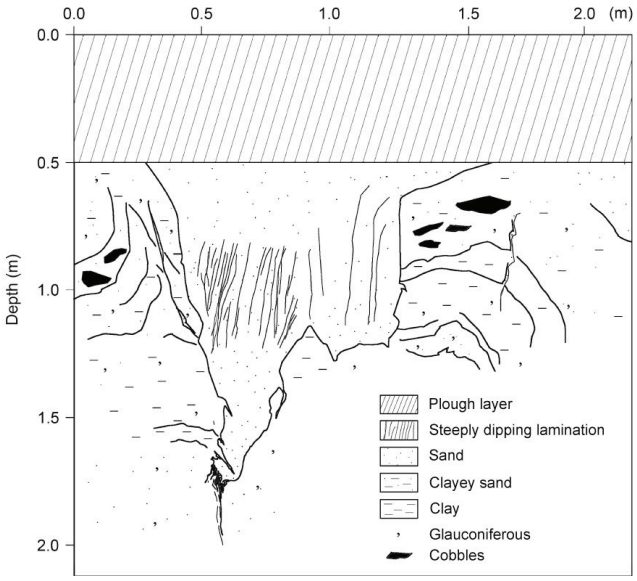


Figure 1. Vertical cross-section of a composite-wedge pseudomorph in Belgium (Ghysels & Heyse 2006). Note the upturned host sediments and the vertical laminated infill, pointing to the progressive infilling of thermal contraction cracks with sand, sand-ice, and ice. Downturned host strata and steeply-dipping tongues of host sediment likely formed as ice melted (Murton & French 1993).


Figure 2. Vertical cross-section of a complex wedge comprising a relict sand wedge (AAL4) which dissects an older composite-wedge pseudomorph (AAL3), Low-Belgium. Numbers refer to the OSL ages (Buylaert et al., accepted).

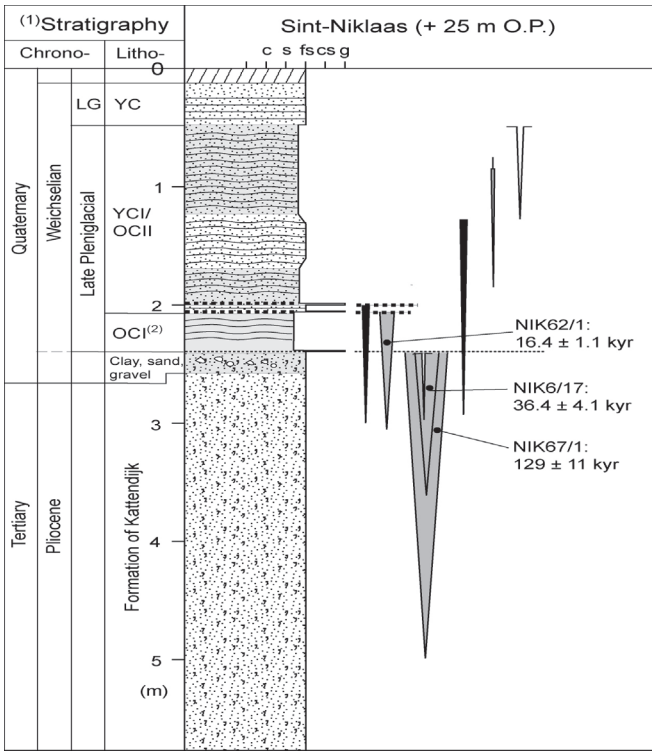


Figure 3. Schematic cross-section of Quaternary deposits showing different wedge levels. Grey wedges indicate wedges with a composite infilling. OSL dates are also indicated (in kyr: kiloyear).

and contraction of the frozen soil due to the lack of an insulating boundary layer (Murton & Kolstrup 2003). As a consequence, it cannot be excluded that wedges grew at higher mean annual air temperatures (MAAT ≤ -3°C) than previously suggested (e.g., MAAT ≤ -6°C in Huijzer & Vandenberghe 1998).

Finally, OSL dating of the aeolian wedge fillings provides direct age estimates for these cold-climate soil processes. The majority of the results points to extensive thermal contraction cracking during Marine Isotope Stage (MIS) 2 (Late Pleni-Weichselian–Lateglacial), peaking around 15,000 and 20,000 years ago (Fig. 2). A few data even suggest the possibility of earlier phases of wedge growth (during MIS 3 or Middle Pleni-Weichselian and MIS 6 or Saalian) (Fig. 3).

## References

Buylaert, J.-P., Ghysels, G., Murray, A.S., Vandenberghe, D., De Corte, F., Heyse, I. & Van den haute, P. Accepted. Optical dating of relict sand wedges and composite-wedge pseudomorphs in Flanders (Belgium). *Boreas*.

De Moor, G., Heyse, I. & De Grootte, V. 1978. An outcrop of Eemian and Weichselian deposits at Beernem (N.W. Belgium). *Bulletin de la Société belge de Géologie* 87: 27-36.

Ghysels, G. 2008. *Bijdrage tot de Studie van de Kenmerken, de Genese en de Datering van Periglaciale Polygonale Wigstructuren in België*. Unpublished PhD Thesis, University of Ghent, 266 & 357.

Ghysels, G. & Heyse, I. 2006. Composite-wedge pseudomorphs in Flanders, Belgium. *Permafrost and Periglacial Processes* 17: 145-161, doi:10.1002/ppp.552.

Heyse, I. 1983. Cryoturbation types in eolian Würm Late Glacial sediments in Flanders, Belgium. *Polarforshung* 53: 87-95.

Heyse, I. 2000. Fossil periglacial remnants in the Beernem-Mouton excavation in Flanders (Belgium). *Biuletyn Peryglacjalny* 39: 53-68.

Huijzer, B. & Vandenberghe, J. 1998. Climatic reconstruction of the Weichselian Pleniglacial in northwestern and central Europe. *Journal of Quaternary Science* 13: 391-417.

Murton, J.B. 1996. Morphology and palaeoenvironmental significance of Quaternary sand veins, sand wedges, and composite wedges, Tuktoyaktuk Coastlands, western Arctic Canada. *Journal of Sedimentary Research* 66: 17-25.

Murton, J.B. & French, H.M. 1993. Thaw modification of frost-fissure wedges, Richards Island, Pleistocene Mackenzie Delta, Western Arctic Canada. *Journal of Quaternary Science* 8: 185-196.

Murton, J.B. & Kolstrup, E. 2003. Ice-wedge casts as indicators of palaeotemperatures: precise proxy or wishful thinking? *Progress in Physical Geography* 27: 155-170.

Murton, J.B., Worsley, P. & Gozdzik, J.S. 2000. Sand veins and wedges in cold aeoilan environments. *Quaternary Science Reviews* 19: 899-922.

Vandenberghe, J. & Pissart, A. 1993. Permafrost changes in Europe during the Last Glacial. *Permafrost and Periglacial Processes* 4: 121-135.

# Response of Arctic and Subarctic Soils in a Changing Earth (RASCHER) – Project of IPY: Methodology, Activity, Results

Sergey V. Goryachkin
*Institute of Geography, Russian Academy of Science, Moscow, Russia*
John M. Kimble
*Soil Consultant, Addison, NY, USA*
Nimazhap B. Badmaev
*Institute of General & Experimental Biology, Russian Academy of Science, Siberian Branch, Ulan-Ude, Russia*
Marek Drewnik
*Jagiellonian University of Krakow, Krakow, Poland*
Dmitri G. Fedorov-Davydov
*Institute of Physico-Chemical & Biological Problems of Soil Science, Russian Academy of Science, Puschino, Russia*
Stanislav A. Iglovski
*Institute of Ecological Problems of the North, Russian Academy of Science, Ural Branch, Arkhangelsk, Russia*
Elena M. Lapteva
*Institute of Biology, Komi Scientific Centre, Russian Academy of Science, Syktyvkar, Russia*
Galina M. Mazhitova
*Institute of Biology, Komi Scientific Centre, Russian Academy of Science, Syktyvkar, Russia*
Nikita S. Mergelov
*Institute of Geography, Russian Academy of Science, Moscow, Russia*
Vladimir E. Ostroumov
*Institute of Physico-Chemical & Biological Problems of Soil Science, Russian Academy of Science, Puschino, Russia*
Eva-Maria Pfeiffer
*Institute for Soil Science, Hamburg University, Hamburg, Germany*

RASCHER (Response of Arctic and Subarctic Soils in a Changing Earth) is the International Polar Year (IPY) project which involves over 20 specialists from different countries. It addresses how climate variability and change can affect the soil systems of the Polar Regions and their sustainability with a changing climate. To provide accurate projections of the impact of climate change requires improved knowledge of its components and their linkages. Soil has both very inert and changeable parameters which are altered differently because of climate change. RASCHER mainly focuses on the study of temporal change of labile soil characteristics (temperature, carbon fluxes and other gas fluxes, microbiota, and microfauna) and of more stable soil characteristics (mineral composition, organic matter content and quality, morphological features, taxonomical status) in different kinds of frontiers (treeline, tundra-bog border, southern border of permafrost, contact zone, and the permafrost table in a profile), which are expected to be changed first due to climate change. The field studies are carried out in the different regions of the Arctic and Subarctic and also in high mountainous landscapes of temperate regions. Their aim is to make a "snapshot" of the current status of soil characteristics in 2007–08. It allows comparison of the inventory data gained in the IPY with results of studies to be carried out at the same locations 30–40 years later, and assessing if any climate-induced change of soil biota will take place. The variability of soil characteristics is taken into account.

The role of thermal factor in composition and functioning of the biotic complex of tundra soils (microbiota, microfauna, and mesofauna) as well as the selective role of negative temperatures on the structure of soil microbiocenoses and the influence of cryogenesis on adaptive functions of soil microorganisms are studied both in the field and in a laboratory, using traditional and new (DNA analysis) methods. For study of the character of polar soil microbocenoses, samples from permafrost-affected soil —Cryozem of the tundra ecosystem of the Lower Kolyma—have been collected and analyzed. The obtained data of the analysis of DNA show that the microbial population of these soils concerns in 14 groups that characterize this soil as the one with high biodiversity comparable with soils of more southern latitudes.

For the inventory study of the soil mesofauna, soil samples in the Vorkuta tundra (northeast of Europe) on soil catena from top to the bottom part of a slope have been collected. Invertebrates have been allocated only from the samples of various layers of the organic horizon. In Barber's traps, there have been caught representatives of five groups (Coleoptera, Hymenoptera, Lepidoptera, Homoptera, Diptera) from a class of insects and species of a class of *Aranei*. Representatives of *Coleoptera* are related to the top and middle part of a slope, while those of *Diptera* are found at the middle and bottom parts of the studied slope. Larvae of *Diptera* have mainly been met in soil samples of the middle part of a slope. In soil microfauna alongside with *Collembola*, there also have been identified ticks: *Gamasidae* and *Oribatei*. The last ones have been found at all sites of the slope mainly in the warmest top

part of soil litters. *Gamasidae* and *Collembola* in the top and middle part of the slope have been met in the whole mass of peaty horizons, while in the wettest bottom part of the slope, they are mostly at the top part of the organic horizons. The general number of *Collembola* in tundra permafrost-affected soils is low. On the average in the top part of the organic horizon, it is nearby 15,300 sp./m$^2$, and in the bottom part – 1,130 sp./m$^2$. At the same time the number of *Collembola* depends on the part of the slope. The wettest bottom part of a slope is characterized by a maximum of *Collembola* which are concentrated in the top part of a litter, while the maximum quantity of *Gamasidae* (2,800 sp./m$^2$) and *Oribatei* (8,400 sp./m$^2$) is related to the middle part of the slope.

The frontier studies concern the non-stability of the soil thermic regimes, shrinking of isolated patches and the northward retreat of permafrost-affected soils, and the assessments of possible soil change related to vegetation transformation on the base of soil studies (carbon fluxes, humus quality, mineral composition, etc.) in different types of ecotones (forest-tundra, tundra-bog, meadow-tundra).

In the Vorkuta tundra, the constant deepening of the permafrost table was observed. Leveling of the permafrost surface revealed that the ground subsidence due to thaw was 18 cm per 7 years, thus the subsidence rate is 2.5 cm/year. The average increment (396 measurements per year) of the soil layer reached 20 cm, and if adjusted to the subsidence is 38 cm per 7 years. Thus, the average thickness of the permafrost involved annually into soil formation is 5.5 cm.

In the tundra of the Lower Kolyma River, the general tendency for decrease of the permafrost table was also revealed, but the process seems to be more complicated and has more fluctuations. It is the result of the influence of 2 factors: (1) lower permafrost temperature at the Eurasian Northeast, and (2) various processes with negative feedbacks resulting in thaw mitigation.

At the southern part of the Cryolithozone, in Buryatia, in 1907–08 in undisturbed Gelic Chernozems, the permafrost table was identified at a depth of 1.5–1.6 m; in the 1960s, 2.0–2.1 m; at present time, 2.5–2.75 m. In loamy Gelic Luvisols, the permafrost at the beginning of the previous century was found at a depth of 1.2–1.3 m; in 1960–70s, 1.5–1.6 m; at present time, 2.2–2.5 m.

The analysis of archives and personal data revealed a shift of the southern permafrost boundary in the region northward from Arkhangelsk since 1933 to 2000. During 67 years, the southern border of the sporadic permafrost has moved northward 20–30 km.

The monitoring of the "forest-bog" ecotone in the sub-arctic zone of the Arkhangelsk region has been conducted. Besides the well-known phenomenon of northern soils bogging, it revealed the ecotone sustainability based on negative feedbacks.

The study of soil and geomorphic processes has been conducted in formerly permafrost-affected Tatra Mountains, which are the highest part of the Central European Carpathians (2655 m a.s.l.). The Tatra Mountains are not glaciated, and nowadays, the presence of permafrost has not been found. However, these mountains are subjected to intense geomorphic processes (rock falls, rock slides, debris and grain flows, solifluction, gelifluction, and others). The soils studied have been localized in the alpine zone (1800–2200 m a.s.l.), where the most intensive geomorphic processes occur (cryo-nivale zone). The soils studied are shallow and contain a considerable amount of clast. They are subjected to the podzolization process, and they can be characterized by thick humus horizons. Slow geomorphic processes (solifluction, soil creep) modify the upper part of the soil profile, comprised of humus horizons and eluvial horizons. The influence of these processes depends on the participation of the phenomena associated with the freeze-thaw action concerning the ground ice. Along with the increased importance of frost action in the movement of regolith, the degree of soil modification increases. The most profound transformation of the soil cover occurs in the case of gelifluction. Within the forms, which developed as a result of secular processes (protuberances, bench terraces, lobes), the soils are modified, although without leading to essential changes in their properties. The soil affected by gelifluction have the properties and morphology of Fluvisols. Catastrophic processes (rock slides, debris and grain flows) cause strong transformation of soil cover and uniformity of soil mass. Further development of soil depends on the geomorphic position; it is different within erosion zones and different within accumulation zones; so the soils above the upper timberline in the Tatra Mountains are young forms. In relatively stable areas or those subjected to only moderate geomorphic processes, they often display the features of polygenesis associated with changing climatic and geomorphic conditions.

The other part of the frontier studies is the detailed analysis of soil process at the interface of the soil and permafrost tables. It concerns the study of the biochemical and geochemical barrier on this interface and the study of the process of cryogenic lateral transportation at the contact zone of the soil and the permafrost table. This interface is the zone of high concentration of organic matter and other compounds, including pollutants. These detailed physico-chemical studies allow for a determination of the fate of these materials as affected by permafrost thawing due to climate change or anthropogenic impact.

The important feature of the cryogenic structure of the transitional layer is the zone of concentration of labile substances which are situated in the zone of the segregative ice. In depressions of the permafrost surface, there are local zones of accumulation of labile substances—cryogenic geochemical traps. The chemical analysis showed that the general salinity and composition of soluble substances concentrated in these traps differ from the composition of intrasoil ice. The differences observed can be explained by cryogenic transformation of suprapermafrost water and selective penetrability of the cryogenic geochemical barrier.

Local accumulation of labile substances in geochemical permafrost traps is the essential part of geochemical balance. If the soil thawing depth increases, then the elements concentrated in permafrost geochemical traps could escape into the surface-water flow.

# Monitoring of the Floodplain Talik Downstream From the Ust'-Srednekan Reservoir

S.A. Guly, V.M. Mikhailov
*North-Eastern Research Station of the Melnikov Permafrost Institute, SB RAS, Magadan, Russia*

In the continuous permafrost area of northeastern Asia, taliks exist only in river valleys and under large lakes. Many of them develop due to intensive convective heat exchange with rivers and occupy the entire floodplain. A generally accepted indicator of such taliks are phytocenoses of thick mixed woods in which large deciduous trees (*Chosenia arbutofolia* and *Populus Suaveolens*) are often most abundant. These woods stand out sharply against the background of sparse growths of trees (almost exclusively larch) dominating in the lower belt of mountains and over flat interfluves (Fig. 1). Many authors, following Vaskovsky (1958), call them an expressive name—tundra-forest—which accentuates the depression of trees.

The largest floodplain talik begins in the Kolyma River valley between Ust'-Srednekan and Seimchan, and extends downstream for more than 500 km, somewhat lower than Ziryanka (Fig. 2). Its width varies from 2.5–3 to 4–5 km or more. Thus, in this reach of the Kolyma River floodplain, a unique natural complex exists, the main constituents of which are the outstandingly huge block of unfrozen ground and the vast woodland north from the taiga forests.

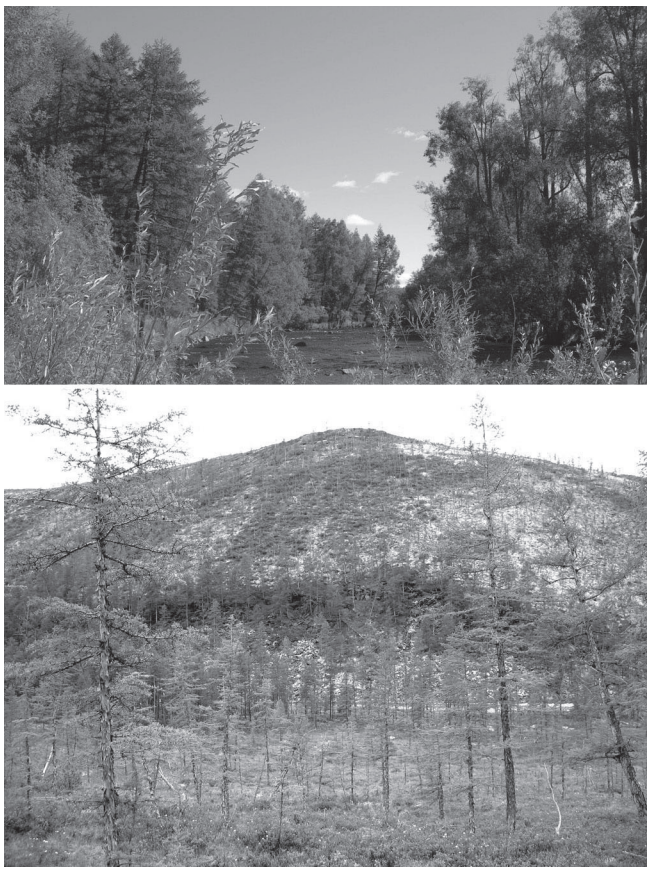

Figure 1. Two typical landscapes of northeastern Asia: mixed forest on a floodplain talik (above) and dominating tundra-forest (below).

In a few years the hydroelectric power station will be put into action 14 km upstream from Ust'-Srednekan. It is common knowledge that reservoir regulations induce significant decreases in temperature and discharge of rivers downstream from dams during summer. Such changes cannot but influence the hydrothermal regimes of contiguous aquifers.

Convective heat exchange is caused by a two-way water exchange (developing due to very high alluvium permeability); in each "elementary" river segment, infiltration of water into ground is accompanied by groundwater recharge. The resulting heat flux into a floodplain talik ( $q_{conv}$ ) is defined by the formula (Mikhailov 2002):

$$q_{conv} = C(\omega^{-}T - \omega^{+}T_f) ,$$

where $C$ is water volumetric specific heat; $\omega^{-}$ is specific (i.e., related to the unit river surface area) rate of water infiltration into alluvium; $\omega^{+}$ is the same, only of groundwater recharge into a river; $T$ is water temperature in a river; and $T_f$ is weighted mean groundwater temperature ("weights" are point rates of recharge). Hereafter all dimensions are in SI; specifically, water exchange characteristics $\omega^{-}$ and $\omega^{+}$ are measured in $m^3/(s\cdot m^2)$. Water surface area may vary greatly over short time periods, so the influence of convective heat exchange on the thermal regime of a talik is better described by the product of $q_{conv}$ by a river width ($B$).

Characteristics of water exchange do not depend substantially on river discharge, while $B$ is directly related to it. Therefore, both above-mentioned changes will diminish the amount of heat supplied to the Kolyma River floodplain with unpredictable consequences for the talik.

The situation has no precedent because never before was

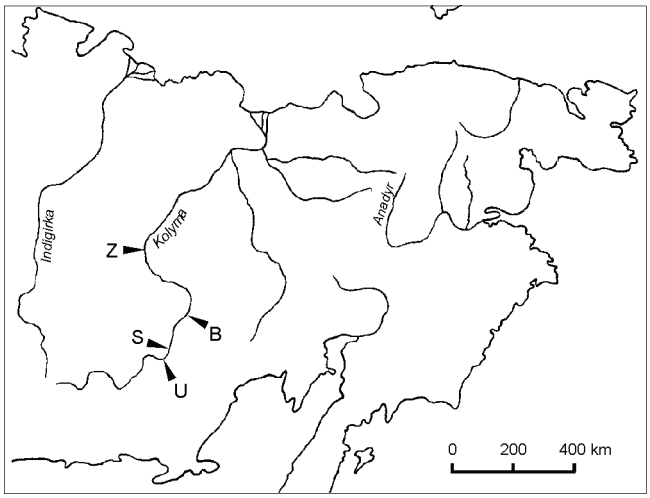


Figure 2. Locations of the gauging stations on the Kolyma River: U – Ust'-Srednecan; S – Seimchan; B – Baligichan; Z – Ziryanka.

a river dam constructed upstream from a floodplain talik; so there is no way to tell how much these changes can influence the natural complex under discussion. Very probably, they will cause reduction of the talik followed by degradation of the woods. To prevent such a trend of developments, it is necessary to perform continuous monitoring of the talik condition downstream from the dam and, in the case of a real threat, to propose efficient ways to reduce the damage to a minimum. Unfortunately, the methods traditionally used in permafrost science are hardly suitable for accomplishing even the first of these aims, because a reasonable degree of accuracy requires numerous measurements that are very labor consuming. Less laborious biological methods are only capable of ascertaining the ecological disturbance when it becomes irreparable.

The most practical approach is based on our recent research of convective heat exchange between rivers and contiguous aquifers by means of estimates of rivers' heat balance (Mikhailov 2002, 2008). Accounting for all commonly considered components, the residual is total heat flux into ground ( $q_{gr}$ ) of which the conductive constituent is virtually a negligible part (Mikhailov 2002). All other heat fluxes can be calculated accurately enough, thus the same is true for the sought quantity. Long-term estimates of $q_{gr}$ were made for large sections of 6 rivers (Mikhailov 2008). As a result, the general patterns of seasonal variation of this value have been established. One of these sections is located on the Kolyma River between Seimchan and Baligichan (see Fig. 2). It belongs to the upper part of the floodplain talik under discussion, subjected to the strongest influence of the reservoir regulations.

Developing further this approach, the pattern of variations of $q_{gr}$ in this section can be determined as dependent on hydrometeorological conditions during the whole period of observations. Comparison of these data sequences with those obtained after the dam construction will bring to light the influence of reservoir regulations. The results of such analyses will become more and more reliable with time. As a first approximation, a steadfast tendency of decrease of $q_{gr}$ (all other factors being equal) will be indicative of the forthcoming reduction of the talik.

Apparently, the only way to increase heat transfer to the floodplain talik is either by specifying additional flushes from the reservoir or manipulating the parameters of the regular ones (e.g., needed for the shipping). But it is a comprehensive analysis of the dynamics of the river temperature and discharge, together with the $q_{gr}$ values, that can enable a rational choice of optimal periods and minimal durations and volumes of the flushes.

The most essential advantages of the approach discussed are the following:

1. Decrease of $q_{gr}$ precedes any significant changes of both the talik size and—all the more—the conditions of floodplain phytocenoses. It gives time to elaborate and discuss with the authorities proposals for necessary adjustments in the reservoir regulations.

2. Analysis of the fundamentally new information obtained in the course of monitoring will undoubtedly improve our knowledge of regularities of convective heat exchange in river valleys. Besides the basic significance, in the practical aspect it will make the aforesaid proposals more realistic.

3. The most necessary part of data for estimating $q_{gr}$ is standard hydrometeorological information. Additional research will be needed only to improve the accuracy of the results obtained and (probably) to verify the fact of the talik reduction.

It is also important that the Ust'-Srednekan hydroelectric power station will function together with the existing one (Kolymskaya station). Such a complex is far more flexible than a single station and in principle allows for more considerable adjustments. This offers grounds for optimism as regards the acceptability of the would-be proposals for governmental and economic bodies. In that case, we may have a good example of sensible compromise between conflicting interests and demands based on improved knowledge of the functioning of natural complexes.

## References

Mikhailov, V.M. 2002. Quantitative methods of indication of floodplain taliks (theoretical premises). Kriosfera Zemli (Cryosphere of Earth) 6: 20-28 (in Russian).

Mikhailov, V.M. 2008. Convective heat exchange between rivers and floodplain taliks. *Proceedings of the Ninth International Conference on Permafrost, Fairbanks, Alaska, June 29–July 3, 2008* (this proceedings).

Vaskovsky, A.P. 1958. New data on the distribution limits of cenoses-forming trees and shrubs in the Far North-East of the USSR. In: Materials on Geology and Minerals in the North-East of the USSR 10: Magadan, 187-204 (in Russian).

# Retrogressive Thaw Slump Impacts on Inconnu Spawning Habitat in the Selawik River, Alaska

Raymond Hander
*U.S. Fish and Wildlife Service, Fairbanks Fish and Wildlife Field Office, Fairbanks, AK, USA*
Kenji Yoshikawa
*Institute of Northern Engineering, Water and Environmental Research Center, University of Alaska Fairbanks, USA*
Nathan Olson
*U.S. Fish and Wildlife Service, Selawik National Wildlife Refuge, Kotzebue, AK, USA*

## Introduction

One of the most dramatic changes and concerns of climate warming is the increased rate of thawing permafrost and its related environmental shifting, such as changing the hydrological regime of river systems. The Kotzebue Sound area of northwestern Alaska is widely recognized as one of the most ice-rich and thaw-sensitive areas in Alaska (Fig. 1). In particular, glaciated areas are prone to develop retrogressive thaw slumps (RTS) by the thawing of buried glacial ice bodies.

In the spring of 2004, a large RTS occurred in the upper Selawik River drainage above important inconnu *Stenodus leucichthys* spawning habitat within the Selawik National Wildlife Refuge (Refuge) (Fig. 2). This event changed the water from a clear to a glacial-colored river that was noticed by Refuge personnel and persons from Selawik. The Selawik River is habitat for a number of whitefish species, including inconnu that support an important subsistence fishery and occupy an important ecological role in the Kotzebue, Alaska area.

Little is known about the physical spawning habitat requirements for inconnu, especially sensitivity to the accretion of sediments. There is potential that sediment could fill interstitial spaces between the gravel and cobble substrate where fertilized eggs need to settle, overwinter, and mature.

Since 2004, the RTS has continued to erode and influence the river with no apparent end in sight. The RTS is caused by ice-rich permafrost degradation resulting in slope failure (Jorgenson & Osterkamp 2005). Also, increasing thermokarst activity has been identified in a 5,000 km$^2$ survey area in the adjacent Noatak National Preserve by Bowden et al. (2007).

*Preliminary RTS analysis*

We attempted to provide an estimate of the volume of sediment/ground ice that has eroded into the Selawik River from the RTS since 2004 using stereophotogrammetric analysis methods of aerial remote sensed imagery (Fig. 3).

This analysis indicated that approximately 25,000,000 to 60,000,000 kg of sediment were released from the RTS in the 2007 melting season. Since 2004, the RTS was discharging 267 g/L of suspended sediments and discharging more than 100 L/sec from thawing permafrost during the melting season. At the inconnu spawning area in August 2007, deposited sediment was observed, and suspended sediments were measured to be at least 375 mg/L.

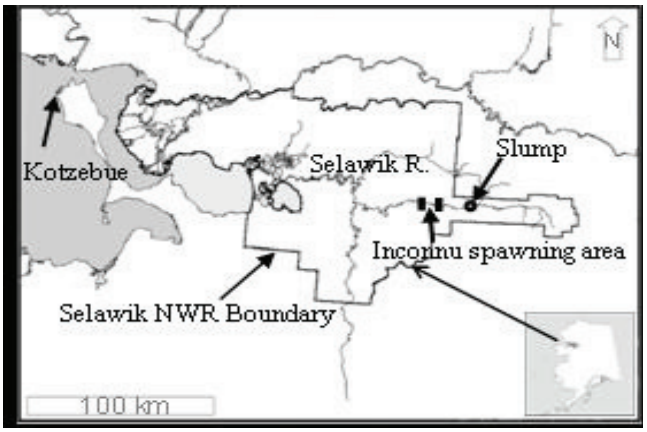


Figure 1. Map of the Selawik River, inconnu spawning area, and the retrogressive thaw slump location.

Figure 2. Selawik River retrogressive thaw slump, 2005. White circle is around a person and provides a slump-size scale.

*Inconnu habitat and RTS monitoring and research*

Impacts to the Selawik River inconnu population may not be known until the age cohorts from eggs deposited during sediment discharge years reach maturity and return to spawn in about 7 to 12 years (Brown 2000). Work is planned to assess the spawning habitat area for silt accretion on the spawning ground. Also, assessment of inconnu egg distribution relative to stream substrate characteristics will be explored to gain an understanding of specific habitat(s) where eggs reside for overwintering and maturation.

Continued RTS analysis in 2007 will include assessing the

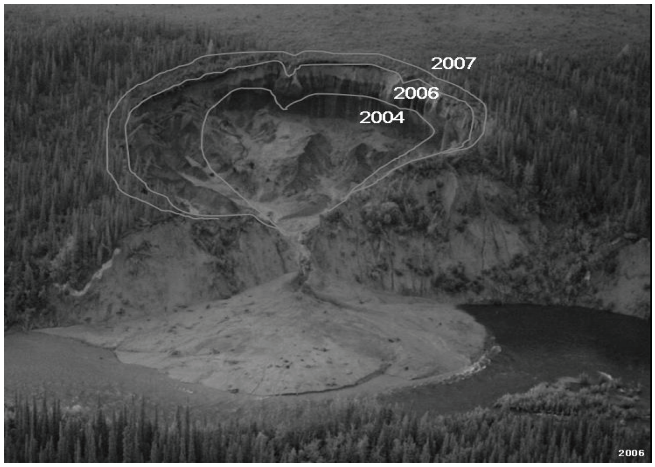


Figure 3. Selawik River retrogressive thaw slump progression from 2004 to 2007.

spatial and temporal distribution of the amount of suspended sediment, profiling river bed geomorphology, assessing spatial distribution of the RTS sediments deposited since 2004, and estimating the total volume of the suspended sediments and discharge volume.

The life expectancy of the RTS is dependent upon its reaching a stable thermal condition induced by the overburden material cover and more stable angles of the RTS walls. Lantuit & Pollard (2005) indicated that it often takes 5 to 10 years for the floor of a slump of dimensions of 100 m and more from the headwall to stabilize.

## Acknowledgments

We thank the Selawik National Wildlife Refuge for field support and University of Alaska Fairbanks, Water and Environmental Research Center staff members and students for help with laboratory analyses and field support.

## References

Bowden, B., Gooseff, M., Jones, J., Balser, A. & Lawler, J. 2007. *Thermokarst Distribution and Characterization in the National Park Service Arctic Network.* Unpublished progress report.

Brown, R.J. 2000. *Migratory patterns of Yukon River inconnu as determined with otolith microchemistry and radio telemetry*. M.S. Thesis, University of Alaska Fairbanks.

Jorgenson, M.T. & Osterkamp, T.E. 2005. Response of boreal ecosystems to varying modes of permafrost degradation. *Canadian Journal of Forest Research* 35: 2100-2111.

Lantuit, H. & Pollard, W.H. 2005. Temporal stereophotogrammetric analysis of retrogressive thaw slumps on Herschel Island, Yukon Territory. Natural *Hazards and Earth System Sciences* 5: 413-423, European Geosciences Union.

Waters, T.F. 1995. *Sediment in Streams: Sources, Biological Effects, and Control*. Bethesda, Maryland: American Fisheries Society Monograph 7, 251 pp.

# Climatic Change and Permafrost Stability in the Eastern Canadian Cordillera

Stuart A. Harris
*Faculty Professor, Department of Geography, University of Calgary, Calgary, T2N 1N*

## Introduction

Permafrost is the result of cold climatic conditions, so the stability of the climate is crucial to permafrost stability. It has been predicted by modeling that Alaska and the Yukon Territory should exhibit the maximum degree of climatic warming in the next century (Anisomov & Poliakov 2003), but Harris (2007) and Sergeev (2007) found that the available climatic data from the most reliable government sources indicated no strong warming trends in large parts of these areas. This paper explores the matter further by extending the study south along the Canadian Cordillera and relating the results to the evidence of associated permafrost stability.

## Sources of Data

When commencing the study of permafrost distribution in the Eastern Canadian Cordillera in 1974, weather stations equipped with temperature recorders were used at key sites together with ground temperature cables. Observations are continuing at the key stations (Fig. 1), which provide a record of the mean annual air temperature (MAAT), the seasonal thawing index (STI= the sum of the positive mean daily air temperatures from January 1 to December 31, inclusive) and the seasonal freezing index (SFI= the sum of the negative mean daily air temperatures from July 1 to June 30). The data represent the only available long-term climatic data from high altitudes south of the 60th parallel. The network was expanded north into the Yukon Territory, where the data supplement the data collected by the AES up to 1993 (AES 1993) and the climatic data from the Class 1 weather stations run by the U.S. National Weather Service. These are the best available data sources for northwest North America.

## Results

Figure 2 shows the regional pattern of climatic change since 1980, based on the published climatic data (Harris 2007) and the present study. Along the Arctic coast of Alaska, the east slope of the Cordillera and the Mackenzie Valley, and in northern British Columbia, there is evidence for substantial warming. This manifests itself in thawing of permafrost north of the crest of the Brooks Range (Osterkamp & Romanovsky 1999) and east of the crest of MacMillan Pass along the North Canol road (Kershaw 2003). The SFI has been decreasing and the MAAT and STI, increasing since 1980.

The main block of the mountains across central and southern Alaska and the Yukon Territory, as well as south of 52°25′N in the Eastern Cordillera, shows only minor long-term changes in MAAT. The SFI has been decreasing since 1972 in the Watson Lake area, though both the STI and SFI have increased slightly since 1985 at Tuchitua. The permafrost landforms such as palsas and lithalsas show negligible signs of degradation except where beavers have raised the local water level resulting in degradation of the adjacent landform, for example, at Wolf Creek (Lewkowicz 2003) and at Fox Lake, or where human activity has altered the water level (Marsh Lake, north shore, 2007) or through road construction, east of Tagish, Y.T. Where the water level is lowered artificially, the ground temperatures in the landforms cool, and the landforms grow in area (Fig. 3) as at Tuchitua. Kershaw (2003) thought that the west side of the MacMillan Pass was also warming due to slow degradation of two floating palsas, but the ponds in which they are found are becoming shallower and, therefore, warm up more in summer. The peat mounds nearby are not showing increasing ground temperatures, and the nearby large palsa fields on the floodplain of the MacMillan River are not showing evidence of degradation. It is concluded, therefore, that there is a climatic divide along the crest of the mountains separating the Northwest Territories from the Yukon Territory.

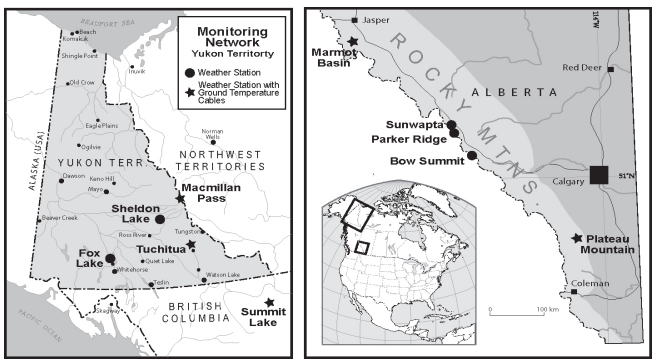

Figure 1. Location of the study sites.

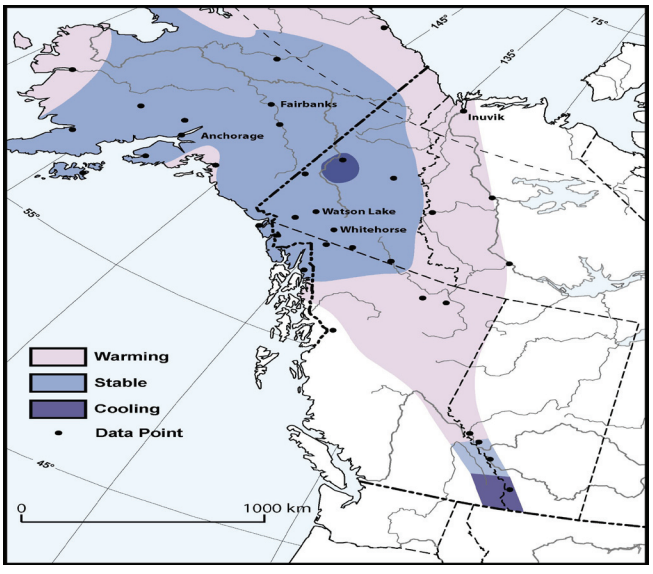

Figure 2. The regional pattern of temperature changes from 1970 to 2006 (partly after Harris 2007).

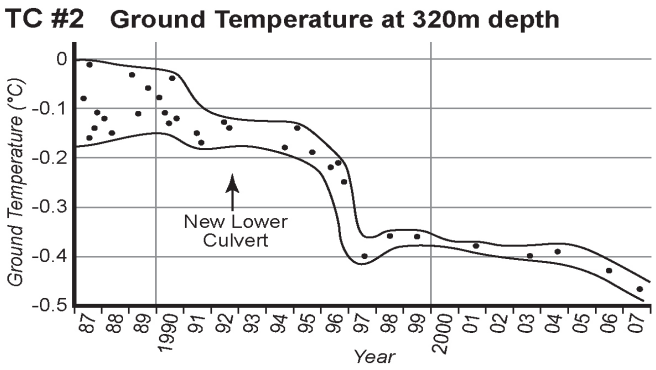


Figure 3. Ground temperature changes at 320 cm depth after the lowering of the adjacent water table, Tuchitua.

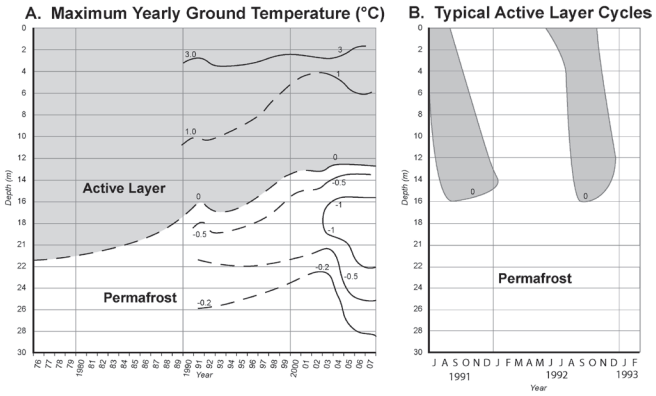


Figure 4. Changes in maximum annual ground temperature a n d active layer, as measured on a yearly basis (A) and on a daily basis (B).

The Summit Lake site showed a spectacular increase of 4.85°C in MAAT between 1982 and 1994 followed by relative stability. The SFI decreased by 40% while the STI increased by 50%. In about 1992, large thaw-flow slides appeared on the hill slopes at 1200 m elevation, and these started to appear up to 1400 m by 2004. The active later thickness increased from 1.5 m in 1982 to >5 m in 2007. The warming decreases southwards to Jasper, where there is only a minor increase in MAAT (0.6°C in 27 years). SFI has decreased considerably as has the mean annual snowfall, but the STI has increased. South to Calgary, the MAAT has remained unchanged with both STI and SFI decreasing (see also Clark et al. 2000).

Plateau Mountain exhibited a decrease in MAAT from 1974 until 1990, but has been fairly stable since then. Both the SFI and STI decreased. The active layer has decreased in thickness, and the upper part of the permafrost has cooled in response to these changes (Fig. 4).

## Causes

The first obvious result is that the climatic changes are local rather than global. In the main mass of the mountains of Alaska and Yukon, inversions of air with their associated cloud cover, steam fog in the fall when the air temperature over lakes is lower than the water temperature, and cold air drainage serves to buffer the valleys from climatic changes (Harris 2007). Along the Arctic coast, changes in surface cover from snow to soil and water enhance the effects of any warming.

Almost all stations indicate a decrease in the SFI, this being most marked at Summit Lake. This appears to indicate a weakening of the air pressure north of the 60th parallel, resulting in warmer air and the associated jet stream moving further north as far as Summit Lake from its previous position further south (see also Nkemdirim & Budikova 2001). The cP air mass is thinner and moves further east rather than swinging south along the mountain front

## Acknowledgments

Roger J.E. Brown of the Building Research Division, National Research Council of Canada funded the original study. It has also been funded in some years by the Geological Survey of Canada (Alan Heginbottom and Sharon Smith) and NSERC operating Grant A-7483. Parks Canada, Alberta, and BC Parks kindly provided the necessary collecting permits.

## References

AES. 1993. CD-Rom of the climatic data collected by the Atmospheric Environment Service at Canadian Weather Stations.

Anisomov, O.A. & Poliakov, V.Yu. 2003. GIS assessment of climatic change impacts in permafrost regions. *ICOP 2003, Permafrost* (1): 9-14.

Clarke, J.S., Yirode, E.K., Burns, N.D. & Astatkie, T., 2000. Regional climate change: trend analysis and precipitation series at selected Canadian sites. *Canadian Journal of Agricultural Economics* 48: 27-38

Harris, S.A. 2007. Reaction of continental mountain climates to the postulated "global warming," evidence from Alaska and the Yukon Territory. *Earth Cryosphere* 11(3): 78-84 (in Russian).

Kershaw, G.P. 2003. Permafrost landform degradation over more than half a century, MacMillan/Caribou Pass region, NWT/Yukon, Canada. *ICOP 2003, Permafrost* (1): 543-548.

Lewkowicz, A.G. 2003. Palsa dynamics in a subarctic mountainous environment, Wolf Creek, Yukon Territory, Canada. *ICOP 2003, Permafrost* (1): 163-168.

Nkemdirim, L.C. & Budikova, D. 2001. Trends in sea level pressure across western Canada. *Journal of Geophysical Research* 106(D11): 11801-11812.

Osterkamp, T.E. & Romanovsky, V.E. 1999. Evidence for warming and thawing of discontinuous permafrost in Alaska. *Permafrost and Periglacial Processes* 10: 17-37.

# Idealized Modeling of the Impact of Atmospheric Forcing Variables on Mountain Permafrost Degradation

Christian Hauck
*Institute for Meteorology and Climate Research, Karlsruhe Institute of Technology (KIT), Germany*
Nadine Salzmann
*National Center for Atmospheric Research (NCAR), Boulder, USA*

## Introduction

The high-mountain Alpine cryosphere is a particularly sensitive system to climate change due to its proximity to melting conditions. In view of probable accelerating rates of ongoing changes concerning atmospheric, surface, and subsurface processes in mountain regions (IPCC 2007), a great need for increased understanding of permafrost degradation processes and corresponding new modeling tools has been identified. Traditional mountain permafrost model approaches focus on spatial distribution models, using physically-based or empirical and statistical approaches to predict the permafrost distribution over larger areas (e.g., Noetzli et al. 2007).

However, to predict possible future changes in the permafrost distribution, the link between small-scale subsurface characteristics, including latent heat processes and predictions from climate models, has to be established. Whereas there is a steadily increasing number of studies using Global and Regional Climate Model (GCM, RCM) simulations to assess permafrost evolution and its impact in arctic regions (e.g., Anisimov & Nelson 1997, Stendel et al. 2007), similar efforts for mountainous terrain have only started very recently (Salzmann et al. 2007a, b). Thereby, regional to local climate scenarios, and especially mountain regions, are among the most ambitious areas for simulating future climate conditions (e.g., Frei et al. 2003). In most GCM/RCM simulations, small-scale processes and influencing variables such as surface characteristics, a realistic snow cover, topography, and lithospheric heterogeneities, as they are typical for mountain regions, cannot be included (Stendel et al. 2007).

Among those influencing variables, the duration of a significant snow cover plays a special role, as it determines the amount of energy exchange between atmosphere and ground and the degree of coupling between both spheres (Hoelzle & Gruber 2008). Climate warming, therefore, can only act upon the permafrost during the snow-free period, which is usually restricted to the summer months in many regions of the European Alps.

On the other hand, the strong decoupling of atmosphere and permafrost during most of the year can be used to simplify the necessary linking procedure between RCM results and subsurface models. The focus of this study is to use idealized modeling of the impact of changes in air temperature and snow cover duration on the subsurface permafrost temperatures. In a next step, permafrost-relevant information (e.g., possible trends concerning air temperature or snow cover duration) from control and scenario time series of RCM simulations can be extracted using the approaches described by Salzmann et al. (2007a).

## Atmospheric Forcing Variables

Figure 1 shows a typical example of the influence of net radiation and snow cover on ground temperatures in mountain permafrost regions. The example is taken from the 2900 m high-altitude permafrost station Schilthorn, Swiss Alps, where a more than 100 m thick permafrost layer exists (Hauck 2002, Hilbich et al. 2008). Figure 1a shows the total ground temperature change with time within the uppermost 10 m of a borehole. During the time when a significant snow cover was present (Fig. 1c and vertical black lines), temperatures within the uppermost 10 m of the borehole remained almost constant, as the ground temperature regime was effectively decoupled from atmosphere. After melting of the snow cover in June, temperature variability in the borehole is high, coinciding well with the observed variability of the radiation balance (Fig. 1b). This agreement confirms the dominant role of the radiation balance for ground temperatures in mountain permafrost terrain in the European Alps.

The only exception is seen right after the beginning of snowmelt in May, where small-scale variability of the total ground temperatures is present (Fig. 1a). Scherler et al. (submitted) showed that this feature is most probably due to infiltrating meltwater from the snow cover.

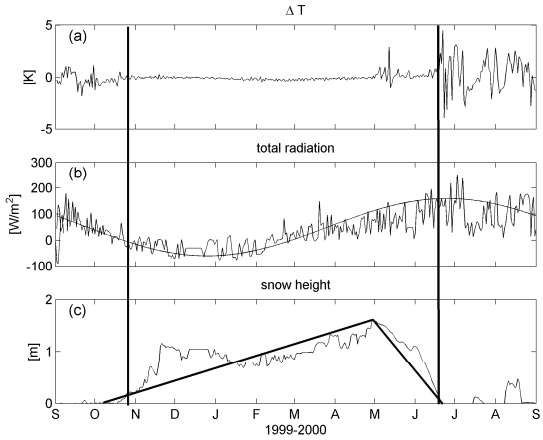


Figure 1. (a) Total temperature difference per day in the uppermost 10 m in the borehole, (b) net radiation at the energy balance station, and (c) snow height at Schilthorn, Swiss Alps.

## Approach

For idealized simulations, the annual variability of radiation (or air temperature) can be approximated by a sinusoidal variation, as indicated in Figure 1b. Similarly, the evolution of the snow cover can be approximated by a continuous linear increase in early winter and a sharp linear decrease in early summer (Fig. 1c). For idealized modeling of the impact of atmospheric forcing on the evolution of mountain permafrost, only four atmospheric parameters need to be varied:

1. accumulated summer air temperature (e.g., approximated by the amplitude of the sinusoidal curve);
2. air temperature at the beginning of the permanent snow cover (autumn);
3. time of the buildup of the permanent snow cover; and
4. time of vanishing of the permanent snow cover.

The rationale for this approach can be further illustrated by analyzing multiyear time series of air temperature and snow cover duration (Fig. 2), as well as comparing them to subsurface temperatures. This was done in detail by Hoelzle & Gruber (2008) for two sites in the Swiss Alps (including Schilthorn), indicating that snow cover duration and air temperature are indeed the dominant forcing variables for permafrost temperatures and active layer thickness.

Our approach focuses on determining subsurface temperatures, water, and ice content evolution with a one-dimensional coupled heat and mass transfer model simulating mass and energy balance of the soil-snow-atmosphere system (COUP-model, Jansson & Karlberg 2001). This model has been successfully applied to simulate water and energy at Schilthorn (Scherler et al. submitted). As a first step to using downscaled RCM scenario time series, we use idealized atmospheric forcing time series to analyze the possible impacts of increasing summer air temperatures, for example, or a shift in the snow cover duration on the permafrost temperatures. In a next step, these characteristics will be extracted from simulated RCM scenario time series for longer time scales. For the idealized simulations, combinations of the four atmospheric parameters listed above will be used.

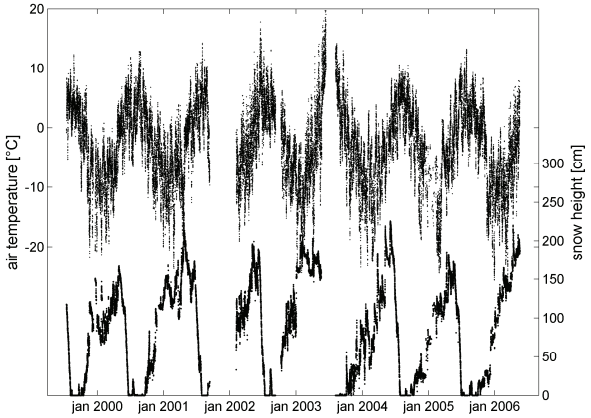


Figure 2. Air temperature and snow height at Schilthorn, Swiss Alps, between autumn 1999 and 2006 (data courtesy of M. Hoelzle and PERMOS).

## References


Anisimov, O.A. & Nelson, F.E. 1997. Permafrost zonation and climate change in the Northern Hemisphere: results from transient general circulation models. *Climatic Change* 35: 241-258.

Frei, C. et al. 2003. Daily precipitation statistics in Regional Climate Models: Evalution and intercomparison for the European Alps. *J. Geophys. Res. 108*(D3): ACL 9-1– 9-19.

Hauck, C. 2002. Frozen ground monitoring using DC resistivity tomography. Geophysical Research Letters 29(21): 2016, doi:10.1029/2002GL014995.

Hilbich, C. et al. 2008. Monitoring mountain permafrost evolution using electrical resistivity tomography: A 7-year study of seasonal, annual, and long-term variations at Schilthorn, Swiss Alps, *J. Geophys. Res*. 113: F01S90, doi:10.1029/2007JF000799.

Hoelzle, M. & Gruber, S. 2008. Borehole and ground surface temperatures and their relation to meteorological conditions in the Swiss Alps. *Proceedings of the Ninth International Conference on Permafrost, Fairbanks, Alaska*.

Intergovernmental Panel on Climate Change (IPCC) 2007. *Climate Change 2007: The Physical Science Basis*. Summary for policy makers, 18 pp., http://www.ipcc.ch/.

Jansson, P.-E. & Karlberg, L. 2001. *Coupled Heat and Mass Transfer Model for Soil-Plant-Atmosphere Systems*. Stockholm: Royal Inst. of Technology, Dept. of Civil and Environmental Engineering, 321 pp.

Noetzli, J., Gruber, S., Kohl, T., Salzmann, N. & Haeberli, W. 2007. Three-dimensional distribution and evolution of permafrost temperatures in idealized high-mountain topography, J. Geophys. Res. 112 (F2): F02S13, doi:10.1029/2006JF000545.

Salzmann, N. et al. 2007a. The application of Regional Climate Model output for the simulation of high-mountain permafrost scenarios. *Global and Planetary Change* 56 (1–2): 188-202.

Salzmann, N. et al. 2007b. RCM-based ground-surface temperature scenarios for complex high-mountain topography. *J. Geophys. Res.* 112: F02S12, doi:10.1029/2006JF000527.

Scherler, M. et al. Submitted. Investigation of meltwater infiltration into the active layer of an alpine permafrost site on Schilthorn, Switzerland. *Water Resources Research.*

Stendel, M. et al. 2007. Using dynamical downscaling to close the gap between global change scenarios and local permafrost dynamics. *Global and Planetary Change* 56(1–2): 203-214.

# A Method for the Analysis of the Thermal Permafrost Dynamics

M.A. Hidalgo, J.J. Blanco, M. Ramos, D. Tomé
*Physics Department, University of Alcala, Spain*
G. Vieira
*Centre for Geographical Studies, University of Lisbon,* Portugal

## Introduction

Antarctica is one of the most sensitive areas to climate change in the world. This is close to the upper limit for permafrost viability and, therefore, studying the distribution and the state of the permafrost, we can monitor climate evolution. Livingston Island (62°39′S, 60°21′W – South Shetland archipelago) is located 50 km west of the Antarctic Peninsula. Almost 90% of the island is glacierized, and the rest has a seasonal snow cover, coinciding with the periglacial domain.

## Experiment Description

The Incinerador borehole drilled in quartzite bedrock has a depth of 2.4 m with a diameter of 90 mm. There is a logger chain inside the borehole pipe. Since January 2004, the chain is composed of 6 loggers placed at different depths: 5, 15, 40, 90, 150, and 230 cm. The time interval between consecutive measurements is 1 hour and the accuracy of the dataloggers (tiny talk Gemini Co.) is 0.2°C.

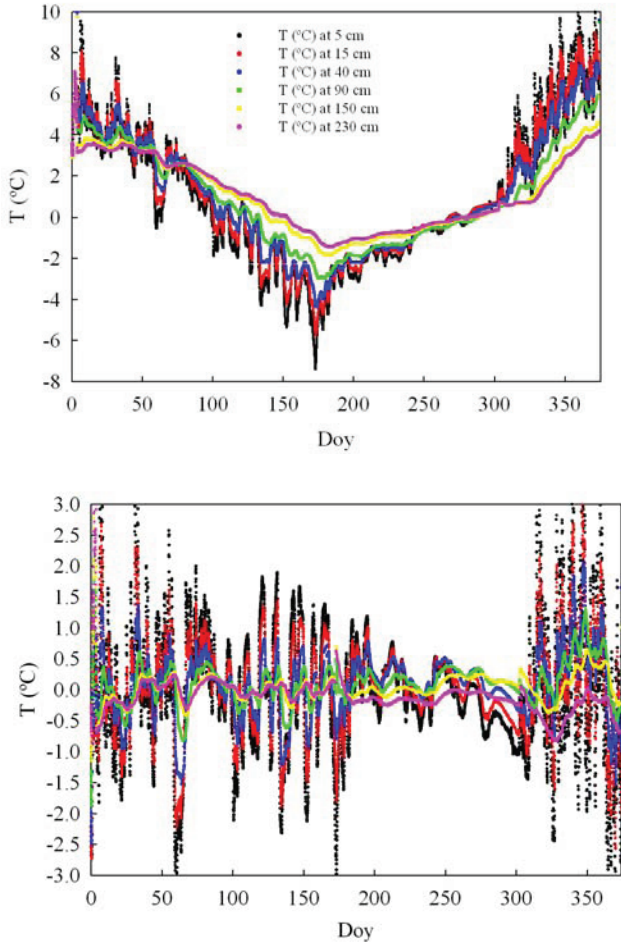


Figure 1. Temperatures recorded during the year 2005 at the different depths (indicated with the legend insert): (1a) the original data, (1b) the data after detrending.

## Data Analysis

In Figure 1a, we show the temperatures at the different depths mention above recorded during the year 2005 as a function of the day of year (doy).

Previous to the FFT analysis, a detrending process over the data corresponding to every record was made (Fig. 1b). After that, the FFT power spectrum obtained is shown in Figure 2.

## Model Description

The study of the permafrost and thermal regime of the active layer require the knowledge of their thermal diffusivity. This parameter is the key to understanding the thermal response of the soil—in particular, the exponential attenuation of the temperature wave with depth and the lag in phase. (In all the presented study, we assume that there are no thermal sources along all the depths considered).

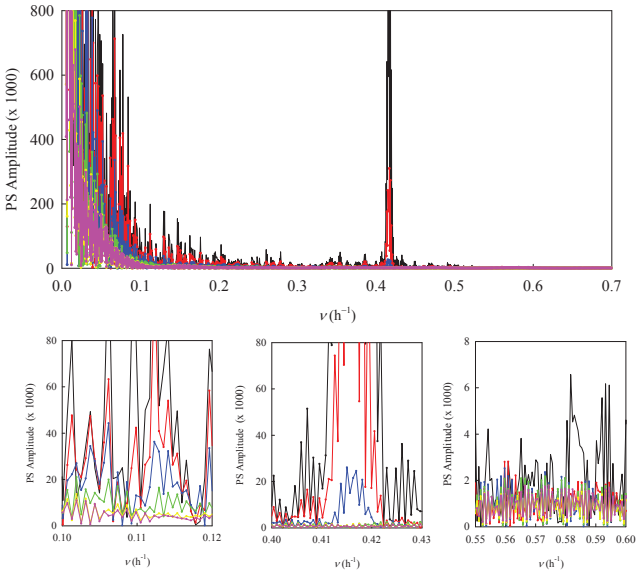


Figure 2. Power spectrum from the FFT analysis made over the detrending data of Figure 1b: (2a) the power spectrums in all the frequency range for the different depths (the colour legends are the same as in Figure 1; (2b)–(2d) details at different frequency ranges.

The temperature regime is determined by the well-known heat conduction equation:

$$\frac{\partial T}{\partial t} = a^2 \frac{\partial^2 T}{\partial z^2} \quad (1)$$

where $T$ is the temperature, $t$ and $z$ the time and depth variables, respectively, and $a$ the thermal diffusivity, given by

$$a = \sqrt{\frac{\kappa}{c\rho}}$$

with $\kappa$ the thermal heat coefficient, $\rho$ the soil density and $c$ its specific heat. Our starting point is the resolution of equation (1) with the single harmonic boundary condition $T_n(z=d,t)=0$ and $T_n(z=0,t)=T_n^0 \cos(\omega_n t)$. Using the separation variables method, the solution of equation (1) is given by the expression

$$T_n(z,t) = T_n^0 \frac{\sin(\gamma_n(d-z))}{\sin(\gamma_n d)} exp(-i\omega_n t)$$

where

$$\gamma_n = \sqrt{\frac{\omega_n}{2a^2}}(1+i)$$

Developing the solution, we obtain

$$T_n(z,t) = \frac{T_n^0}{\left(\cosh^2\beta_n - \cos^2(\beta_n)\right)} \times \times \left[A_n \cos(\omega_n t) + B_n \sin(\omega_n t)\right] \quad (2)$$

where

$$A_n = \sin(\alpha_n)\sin(\beta_n)\cosh(\alpha_n)\cosh(\beta_n) + + \cos(\alpha_n)\cos(\beta_n)\sin h(\alpha_n)\sinh(\beta_n)$$

and

$$B_n = \sin(\alpha_n)\cos(\beta_n)\cosh(\alpha_n)\sinh(\beta_n) - - \cos(\alpha_n)\sin(\beta_n)\sin h(\alpha_n)\cosh(\beta_n)$$

with

$$\alpha_n = \sqrt{\frac{\omega_n}{2a^2}}(d-z) \text{ and } \beta_n = \sqrt{\frac{\omega_n}{2a^2}}d \quad (3)$$

adding now all the harmonics corresponding to the temperature data recorded at the depth $z$=0 (and consequence of its Fourier analysis), $T(z=0,t) = \sum_n T_n^0 \cos\omega_n t$ , and also considering the boundary condition $T(z=d,t)=0$ .

Hence, we can predict and reconstruct the expectable temperature record at any depth, using the linear superposition principle. Simultaneously, this solution allows us to estimate the behaviour of the diffusivity at different depths (see below).

## Discussion

Although snow in the surface is thought to be a low-pass filter for the temperature signal (Goodrich, 1982), we find that the dependence of the diffusivity with depth is complex and determinant for interpreting the experimental data. Thus, looking at the results of the FFT power spectrum analysis of the temperature signal at different depths (Fig. 2a–2b), it is clearly seen the strong dependence of the thermal wave with frequency. Figure 2b shows the results for frequencies around $\nu_n \approx 0.11$ Hz , where an almost linear decay of the corresponding amplitude $T_n$ is observed, according with its linear dependence with depth reflected in the term $\alpha_n$. On the other hand, to explain the tendencies shown for the amplitudes at frequencies $\nu_n \approx 0.41\ h^{-1}$ and $\nu_n \approx 0.55\ h^{-1}$ we necessarily assume an increase of the term $\beta_n$ with depth, what implies a decrease of the diffusivity with it. This non-uniform diffusivity is a consequence of the variation of some of the magnitudes, and depends on the density, the conductivity, or the specific heat. Because it does not seem to justify a significant variation in either density or specific heat in the depths we are considering, the decrease seems to be related to thermal conductivity. Of course, a good knowledge of behaviour of the diffusivity with depth allows a better forecasting of the thermal evolution of the soil.

Using the presented method to analyse temperatures, data recorded in periods of several years will allow us to make a precise determination of the soil properties under interest, the evolution of the active layer, and their implication on climate. Thus, we will develop a tool implemented with the commercial program IDL with which we will analyse automatically the behaviour of the active layer. Even more, we will extend the presented model, taking into account thermal sources along the depth of interest, which could be very interesting for the study of the evolution of the active layer in soils.

## Acknowledgments

This research was founded by the Spanish Ministerio de Educación y Ciencia project, reference code: POL2006-01918/CGL.

## References

Blanco, J.J. et al. 2007. Active layer apparent thermal diffusivity and its dependence on atmospheric temperature (Livingston Island, Maritime Antarctic). *U.S. Geological Survey and the National Academies*, USGS OF-2007-1047, Extended Abstract.

Goodrich, L.E. 1982. The influence of the snow cover on the ground thermal regime. *Canadian Geotechnical Journal* 19: 421-432.

Hauck, C. et al. 2007. Geophysical identification of permafrost in Livingston Island, Maritime Antarctica. *Journal of Geophysical Research* (in press).

Ramos, M. & Vieira, G. 2003**.** Active Layer and Permafrost Monitoring in Livingston Island, Antarctica, first results from 2000 and 2001. In: M. Phillips, S.M. Springman, & L.U. Arenson (eds), *Permafrost* 2: 929-933. ICOP 2003. A.B. Balkema. Rotterdam.

# Ground Truth Observations of the Interior of a Rock Glacier as Validation for Geophysical Monitoring Datasets

Christin Hilbich
*Department of Geography, University of Jena, Germany*
Isabelle Roer
*Department of Physical Geography, University of Zurich, Switzerland*
Christian Hauck
*Institute for Meteorology and Climate Research, Karlsruhe Institute of Technology (KIT), Germany*

## Introduction

Monitoring the permafrost evolution in mountain regions is currently one of the important tasks in cryospheric studies, as little data on past and present changes of the ground thermal regime and its material properties are available. In addition to existing borehole temperature monitoring networks, techniques to determine and monitor the ground ice content have to be developed. A reliable quantification of ground ice is especially important for modeling the thermal evolution of frozen ground and for assessing the hazard potential due to thawing permafrost- induced slope instability.

Near-surface geophysical methods are increasingly applied to detect and monitor ground ice occurrences in permafrost areas. Commonly, characteristic values of electrical resistivity and seismic velocity are used as indicators for the presence of frozen material. However, validation of the interpretation of geophysical parameters can only be obtained through boreholes, limited to vertical temperature profiles. Ground truth of the internal structure and the ice content is usually not available.

During the construction of a ski track in summer 2007 we had the unique opportunity to conduct geophysical measurements (Electrical Resistivity Tomography [ERT] and Refraction Seismic Tomography [RST]) on a partly excavated rock glacier near Zermatt (Valais, Swiss Alps) and to calibrate the data with direct observations. (For further description of the study site, impacts, and investigations, see Maag et al. 2008 and Wild et al. 2008).

## Rock Glacier Composition

The general stratigraphy of rock glaciers is described by several authors (e.g., Barsch 1996, Burger et al. 1999) as a sequence of 3 main layers: (1) The uppermost 1–5 m consist of big boulders riding on (2) an ice-rich permafrost layer (with 50–70% ice and ca. 30% finer-grained material (Barsch 1996), which is creeping downslope. (3) The lowermost layer consists of larger rocks, which were deposited at the rock glacier front and subsequently overrun by the other layers. Despite numerous investigations of rock glaciers worldwide, direct observations of the internal structure of rock glaciers are rare. More detailed studies on stratigraphy result from direct observations in boreholes (e.g., Haeberli et al. 1998, Arenson et al. 2002) and indirect geophysical data (e.g., Vonder Mühll 1993, Hauck 2001, Maurer & Hauck 2007).

*Observed composition of the Gornergrat rock glacier*

Trenches cut during the construction of the ski track (up to 12 m) provided insight into the composition of the blocky active layer, a frozen mix of blocks, fine sediment and ice underneath, followed by a massive ice core. To validate the geophysical data, the respective fractions of rock, ice, water, and air were roughly estimated by visual inspection (Table 1).

Table 1. Estimated fractions (f) of rock, ice, air, and water for different layers observed during the final construction stage.

| | $f_{rock}$ | $f_{air}$ | $f_{water}$ | $f_{ice}$ |
|---|---|---|---|---|
| Active layer (2-3 m) | | | | |
| Coarse blocks | 0.6-0.7 | 0.3-0.4 | 0 | 0 |
| Mix of blocks and fine sediment | 0.8 | ? | ? | 0 |
| Intermediate layer (3-5 m) | | | | |
| Blocks with interstitial ice | 0.5 | 0 | 0 | 0.5 |
| Lowest observed layer | | | | |
| Massive ice with few blocks | 0.2-0.4 | 0 | 0 | 0.6-0.8 |

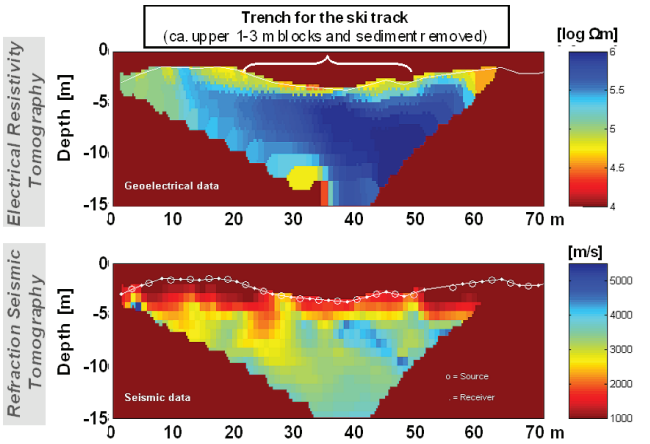


Figure 1. Inversion results for electrical resistivities and *P*-wave velocities obtained at the survey line.

## Geophysical Data

In the beginning of the construction of the ski track, while only little material had been removed so far, we conducted ERT and RST measurements on a longitudinal profile (70 m) in the upper part of the rock glacier (Fig. 1).

High resistivity zones coincide with high velocity zones, indicating a high ice content within the rock glacier, especially in the upper (right) part of the profile. The active layer is clearly delineated by smaller resistivities and velocities in the uppermost 2–3 m of the profile. In the central part, the active layer had already been disturbed by the construction work.

## Quantification of Material Properties

*The Four Phase Model (FPM)*

The indirect nature of geophysical soundings requires a relation between the measured variable (electrical resistivity, seismic velocity) and the rock/soil, water, air, and ice contents. The so-called Four Phase Model (FPM) (Hauck et al. 2008) determines volumetric fractions of these four phases from tomographic electrical and seismic datasets. It is based on geophysical mixing rules for electrical resistivity and seismic *P*-wave velocity. Observed resistivity and velocity data are used as input data on a two-dimensional grid (Fig. 1).

Application of this model to the geophysical dataset of the rock glacier allows for an estimation of the total fractions of ice, water, air, and the rock matrix with non-intrusive methods. Direct observations from the trenches cut for the ski track provide a unique opportunity to validate the FPM results and to evaluate the performance of the model.

*Modeled composition of the Gornergrat rock glacier*

Dominant materials calculated by the FPM are rock and ice with an average ratio of about 50%:40%. The contents of air and water are negligible below the uppermost 3 m, and do not exceed 10% (water) and 40% (air) within the active layer.

A critical parameter is the resistivity of the pore water $\rho_W$, which has to be prescribed beforehand. This parameter was measured in the field, but yielded 2 different values: 274 Ωm for melted ice (from a previously frozen ice sample), and 69 Ωm for collected meltwater, running out of the rock glacier. The FPM was calculated for both values, resulting in distinct differences for the content of unfrozen water: up to 10% (for 274 Ωm), and less than 5% (for 69 Ωm). Consequences for the other phases are small; only a slight increase in ice content is observed for higher values of $\rho_W$, but with a slightly lower saturation of the available pore space.

Separated into active layer and the underlying ice core, the respective fractions can be averaged (Table 2).

## Discussion

A comparison of modeled and observed (visually estimated) fractions of all four phases in the trenches cut for the ski track yields a very good accordance in terms of geophysical identification of solid (ice, rock), gaseous, and liquid phases. The differentiation between ice and rock is difficult, since seismic velocities of both phases can be very similar. Also, it has to be noted that direct observations/estimations were only made in several outcrops, and showed considerable small-scale heterogeneity of the rock-ice distribution. However, despite the remaining uncertainties of the FPM, the preliminary results seem realistic in terms of identification of the four phases and their relative distribution.

In a further step, relative changes of electrical resistivities and seismic velocities derived from geophysical monitoring data will be used to estimate total seasonal or annual changes in the contents of ice and unfrozen water to quantify permafrost degradation due to climate change.

Table 2: Calculated fractions of rock, air, water, and ice.

| | $f_{rock}$ | $f_{air}$ | $f_{water}$ | $f_{ice}$ |
|---|---|---|---|---|
| Active layer | 0.4-0.6 | 0.3-0.4 | 0.02-0.08 | 0-0.4 |
| Ice core | 0.4-0.5 | 0 | 0-0.03 | 0.4-0.6 |

## References


Arenson, L., Hoelzle, M. & Springman, S. 2002. Borehole deformation measurements and internal structure of some rock glaciers in Switzerland. *Permafrost and Periglac. Process.* 13(2): 117-135.

Barsch, D. 1996. *Rockglaciers: Indicators for the Present and Former Geoecology in High Mountain Environments*. Berlin, Springer.

Burger, K.C., Degenhardt, J.J. & Giardino, J.R. 1999. Engineering geomorphology of rock glaciers. *Geomorphology* 31(1–4): 93-132.

Haeberli, W., Hoelzle, M., Kääb, A., Keller, F., Vonder Mühll, D. & Wagner, S. 1998. Ten years after drilling through the permafrost of the active rock glacier Murtèl, eastern Swiss Alps: answered questions and new perspectives. *Proceedings of the Seventh International Conference on Permafrost*, *Yellowknife, Canada*.

Hauck, C. 2001. *Geophysical Methods for Detecting Permafrost in high Mountains*. Mitt. der Versuchsanst. für Wasserbau, Hydrol. und Glaziol. der Eidg. Tech. Hochsch. Zurich, Nr. 171: 204 pp.

Hauck, C., Bach, M. & Hilbich, C. 2008. A 4-phase model to quantify subsurface ice and water content in permafrost regions based on geophysical datasets. *Proceedings of the Ninth International Conference on Permafrost, Fairbanks, Alaska, 29 June–3 July 2008.*

Maag, C., Wild, O., King, L., Baum, M., Klein, S. & Hilbich, C. 2008. Permafrost characteristics and climate change consequences at Stockhorn and Gornergrat (Swiss Alps). *Proceedings of the Ninth International Conference on Permafrost, Fairbanks, Alaska, 29 June–3 July 2008.*

Maurer, H. & Hauck, C. 2007. Geophysical imaging of alpine rock glaciers. *Journal of Glaciology* 53(180): 110-120.

Vonder Mühll, D.S. 1993. *Geophysikalische Untersuchungen im Permafrost des Oberengadins*. ETH Zürich, Diss. ETH Nr. 10107: 222.

Wild, O., Roer, I., Gruber, S., May, B. & Wagenbach, D. 2008. Scientific opportunities and environmental impacts related to ski run construction, Zermatt, Swiss Alps. *Proceedings of the Ninth International Conference on Permafrost, Fairbanks, Alaska, 29 June–3 July 2008.*

# Internal Structure of Rock Glacier Murtèl Delineated by Electrical Resistivity Tomography and Forward/Inverse Modeling

Christin Hilbich
*Department of Geography, University of Jena, Germany*

## Introduction

Rock glacier Murtèl (Engadine, Swiss Alps) is one of the most intensely investigated rock glaciers worldwide. Borehole temperatures have been recorded since 1987 (Vonder Mühll & Haeberli 1990, Haeberli et al. 1998, Vonder Mühll et al. 1998, Vonder Mühll et al. 2007), providing one of the longest temperature records in Alpine permafrostFrom the broad range of investigations on this rock glacier, it has been learned that:

- The rock glacier Murtèl consists of a considerable amount of massive ice (up to 80–100% in a ca. 25 m thick layer below the active layer) (Vonder Mühll & Haeberli 1990).
- The active layer depths vary only slightly throughout the years (by max. 0.5 m) (Vonder Mühll et al. 2007).
- Rock glacier creeping is generally rather slow with velocities between 5 and 15 cm/a (determined over the period 1987–1996) (Kääb et al. 1998).
- A shear zone exists in 30 m depth, where most of the horizontal movement is concentrated (Arenson et al. 2002).

Apart from the borehole observations, no direct observations of the interior exist at rock glacier Murtèl. However, indirect information could be inferred from geophysical measurements (Vonder Mühll 1993, Hauck & Vonder Mühll 2003, Maurer & Hauck 2007).

In general, rock glacier Murtèl is considered an active rock glacier under stable conditions. The internal structure is assumed to be homogeneous without any distinct degradation phenomena.

## Geoelectrical Monitoring

In summer 2005 a longitudinal Electrical Resistivity Tomography (ERT) monitoring profile was installed at rock glacier Murtèl. The horizontal distance of the profile is 235 m (crossing the borehole and the tongue). Results from the ERT monitoring give rise to an interesting inhomogeneity in the central part of the rock glacier.

The general resistivity pattern (Fig. 1) clearly confirms the stratigraphy derived from borehole measurements: the active layer is represented by relatively low resistivities between 15 and 30 kΩm in the upper 3 m. Beneath the active layer there is a sharp increase in resistivities to values between 500 kΩm and 1.9 MΩm, indicating the presence of massive ice. In the central part of the rock glacier, this pattern is interrupted by a vertical anomaly with smaller resistivity values (300–400 kΩm). The monitoring results indicate that this feature is much more pronounced in summer than in winter.

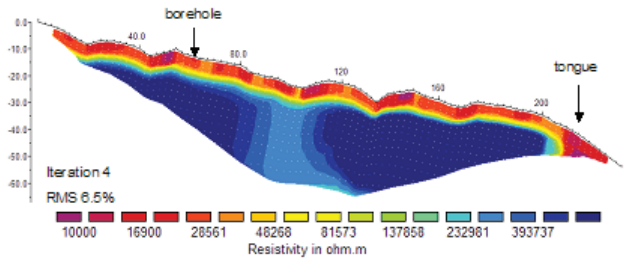


Figure 1. ERT tomogram from rock glacier Murtèl, measured on August 17, 2006.

To assess whether this anomaly is an artefact of the inversion process (cf. Hauck & Vonder Mühll 2003) or produced by a real structural inhomogeneity the resistivity distribution of the rock glacier was analysed by means of synthetic datasets and forward/inverse modeling using the software Res2DMod and Res2DInv (Loke & Barker 1995, Loke 2002). In forward/inverse modeling approaches, apparent resistivities are calculated from a synthetic model of the assumed resistivity distribution. The resulting inversion result can then be compared to the corresponding inversion result of the measured data. If the results are similar in terms of both resistivity distribution and total values, the synthetic model can be evaluated as a realistic model of the subsurface resistivity distribution.

This procedure was performed for a variety of geomorphological situations that may explain the inhomogeneity within rock glacier Murtèl.

Best results were obtained for a simulated crevasse in the massive ice body of the rock glacier, which is, at least partly, filled with unfrozen water. This result is surprising, as the rock glacier does not show indications of disintegration at the surface. An interpretation of this feature in terms of a degradation phenomenon seems likely, but cannot be supported by other data from the rock glacier.

## Conclusions

The forward/inverse modeling showed that the resistivity anomaly in the central part of the rock glacier is very likely due to a crevasse-like structure within the ice core. These findings are of interest in the context of the observed speed-up of many rock glaciers in the Alps, which is often associated with disintegration of the surface and the formation of crevasses (Roer et al. 2005, Kääb et al. 2007). Since comparable developments (speed-up, formation of crevasses at the surface) are not known for rock glacier Murtèl so far, further studies are necessary to verify the assumptions resulting from forward/inverse modeling.

## References


Arenson, L., Hoelzle, M. & Springman, S. 2002. Borehole deformation measurements and internal structure of some rock glaciers in Switzerland. *Permafrost and Periglacial Processes* 13: 117-135.

Barsch, D. 1996. *Rock Glaciers – Indicators for the Present and Former Geoecology in High Mountain Environments*. Berlin: Springer.

Burger, K.C., Degenhardt, J.J. & Giardino, J.R. 1999. Engineering geomorphology of rock glaciers. *Geomorphology* 31(1–4): 93-132.

Haeberli, W., Hoelzle, M., Kääb, A., Keller, F., Vonder Mühll, D. & Wagner, S. 1998. Ten years after drilling through the permafrost of the active rock glacier Murtèl, eastern Swiss Alps: Answered questions and new perspectives. *Proceedings of the Seventh International Conference on Permafrost, Yellowknife, Canada.*

Hauck, C. & Vonder Mühll, D. 2003. Inversion and interpretation of two-dimensional geoelectrical measurements for detecting permafrost in mountainous regions. *Permafrost and Periglacial Processes* 14: 305–318.

Kääb, A., Gudmundsson, G.H. & Hoelzle, M. 1998. Surface deformation of creeping mountain permafrost. Photogrammetric investigations on rock glacier Murtél, Swiss Alps. *Proceedings of the Seventh International Conference on Permafrost, Yellowknife, Canada:* 531-537.

Kääb, A., Frauenfelder, R. & Roer, I. 2007. On the response of rock glacier creep to surface temperature increase. *Global and Planetary Change 56*(1–2): 172-187.

Loke, M.H. & Barker, R.D. 1995. Least-squares deconvolution of apparent resistivity. *Geophysics* 60: 1682-1690.

Loke, M.H. 2002. *RES2DMOD, Ver. 3.01*: Rapid 2D resistivity forward modelling using the finite-difference and finite-element methods.

Maurer, H. & Hauck, C. 2007. Geophysical imaging of alpine rock glaciers. *Journal of Glaciology* 53(180): 110-120.

Roer, I., Kääb, A. & Dikau, R. 2005. Rock glacier acceleration in the Turtmann valley (Swiss Alps): Probable controls. *Norwegian Journal of Geography* 59: 157-163.

Vonder Mühll & Haeberli 1990

Vonder Mühll, D.S. 1993. Geophysikalische Untersuchungen im Permafrost des Oberengadins. *ETH Zürich, Diss. ETH* 10107: 222.

Vonder Mühll, D., Stucki, T. & Haeberli, W. 1998. Borehole temperatures in alpine permafrost: a ten years series. *Proceedings of the Seventh International Conference on Permafrost, Yellowknife, Canada*.

Vonder Mühll, D., Noetzli, J., Roer, I., Makowski, K. & Delaloye, R. 2007. *Permafrost in Switzerland 2002/2003 and 2003/2004.* Glaciological Report (Permafrost) No. 4/5 of the Cryospheric Commission (CC) of the Swiss Academy of Sciences (SCNAT) and the Department of Geography, University of Zurich: 106.

# Permafrost Degradation Beneath a Heat-Producing Coal Waste Rock Pile, Svalbard (78°N)

Jørgen Hollesen
*Department of Geography and Geology, University of Copenhagen, Copenhagen, Denmark*
*UNIS, Longyearbyen, Svalbard*
Bo Elberling
*Department of Geography and Geology, University of Copenhagen, Copenhagen, Denmark*
*UNIS, Longyearbyen, Svalbard*

## Introduction

In Arctic areas, permafrost and low annual air temperatures are considered to keep the chemical activity within sulphide-containing waste rocks low. This has led to a general acceptance that permafrost environments are well suited for storing waste rocks. Although temperatures below 0°C reduce the oxidation rate of sulphide minerals, they do not eliminate oxidation (Elberling 2001). Furthermore, the oxidation of sulphide minerals is strongly exothermic producing 1409 KJ of heat for every mole oxidized. Because the oxidation rate of sulphides increases with temperature (Elberling 2005), the release of heat can result in a positive feedback on the oxidation process, causing subsurface temperatures to become self-increasing (Lefebvre et al. 2001). Depending on the local meteorological conditions, the sulphide content of the waste material and the physical design of the waste rock pile, subsurface temperatures can become so high that weathering processes continue year-round within the waste rock pile (Elberling et al. 2007). This is not only important to the overall amounts pollutants released but also to the stability of the permafrost beneath the pile which could be degraded, causing the foundation of the waste rock pile to destabilise.

The objective of this study is to investigate the thermal regime within a coal waste rock pile on Svalbard and to simulate subsurface temperatures due to current weather conditions, physical properties of the waste rock material, and subsurface heat generation. The simulations will be carried out using the one-dimensional heat and water flow model, CoupModel (Jansson & Karlberg 2001), which will be calibrated and validated based on data from the study area. The validated model will be used to investigate how the permafrost beneath the waste rock pile is influenced by the oxidation processes.

## Study Site

In this High Arctic study, an abandoned coal waste rock pile near Longyearbyen, Svalbard (78°20′N, 15°40′E) is investigated. Based on data from 1975–2005, the mean annual air temperature of the area is -5.8 ± 1.3°C and the annual amount of precipitation is 187 ± 44 mm, of which approximately 50% falls as snow. Svalbard is located within the region of continuous permafrost with an active layer thickness of 1.0 to 1.5 m. The construction of the waste rock pile was initiated in 1986 and completed in 1990 with a height of 20 m (roughly 200,000 $m^3$ of waste rock). It stands out in the landscape with steep sides and is highly exposed to winds.

The waste rock pile has previously been described by Elberling et al. (2007). The waste rock material is very coarse and heterogeneous with only 16% ± 6% being less than 2 mm in diameter and 40% being above 100 mm in diameter. It is dominated by 1–10 mm rocks, but contains rocks more than 0.5 m in diameter. Heat production rates due to pyrite oxidation range from 0.5 to 2.5 μW $g^{-1}$ and a significant exponential increase in heat production has been noted with increasing temperatures ($R^2$ = 0.98, $p$ = 0.001) which is equal to a $Q_{10}$ of 2.6.

## Methods

Based on climatic inputs (air temperature, wind speed, wind direction, relative humidity, radiation, pressure, and snow depth), grain size distribution, porosity and microbial and chemical heat production rates from pyrite oxidation, the CoupModel is used to simulate subsurface temperatures within and below the waste rock pile. The model is calibrated using measurements of subsurface temperatures from 1 October 2004 to 19 August 2005 and validated using measurements from 1 October 2005 to 19 August 2006.

## Results

Despite freezing air temperatures 240 days per year subsurface temperatures within the investigated pile were stable around 4.3 ± 0.5°C at 7 m depths throughout the year. Seasonal temperature readings indicate that an outer layer of less than 1 m remained frozen during the six-month winter period. Observations of nearby natural permafrost-affected talus slopes confirm that, without subsurface heat generation, only a thin near-surface layer of less than 2 m thaw every summer (Fig. 1).

The CoupModel setup is successfully calibrated and validated. With $r^2$ values ranging from 0.99 to 0.64 and $p$ values being <0.001, the linear correlations are highly significant in all depths. The mean temperature differences range from 0.04°C to 1.15°.

Simulations show that the underlying permafrost is strongly influenced by the heat from the waste rock pile. The zone of thaw has changed from 1–2 m in 1986 to 25 m in 2006, and in 2006, temperatures are influenced down to a depth of 50 m (Fig. 1).

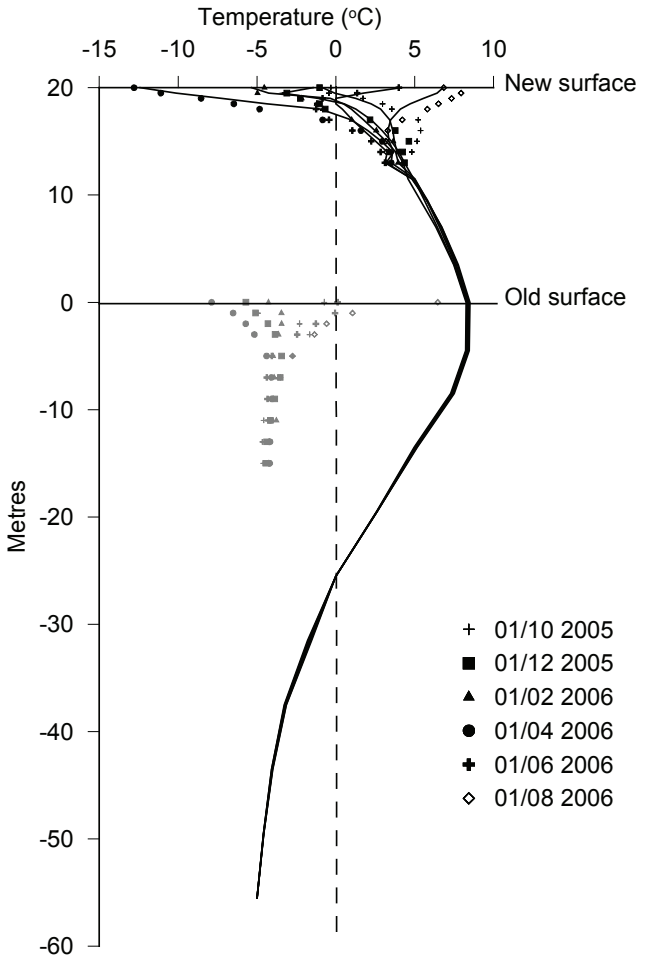


Figure 1. Observed and simulated subsurface temperatures within and beneath the waste rock pile in Bjørndalen (black symbols and lines, respectively). The grey symbols show subsurface temperatures within a nearby talus slope (provided by N. Matsuoka, pers. com., 2008).

## Discussion

It is not possible to measure temperatures beneath the waste rock pile; thus the actual thaw depth is unknown.

Observations of the water runoff coming from the pile do show, however, that high concentrations of reduced Fe are coming out at the foot of the pile (Søndergaard et al. 2007). This suggests that water draining from the pile is at least partly infiltrating the newly formed and saturated active layer below the pile.

Many Arctic waste rock piles are located in near-coast regions; thus destabilisation due to permafrost degradation could cause the pollution to spread to the marine environment. There is no evidence that the melting of the permafrost has influenced the stability of the waste rock pile in Bjørndalen. However, as the pile is located on a downward slope the risk still exists, especially if temperatures increase further due to climate change.

## References

Elberling, B. 2001. Environmental controls of the seasonal variation in oxygen uptake in sulfidic tailings deposited in a permafrost-affected area. *Water Resources Research* 37: 99-107.

Elberling, B. 2005. Temperature and oxygen control on pyrite oxidation in frozen mine tailings, *Cold Regions Science and Technology* 41(2): 121-133.

Elberling, B., Søndergaard, J., Jensen, L.A., Schmidt, L.B., Hansen, B.U., Asmund, G., Balic-Zunic, T., Hollesen, J., Hansson, S., Jansson, P.E. & Friborg, T. 2007. Arctic vegetation damage by winter-generated coal mining pollution released upon thawing. *Environ. Sci. Technol.* 41(7): 2407-2413.

Jansson, P.E. & Karlberg, L. 2001. Coupled *heat and mass transfer model for soil-plant-atmosphere systems*. Royal Institute of Technology, Dept of Civil and Environmental Engineering, Stockholm, Sweden.

Lefebvre, R., Hockley, D., Smolensky, J. & Gelinas, P. 2001. Multiphase transfer processes in waste rock piles producing acid mine drainage 1: Conceptual model and system characterization, *Journal of Contaminant Hydrology* 52(1–4), 137-164.

Søndergaard, J., Elberling, B., Asmund, G., Gudum, C. & Iversen, K.M. 2007. Temporal trends of dissolved weathering products released from a high Arctic coal mine waste rock pile in Svalbard (78°N). *Applied Geochemistry* 22: 1025-1038.

# Patterns in Soil Carbon Distribution in the Usa Basin (Russia): Linking Soil Properties to Environmental Variables in Constrained Gradient Analysis

Gustaf Hugelius, Peter Kuhry
*Department of Physical Geography and Quaternary Geology, Stockholm University, Sweden*

## Introduction

Arctic and subarctic ecosystems harbour large reservoirs of soil organic matter (SOM) and are considered key components in the global carbon (C) cycle (White et al. 2000). To a large degree, this C is found in cryosols and cryic histosols, where subzero temperatures limits decomposition (Davidson & Janssens 2006). We compile and analyse a database describing soil C properties, permafrost conditions, and vegetation in the Usa Basin of Northeastern European Russia. We update previous calculations of landscape soil C storage for the whole Usa Basin and describe general patterns of landscape C allocation with respect to vegetation and permafrost. We analyse a subset of the database in constrained gradient analysis combined with Monte Carlo permutations to determine how an array of environmental variables are linked to site-specific soil quantity and quality.

## Study Area

The Usa River Basin straddles the Arctic Circle in Northeastern European Russia, covering some 93,500 km$^2$. Spruce dominated taiga covers the southern parts of the basin and gradually gives way to open ground in a wide taiga-tundra transition zone. Isolated permafrost first appears in peatlands of this transition zone, but increases as tundra begins to dominate the landscape. The northern lowland parts of the basin are dominated by tundra and peatland with extensive permafrost. Subalpine forests of Larch and Fir grow in the foothills of the Ural Mountains, which denote the eastern border of the basin.

## Methods

The analysed database contains soil chemical and physical descriptions from 363 different sites and includes both upland soils and peat. For each site, the soil database lists vegetation cover, soil type (FAO-WRB), depth of soil genetic horizons, top organics, and active layer (if permafrost is present). Carbon storage is calculated to 30 and 100 cm reference depths in mineral soils and to full depth in peatlands. For a subset of the database there is also data on nitrogen (N) content. The C:N ratio of peat decreases as the material is degraded and is considered a useful proxy for quality (Kuhry & Vitt 1996). We also analyse a GIS database of the Usa Basin containing maps of soils (Mazhitova et al. 2003) and permafrost (Oberman & Mazhitova, 2003) as well as 100 m resolution Digital Elevation Model (DEM) and a satellite Land Cover Classification (LCC, 30*30m Landsat TM data, Virtanen et al. 2004). Climate data is interpolated from the 16 km grid of the HIRHAM regional climate model (Christensen & Kuhry 2000).

## Analyses

For the purpose of Soil C calculations and upscaling, the Usa Basin is divided into ecoclimatic regions (Fig. 1). The sites in the database are ordered according to region and vegetation. Mean soil C content is then calculated for each vegetation type in the separate regions. We also calculate the proportion of C that is stored in Cryosols. The results are upscaled to full areal coverage using vegetation data from the LCC.

For a subset of lowland sites ($n$ = 68), soil properties are analysed with Redundancy Analysis (RDA). This constrained ordination technique is used to assess the relationships within and between two separate data matrices of response and environmental variables.

For each pedon, a total of nine soil response variables are included: **1–3:** Carbon storage (kgC/m$^2$) in three depth intervals (0–30 cm, 30–100 cm, and >100 cm); **4–6:** percentage of C that is in top organics, in peat and in permafrost; **7:** Bulk Density (BD, g/cm3); **8–9:** C:N ratio of organic soil horizons and C:N ratio of mineral soil horizons.

The environmental variables permafrost, vegetation, and soil are available from field observations as well as geomatic sources. The Topographic Wetness Index is calculated from a DEM. Climate variables are derived from the HIRHAM model.

We perform RDAs of the response variables, separately using each environmental variable to constrain the ordination (software CANOCO 4.5). The explanatory power of each

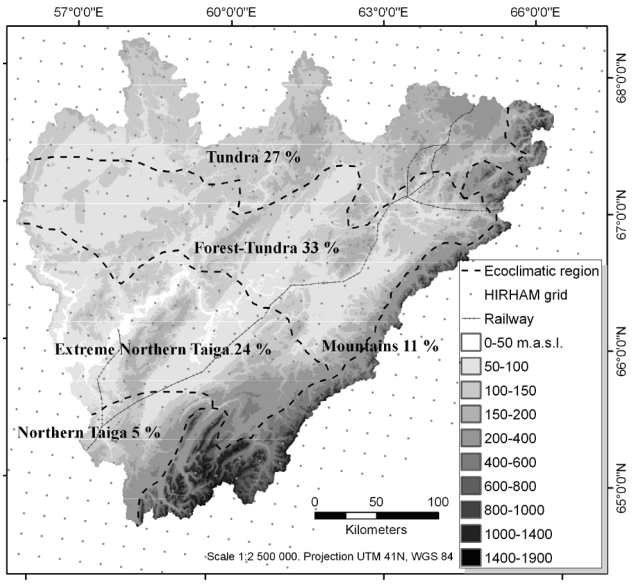


Figure 1. Map showing the coverage of ecoclimatic regions in the Usa Basin with the HIRHAM grid, railway, and topography.

environmental variable is determined through Monte Carlo permutations of the canonical eigenvalues of each RDA (999 permutations).

To further constrain the ordination, the variables that are found to be statistically significant are tested together in a RDA *Monte Carlo forward selection* process ($p$-value <0.05, Bonferroni correction applied). For this process, the site-corresponding variables from site-specific and geomatic sources were separated and tested in two independent RDAs.

## Results

*Storage and partitioning*

Estimates of soil C storage for 30 cm, 100 cm, and full depth of peatlands in the five ecoclimatic regions are summarised in Table 1. The mean for the entire catchment is 34.8 kgC/m$^2$ when full depth of peatlands is included. Kuhry et al. (2002) estimated a total storage of 33.0 kgC/m$^2$ in the Usa Basin for the same depths.

When looking at separate vegetation classes, it is evident that peatlands store a disproportionate portion of soil C. Fen and bog peatlands cover some 30% of the Basin, but hold more than two-thirds of all C. Bogs alone cover less than a fifth, but hold more than half of all C in the Basin.

Carbon storage in permafrost terrain is dominated by bog peatlands. Bogs hold some 90% of permafrost C and >95% of perennially frozen C in the Usa Basin. While there is extensive permafrost underlying northern tundra vegetation, the active layer boundary is generally below the C-rich top organic layer.

Table 1. Area and C storage for regions and whole basin.

| Region | Area km$^2$ | 30 cm kgC/m$^2$ | 100 cm kgC/m$^2$ | Total kgC/m$^2$ |
|---|---|---|---|---|
| Northern Taiga | 4,709 | 10.4 | 22.3 | 31.0 |
| Extreme N. Taiga | 22,600 | 11.2 | 27.3 | 38.3 |
| Forest-Tundra | 31,245 | 11.5 | 27.4 | 37.3 |
| Tundra | 24,720 | 11.2 | 27.1 | 38.1 |
| Mountains | 10,210 | 7.1 | 12.7 | 12.8 |
| Whole Basin | 93,484 | 10.8 | 25.5 | 34.8 |

Table 2. Summary of tested environmental variables.

| Variable Type | Variable | $p$-value |
|---|---|---|
| Site | Permafrost | *<0.01** |
| " | Vegetation | *<0.01** |
| " | Soil | *<0.01** |
| Climate | Annual mean temperature | 0.09 |
| " | July temperature | 0.17 |
| " | Summer precipitation | *<0.05* |
| " | Winter precipitation | *<0.05** |
| " | Frost index | 0.14 |
| Climate / Geomatic | Conrads continentality index | 0.48 |
| Geomatic | Permafrost map | *<0.05* |
| " | Satellite LCC | *<0.01** |
| " | Soil map | *<0.01** |
| " | Topographic Wetness Index | 0.77 |

The $p$-values of variables that were significant when tested separately are in italic. The variables that were further identified in the *forward selection* process are marked with an asterix*.

*Constrained gradient analysis*

Table 2 summarizes the environmental variables and their significance as explanatory variables. Permafrost, vegetation, and soil are all significant from both site specific and geomatic sources. This indicates that geomatic sources may be used to replace when actual field data is lacking.

Both summer and winter precipitation significantly explains the response variables. While July temperature, mean annual temperature, and the frost index should all affect permafrost occurrence, they are not significant explanatory factors here.

The RDA *forward selection* process further constrains the ordination by removing weak or redundant (collinear) variables. Summer precipitation is highly correlated to winter precipitation and does not contribute to the model. The Permafrost map was partly based on the soil map and satellite LCC, and is also found to be redundant.

## Acknowledgments

Much of the material was collected and compiled in the EU 4th Framework TUNDRA project. Further compilation and analyses are funded through the EU 6th Framework CARBO-North project, and a grant of the Swedish Research Council.

## References

Christensen, J.H. & Kuhry, P. 2000. High resolution regional climate model validation and permafrost simulation for the East-European Russian Arctic. *J. of Geophys. Res.* 105(D24): 29647-29658.

Davidson, E.A. & Janssens, I.A. 2006. Temperature sensitivity of soil carbon decomposition and feedbacks to climate change. *Nature* 440: 165-173.

Kuhry, P. & Vitt, D.H. 1996. Fossil Carbon/Nitrogen ratios as a measure of peat decomposition. *Ecology* 77(1): 271-275.

Kuhry, P. et al. 2002. Upscaling soil organic carbon estimates for the Usa Basin (Northeast European Russia) using GIS-based landcover and soil classification schemes. *Danish J. of Geog.* 102: 11-25.

Oberman, N.G. & Mazhitova, G.G. 2003. Permafrost mapping of Northeast European Russia based on the period of climatic warming 1970–1995. *Norwegian J. of Geog.* 57(2): 111-120.

Mazhitova, G.G. et al. 2003. Geographic Information System and Soil Carbon Estimates for the Usa River Basin, Komi Republic. *Eurasian Soil Science* 36(2): 123-135.

White, A. et al. 2000. The high-latitude terrestrial carbon sink: A model analysis. *Global Change Biology* 6: 227-245.

# Total Storage and Landscape Distribution of Soil Carbon in the Central Canadian Arctic Using Different Upscaling Tools

Gustaf Hugelius, Peter Kuhry
*Department of Physical Geography and Quaternary Geology, Stockholm University, Sweden*
Charles Tarnocai
*Agriculture and Agri-Food Canada, Ottawa, Canada*
Tarmo Virtanen
*Department of Biological and Environmental Sciences, University of Helsinki, Finland*

## Introduction

The arctic landscape displays variation on many different spatial scales, and different methods for calculating landscape C pools demand varying approaches to sampling.

In this study we assess the total storage and spatial distribution of soil C in continuous permafrost terrain of Central Canada. The landscape allocation of soil C is assessed using a transect-based soil sampling program carried out in the summer of 2006 at the shore of Lake Tulemalu, northern Kazan Basin (62°55′N, 99°10′W, Fig. 1). We combine and compare three upscaling methods of increasing sophistication: (1) arithmetic mean, (2) transect upscaling, and (3) landscape upscaling. For the latter, we compare land cover and geomorphological landscape elements as spatial proxies for upscaling.

Figure 1. Oblique air photograph facing southwards over the northernmost transect.

## Methods

*Field sampling and sample analyses*

Soils were sampled along three 1 km transects, which were chosen to represent main vegetation types and geomorphology of the landscape. Once the transects were established, however, pedons were collected equidistantly every 100 m without further bias (33 sites). This sampling scheme combined selective representation of what was considered representative with a measure of randomization introduced by small-scale vegetation and micro-topography patterns. Sampling includes upland soils (to 1 m depth) and peat deposits (to mineral contact). At all non-peatland sites, three additional samples of the top organic layer were collected.

Samples from all sites were analyzed in 10 cm depth increments for bulk density and loss on ignition (LOI at 550°C and 950°C) to determine organic content. A subset of samples is tested in an elemental analyzer to accurately determine C and N content. For remaining samples a LOWESS regression model is constructed to translate LOI to C content. The age of basal peat samples from 8 selected sites is determined through radiocarbon dating.

*Landscape classification and upscaling*

To enable interpretation and landscape upscaling of soil sampling results, we mapped land cover and geomorphology in the larger surrounding area. A land cover classification (LCC) based on Landsat ETM+ imagery was produced and verified using inventoried ground truth points. The classification covers some 400 km$^2$ around the sampled transects, and the main land cover types are water bodies (35% coverage), fen and bog peatlands (16% and 11%, respectively), dry, moist and wet shrub tundra (6%, 20%, and 8% coverage, respectively), lichen tundra (3.5%) and non-vegetated ground (0.5% coverage). We focus our landscape upscaling on a smaller, 42 km$^2$, intensive study area, delineated to be representative of the sampled sites. Some 20 km$^2$ of this is water and will be excluded from the upscaling. A simplified land cover map of this area is shown in Figure 2. A geomorphological map was produced using black and white aerial imagery combined with multispectral satellite scenes. The map identifies features such as recent and relict raised shorelines and separates well-drained upland till soils from local hollows.

In the simplest upscaling method, we calculate an arithmetic mean of soil C storage at all 33 sites. For transect upscaling, the soil sampling results are upscaled according to the proportional distribution of land cover types and landscape elements along the inventoried transects. For the landscape upscaling, we use information from the land cover and geomorphology mapping to calculate total C pool, also assessing land cover and geomorphology proxies separately.

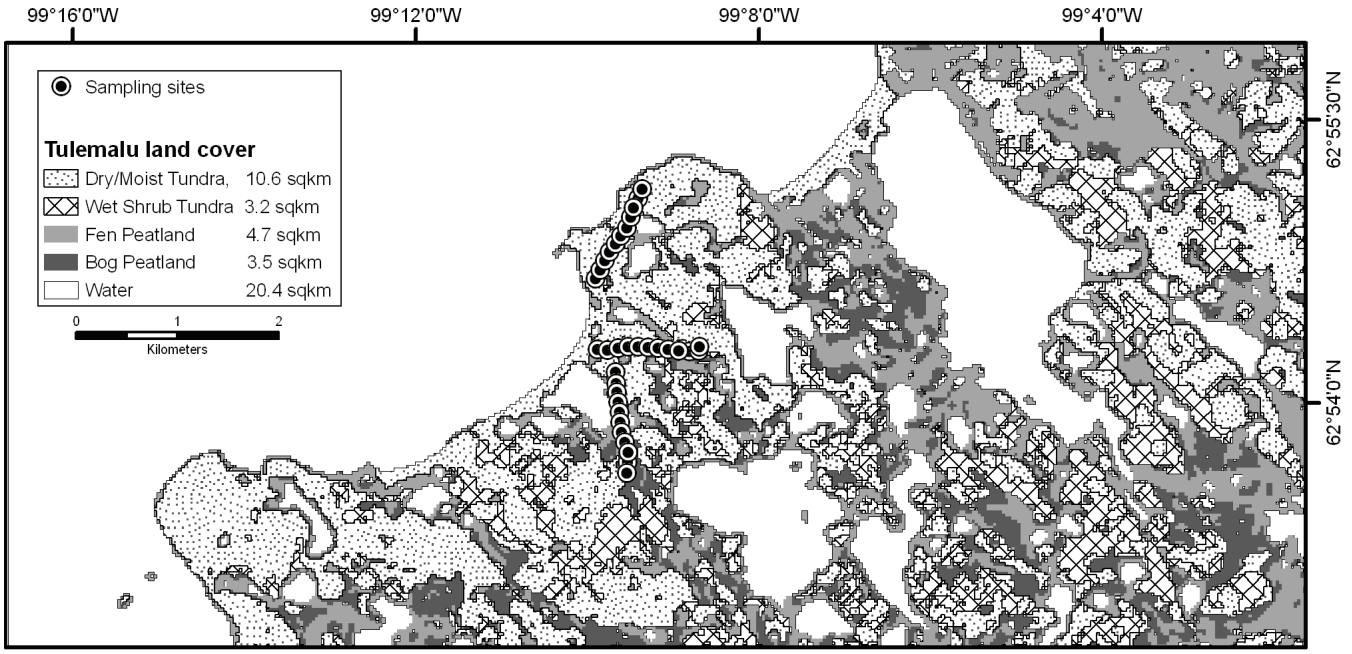


Figure 2. Map of the intensive study area showing land cover and sampling sites. Land cover is simplified with Bare ground, lichen tundra and dry/moist shrub tundra combined into one class.

Table 1. Summary of samples and land cover type coverage

| Land cover type | Samples n / % | Organic layer | Transect coverage | Landscape coverage |
|---|---|---|---|---|
| Dry lichen tundra | 3 / 9 % | 3 cm | 4 % | 2 % |
| Dry shrub tundra | 4 / 12 % | 5 cm | 5 % | 9 % |
| Moist shrub tundra | 12 / 35 % | 6 cm | 34 % | 35 % |
| Wet shrub tundra | 4 / 12 % | 19 cm | 12 % | 14 % |
| Fen peatland | 7 / 21 % | 32 cm | 21 % | 21 % |
| Bog peatland | 4 / 12 % | 65 cm | 21 % | 16 % |

## Results

A summary land cover type representation in samples, transects, and the intensive study area is presented in Table 1. The land cover type Bare ground is only represented at the landscape level (2% of the intensive study area), and is not included. As no lake sediments have been sampled, water is also excluded.

The percentage representation for the three different upscaling techniques is quite similar. Dry lichen and shrub tundra is somewhat over represented in the number of samples collected, while Bog peatlands are under-sampled.

The mean depth of the top organic layers of tundra habitats seem to gradually increase along a moisture gradient. Average peat thickness in raised permafrost bogs is considerably higher than in fen peatlands. Radiocarbon dating shows that bogs are generally older than fens; the oldest basal peat from a bog is 5220 ± 50 $C^{14}$y BP while the corresponding age for fens is 1405 ± 30 $C^{14}$y BP.

Preliminary analyses indicate that most of the C is found in fen and bog peatlands. Calculated from arithmetic means, about three-quarters of the C is stored in peat or peaty tundra top organics. The wet shrub tundra stores significantly more C than do moist or dry shrub tundra classes, showing that it is important to make a distinction between shrub tundra classes for the landscape upscaling. Bog peatlands stand out with regard to storage of frozen C.

More than a third of all stored C is perennially frozen beneath the active layer boundary, mainly in histic Cryosols. The soils in the study area are heavily cryoturbated and a tenth of all C is found in cryoturbated soil layers.

An additional objective of this study is to compare average soil carbon storage derived from these intensive landscape analyses with previously published local/regional estimates as well as more general databases such as those provided by The Soil Organic Carbon of Canada Map (Tarnocai & Lacelle 1996).

## Acknowledgments

Fieldwork and analyses was supported through a grant of the Swedish Research Council. We wish to thank Ms. Helen Dahlke for her assistance during fieldwork.

## References

Tarnocai, C. & Lacelle, B. 1996. *Soil Organic Carbon of Canada Map*. Ottawa, Ontario: Eastern Cereal and Oilseed Research Centre, Agriculture and Agri-Food Canada, Research Branch.

# Liquid Water Destabilizes Frozen Debris Slope at the Melting Point: A Case Study of a Rock Glacier in the Swiss Alps

Atsushi Ikeda, Norikazu Matsuoka
*Graduate School of Life and Environmental Sciences, University of Tsukuba*

## Introduction

Positive correlation between temperatures and surface velocities of rock glaciers in various time scales indicates that ground warming accelerates rock glaciers (e.g., Kääb et al. 2007). In particular, rock glaciers lying close to the lower limit of local permafrost occurrence show high surface velocities (>0.2 m $a^{-1}$) and significant acceleration which appears to follow seasonal to decadal warming trends (Frauenfelder et al. 2003, Roer et al. 2005, Kääb et al. 2007, Delaloye et al. 2008). Such acceleration has been attributed to gradual heat conduction from the ground surface to the creeping layer lying below several meters' depth. In this report, we propose another model of acceleration by water infiltration, based on in situ monitoring of permafrost creep at the melting point (see also Ikeda et al. 2008).

## Study Site

The studied rock glacier is the upper lobe of Büz North rock glacier (BNU), located on the northeastern slope of a peak named Piz dal Büz (lat. 46°32′N, long. 9°49′E, 2955 m a.s.l.) in the Upper Engadin, Switzerland (see also Ikeda & Matsuoka 2006 for detailed information). BNU originates from the foot of a talus slope at 2840 m a.s.l. and terminates at 2810 m a.s.l. The horizontal dimension (70 m long and 120 m wide) represents almost the minimum size identified as a rock glacier. The steep frontal slope is 10 m high, sloping at 35°. The upper surface is smooth and the average slope angle is 25°.

A pit and borehole indicated that the major components of BNU are platy shale pebbles and cobbles, the interstices of which are partly filled with sand and silt. Below the frost table, the debris was entirely ice-cemented to the bottom of the hole at 5.4 m depth. The gravimetric ice content of borehole cores (c. 10 cm long) was 50% at 4 m depth and 28% at 5 m depth.

## Methods

Inclinometers (BKJ-A-10-D, manufactured by Kyowa Electronic Instruments, Japan) 35 cm long and 2.7 cm in diameter, installed at 4 m and 5 m depths in the borehole on August 9, 2000, measured the deformation of the perennially frozen debris continuously. Each inclinometer sensed inclinations along two directions perpendicular to each other within ±12.2° from the vertical with a resolution of 0.005°. The inclinations were recorded at 3 h or 6 h intervals by a datalogger until August 2, 2007. Ground temperatures (0.1°C resolution) at depths of 0, 0.5, 1, 2, 3, 4, and 5 m were also monitored for the same period.

Downslope inclination at a certain depth was calculated from the sum of the horizontal vectors, which were defined as the tangents of the measured inclinations for the two axes. Strain rates (i.e., vertical velocity gradients) at the two depths were also calculated. Note that inclination for one of the two axes at 5 m depth exceeded the measurement limit on February 3, 2003. From the day to July 2005, the inclination at 5 m depth was estimated from the measured inclination for the other axis using the former linear relationship between the two-axes' inclinations ($r^2 = 0.9995$).

## Findings and a Presumed Model

Both inclinometers showed fast continuous deformation (on average, 2.4° $a^{-1}$ and 6.0° $a^{-1}$) with large seasonal and interannual variations, while the permafrost temperatures remained almost at the melting point (Fig. 1). The movement of the inclinometers coincided with interannual changes in the surface velocities (Ikeda et al. in press). The strain rates at 5 m depth always surpassed those at 4 m depth, both of which had parallel patterns of seasonal variations. The strain rates rapidly increased in the snowmelt periods, indicated by the constant surface temperature at 0°C in early summer. In contrast, the strain rates gradually decreased below a dry snow cover in winter, except for the 2000–01 winter. When the freezing index at the ground surface was small, the decrease in strain rate tended to be small (or even the rate slightly increased in the 2000–01 winter), and the strain rate remained at a large value at the end of the dry snow period (Fig. 2). The highest strain rates at both depths were recorded when the unusually thick snow cover in 2000–01 was melting, whereas the net increases in the strain rates during a snowmelt period were smallest after the extremely snowless 2001–02 winter. In addition, the magnitudes of the acceleration during the snowmelt periods appeared to correlate with the shearing strain (i.e., net deformation) in the preceding dry snow periods.

These phenomena suggest that the frozen debris is permeable to water (mostly from snow melting), although ice-saturated debris is generally regarded as impermeable. The large annual strain rates (>0.1 $a^{-1}$ at 5 m depth) of the coarse debris filled with ice probably result from thrusting up of debris particles over underlying particles within one year. The resulting dilatant deformation probably creates air voids in the frozen debris, a network of which eventually allows water infiltration. The water infiltration accelerates the deformation by reducing effective stress. The refreezing of the pore water, which depends on the cooling intensity in winter, decelerates the deformation. The combination of these processes, possibly affected by different amounts of annually developed air voids and available snowmelt water, controls the temporal variations in the deformation.

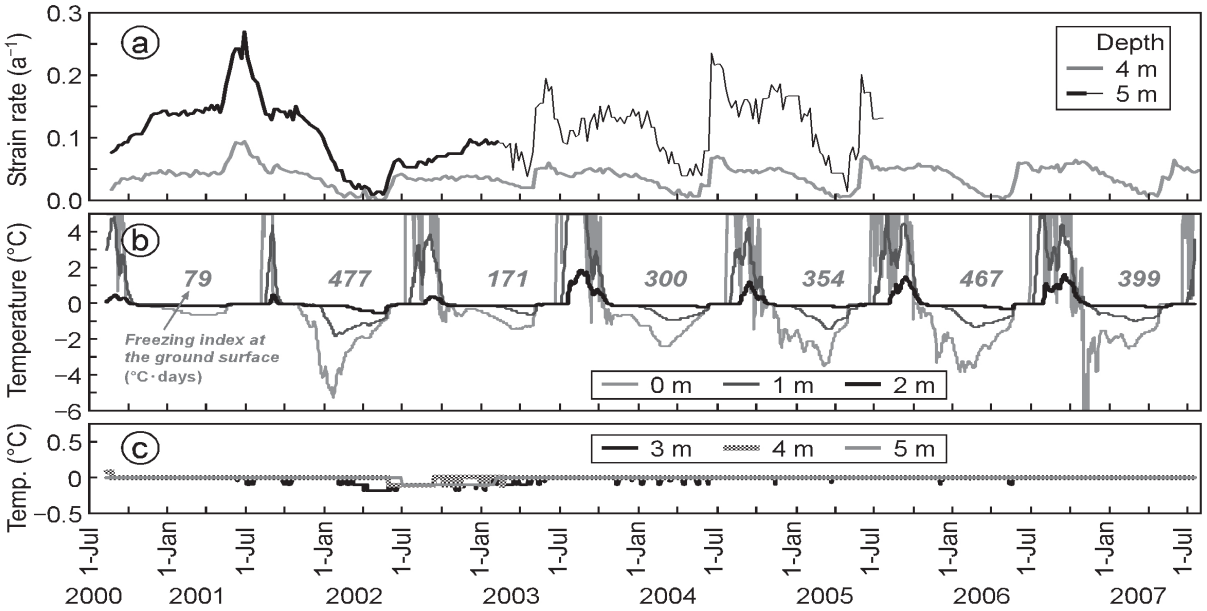


Figure 1. Seven-year records of (a) weekly shearing strain rates, (b) mean daily active-layer temperatures, and (c) permafrost temperatures. The thin line at 5 m depth in (a) is estimated from inclination to one axis after that to the other axis exceeded the measurement limit.

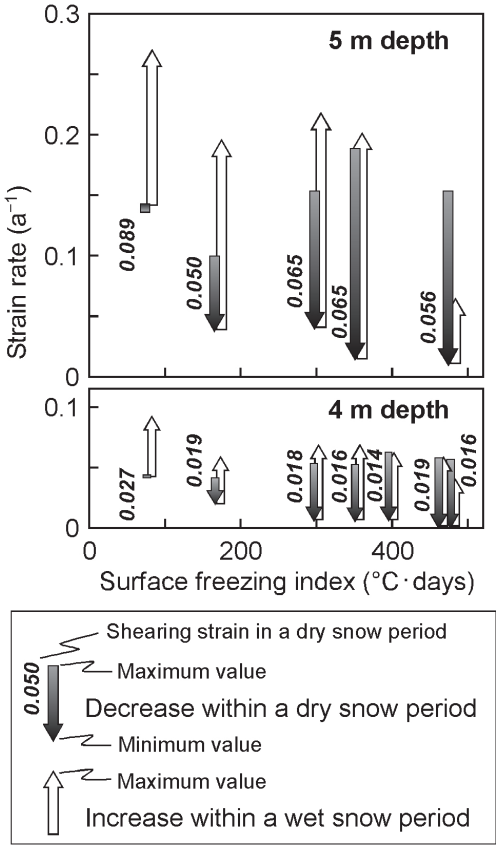


Figure 2. Relationship between surface freezing index and seasonal variations in strain rate. A wet snow period is defined by the constant ground surface temperatures at 0°C in summer and a dry snow period by the preceding subzero temperatures.

## References


Delaloye, R., Perruchoud, E., Avian, E., Kaufmann, V., Bodin, X., Hausmann, H., Ikeda, A., Kääb, A., Kellerer-Pirklbauer, A., Krainer, K., Lambiel, C., Mihajlovic, D., Staub, B., Roer, I. & Thibert, E. 2008. Recent interannual variations of rockglacier creep in the European Alps. *Proceedings of the Ninth International Conference on Permafrost, Fairbanks, USA, June 29–July 23, 2008.*

Frauenfelder, R., Haeberli, W. & Hoelzle, M. 2003. Rockglacier occurrence and related terrain parameters in a study area of the Eastern Swiss Alps. *Proceedings of the Eighth International Conference on Permafrost, Zurich, Switzerland, July 21–25, 2003*: 253-258.

Ikeda, A. & Matsuoka, N. 2006. Pebbly versus bouldery rock glaciers: Morphology, structure and processes. *Geomorphology* 73: 279-296.

Ikeda, A., Matsuoka, N. & Kääb, A. 2008. Fast deformation of perennially frozen debris in a warm rock glacier in the Swiss Alps: An effect of liquid water. *Journal of Geophysical Research* 113 (in press).

Kääb, A., Frauenfelder, R. & Roer, I. 2007. On the response of rockglacier creep to surface temperature increase. *Global and Planetary Change* 56: 172-187.

Roer, I., Kääb, A. & Dikau, R. 2005. Rockglacier acceleration in the Turtmann valley (Swiss Alps): Probable controls. *Norsk Geografisk Tidsskrift* 59: 157-163.

# TSP NORWAY – Thermal Monitoring of Mountain Permafrost in Northern Norway

Ketil Isaksen
*Norwegian Meteorological Institute, Oslo, Norway*
Herman Farbrot
*Department of Geosciences, University of Oslo, Norway*
Bernd Etzelmüller
*Department of Geosciences, University of Oslo, Norway*
Hanne H. Christiansen
*The University Centre in Svalbard, Longyearbyen, Norway*
Lars Harald Blikra
*International Centre for Geohazards, Oslo, Norway*
Kirsti Midttømme
*Geological Survey of Norway, Trondheim, Norway*
Jan Steinar Rønning
*Geological Survey of Norway, Trondheim, Norway*

## Introduction

Permafrost is widespread in the higher mountains of Norway. Extensive studies in southern Norway show that the lower regional altitudinal limit of mountain permafrost is strongly correlated with the mean annual air temperature (MAAT) and decreases eastward with increasing continentality (e.g., Etzelmüller et al. 2008). However, less information is available on the distribution of permafrost in northern Norway, where most investigations have focused on periglacial geomorphology and, in particular, palsas (Isaksen et al. 2008 and references therein).

In 2002 a permafrost monitoring program was initiated in Troms and Finnmark, which are the two northernmost counties of mainland Norway. A series of miniature temperature dataloggers (MTDs) were installed for monitoring ground surface and air temperatures (Isaksen et al. 2008). A gridded mean annual air temperature map indicates a altitudinal gradient for discontinuous permafrost in northern Norway, decreasing from over 1000 m a.s.l. in coastal sites down to below 400 m a.s.l. in the interior and more continental areas (Etzelmüller et al. 2008).

In March 2007, the Norwegian-founded IPY project "Permafrost Observatory Project: A Contribution to the Thermal State of Permafrost in Norway and Svalbard" (TSP NORWAY) was started. In the following, the project is briefly described, and the first results from borehole thermal profiles are presented.

## The TSP Norway Project

The Norwegian-funded IPY project "Permafrost Observatory Project: A Contribution to the Thermal State of Permafrost in Norway and Svalbard" (TSP NORWAY; Christiansen et al. 2007) is a part of the international IPY full project "Permafrost Observatory Project: A Contribution to the Thermal State of Permafrost (TSP)." TSP will obtain a "snapshot" of the permafrost environments as a benchmark against which to assess past and future changes by making standardized temperature measurements in existing and new boreholes throughout the World's permafrost regions. The ultimate payoff is long-term and will serve as validation of current models and understanding of how permafrost conditions are reacting to climate change. Thawing of permafrost in Norway may lead to subsidence of the ground surface, having a substantial impact, for example, on infrastructure and on the stability of mountain slopes.

The main objective of TSP NORWAY is to measure and model the permafrost distribution in northern Norway and Svalbard, including its thermal state, thickness, and influence on periglacial landscape-forming processes.

## Establishment of High Altitude Boreholes

Nine 7–31 m deep boreholes were drilled in bedrock in Troms and Finnmark in August and September 2007. In two of the boreholes, a measurement setup with 15–20 thermistors connected to dataloggers and snow depth sensors, with data recording every six hours, was installed. In one of these boreholes (Kistefjellet) the data are transferred by a modem enabling online presentation. The other seven and two existing boreholes were instrumented with MTDs at selected depths. All boreholes were cased. Periodic recalibration of the installed thermistors is possible, and the holes remain accessible for other probes in the future. Furthermore, a series of MTDs were installed for monitoring surface and air temperatures at selected sites.

## Results

The first estimate of mean ground temperature (MGT) near the bottom of the boreholes is presented in Table 1. Permafrost is presumably present in one of the boreholes (Guolasjavri 1, Fig. 1). In the remaining boreholes, MGT is near or slightly above 0°C. Snow cover conditions seem to be decisive for the permafrost distribution in the investigated altitude ranges. In addition sediment-covered ground may in some cases experience permafrost conditions due to thermal

Table 1. Key information of the TSP-borehole sites in northern Norway, including the first estimate of mean ground temperature (MGT) near the bottom of the boreholes.

| Location | Altitude (m) | Depth (m) | MGT (°C) |
|---|---|---|---|
| Kistefjellet | 990 | 24.8 | 0.7 |
| Lavkavagge 1 | 766 | 14.0 | ?? |
| Lavkavagge 2 | 600 | 30.5 | 2.0 |
| Lavkavagge 3 | 492 | 15.8 | ?? |
| Guolasjavri 1 | 786 | 32.3 | -0.1 |
| Guolasjavri 2 | 814 | 10.5 | <1.4 |
| Guolasjavri 3 | 780 | 10.5 | 0.8 |
| Abojavri 1 | 761 | 6.6 | ?? |
| Abojavri 2 | 570 | 30.3 | 1.1 |
| Iskoras | 572 | 10.7 | ~0 |
| Trolltinden | 848 | 29.4 | 0.5 |

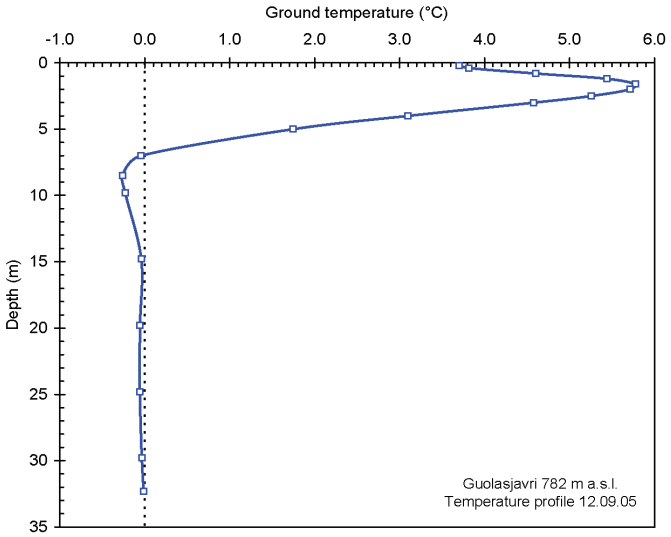


Figure 1. Temperature profile from Guolasjavri 1 borehole, recorded 12.09.2005. Maximum thaw depth is near 7 m.

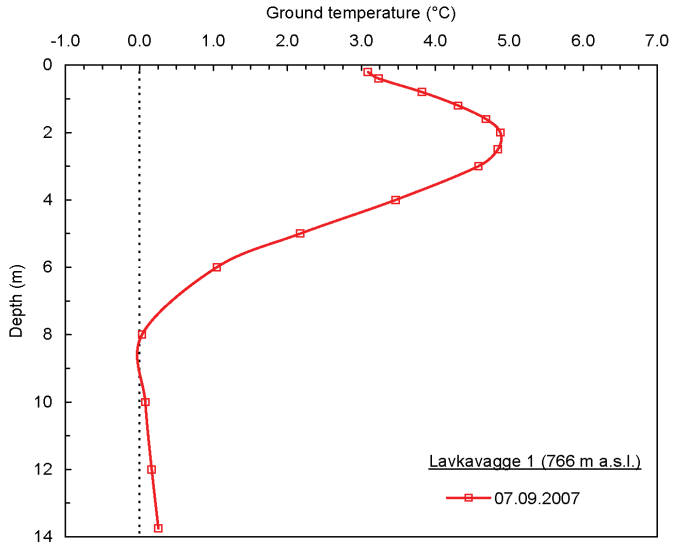


Figure 2. Temperature profile from Lavkavagge 1, recorded 07.09.2007. Seasonal frost reaches a depth of more than 8 m.

offset effects associated with seasonal variation in the heat transfer within the active layer. The seasonal thermal wave may go deep in bedrock, as exemplified by Lavkavagge 1, where seasonal freezing reaches a depth of more than 8 m (Fig. 2).

At Kistefjellet, for example, (Table 1) permafrost is absent. The mean temperature at 24.8 m depth is 0.7°C. The winter snow cover is fairly thick at this site, so permafrost is probably present at nearby wind-swept locations.

## Acknowledgements

This study was financed by the Norwegian Research Council IPY program (NFR contract 176033/S30). In addition the study is part of a Norwegian network project, "*Permafrost og ustabile fjellsider,*" established in 2002.

## References

Christiansen H. et al. 2007. Permafrost Observatory Project: A contribution to the Thermal State of Permafrost in Norway and Svalbard, TSP NORWAY. *Eos Trans. AGU* 88(52), Fall Meet. Suppl., Abstract C21A-0052.

Etzelmüller, B. et al. 2008. Mapping and modeling the distribution of permafrost in the Nordic countries. *Extended abstracts, Ninth International Conference on Permafrost, Fairbanks, Alaska, 29 June–3 July 2008*.

Isaksen, K., Farbrot, H., Blikra, L.H. & Sollid, J.L. 2008. The distribution of permafrost in Finnmark, northern Norway. *Proceedings of the Ninth International Conference on Permafrost, Fairbanks, Alaska, 29 June–3 July 2008*.

# Mapping the Mountain Permafrost in Areas Surrounding Ulaanbaatar City

Ya Jambaljav, A. Dashtseren, D. Battogtokh, D. Dorjgotov
*Institute of Geography, Mongolian Academy of Sciences, Ulaanbaatar, Mongolia*
Y. Iijima, M. Ishikawa, Y. Zhang, T. Kadota, T. Ohata
*Institute of Observational Research for Global Change, JAMSTEC, Yokosuka, Japan*

## Introduction

According to the geographical location and to the climatic condition of Mongolia, the dominating parameters for permafrost occurrence are incoming shortwave solar radiation (ISWSR) and ground moisture. Using threshold values, we have generated a permafrost distribution map in areas surrounding Ulaanbaatar city.

*Study area*

There are three observation sites in our study area: (1) Terelj forest site (Terelj FA) is characterized by north-facing forested slope; (2) Terelj grassland site (Terelj GL) is characterized by south-facing sparse grassed gentle slope; and (3) Nalaikh site is characterized by sparsely grassed plate area with smooth hillocks.

*Data used*

We used the following data: (1) ISWSR at the Nalaikh automatic weather station (Nalaikh AWS), at Terelj GL AWS), and at Terelj FA AWS (Fig. 1). (2) Mean annual ground temperature (MAGT) on the bottom of seasonal freezing and thawing (BSFT) at the above sites and at Sanjai of the Selbe River basin (Table 1). In 5 boreholes, temperatures were measured by CR-10X dataloggers, data marks, and HOBO dataloggers. (3) DEM data from SRTM. (4) Landsat 7ETM image from August 1, 2001, of 131 path and 027 row. We used the temperature data measured by a HOBO datalogger in a borehole located in Sanjai of the Selbe River valley and the temperature data measured by a HOBO datalogger in a borehole located on top of small pingo near Nalaikh AWS.

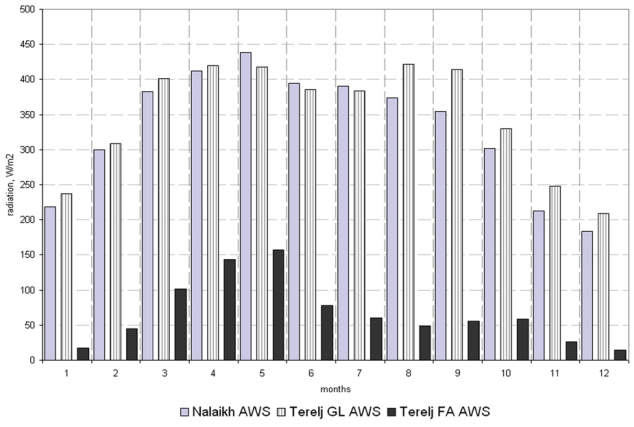


Figure 1. MM of SWSR at Terelj GL AWS, at Terelj FA AWS, and at Nalaikh AWS site.

Table 1. MAGT on BSFT, depth of SFT, and YM of ISWSR.

| | Name of sites | MAGT on BSFT, *C | Depth of SFT, m | YM of ISWSR, $WM^{-2}$ |
|---|---|---|---|---|
| 1 | Terelj GL | +1.9 | 4.0 | 349.3 |
| 2 | Terelj FA | -1.4 | 3.5 | 67.17 |
| 3 | Nalaikh | -0.14 | 5.0 | 330.23 |
| 4 | Nalaikh pingo | -2.2 | 1.45 | 327.67* |
| 5 | Sanjai | +1.75 | 3.2 | 346.9* |

** these data from calculation results*

Table 1 shows the MAGT on BSFT, the depth of seasonal freezing and thawing (SFT), and the yearly mean (YM) of ISWSR

## Modeling the Permafrost Occurrence

One of more important criteria of permafrost occurrence or absence is the MAGT at the BSFT. According to Kudryavtsev (1978), the MAGT at the BSFT is the function of multiparameters. Where the MAGT at the BSFT is lower of the zero, permafrost occurs. In contrast, permafrost is absent. *It is the main criterion of our model.* We calculated the monthly mean of ISWSR at selected sites as the following equations (Fu & Rich 2002):

$$R_{income} = \sum R(dir_{\theta,\alpha}) + \sum R(dif_{\theta,\alpha}) \quad (1)$$

where:

$$R(dir_{\theta,\alpha}) = S_{Const} * \tau^{m(\theta)} * SunDur_{\theta,\alpha} * SunGap_{\theta,\alpha} * \cos(AngIn_{\theta,\alpha})$$

$$R(dif_{\theta,\alpha}) = R_{glb} * P_{dif} * Dur * SkyGap_{\theta,\alpha} * Weight_{\theta,\alpha} * \cos(AngIn_{\theta,\alpha})$$

$$m(\theta) = EXP(-0.000118 * Elev - 1.638 * 10^{-9} * Elev^2) / \cos(\theta)$$

$$AngIn_{\theta,\alpha} = \arccos[\cos(\theta) * \cos(G_z) + \sin(\theta) * \sin(G_z) * \cos(\alpha - G_a)]$$

$$R_{glb} = (S_{Const} \sum (\tau^{m(\theta)})) / (1 - P_{dif})$$

where:

$S_{Const}$ – solar constant ($1367 WM^{-2}$)

$\tau$ – transmitivity of the atmosphere

$\theta$ - solar zenith angle

$\alpha$ - solar azimuth angle

$SunDur_{\theta,\alpha}$ – time durationby sky sector

$P_{dif}$ – the proportion of global normal radiation flux that is diffused

$Dur$ – *the time interval for analysis*

$SkyGap_{\theta,\alpha}$ – *the gap fraction for the sky sector*

*Elev – elevation above sea level*

$G_z, G_s$ – *surface zenith, azimuth angle*

$Weight_{\theta,\alpha} = (\cos\theta_2 - \cos\theta_1)/Div_{azi}$

$\theta_1, \theta_2$ – *the bounding zenith angles of the sky sector*

$Div_{azi}$ – *the number of azimuthal divisions in the sky*

$SunGap_{\theta,\alpha}$ – *gap fraction for the sunmap*

Using equation (1), we calculated the monthly mean of ISWSR at all sites. Figure 2 shows the monthly mean of ISWSR by calculation and by measurement at Terelj GL.

Using the data given in Table 1, we obtained the following regression equation:

$$t_{\xi} = -2.1755 + 0.0116 \; R_{yearly} \quad (2)$$

From regression equation (2) the threshold value below which the permafrost occurs is 187.5WM$^{-2}$.

## Mapping Permafrost Distribution

We generated the map of YM of ISWSR. The YM of ISWSR fluctuates from 50.7WM$^{-2}$ to 409.1WM$^{-2}$, depending on topography and forests. Mountain permafrost distribution was mapped based on the threshold value of 187.5WM$^{-2}$.

The permafrost island exists along the small river valleys (valley permafrost) and on the bottom of depression (depression permafrost), where a YM of ISWSR is more than 187.5WM$^{-2}$. From DEM data, we generated the slope map. From this slope map we have separated the areas with a slope angle between 0–1°. The area with slope angle between 0–1° corresponds to the bottom of depression in Nalaikh. This area of Nalaikh was mapped as a depression permafrost area (relict permafrost). From the slope map we have separated the areas with a slope angle between 0–5°. The areas with 0–5° indicate the small river valleys. In these areas, we have calculated the NDVI and NDWI as follows:

$$NDVI = \frac{NIR - VIS}{NIR + VIS} \quad (3)$$

$$NDWI = \frac{NIR - SWIR}{NIR + SWIR} \quad (4)$$

The areas with high NDVI and NDWI were mapped as wetland areas. NDVI lies between the limits of -0.4667 and +0.7042. A high value of NDVI is between the limits of +0.30 and +0.7042. NDWI lies between the limits of -0.6 and +0.6129. A high value of NDWI is between the limits of 0.0 and +0.6129. The wetland areas overlie the more vegetated areas, and we separated more wetland areas. These areas correspond with the permafrost island areas along the small river valleys.

The study area divides into two areas: permafrost areas and no permafrost areas. The permafrost areas divide into three kinds of permafrost: 1 – mountain permafrost, 2 – depression permafrost (relict permafrost), and 3 – valley permafrost (Fig. 3).

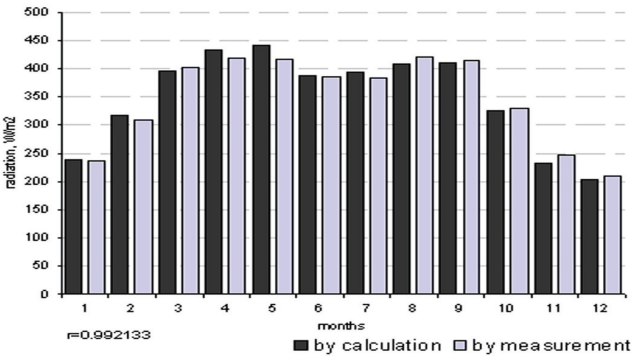


Figure 2. Monthly mean of ISWSR at Terelj GL AWS site.

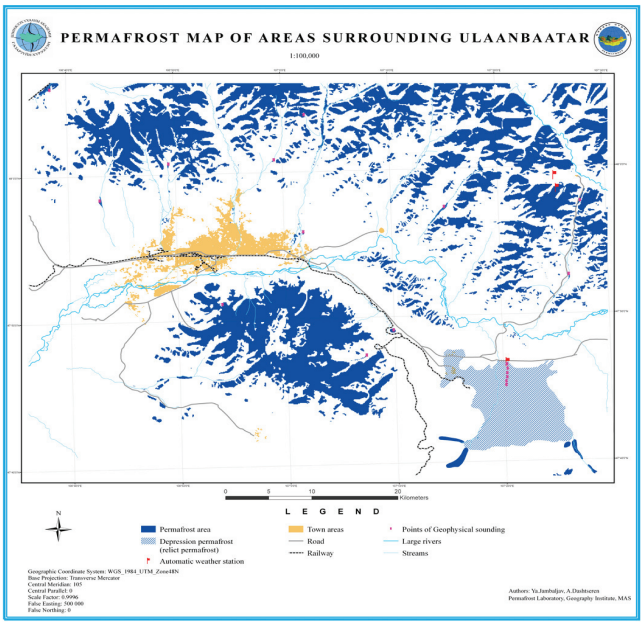


Figure 3. Permafrost map of areas surrounding Ulaanbaatar.

## Conclusion

In summer 2007, we carried out the 1D geophysical measurements by instrument AE-72 on 30 more points and excavated 10 pits in our study area for validation of the permafrost distribution. The probability is about 90%.

## References

Etzelmuller, B. & Hoelzle, M. 2001. Mapping and Modelling the Occurrence and Distribution of Mountain Permafrost. *Status Report at First European Conference on Permafrost, Roma, Italy, March 2001.*

Fu, P. & Rich, P.M. 1999–2000. The solar analyst 1.0. *User Manual*, Helios Environmental Modeling Institute LLC, USA.

Kudryavtsev, V.A. 1978. *General Geocryology.* Moscow: Moscow University Press, 462 pp.

# Historic Change in Permafrost Distribution in Northern British Columbia and Southern Yukon

Megan James
*Department of Geography, University of Ottawa, Ottawa, Canada*
Antoni G. Lewkowicz
*Department of Geography, University of Ottawa, Ottawa, Canada*
Sharon L. Smith
*Geological Survey of Canada, Natural Resources Canada, Ottawa, Canada*
Panya Lipovsky
*Yukon Geological Survey, Whitehorse, Canada*

## Introduction

As a largely climatically-controlled phenomenon, permafrost conditions are impacted by air temperature and precipitation, as well as other local surface and subsurface factors (Smith & Riseborough 1996, 2002). Numerous studies have shown that permafrost should diminish in extent with rising air and ground temperatures (ACIA 2004). However, most of these predictions are based on modeling, and there are very few field-based studies of long-term permafrost change in Canada.

The objective of this study is to directly evaluate the impact of recent climate change on permafrost distribution. We were able to conduct it due to the availability of early baseline permafrost data, which are rare in Canada. In August 2007, we repeated a 1964 permafrost survey undertaken by the late Roger Brown along the Alaska Highway from Whitehorse, YT, to Fort St. John, BC (Brown 1967).

## Study Area

It is difficult to demonstrate climate change impacts on permafrost except in very cold permafrost, where temperatures can rise without much thaw, or in areas of very warm and shallow permafrost, where it may thaw completely (Smith et al. 2005). Even warm, shallow permafrost, like that found in the study area, can take several decades to thaw because far more heat is required for phase change than for warming (Smith et al. 2005).

Brown's sites traverse discontinuous permafrost designated as sporadic (underlying 10–50% of the landscape) or isolated patches (underlying 0–10%) (Heginbottom et al. 1995), which can be expected to be the most sensitive to climate change, because a small change in temperature can result in a transition from a cryotic to a thawed state (Kwong & Gan 1994). According to Smith and Riseborough (2002), the southern limit of discontinuous permafrost approximately coincides with a mean annual air temperature (MAAT) of -1ºC. Table 1 shows the MAATs of the principal communities along the study transect east of Whitehorse.

Table 1. MAATs of communities along the study transect.

| Community | Latitude | Longitude | Normal MAAT (1971–2000) |
|---|---|---|---|
| Whitehorse, YT | 60°42′ N | 135°04′ W | -0.7°C |
| Watson Lake, YT | 60°72′ N | 128°49′ W | -2.9°C |
| Fort Nelson, BC | 58°50′ N | 122°36′ W | -0.7°C |
| Fort St. John, BC | 56°14′ N | 120°44′ W | 2.0°C |

(Environment Canada 2007b)

## Methods

Brown described the 60 locations that exhibited permafrost in 1964, as well as some nonpermafrost sites, in such sufficient detail that it was possible to relocate most of them using milepost information, written descriptions, and photographs. This information was retrieved from Brown's 1967 publication, as well as from cartographic and photographic material archived at the National Research Council of Canada. The research was conducted in the month of August so that the depth of the thawed layer would be near its maximum.

Using UTM coordinates for Brown's sites, derived from archived 1965 Alaska Highway maps, we drove along the route until we were within 500 m of the coordinates for a site and continued for 500 m past. We assessed the landscape on either side of the highway until we could confidently match Brown's photographs and descriptions. At some locations we had to examine an area several hundred metres around the UTM coordinates and look for sites most likely to have permafrost (based on vegetation and drainage), which we would investigate. There were several sites that we were unable to relocate due to inadequate descriptions or profound changes in land cover, such as conversion of spruce forest to farm fields. At each relocated site, 2 ground temperature profiles were measured to 1.5 m or until we encountered the frost table. At sites where a frost table was found, 10 ground probings, roughly 1 m apart, were performed to measure active layer thickness.

Further information on ground thermal conditions will be obtained from six climate stations which were set up to measure air temperature, ground temperatures, and snow depths in order to examine the conditions that have allowed permafrost to endure. These data will be downloaded in summer 2008.

## Results

The results of this survey demonstrate that significant change has occurred in the last four decades. More than half of the positively located sites which had permafrost in the upper 1.5 m in 1964 along the route as a whole no longer exhibited perennially frozen ground in 2007, and this was true of almost three-quarters of the sites in the route segment to the south of Fort Nelson, BC. In addition, where permafrost was still extant in the upper 1.5 m, active layers on average were deeper than in 1964, even though the survey was undertaken one month earlier in the thaw season.

Climate data show that Brown's survey in 1964 followed roughly 20 years of cooling, especially at Whitehorse (Fig. 1). This cooling continued for another decade, and there was then a rapid rise in temperatures. Changes in active layer thickness and permafrost extent observed during the 2007 revisiting of Brown's sites would have been the result of this 1.5–2.0°C rise in temperature over the past 30 years, as well as any change in precipitation quantities and patterns.

## Discussion and Conclusion

Preliminary results suggest that the boundaries of the permafrost zones may have moved substantially northwards since Brown undertook his survey. These results fit with what would be expected given the concurrent air temperature change. However, precipitation is also an important component of climate, and snow depth and duration are significant local factors affecting the ground temperature regime (Smith & Riseborough 1996, 2002). Little is currently known about the snow conditions at the sites, but the climate stations installed in 2007 should reveal relationships between air temperatures, ground temperatures, and snow depths.

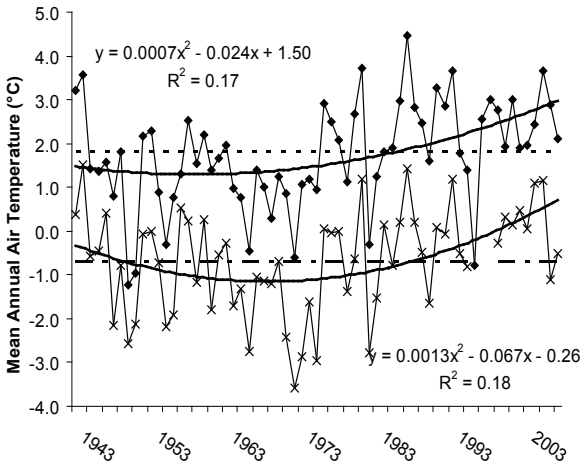


Figure 1. MAATs of Whitehorse, YT (the *x* line) and Fort St. John, BC (the "diamond" line) from 1943–2007 (Environment Canada 2007a). The dashed lines are the long-term MAATs over the time period, and the solid black lines are polynomial lines.

In August 2008, data will be downloaded from the six climate stations and a combination of geophysical techniques and direct drilling will be used to establish current permafrost thicknesses and to install ground temperature cables. This information will be combined with spatial analysis of a highway borehole database on permafrost that is currently being developed at the Yukon Geological Survey.

This study is a step towards filling a research void to provide evidence of loss of permafrost on a multidecadal scale. Careful archiving of information about the research sites should allow repetition of the survey by future generations of permafrost researchers, thus contributing to the legacy of the International Polar Year.

## Acknowledgments

Support for this project has been provided by the Federal Government of Canada's International Polar Year Program (Thermal State of Permafrost in Canada), the NSERC Northern Internship Program, the Northern Student Training Program, DIAND, and the Yukon Geological Survey. Catherine Henry provided field assistance.

## References

Arctic Climate Impact Assessment (ACIA). 2004. *Impacts of a Warming Climate*. New York: Cambridge University Press, 139 pp.

Brown, R.J.E. 1967. *Permafrost Investigations in British Columbia and Yukon Territory*. Division of Building Research Technical Paper 253. Ottawa: National Research Council of Canada.

Environment Canada. 2007a. *Canadian Climate Data*. http://climate.weatheroffice.ec.gc.ca/climateData/canada_e.html.

Environment Canada. 2007b. *Canadian Climate Normals or Averages 1971–2000*. http://climate.weatheroffice.ec.gc.ca/climate_normals/index_e.html.

Heginbottom, J.R., Dubreuil, M.A. & Harker, P.T. 1995. Canada Permafrost. (1:7,500,000 scale). In: *The National Atlas of Canada*, 5th Edition, sheet MCR 4177. Ottawa: National Resources Canada.

Kwong, Y.T. & Gan, T.Y. 1994. Northward Migration of Permafrost along the Mackenzie Highway and Climatic Warming. *Climatic Change* 26(4): 399-419.

Smith, M.W. & Riseborough, D.W. 1996. Permafrost monitoring and detection of climate change. *Permafrost and Periglacial Processes* 7: 301-309.

Smith, M.W. & Riseborough, D.W. 2002. Climate and the limits of permafrost: A zonal analysis. *Permafrost and Periglacial Processes* 13: 1-15.

Smith, S.L., Burgess, M.M., Riseborough, D. & Nixon, F.M. 2005. Recent trends from Canadian permafrost Thermal Monitoring Network sites. *Permafrost and Periglacial Processes* 16: 19-30.

# Improve the Active Layer Temperature Profile Estimation by the Data Assimilation Method

Rui Jin, Xin Li
*Cold and Arid Regions Environmental and Engineering Research Institute, Chinese Academy of Sciences*

## Introduction

The heat and hydrological regimes of the frozen ground, especially its active layer dynamics, have important impacts on the energy and water exchange between the land and atmosphere, runoff, the carbon cycle, and crop growth.

There are two methods widely used in frozen ground research including the physically based model and in situ/ remote sensing observation. However, there are some uncertainties in the model simulation. The observation has instrumental and representative errors as well. The in situ stations are distributed sparsely. Additionally, although remote sensing can provide a regional view, the direct application of remote sensing was to detect the soil surface freeze-thaw status by microwave bands.

Land data assimilation provides a new methodology to merge the observations into the dynamics of the land surface model for improving the estimation of land surface state (Li et al. 2007).

## Framework of Active Layer Data Assimilation System

The active layer data assimilation system comprised four components:

1. Model operation: The SHAW (Simultaneous Heat and Water) (Flerchinger & Saxton 1989) model was used to provide the dynamical framework.

2. Observation operator: The microwave radiative transfer model $T_b = e \cdot T_{eff}$ (Liou 1998) was used to convert the predicted model state variable to the simulated brightness temperature.

3. Assimilation strategy: The ensemble kalman filter (Evensen 2003) is a new sequential data assimilation algorithm, which can deal with the nonlinearity and discontinuity of the model.

4. Dataset: It includes atmospheric forcing data, land surface parameters, in situ SMTMS (Soil Moisture and Temperature Measurement System) observation, and SSM/I data.

The assimilation experiments were carried out at AMDO (32.2°N, 91.6°E, 4700 m) station on the Tibet plateau, which is located in the island permafrost region.

*Assimilating the 4 cm depth soil temperature observation*

The 4 cm depth soil temperature observation was assimilated because it contributed to the microwave emission and was less influenced by the environmental conditions than the soil surface temperature.

The experiment of assimilating hourly 4 cm depth soil temperatures showed the result matched well with the

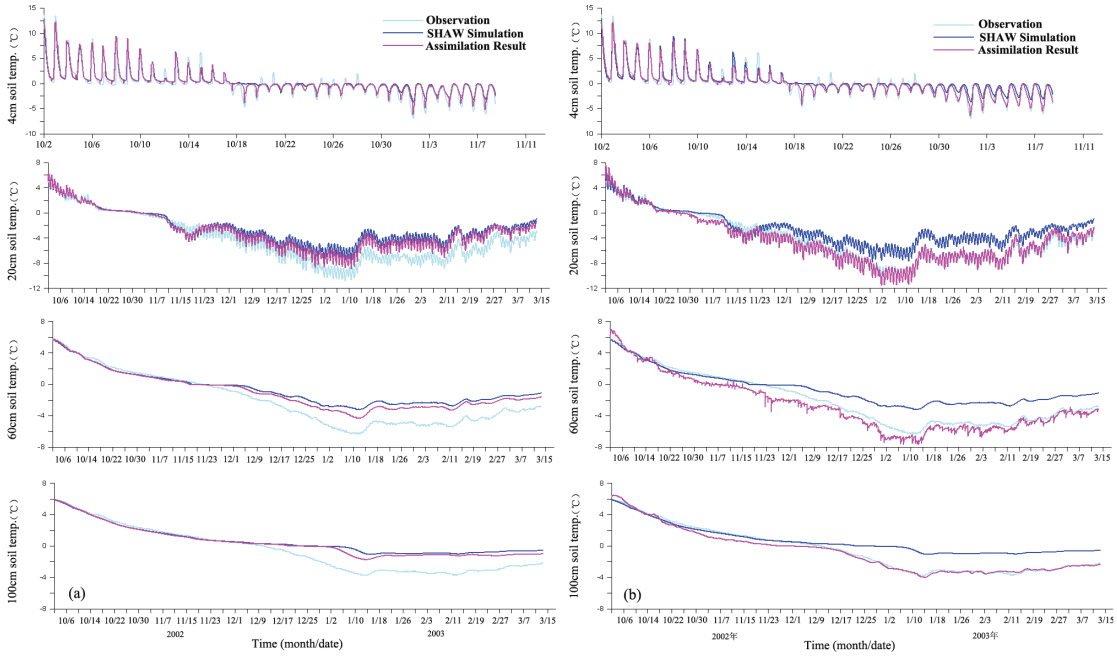


Figure 1. The assimilation result of 4 cm, 20 cm, 60 cm, and 100 cm soil temperature by introducing the 4 cm depth soil temperature observation: (a) the non-diagonal element equals to 0; (b) the non-diagonal element is determined by the model error and the correlation analysis.

Table 1. The soil temperature RMSE (K) of SHAW simulation against the result of assimilating the SSM/I brightness temperature.

| Soil Layer (cm) / RMSE (K) | 0 | 4 | 10 | 20 | 40 | 60 | 80 | 100 | 130 | 160 | 200 | 258 |
|---|---|---|---|---|---|---|---|---|---|---|---|---|
| SHAW Simulation | 10.09 | 3.03 | 2.43 | 2.07 | 1.65 | 1.75 | 1.67 | 1.61 | 1.20 | 0.81 | 0.36 | 0.04 |
| Assimilating SMTMS | 8.05 | 1.61 | 0.91 | 0.60 | 0.99 | 0.79 | 0.63 | 0.38 | 0.42 | 0.51 | 0.31 | 0.04 |
| Assimilating SSM/I | 8.60 | 1.89 | 1.23 | 1.15 | 1.44 | 1.06 | 0.73 | 0.61 | 0.62 | 0.64 | 0.34 | 0.04 |

observations. The RMSE (root mean square error) of the assimilated result of 4 cm soil temperature is 0.16 K, which is significantly less than that (3.03 K) by running the SHAW model alone.

Assimilating the 4 cm depth observation not only improves the state estimation of the corresponding layer, but also can improve the estimation of the whole soil profile state when given reasonable model error covariance matrix (Hoeben & Troch 2000).

Figure 1 showed the assimilation results of the non-diagonal elements equal to zero (Fig. 1a) and equaling the values determined by the correlation analysis (Fig. 1b). For clarity, part of the assimilation result at the 4 cm layer was shown here. The zero non-diagonal elements mean the soil temperature of each layer is independent; only soil temperature at 4 cm can be updated after assimilating the corresponding soil temperature observation. The deep soil temperature can only be influenced slowly by the process of interlayer flow described in the SHAW, so the data assimilation efficiency is very low. The error covariance matrix with non-diagonal elements not equal to zero can play the key role of transferring the updated surface state information to the deep soil quickly, achieving improved estimation of the soil temperature profile. After assimilating the 4 cm depth soil temperature observation, the RMSE of soil temperature decreased 1 K on average, compared to SHAW simulation. The RMSE of assimilation with reasonable covariance decreased about 0.7 K compared to assimilation with covariance as zero.

*Assimilating the 19 GHz SSM/I brightness temperature*

For the regionally frozen ground research, the available in situ observation is sparse. Remote sensing, especially the passive microwave radiometers, would be a promising observation method because of its frequent revisit cycle and global/regional coverage.

The key to merging the brightness temperature observation into the assimilation system is the microwave radiative transfer model, which can act as the bridge between the model state variables predicted by SHAW and brightness temperature observed by the radiometer. The volume-scattering effect was not considered in the LSP/R model, so the 19 GHz brightness temperatures, having the longest wavelength in the SSM/I frequencies, were chosen as the observations to be assimilated.

After assimilating the SSM/I 19 GHz brightness temperature, the RMSE of soil temperature decreases 0.76 K on average (Table 1). Especially the improvement of 0–100 cm layer soil temperature was obvious, nearly 1–2 K. The improvement by assimilating the brightness temperature is lower than assimilating in situ observation, because the brightness temperature is an indirect observation, and there exist uncertainties in the microwave radiative transfer model.

## Conclusion

The one-dimensional assimilation experiments showed that assimilating the in situ observations and the passive microwave brightness temperature can remarkably improve the estimation of a soil temperature profile.

The regional four-dimensional active layer data assimilation system can be developed based on the current one-dimensional system. It will be able to provide soil temperature, water content, ice content, and other datasets with spatiotemporal and physical consistence. The datasets can be used in frozen soil and climate change interaction research, promoting the in-depth and quantitative understanding of frozen soil dynamics.

## Acknowledgments

The authors thank the support from the National Natural Science Foundation of China (40701113; 40601065). The data used in the paper are generously provided by the CEOP and NSIDC.

## References

Evensen, G. 2003. The ensemble kalman filter: Theoretical formulation and practical implementation. *Ocean Dynamics* 53: 343-367.

Flerchinger, G.N. & Saxton, K.E. 1989. Simultaneous heat and water model of a freezing snow-residue-soil system Ⅰ: Theory and development. *Transactions of the ASAE* 32(2): 565-571.

Hoeben, R. & Troch, P.A. 2000. Assimilation of active microwave observation data for soil moisture profile estimation. *Water Resources Research* 36(10): 2805-2819.

Li, X., Huang, C.L., Che, T., Jin, R., Wang, S.G., Wang, J.M., Gao, F., Zhang, S.W., Qiu, C.J. & Wang, C.H. 2007. Development of a Chinese land data assimilation system: Its progress and prospects. *Progress in Natural Science* 17(8): 881-892.

Liou, Y.A. & England, A.W. 1998. A land surface process/radiobrightness model with coupled heat and moisture transport in soil. *IEEE Transactions on Geoscience and Remote Sensing* 36(1): 273-286.

# Long-Term Winter Seismic Vehicle Impacts in Permafrost Terrain

Janet C. Jorgenson
*Arctic National Wildlife Refuge, U.S. Fish and Wildlife Service*

Seismic exploration was conducted on the coastal plain of the Arctic National Wildlife Refuge, Alaska, during the winters of 1984 and 1985. Approximately 2000 km of seismic line were completed in a 5 x 20 km grid. At least 2000 km of additional trails were created adjacent to the seismic lines by D-7 Caterpillar tractors, pulling ski-mounted trailers between camps. U.S. Fish and Wildlife Service initiated a monitoring program in 1984 to document vegetation and soil disturbance and natural recovery (Felix & Raynolds 1989, Emers & Jorgenson 1997).

Color-infrared aerial photographs were taken of 20% of the trails in 1985 and 1988, and disturbance levels were photo-interpreted at 4914 systematic plots (Raynolds & Felix 1989). A two-stage cluster sample was used to randomly choose 200 of the plots to monitor in the field. Twenty 3-km transects, each consisting of ten 18-m diameter circular plots spaced 300 m apart, were randomly selected. A semi-quantitative system for ranking vehicle disturbance based on vegetation and soil changes was used. Ranks were assigned initially in 1985 by photo-interpretation and subsequently by field evaluations in 1989, 1993, 1998, 2002, and 2005. All plots were visited in 1989. From 1993 to 2005, plots rated as undisturbed in a previous year were assumed to remain undisturbed thereafter and were not revisited.

Disturbance and recovery were summarized by trail type (seismic line or camp-move trail) and vegetation types, which included Wet Sedge Tundra, Moist Sedge-Willow Tundra, Moist Sedge-Dryas Tundra, Moist Sedge-Tussock tundra, Low Shrub Tundra on high-centered polygons, Riparian Shrublands, and Partially Vegetated. The vegetation type Dryas River Terrace was not represented in the 200-plot sample, but data were available from the larger photo-interpreted sample. Ten Dryas River Terrace plots were visited in 2007 to assess recovery.

Snow was usually less than 30 cm deep and did not provide complete protection from vehicle damage. The following summer, most trails had at least some scuffing of vegetation and deeper summer-thawed soil. The greatest damage was destruction of shrubs and sedge tussocks, scraping of ground cover to bare soil, and standing water on trails. Tussock Tundra, Low Shrub Tundra, and Dryas River Terrace were the vegetation types with the highest initial disturbance. About one-half of these plots had medium- and high-level disturbance in 1985. Sedge-Dryas Tundra and Sedge-Willow Tundra were intermediate in disturbance levels, with medium- and high-level disturbance found at about one-third of the plots. Medium- and high-level disturbance was absent in Riparian Shrublands, which collect deep snow, and occurred in <10% of plots in Wet Sedge Tundra. Partially Vegetated areas had no damage.

Recovery was rapid in the first decade as the percentage of disturbed plots decreased from 79% in 1985, to 48% in 1989, and to 11% in 1993. After 1993, the remaining disturbance recovered only slightly. Five percent of plots were still disturbed in 2005. For points that initially had low-level disturbance, recovery was rapid. Twenty-three percent of all points had medium to high levels of disturbance in 1985, and these recovered more slowly.

Figure 1. Repeat photographs of study plot on a trail on Moist Sedge-Dryas Tundra. Parallel ruts and crushed vegetation were evident in 1984, the summer following disturbance (top). An undisturbed reference plot adjacent to this trail had a mean of 37% excess ice content (% volume) near the surface of the permafrost. By 2002, a network of sedge-filled troughs had developed, where melting ice wedges caused ground subsidence (bottom) not seen in the reference plot off the trail.

Vegetation types that tend to have greater amounts of excess ice in the upper permafrost (measured at other plots associated with this study) had the poorest recovery. High disturbance persisted for 23 years only where vehicle traffic had broken the insulating vegetative mat, allowing warming of the soil and permafrost degradation that led to thaw settlement. Changes on these trails included increased moisture, transient increases in nutrient flux, increased cover of a few hydrophytic sedge species, and long-term, large decreases for evergreen shrubs and mosses. In contrast, trails

on the ice-poor gravel substrates of riparian areas (Dryas River Terrace and Riparian Shrublands) did not subside, and vegetation recovered steadily even after severe initial damage.

Tussock Tundra and Sedge-Willow Tundra plots recovered well except for a few that subsided into troughs. Sedge-Dryas Tundra frequently subsided, even when initial disturbance was not high, and over two-thirds of the plots were still disturbed in 2005, with substantial changes in plant community composition (Fig. 1). Low Shrub Tundra and Dryas River Terrace had some low-level disturbance remaining in 2005–2007, mainly patchy subsidence and vehicle ruts that did not subside, with more subtle plant community composition changes.

Figure 2. Repeat photographs of trail on Moist Sedge-Willow Tundra in 1985 (top) and 2007 (bottom). An undisturbed reference plot adjacent to this trail had a mean of 28% excess ice content near the surface of the permafrost. Trail subsidence caused increases in hydrophytic sedges and decreases in all other plants.

Camp-move trails were made by vehicles with higher ground pressure than seismic lines and had more initial damage and slower recovery. By 1989, 32% of seismic trails were still disturbed compared to 64% of camp trails, including 41% at medium- and high-level disturbance. By 2005, all seismic trail plots had recovered to a negligible disturbance level, whereas 10% of the camp trail plots were still disturbed and one-half of those had medium- and high-level disturbance. Overall, 5% of plots were still disturbed in 2005. This translates to 200 km of disturbed trail, out of the original 4000 km of trails.

Previous studies of winter seismic vehicle disturbance in the Arctic predicted only short-term and mostly aesthetic impacts. Long-term monitoring showed that most of the disturbance disappeared gradually, but that impacts to tundra vegetation persisted on a small percentage of the trails up to 23 years after disturbance (Fig. 2).

## References

Emers M. & Jorgenson, J.C. 1997. Effects of winter seismic exploration on the vegetation and soil thermal regime of the Arctic National Wildlife Refuge. In: R.M.M. Crawford (ed.), *Disturbance and Recovery in Arctic Lands: an Ecological Perspective.* Dordrecht, the Netherlands: Kluwer Academic Publishers.

Felix, N.A. & Raynolds, M.K. 1989. The effects of winter seismic trails on tundra vegetation in northeastern Alaska, U.S.A. *Arctic and Alpine Res*. 21(2): 188-202.

Raynolds, M.K. & N.A. Felix. 1989. Airphoto analysis of winter seismic disturbance in northeastern Alaska. *Arctic* 42(4): 362-367.